Synthesis and Application of New Bodipy-tagged NHC Metal Complexes

Design and study of novel Bodipy-tagged NHC-transition metal complexes using fluorescence spectroscopy. Application of novel systems to evaluate the steric and electronic properties of NHC ligands and to gain insight into the assembly/disassembly of organometallic complexes.

TECHNISCHE UNIVERSITÄT DARMSTADT

Vom Fachbereich Chemie

Der Technischen Universität Darmstadt

Zur Erlangung des akademsichen Grades eines

Doctor rerum naturalium (Dr. rer. nat.)

genehmigte

Dissertation

eingereicht von

Stepan Popov

Aus Kramatorsk, Ukraine

Referent: Prof. Dr. Herbert Plenio
Korreferentin: Prof. Dr. Christina M. Thiele

Darmstadt 2023

Stepan Popov:

Synthesis and Application of New Bodipy-tagged NHC Metal Complexes

Tag der Einreichung: 20 Juli 2023
Tag der mündlichen Prüfung: 23 Oktober 2023

Darmstadt, Technische Universität Darmstadt
Jahr der Veröffentlichung der Dissertation auf TUprints: 2023
URN: urn:nbn:de:tuda-tuprints-263692

Acknowledgements

I would like to express my sincere gratitude to Prof. Dr. Herbert Plenio for the opportunity to work in his research group. I am deeply thankful for his mentorship, continuous encouragement, and support throughout my PhD journey. Working with Prof. Dr. Herbert Plenio has been a pleasure, and I was happy to be a part of his research team.

I´m particularly thankful to Eleonore Pfeifer for her endless kindness and support during all these years. I am very happy to have vivid memories and moments that we shared.

I am grateful to the past and current members of AK Plenio: M. Sc. Alexander Kaps, M. Sc. Dorian Müller-Borges, Dr. Yoshinao Shinozaki, M. Sc. Yuki Kanai, Dr. Maximillian Heidrich, Dr. Pavlo Kos, Dr. Götz Hoffmann, Dr. Roman Vasiuta, M. Sc. Sondre Lomeland, and M. Sc. Anusree Ghosh. Over these years in the research group, I found not only great co-workers and team members but also friends and kind people that always shared their constant support and help with me.

Additionally, I would like to express my gratitude to all TU Darmstadt members and departments that directly or indirectly helped and supported me during my PhD. In addition, I am deeply thankful to all the teachers and mentors who have played a significant role in my personal and academic development—their efforts in sharing knowledge and teaching significantly contributed to my growth.

It is challenging to find enough words to express my appreciation to my family, which plays a crucial part in my life. Their endless support and tireless patience have been essential in my achievements and development. I am deeply thankful to them for their constant presence and faith.

Finally, I would like to express my sincere gratitude to my wife, Anastasiia Kremen. Her patience, faith and support with sincere kindness have been my constant source of strength throughout these years and my day-to-day life.

Die vorliegende Arbeit wurde am Eduard-Zintl-Institut für Anorganische und Physikalische Chemie der Technischen Universität Darmstadt unter der Leitung von Prof. Dr. H. Plenio in der Zeit von August 2018 bis Oktober 2022 angefertigt.

Teile dieser Arbeit sind bereits veröffentlicht oder zur Veröffentlichung eingereicht Ergebnisse:

Veröffentlichungen

[1.] **S. Popov**, H. Plenio, "*Determination of Stereoelectronic Properties of NHC Ligands via Ion Pairing and Fluorescence Spectroscopy*", *Eur. J. Inorg. Chem*. **2021**, *36*, 3708.

[2.] **S. Popov**, H. Plenio, "*Ligand Exchange Triggered Photosensitizers – Bodipy-Tagged NHC-Metal Complexes for Conversion of $^3O_2$ to $^1O_2$*", *Eur. J. Inorg. Chem.* **2022**, *27*, e202200335.

[3.] **S. Popov**, H. Plenio, "*Switched fluorescence and photosensitization based on reversible ion-pairing*", *Chem. Commun*., **2022**, *58*, 12669.

[4.] Y. Shinozaki, **S. Popov (shared first author)**, H. Plenio, "*Fluorescent organometallic dyads and triads: establishing spatial relationships*", *Chem. Sci*., **2023**, *14*, 350.

Table of Contents

1. Introduction

Fluorescence spectroscopy has become an important tool in various fields of modern science, including organic chemistry and advanced materials development. The measurement of fluorescence can detect small amounts of luminescent materials in target systems, expanding the limits of classical analytical techniques. In homogeneously catalyzed transformations, transition metal-based complexes are typically present in small quantities relative to the reaction substrate compounds. As a result, the tunable properties of fluorescence signal can be effectively leveraged to gain insights about the state of the metal complex or catalytically active species in real-time conditions. In addition to high efficiency of fluorescence spectroscopy in the quantitative and qualitative detection of analytes, it also offers the advantage of inducing dynamic photophysical changes in fluorophore molecules connected to transition metal complexes. These changes result in different transformations of the emission signal. Such fluorogenic modulations are potentially important triggers for evaluating various aspects of transition-metal ligand interactions, molecular sensing, organometallic-based reactions, triplet sensitizers, *etc*. Labeling transition-metal complexes with appropriate fluorophores is a crucial requirement for conducting research in this scientific area.

The current chapter presents a brief overview about fluorescence spectroscopy and general information about pathways in tunability of the fluorescence properties of Bodipy fluorophore *via* structure modification. It also includes a short up-to-date review of field-related data about the development and applications of transition metal-fluorophore based systems.

1.1. Phenomena of luminescence

The luminescence process involves the emission of light by a molecule from an electronically excited state triggered by physical, mechanical, chemical, or electrochemical mechanisms. Different ways of substance excitation result in different categories of luminescence, such as chemiluminescence, mechanoluminescence, electroluminescence, thermoluminescence, and photoluminescence. Phenomena of photoluminescence are divided into two types based on the nature of the excited state: fluorescence and phosphorescence. It occurs when a chromophore absorbs radiation, initiating a transition to the electronically excited state, and then returns to the ground state, resulting in light emission. Fluorescence is a radiative transition between electronic states of the same multiplicity, while phosphorescence is a radiative transition between states of different multiplicity.

The Jablonski diagram visually represents all photoinduced molecule processes in various excited states, starting from light absorbance that does not cause chemical modification (Figure 1). It represents the singlet ground state S_0 of the molecule, the first S_1 and second S_2 excited singlet states, and T_1 as the first excited triplet state, where the name of each vibrational state is based on the configuration of angular momentum. These electronic states can exist in various vibrational energy levels, depicted by numbers 0, 1, 2, and 3 and illustrated as horizontal lines. The vertical lines represent transitions from the ground to a higher electronic state that occur in the timescale of about 10^{-15} s, *i.e.* there is no time for a molecular motion due to the fast occurrence of absorbance. Therefore, displacement of nuclei is negligible according to the Frank-Condon principle. After absorption of radiation molecule is promoted to the higher vibrational level S_1 or S_2. Molecules in the thermally equilibrated S_1 state can undergo a rapid relaxation to a ground energy state S_0 by emission of a photon (fluorescence) or a radiationless transition

with spin conversion to the first triplet state T_1. Such transition from S_1 to T_1 isoenergetic vibrational levels is called intersystem crossing (ISC).

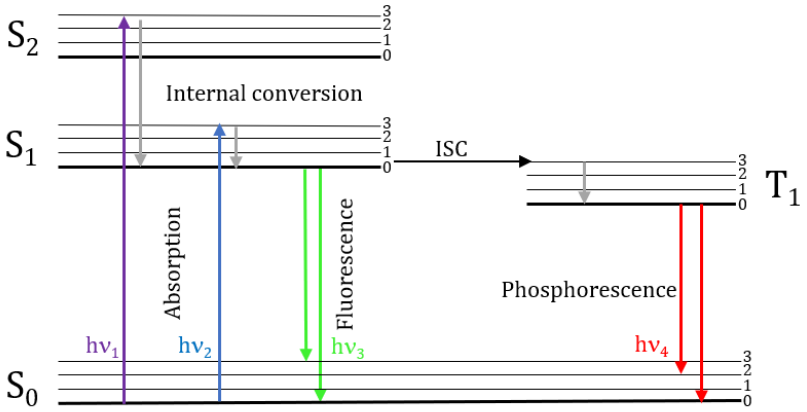

Figure 1 Jablonski energy diagram of a photoluminescent procces.

The molecular transition form T_1 to S_0 results in emission called phosphorescence that usually has a stronger bathochromic shift in comparison to fluorescence. The fluorescence emission rate is relatively fast at 10^{-8} s^{-1} compared to slow phosphorescence rates in the range of 10^{-3} to 10 s^{-1}. This slow transition is forbidden because triplet and singlet wavefunctions are orthogonal.

Loss of excitation energy can occur due to various processes such as vibrational relaxation, internal conversion, solvent effects, excited-state reaction, energy transfer, *etc*. Internal conversion and vibrational relaxation are important energy dissipation mechanisms to consider when analysing fluorescence emission. The non-radiative process of vibrational relaxation occurs within an electronic state and moves from a high to a low vibrational energy level. In the case of internal conversion (IC), a molecule can follow non-radiative relaxation process with change in the electronic state from the higher S_2 to the lower S_1 singlet excited state without light emission, usually occurring in 10^{-12} s. As a result of rapid decay to the lowest vibrational level energy S_1, emitted photons have less energy than initially absorbed light (absorption). Such phenomenon where the maximum wavelength of emission spectra is longer than absorbance is known as Stokes Shift. Another important characteristic of the efficiency of fluorescence emission is fluorescence quantum yield (Φ) and can be defined as ratio of all emitted photons to the number of absorbed photons in all directions. Molecules with brightest emission display high fluorescence quantum yield that depends on environmental factors like solvent polarity, viscosity, pH, temperature, and chemical properties of fluorophore.[1]

1.2. Fluorescence quenching mechanisms

A variety of processes can modulate the intensity of fluorescence. Application of fluorescence spectroscopy strongly relies on the modulation of the fluorescence signal originating from the different mechanisms of fluorescence quenching. This chapter will briefly describes some quenching mechanisms as primary tools of fluorescence modulation in transition metal-based fluorogenic systems.

Fluorescence can be diminished because of molecular collisions (dynamic quenching) or the formation of stable complexes (static quenching). The main requirement for efficient quenching is presence of close-distance interactions between fluorophore (F) and quencher (Q) with corresponding overlapping of molecular orbitals and strong localization of electron clouds. Such contact can be affected by different

molecular factors, including steric and electrostatic effects. In a moment of quencher contact with a fluorophore in the excited state, the excited electron of fluorophore returns from LUMO to the ground state, while the quencher may remain in the ground state. In this situation, emission does not occur, and energy is released as heat.

For specific mechanisms, the quencher can undergo excitation to the higher vibrational energy level, which then returns to the ground electronic state. This description of the quenching process is considered only phenomenological and can vary depending on the character of the interactions between F and Q.

Intersystem crossing (ISC). The intersystem crossing is normally a forbidden transition that arises from spin-orbit coupling between electronic states of different multiplicity and results in a non-radiative transition from the singlet to a triplet electronically excited state (Figure 1). The probability of such transition can be increased by incorporating heavy atoms into the molecular structure due to increase in the spin-orbit coupling constant according to the fourth power of the effective nuclear charge and usually can be observed in the presence of heavy elements like I, Br, Ir, Rh, Pd, Pt, Au, Ru, Re, *etc*. Because of the typically long lifetimes of the excited triplet state, it can be quenched (similarly to the singlet state) to the ground state (*e.g*. by molecular oxygen, internal conversion). It is not always obvious to know from the fluorophore molecular structure which quenching mechanism of the singlet state is predominant. Some literature mentions the presence of mixed quenching mechanisms by halogens and molecular oxygen involving ISC, charge transfer, and electron exchange.[2,3] Hence it is often difficult to predict which mechanism is responsible for fluorescence quenching.[1]

Electron-Exchange Quenching. Electron-exchange or Dexter interaction is a quantum-chemical effect associated with quenching and illustrated schematically in Figure 2. Basically, electron in the LUMO orbital of the excited donor molecule (D_e*) can be transferred to the LUMO orbital of an electron acceptor (A_e). Consequently, the acceptor (A_e) follows the return of the electron back to the donor from its (A_e) HOMO orbital and remains in an excited state.

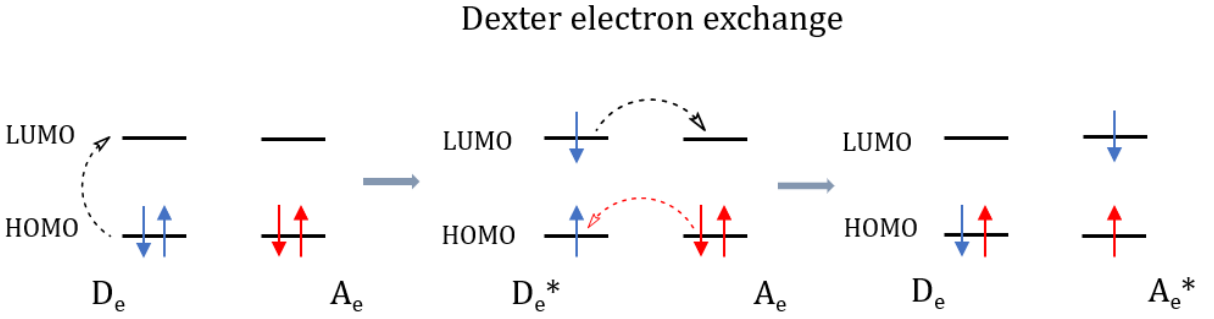

Figure 2 General representation of Dexter electron exchange quenching mechanism.

The nature of the Dexter interaction is similar to the resonance energy transfer (RET) due to energy transfer to the acceptor and dependent on spectral overlapping of donor and acceptor molecules. However, this electron transfer may occur only at short distances (below 1 nm) between molecules and usually occurs at high concentrations compared to relatively large distances of RET under much lower concentrations.

Photoinduced Electron Transfer (PET). PET is an intermolecular photophysical phenomenon of fluorescence quenching derived from total energy change due to an excited electron transfer. Fluorophores can exhibit enhanced oxidative and reductive capabilities in the electronically excited state. As a result, the electron donor and acceptor provide a charge transfer complex that returns to the ground excited state radiationless. Excessive electron is returned to the donor from the acceptor molecule after complex

dissociation. The direction of PET can be predicted from the respective ground and excited state redox potentials and the thermodynamic arrangement of an excited fluorophore and quencher molecule. The reaction of the charged complex formation D^+A^-, which includes redox electron transfer, is illustrated in Figure 3.

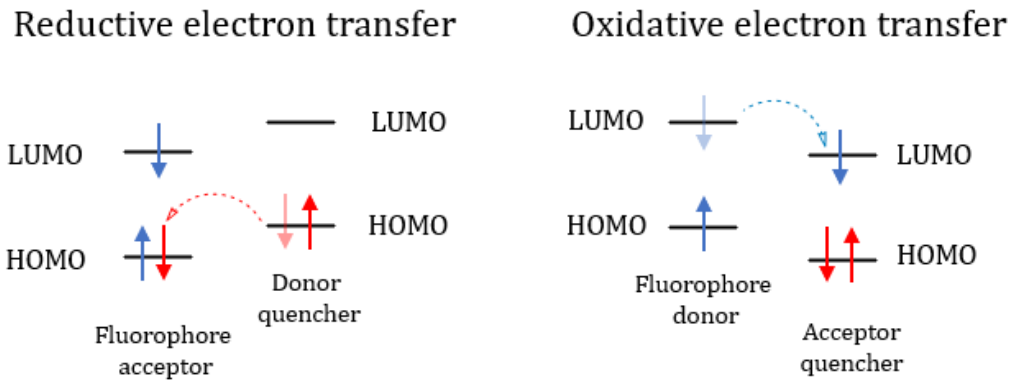

Figure 3 Reductive and oxidative photoinduced energy transfer.

In some cases, emissive excited-state complexes (exciplex) are formed by a collision between the molecule in the excited state and the identical molecule in the ground state. Initiated species in the excited states do not identify the donor´s or acceptor's nature compared to RET, where a fluorophore always represents the donor molecule. The origin of the PET can be represented by situations when fluorophore in the excited state plays the role of the electron acceptor or donor.

The reduction in the overall energy of the charge transfer complex is a crucial aspect of PET process. The capability of an excited fluorophore to donate or accept electrons can cause this energy drop because excitation provides the energy needed to force charge separation. Hence, the charge transfer complex formation process between donor and acceptor through their ground state is energetically unfavorable. The standard Gibbs energy for PET is described by the Rehm-Weller equation using redox potentials of the donor and acceptor:

$$\Delta G = E(D^+/D) - E(A/(A^-) - \Delta G_{exc} - e^2/\varepsilon d \qquad (1.1)$$

where ΔG_{exc} is the excitation energy of fluorophore transition from the lowest vibrational levels of ground S_0 and excited S_1 state; it includes Columbic energy of the formed ion pair where ε is a dielectric constant (permittivity) of the solvent, d is a distance between two formed ions and e is the electron charge.[1,4]

Resonance Energy Transfer (RET). RET is also known as electronic energy transfer (EET) or Förster resonance energy transfer (FRET). Like fluorescence quenching, RET is an electrodynamic phenomenon that always competes with Dexter energy transfer at short donor-acceptor distances, where the fluorescence intensity of the initially excited molecule (donor) can be transferred to the acceptor molecule. During the resonance energy transfer electrons are attached to the molecular cores and typically exist in their valence molecular orbitals and remaining to be dynamically active. Due to non-overlapping wavefunctions of the molecular orbitals of the corresponding molecules, the electrons do not move across them during the energy transfer process and rather move between different electronic states of each molecule. Therefore, RET is fundamentally different from the short-distance nature of Dexter energy transfer, for which electrons move between molecules through covalent bonds.[5] The theoretical concept is based on

considering fluorophore (donor) as an oscillating dipole that can exchange energy with a similar dipole resonance frequency of a second molecule. A general schematic representation of resonance energy transfer is illustrated using the Jablonski diagram (Figure 4). First, a donor fluorophore with two electrons in its HOMO orbital absorbs light, which promotes the electron to the LUMO orbital. The corresponding donor molecule, during the relaxation to the ground electronic state process, releases excitation energy that is simultaneously transferred to the acceptor fluorophore through long-range dipole-dipole interactions and raises the electron of the acceptor molecule to the higher excited-state orbital. The resulted acceptor molecule can be a fluorogenic material that releases accepted energy as an emission or undergoes a radiationless pathway and dissipates energy as heat. In general, molecules involved in energy transfer have low dependence on the permittivity of the surrounding solvent because it has short-range effects compared

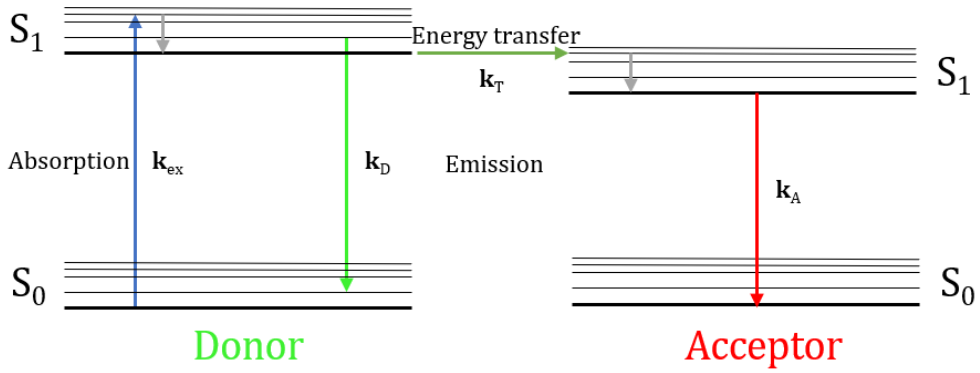

Figure 4 Jablonski diagram for a FRET process. S_0 – ground state, S_1– singlet excited states, k_T – rate of energy transfer, k_D, k_A – donor and acceptor fluorophore fluorescence emission rates, k_{ex} – excitation rate.

to RET as a much longer distanced process between donor and acceptor fluorophore. The solvent's nature significantly impacts the fluorophores' individual spectral properties and can be an essential parameter in developing suitable FRET pairs.[1]

Specific criteria must be considered for FRET to take place:

- The absorbance spectra of the fluorophore acceptor must overlap with the emission spectra of the fluorophore donor;
- Donor and acceptor fluorophores must be placed in the range of approximately 1 – 10 nm from one to another;
- Orientation of transition dipole of donor and acceptor fluorophores must be parallel to each other;
- The fluorescence lifetime must be long enough for the possibility of FRET process to occur.

The efficiency of RET at 50% can be observed at specific distances in the range of 2 – 6 nm and called Förster distance. In other words, this is the distance at which half of the excitation energy of the donor (D) is transferred to the acceptor (A) fluorophore. The rate energy transfer is described by equation (1.2.) and depends on the spectral overlap integral of the donor and acceptor:

$$k_T = \frac{1}{\tau_D}\left(\frac{R_0}{r}\right)^6 \qquad (1.2)$$

where τ_D is the fluorescence lifetime of the donor, r is the distance between the donor and acceptor, R_0 is Förster distance. Energy transfer efficiency is given by:

$$E_{FRET} = \frac{k_T}{k_r + k_{nr} + k_T} = \frac{R_0^6}{R_0^6 + r^6} \quad (1.3)$$

where k_r and k_{nr} are the corresponding rate of radiative and radiationless decays of the donor fluorophore.

Distant dependence of RET and quenching. In general, the quenching rate k_q of fluorescence depends on the degree of interaction between molecular orbitals (electron exchange) of fluorophore and quencher. The quenching rate is assumed to have exponential dependence with an increased distance to the nuclei and can be described by the equation:

$$k_q = C \exp\left[-\beta(R - R_c)\right] \quad (1.4)$$

where β is a constant scaling distance dependence with a distinctive value near 0.1 nm^{-1}; R_c is distance of the nearest molecular contact; R is distance between the center of fluorophore and center of quencher; C represents quenching rate below contact distance and has a value around 10^{13} s^{-1}.[1,6]

Equations 1.2 and 1.4 can be used to compare fluorescence efficiencies *via* distance dependence for RET and quenching, represented in Figure 5.

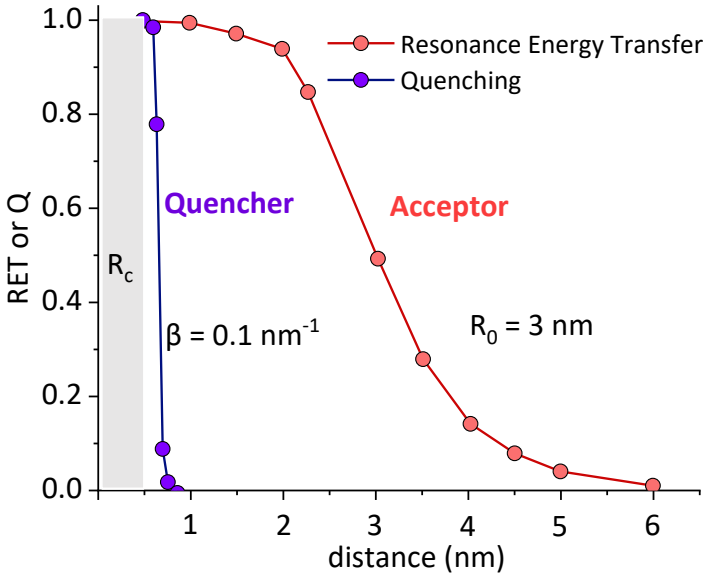

Figure 5 Distant dependence of quenching and resonance energy transfer efficiency.

This data illustrates that RET is indeed more efficient over long distances. At the same time, quenching is efficient only at low-range distances because of the necessity of electron exchange interaction within 0.2 nm between molecular orbitals of fluorophore and quencher.[1]

1.3. Bodipy fluorophores

1.3.1. Fluorophores

Fluorophores play a central role in fluorescence spectroscopy and are often applied as a powerful tool for non-invasive investigations and developments at the single-molecular level in different fields, such as material science, molecular biology, drug discovery, (in)organic chemistry, biotechnology, *etc*.[4,7] Therefore, the choice of fluorophore is often crucial and determined by the specific application needs.[1,4,8] Small fluorogenic organic dyes have many advantages due to their small molecular size, simple tunability of photophysical properties, and molecular functionalization. Hence organic dyes can be applied in various research areas.[9] The perfect organic fluorophore should have a broad scope of desirable physical and chemical properties, such as high fluorescence quantum yield (Φ), molar absorbance coefficient (ε), fluorescence excitation and emission in the specific range of the wavelength, stability towards light and chemicals, good solubility, a large Stokes shift, tunability of properties and facile synthesis. Despite the current availability of different highly fluorescent organic molecules like xanthenes, coumarins, squaraines, acridines, cyanines, pyrenes, anthracenes, *etc.,* non of them fully meets all above-mentioned parameters in parallel. Hence, the development and pursuit of practical fluorescent molecules remain challenging in fluorescence research and application.

1.3.2. Bodipy

Among numerous fluorogenic materials, difluoro*bo*ron *dipy*rromethene complexes (4,4-difluoro-4-bora-3*a*,4*a*-diaza-*s*-indacene, abbreviated as BODIPY and denoted further in this thesis as "Bodipy") become an increasingly practical class of organic fluorophores. It was generally applied in bioimaging[10,11], chemosensing[12,13], triplet photosensitizes[14,15], organic emitting devices[16], photocatalysis[17], laser dyes[18], drug delivery agents[19], *etc*.

Boron dipyrromethene dyes typically exhibit narrow absorption and emission bands, accompanied by small Stokes shifts. These dyes tend to absorb and emit light within the visible spectrum and frequently possess high fluorescence quantum yields. Bodipy dye is small, chemically robust (except strong acids and bases) and neutral molecule with a high thermo- and photostability. From the viewpoint of organic synthesis, these fluorophores are very versatile for molecular modification *via* attachment of different groups at the core structure of Bodipy. This tunability allows researchers to obtain control over the variability of (photo)physical and (electro)chemical properties. In contrast to many other fluorophores that do not have the same level of functionalization, choosing specific substitution parameters of Bodipy core allows variation of the fluorescence emission and absorbance at the entire visible spectrum and near-infrared (NIR) region.

Bodipy molecule derived from the complexation of dipyrromethene ligand with BF_2 unit and can be considered as rigidified monomethine cyanine dye type derivative with full planarity and π-conjugated electronic system. Numbering of substituents of the Bodipy structure derived from the analogous structure of tricyclic *s*-indacene molecule, where positions are often referred as *meso, α* and *β* (Figure 6).

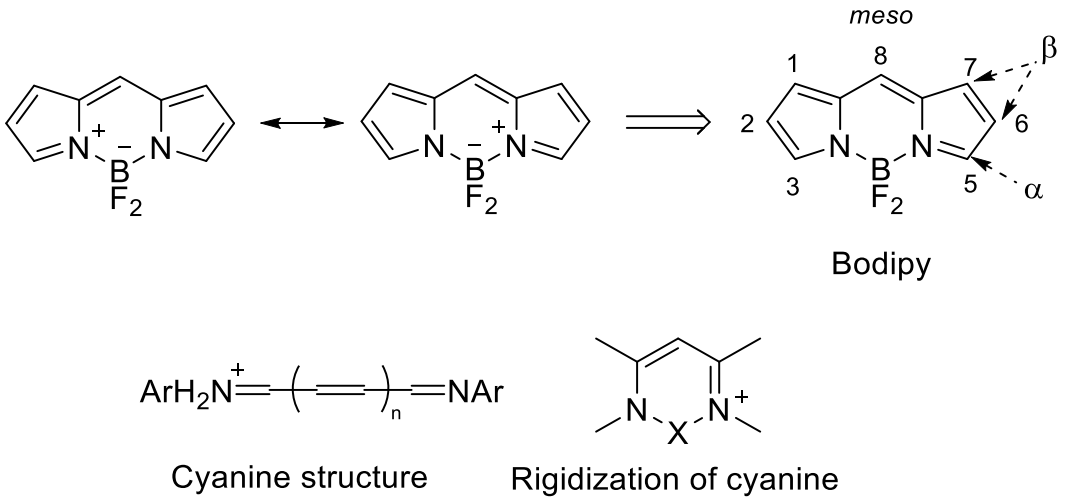

Figure 6 General structure of Bodipy and cyanine dyes.

A molecular dipole moment (μ) is oriented toward the axis where the positive charge is located near *meso* position and the negative charge is at the fluorine atoms. HOMO-LUMO transition dipole moment (M) is correspondingly pointed along the long molecular axis (Figure 7).[20]

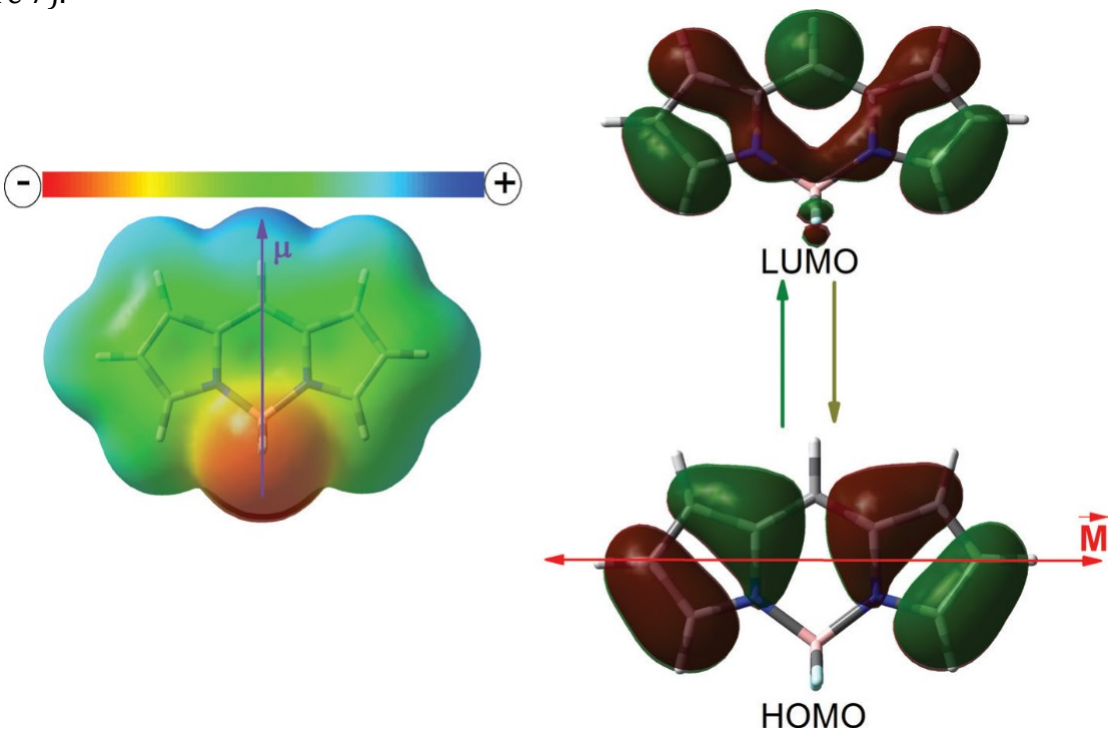

Figure 7 The charge density distribution of the frontier molecular orbitals. Molecular dipole moment and transition dipole moment of the Bodipy molecule.[20]

This chapter will include only a small part of the extensive information about Bodipy fluorophore's general properties and characteristics. It highlights main approaches of Bodipy fluorophores synthesis, pre- and post-functionalization that leads to modulations of different photophysical parameters and presents examples of the application of Bodipy dyes in organometallic chemistry.

1.3.3. Synthesis of Bodipy dyes

The Bodipy fluorophore gained widespread popularity only in the 1990s following the first reported synthesis of 2,4-dimethyl substituted Bodipy by Treibs and Kreuzer in 1968.[21] One of the reasons for its delayed application is that unsubstituted dipyrromethene is a rather unstable compound and decomposes at temperatures above 40 °C.[22] This fluorophore is also highly sensitive toward nucleophilic substitution with the formation of 4,4-difluoro-3-(pyrrol-2-yl)-4-bora-3*a*,4*a*-diaza-*s*-indacene derivative.[23]

Bodipy core synthesis starts from the preparation of the corresponding dipyrromethene or dipyrrinium salt derivative, followed by deprotonation with a non-nucleophilic base like Et_3N or DIPEA and complexation with $BF_3{\cdot}OEt_2$ (Scheme 1). This approach originated from porphyrin chemistry *via* well-established reactions of pyrrole condensation. Formation of the methene bridge within dipyrromethene structure is usually performed using highly electrophilic carbonyl derivatives such as aldehydes (also known as the Lindsey method[24]), acetyl chlorides and acid anhydrides. Asymmetric Bodipy dyes can be prepared *via* condensation reaction of 2-unsubstituted pyrrole and acylated pyrrole in the presence of $POCl_3$ (Scheme 1).

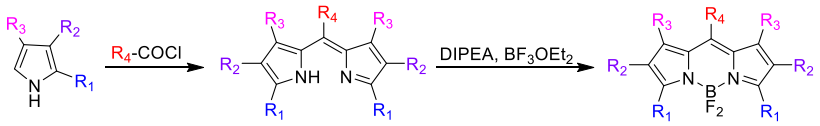

a) Synthesis from pyrrole and acid chlorides

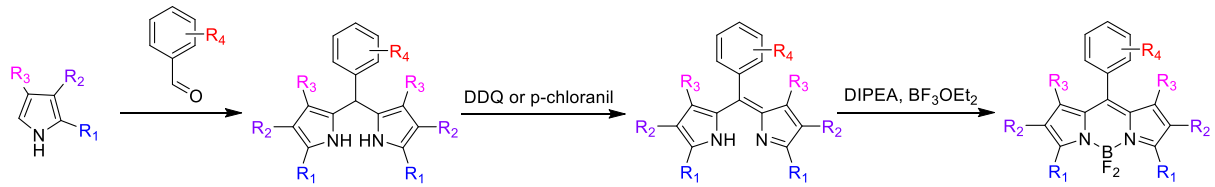

b) Synthesis from pyrroles and aldehydes (aromatic and aliphatic)

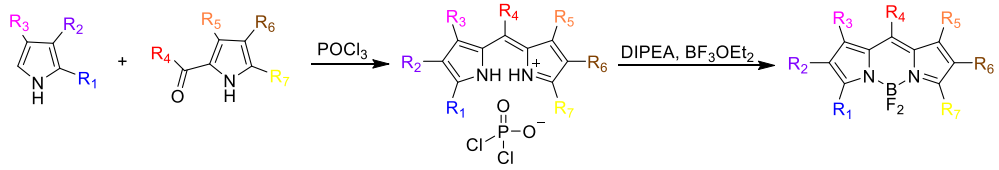

c) Synthesis from pyrroles and ketopyrroles

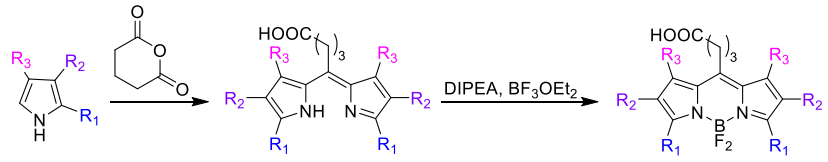

d) Synthesis from pyrroles and acid anhydrides

Scheme 1 General procedure of synthesis symmetrical and asymmetrical Bodipy dyes.

Dipyrromethanes are generally prepared *in situ* because of the high sensitivity to exposure of light, air, and acids. Oxidation of dipyrromethanes is performed using oxidative agents like 2,3,5,6-tetrachloro-1,4-benzoquinone (*p*-chloranil) or 2,3-dichloro-5,6-dicyano-1,4-benzoquinone (DDQ). The resulting products of dipyrromethene oxidation (dipyrrin) are usually challenging to purify by column chromatography due to low stability. Therefore, all reactions starting from pyrrole to the final Bodipy condensation step are often performed sequentially in a one-pot reaction by stepwise addition of all necessary reagents.

Biellmann and coworkers provided an alternative way of Bodipy core synthesis[25], which avoids the standard Lindsey approach. In this methodology, pyrrole reacts with thiophosgene and forms a dipyrrothioketone derivative **1** in decent yields (Figure 8). Simple alkylation reaction of thioketone by methyl iodide resulting in formation of thiomethyl dipyrrinium salt **2**. The corresponding deprotonation of the salt with an excess of Et_3N and complexation with $BF_3{\cdot}OEt_2$ produce 8-thiomethyl Bodipy **3**.

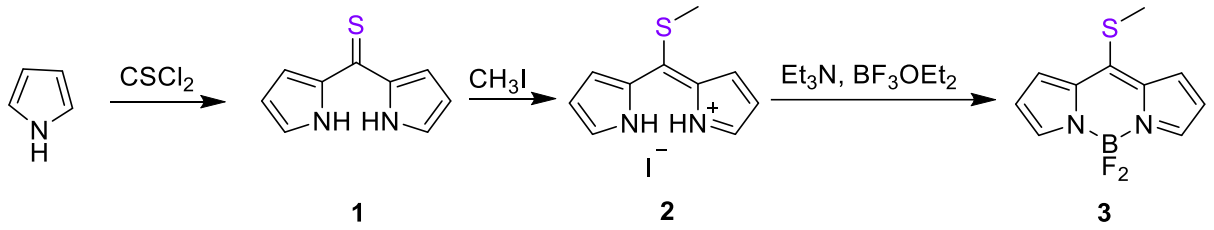

Figure 8 Synthesis of 8-thiomethyl Bodipy by Biellman *et al*.

Leen *et al*. in 2012 reported the synthesis of an alternative to the 8-thiomethyl Bodipy *i.e.* **3** symmetrical *meso*-halogenated Bodipy **5** (Figure 9).[26] This methodology includes synthesis of the di(pyrrol-2-yl)methanone **4** that can be obtained either from the reaction of phosgene (or trisphosgene) with desirable pyrrole or *via* oxidation by H_2O_2 of the above-mentioned dipyrrylthioketone derivative **1**. Halogenation reaction by $POCl_3$ or $POBr_3$ converts dipyrrylketone to the corresponding dipyrrinium salt, which undergoes *in situ* deprotonation and complexation reaction producing 8-halogenated Bodipy **5**.

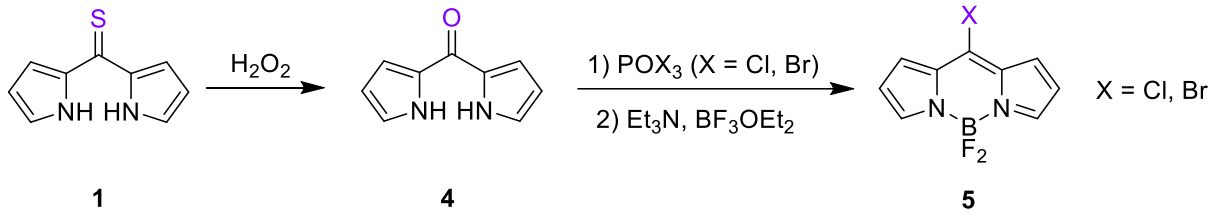

Figure 9 Synthesis of a *meso*-halogenated Bodipy according to Leen *et al*.

It is also important to mention the synthesis of aza-Bodipy fluorophore **10** reported by O'Shea *et al.* (Figure 10).[27] Preparation of this dye starts from the synthesis of α,β-unsaturated ketones (chalcones) following Michael addition to nitromethane in the presence of diethylamine produces 1,3-diaryl-4-nitrobutan-1-one **7**. The condensation reaction of **7** in the presence of an excess of ammonium acetate under reflux conditions forms 2,4-diphenyl-pyrrole **8**, which is sequentially converted to tetraarylaza-dipyrromethene **9**. Deprotonation by DIEA and complexation with $BF_3{\cdot}OEt_2$ provide corresponding aza-Bodipy dye **10** (Figure 10).[34] Unfortunately, synthesis of aza-Bodipy fluorophores is limited using only annelated or 2,4-diaryl substituted pyrrole derivates due to unsuccessful efforts of obtaining alkyl-substituted aza-dipyrromethene derivate systems.[28]

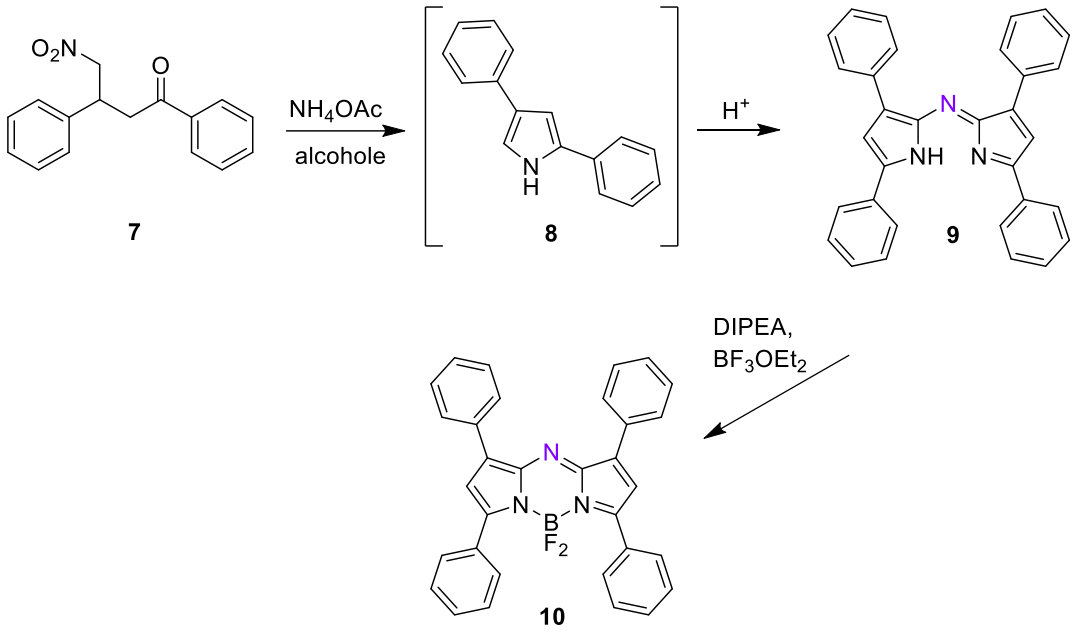

Figure 10 Synthesis of the aza-Bodipy.

1.3.4. Functionalization of Bodipy structure

From the point of view of a synthetic chemist, synthesis of the Bodipy molecule has different advantages due to the accessibility of pyrrol-based starting materials. Various review articles cover the design and production of diverse boron dipyrromethene structures[15,29] and present extensive information about the functionalization methodologies of Bodipy core (Scheme 2).[30–32]

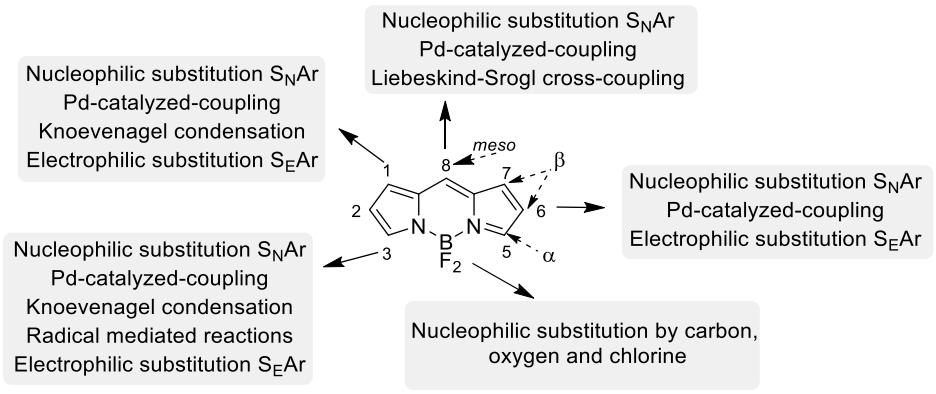

Scheme 2 General strategy of Bodipy core functionalization.

Examples of functionalized Bodipys are represented in Scheme 3 and include modifications of halogenated and thioether derivatives or through the C-H activation of unsubstituted boron dipyrromethene core. Among them are electrophilic (S_EAr)[33,34] and nucleophilic (S_NAr) aromatic substitution reactions[35,36], substitutions of fluorine atoms on the boron atom[37,38], nucleophilic[39,40] and radical[41] substitution of hydrogen atoms, reactions of Knoevenagel-type condensation[42], transition-metal catalyzed cross-coupling reactions[43,44], styrilation reactions[40]. According to the literature sources, general examples of functionalized Bodipy scaffold at the 8-, 2,6-, and 3,5- positions, and the boron center.

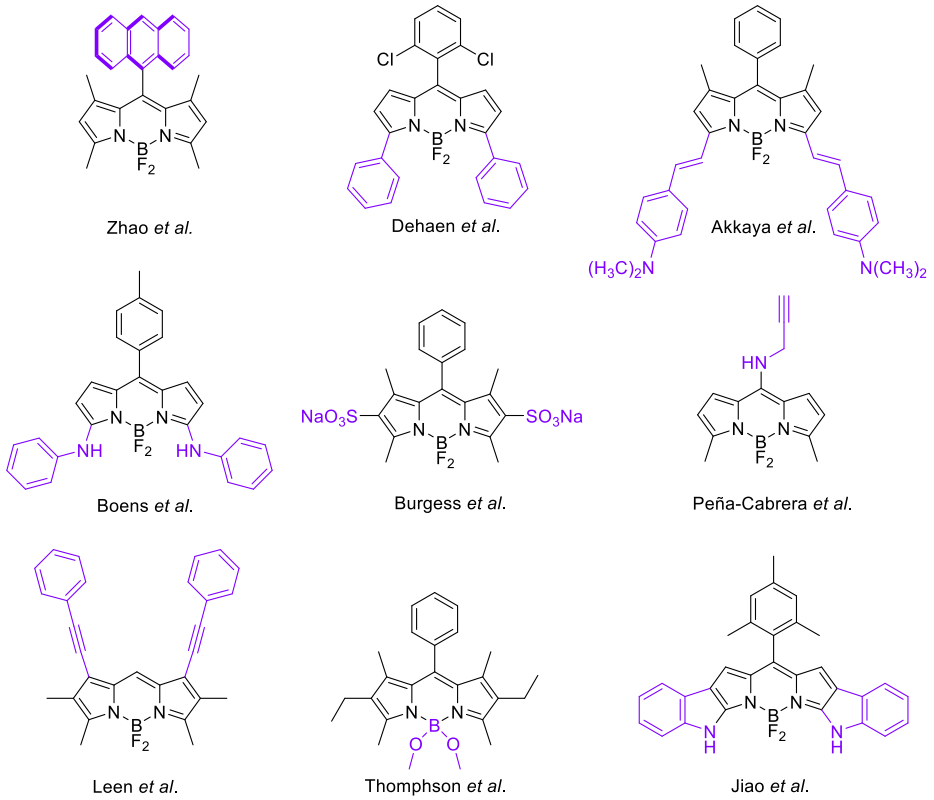

Scheme 3 Example of functionalized Bodipy scaffold.[36,38,41,45,46,47]

1.3.5. Tuning the optical properties of Bodipy dyes

Effects of structure functionalization often directly influence the photophysical characteristics allowing a researcher to apply Bodipy dye for different scientific targets and applications.[20,30,48] Generally, these modification approaches can adjust the absorbance and emission bands in a wide range from the ultraviolet to NIR spectral regions form 400 to 1000 nm (Figure 11).[20]

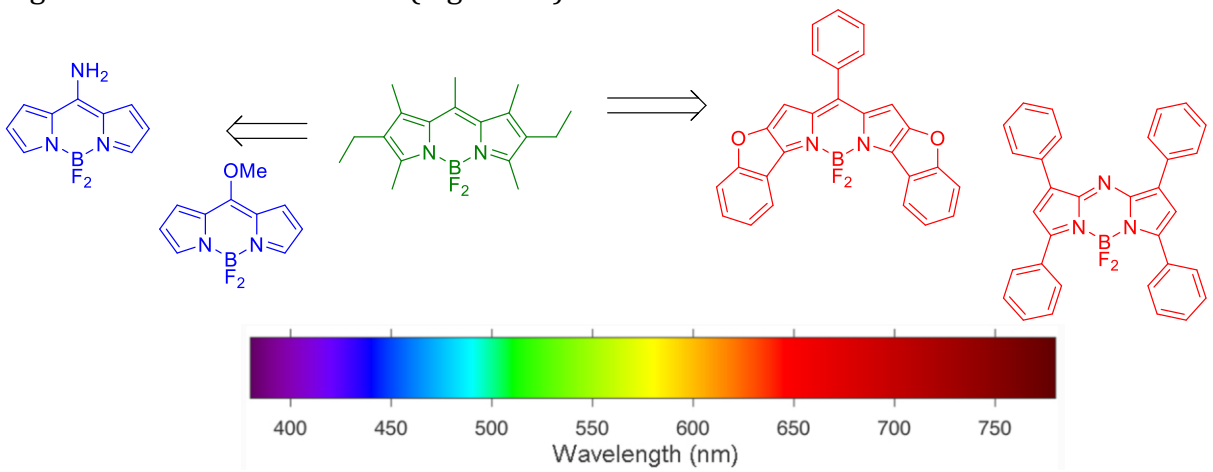

Figure 11 Molecular structure of Bodipy dye and its blue-emitting and red-emitting derivatives.

Patterns of photophysical dependencies of Bodipy dyes usually originate from the various types of substituents at the molecular core. Boens *et al.* have summarized the effects of different electron-donating and withdrawing substituents at common Bodipy

derivatives.[49] In the case of the alkylated basic asymmetrical molecular structures, there are a few differences between the photophysical parameters like UV/Vis absorbance, fluoresce emission, and quantum yield (Figure 12). For instance, bathochromic shifts in absorbance and emission bands appear with an increasing number of alkyl substituents at the Bodipy core.

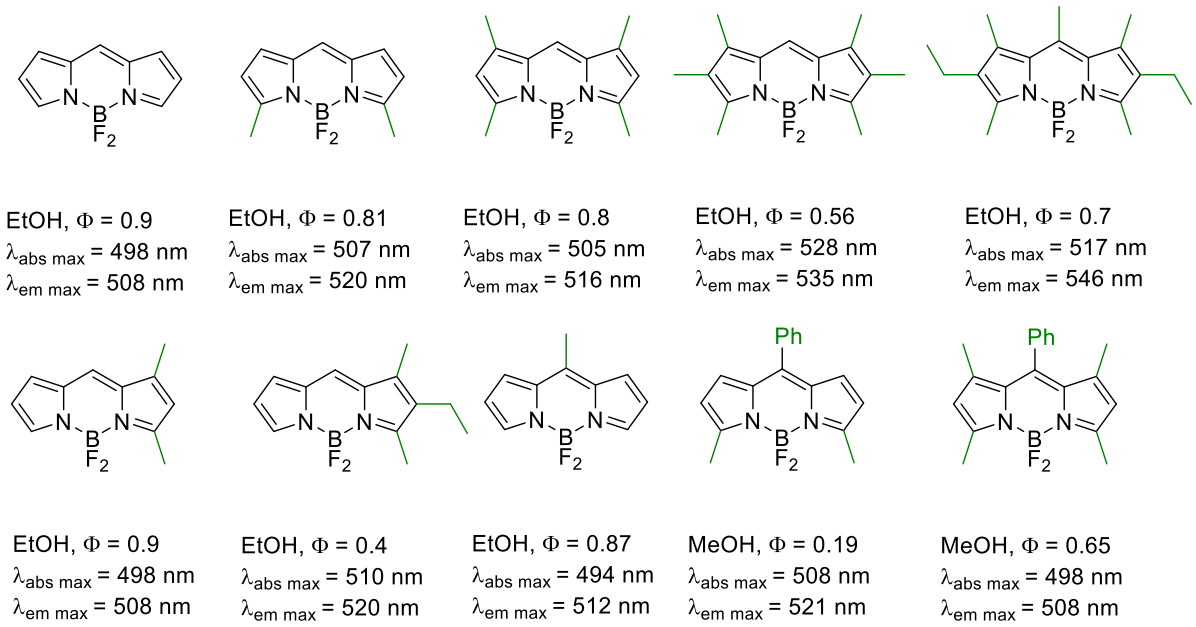

Figure 12 Spectroscopic characteristics of alkyl-substituted Bodipys.[50]

Introduction of the phenyl substituent to the *meso* position has no significant impact on the position of absorbance and emission maxima. However, such modification of *meso* position influences fluorescence quantum yield in the case of arylated derivative compared to alkylated one. This problem can be solved by introducing substituents to the 1,7-position of Bodipy core or substituents to the *ortho* positions at the phenyl ring. Such structural modifications toward steric restriction prevent radiationless loss of excited state energy through the aryl ring's free rotation and increase fluorescence quantum yield.

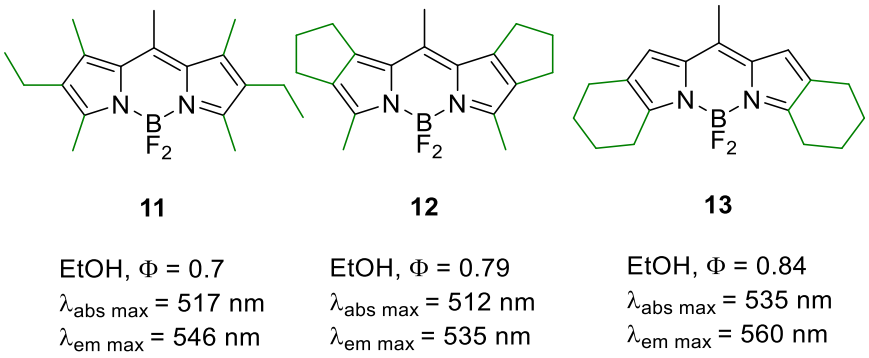

Figure 13 Bodipy dyes with fused aliphatic substituents.

Modification of Bodipy structure *via* fusing of pyrrole parts with aliphatic rings (Figure 13) provides additional rigidity to the molecular core. However, for compounds **11**, **12**, **13,** the prediction of substitution effects does not seem obvious in contrast to acyclic aliphatic substituents. For example, both fluorophores **12** and **11** have fully substituted cores, but **12** provides stronger hypsochromic shifts for the absorbance and

emission compared to **11**. Interestingly, **13** has stronger bathochromic shifts and fewer substituents on the pyrrole ring.[29]

A shift from green to NIR. NIR-fluorophores have broad applications in biomedicine[51], material science[52], bioimaging[11], photodynamic therapy[53,54], and solar cells[55]. Therefore, developing suitable red-emitting Bodipy fluorophores remains to be essential task for many researchers due to the advantages in the robustness and brightness of Bodipy dyes. The general strategy of development of NIR boron dipyrromethene-based dyes includes an extension of the π-conjugated system *via* aromatic framework (*method A*), a fusion of aryls to the indacene core (*method B*), and replacement of carbon atom by nitrogen at *meso* position providing aza-bodipy (*method C*) which represented in Scheme 4. In all mentioned cases provided modification of the molecular core shifts absorbance and fluorescence bands toward red/NIR region.[32]

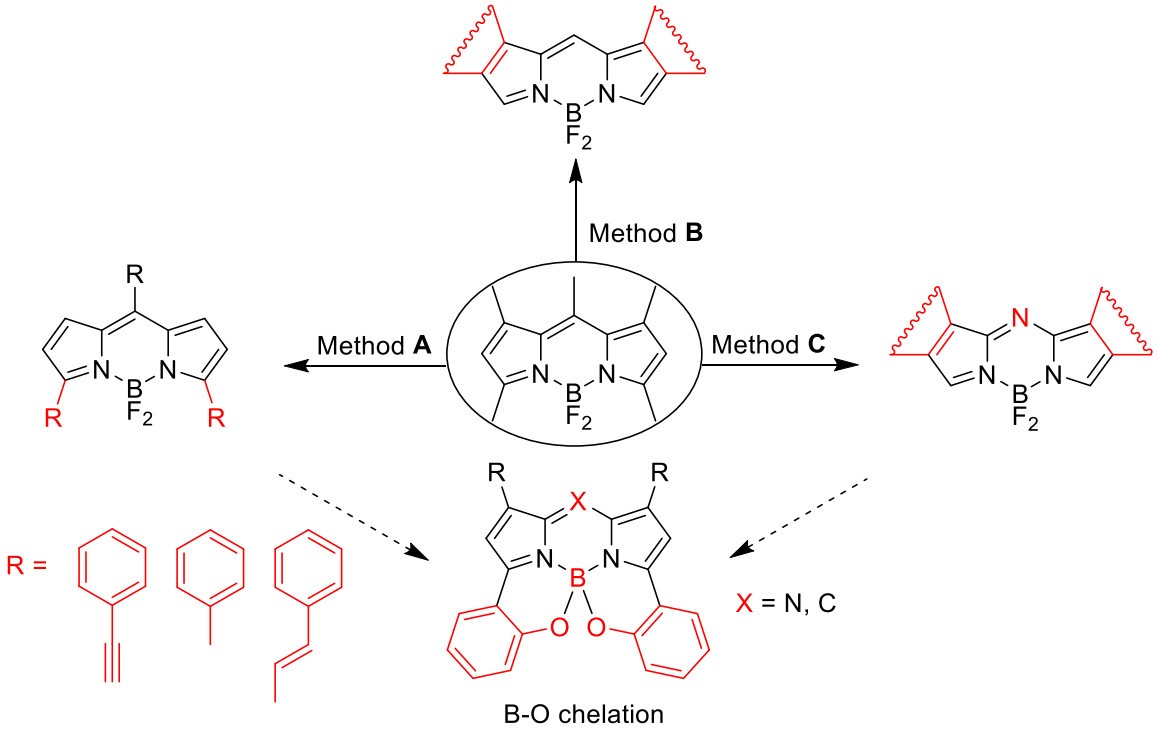

Scheme 4 Structural modifications toward red Bodipy derivatives.

The strategy of peripheral modification of the Bodipy core has three main ways of forming different red-shifted Bodipy derivatives (Figure 14). The first approach relies on nucleophilic **14**[56] and transition-metal catalyzed cross-coupling reactions **15**[34,44] utilizing 3,5-dihalogenated Bodipy with adjustment to obtain both mono- and disubstituted derivatives. The second type of modification includes oxidative nucleophilic reaction at non-substituted 3,5-positions of indacene ring producing compound **16**.[57] This reaction can be performed under oxygen atmosphere depending on the nucleophilicity of substituents. The third approach involves a Knoevenagel-type condensation reaction of methyl substituted Bodipy that provides sufficient acidity for participation in the reaction and results in red-emitting derivate **17**[58]. Disadvantages of this reaction, such as formation of a mixture of condensed products, can be overcome through adjustment of concentration, reaction time, and the ratio of reactants[59].

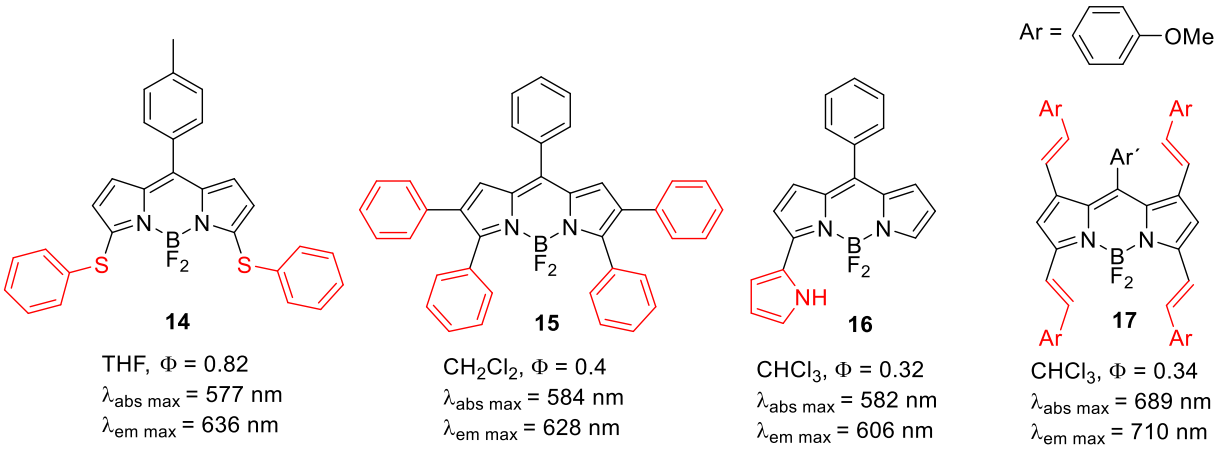

Figure 14 Chemical structures of various peripherally modified Bodipy.

Another approach significantly enhances the emission behavior of fluorophores compared to unconstrained analogues through the restriction of intramolecular rotations and steric hindrance.[60,61] Extended π-conjugation of the indacene plane can be formed through the fusion of benzene rings on the dipyrromethene core or direct synthesis using aromatically ring-fused pyrroles, which usually require more synthetic effort.[62] A strong impact of a ring fusion can be highlighted by comparing compounds **18**, **19**, and **20** (Figure 15).[63] Here, conformational rigidization of **18** leads to the red-shift of the absorbance and emission maximum and the fluorescence quantum yield increase due to the incorporation of sp^3 hybridized carbons that eliminate free rotation of the phenyl groups. In the case of the system with B–O chelation, the absorption and emission maxima have a significant bathochromic shift of ca. 65–80 nm. Similarly to the *meso*-functionalization, substitution reaction at the boron atom impacts the fluorescence quantum yield but has only minor effect on the fluorophore's absorbance and emission bands.[29] Hence, a red-shift of **20** was probably observed because of decreased dihedral angle between the aryl rings and the fluorophore core.[32]

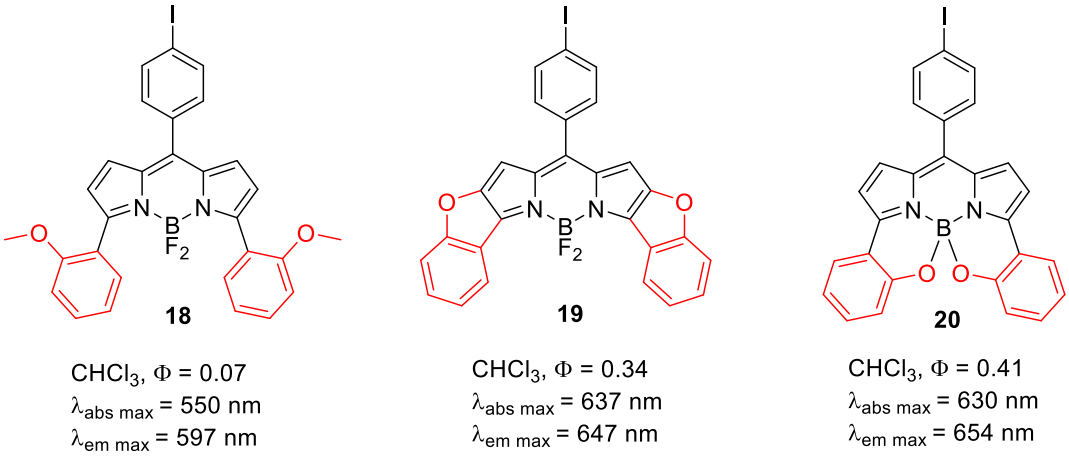

Figure 15 Rigidified red Bodipy dyes.

The previously mentioned aza-Bodipy derivative is another example with a vast potential for synthetic variations and can include all previously mentioned structural modifications (methods **A, B** and **C**). Therefore, the spectroscopical properties of such fluorophores (**21**-**23**)[64] can be extended further in the NIR spectroscopical range (Figure 16). Due to its fascinating functionalization ability, low sensitivity to the solvent polarity,

high photostability, small Stokes shifts and absorption and emission maxima in the NIR-I or NIR-II region, this dye gained popularity in biotechnological applications.[65]

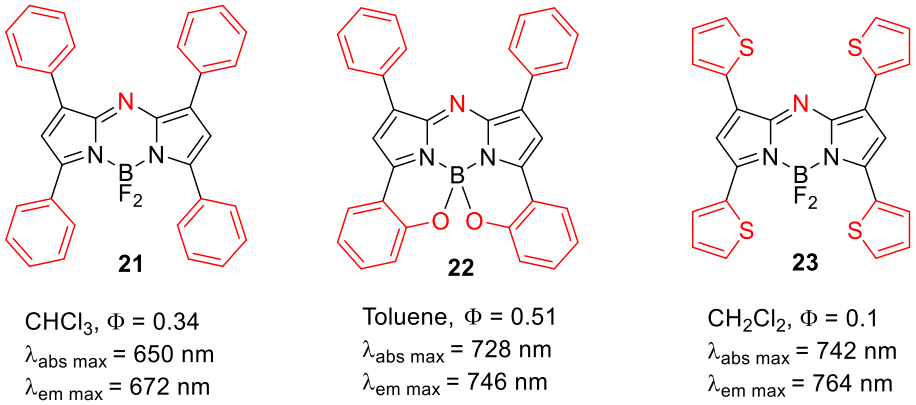

Figure 16 Red-emitting aza-Bodipys.

A shift from green to blue region. Nowadays, blue-emitting fluorophores are applied in various scientific areas, including fluorescence labeling[66], molecular sensing[67], and light-emitting diodes[60,68]. Compared to the wide variety of synthetic approaches for obtaining red-shifted Bodipy derivatives, synthetic strategies for blue-emitting fluorophores remain rather limited.

Biellmann and coworkers first synthesized blue-emitting boron dipyrromethene derivatives in 2006, but the resulting dyes did not provide desirable photophysical characteristics for further application.[25] One of the most common ways of tuning standard fluorescence emission of Bodipy from green to blue spectral region was well-established by Peña-Cabrera *et al.*(Figure 17).[69] This approach relies on the connection of heteroatoms such as oxygen or nitrogen to the *meso* position of the dipyrromethene core, providing blue-emitting Bodipy dye with good photophysical, photochemical, and thermal properties.

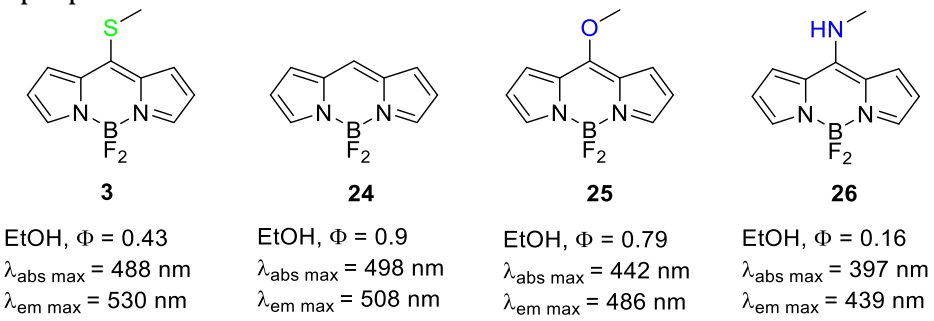

Figure 17 *Meso*-substituted Bodipy derivatives.

Carbon-heteroatom bond formation at the *meso* position was previously reported for the compounds that contain a good leaving group (Cl, Br, or SMe) through the aromatic nucleophilic substitution (S_NAr).[25,26] Therefore, *meso*-chloro or -thiomethyl Bodipy derivatives are usually good candidates for producing blue-emitting dyes (Figure 18).[45,70]

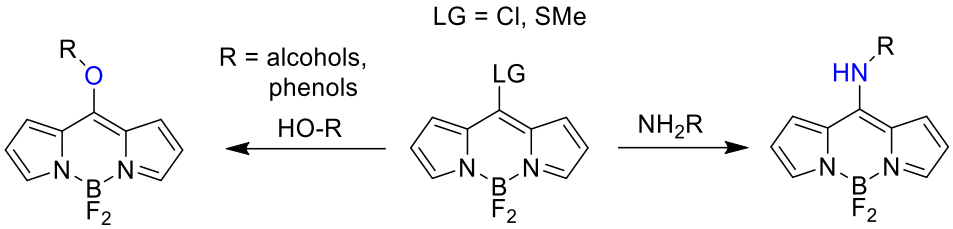

Figure 18 Preparation of blue-emitting Bodipy *via* nucleophilic substitution reaction.

Variation of the type 8-substituted heteroatom at the Bodipy core provides different shifts of fluorescence and absorbance bands to the blue or red spectral region. Here alkylamino- (**26**) and alkoxy- (**25**) derivatives are responsible for the hypsochromic shift, while alkylthio-substituted fluorophore provides red shifts compared to the *meso*-unsubstituted Bodipy. This phenomenon is observed due to differences in electronegativity of the attached heteroatoms and their ability to disturb the electronic delocalization between pyrroles in the dipyrromethene unit (Figure 19). Higher electron-donating effects of the nitrogen have a stronger ability for the formation of a new delocalized π-conjugated system which leads to the corresponding increase of the LUMO energy and respectively different energy gap providing stronger hypsochromic shift.[69]

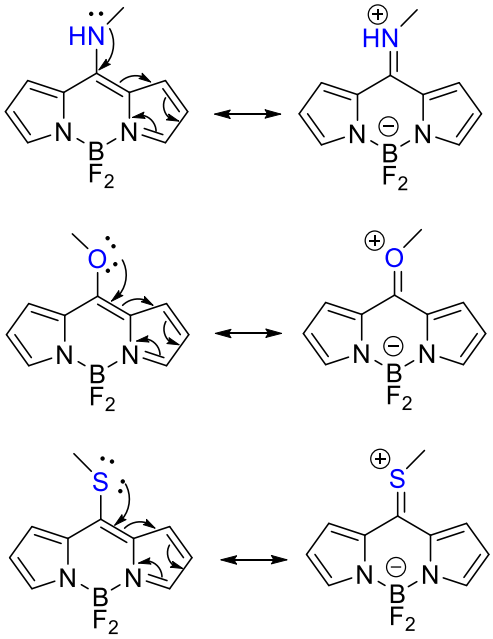

Figure 19 Resonance structure of the Bodipy structures with heteroatom at *meso* position.

To conclude, the Bodipy fluorophores have impressive photophysical and chemical versatility within a single molecular scaffold. In the subsequent section, the discussion will shift from general information about boron dipyrromethene derivatives to the practical applications of this dye in organometallic chemistry.

1.4. Application of Bodipy dyes in organometallic systems

1.4.1. Fluorescent sensors and switches

Fluorescence spectroscopy provides a convenient experimental setup for sensing experiments that can be performed under real-time conditions, with moderate instrumentation costs, the possibility of simple "naked eye" detectability, and low

operating concentrations with high sensitivity down to single molecules. The ability to manipulate fluorescence emission through chemical and physical changes on a molecular scale became the optimal tool for sensing applications.[71,72] Fluorescent probes can be defined as chemical sensors in which the signalling process involves interaction of the analyte with a ligand which can be either part of the fluorophore π- system or isolated from it.[73] Ideally, fluorescent sensors should provide a reversible analytical response after reacting with a targeted species. In many systems, this process is irreversible and encounters limitations in molecular design. Generally, the nature of binding to the target is defined by various parameters like intermolecular forces, hydrogen bonding, metal coordination, Van der Waals interactions, π-π interactions, electrostatic charges, hydrogen bonding, *etc*. A wide range of transition metals can be detected after complexation with chelating ligands at the fluorophore.

Modification of the electronic and/or molecular environment of fluorophore after metal cation inclusion into the cavity of structure leads to a change of the fluorescence properties providing a "turn on/off" response. Photophysical tunability of metal-modified sensors often has complex nature of emission modulation where interaction between partially filled d-orbitals with appropriate energy of the transition metal and the excited state of fluorophore might undergo Dexter energy transfer or photoinduced electron transfer (PET). Another example includes internal charge transfer (ICT), which results in a sufficient shift of the absorbance or emission band wavelength providing a ratiometric type of sensor. Alternatively, to the quenching processes, attachment of the transition metal to a chelating unit of the two fluorophore-tagged molecular systems can induce changes in distance and orientation of molecular structure that can be studied using FRET-based sensors leading to the detectable changes in the ratio of donor/acceptor emission.[72] Numerous review articles describe approaches in the design and application of metal chemosensors.[72,74] Hence, in this section, only the general concept and strategy of developing Bodipy-based chemosensors are provided.

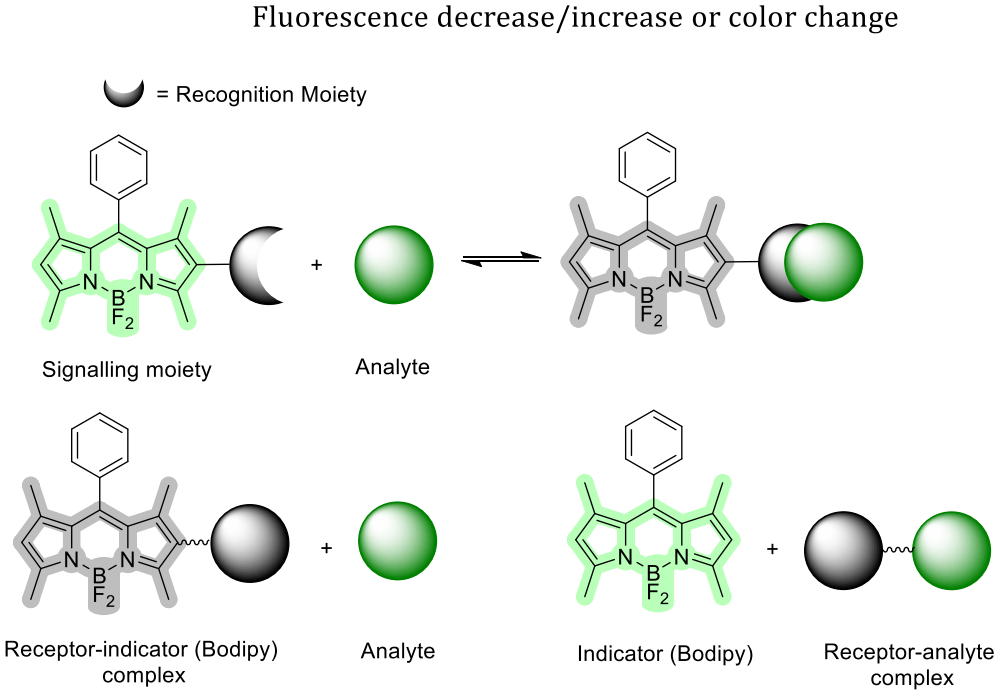

Scheme 5 Representation of indicator displacement assay.[8]

Among numerous fluorophores, Bodipy dye became popular in the application and development of such fluorescence probe systems due to the combination of excellent versatility of photophysical properties and high capability of dipyrromethene core (pre-)postfunctionalization providing a variety of attached mono- or multidentate coordinating groups.[12,75]

In 2022 Ji and coworkers reported the synthesis and application of fluorescence "turn-on" sensor for detecting different heavy metal ions based on the PET quenching mechanism of Bodipy fluorophore (Figure 20).[76] Modification of the Bodipy-core by incorporation of bis(pyridin-2-ylmethyl)-amine **27** provided strong sensitivity and selectivity in recognition of Pb^{2+}, Cr^{3+}, Zn^{2+}, Hg^{2+}, Cd^{2+} and Ba^{2+} cations with an increase "turn-on" of green fluorescence emission.

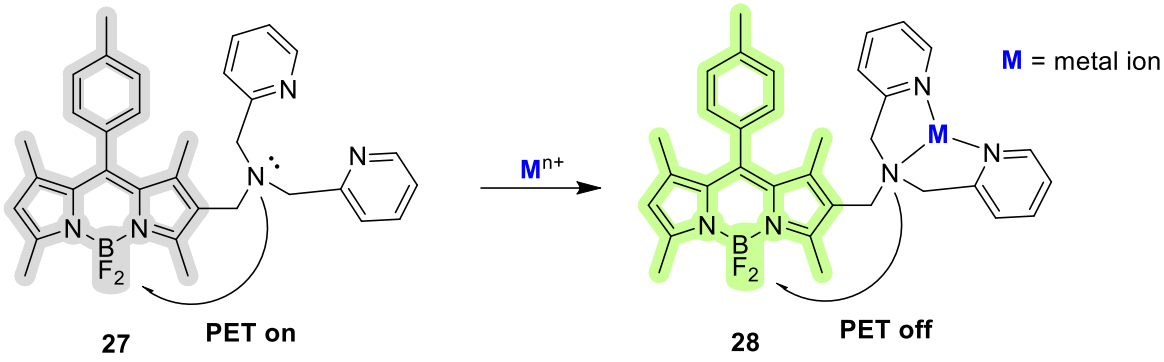

Figure 20 Metal ions induced emission "off–on" probe by Ji *et al*.

It was reported that electron-rich substituents could donate electron density to the Bodipy unit at its excited state resulting in efficient radiationless transitions with quenching of fluorescence intensity *via* PET processes.[77] After the coordination of metals to the DPA unit of quenched Bodipy chromophore **27**, the fluorescence emission of the dye was recovered, resulting in **28** weakening of the electron-donating ability of the nitrogen atom and respective inhibition of PET. In general, the construction of PET chemosensors based on Bodipy with metal chelating ligands such as calix[4]arenes, crown-ethers, bipyridines, cavitands, cyclodextrins, *etc*., allows the development of a variety of sensors and switches.[12]

Förster resonance energy transfer-based probes and sensors became a novel approach for detecting or visualizing ions, small molecules, biomacromolecules, cellular components, and systems with numerous analytes.[78] One of the first examples of Bodipy application in FRET systems is selective detection in ppb (parts per billion) scale of Hg^{2+} ions and was reported by Zhang *et al*.[79] Molecular system was constructed based on the covalently connected Bodipy and rhodamine dyes and thiosemicarbazide unit providing a fluorescent donor-acceptor FRET pair **29** (Figure 21). The reaction of thiosemicarbazide **29** with Hg^{2+} results in cyclization and formation of 1,3,4-oxadiazole **30**, which leads to the open form of the rhodamine spirolactam subunit giving the "FRET-on" stage. At this state of the rhodamine **30** dye FRET occurs, exhibiting fluorescence emission at 589 nm (λ_{exc} = 488 nm), while at "FRET-off" system with non-activated acceptor displays only the fluorescence emission at 514 nm of the donor-Bodipy dye upon excitation (λ_{exc} = 488 nm). In this regard, real-time measurements of the systems upon the addition of Hg^{2+} induce apparent changes in the fluorescence intensity ratio between donor-Bodipy and acceptor-rhodamine subunits, which can be observed by the "naked eye." Such techniques find application in confocal laser scanning microscopy methods in living cells and have strong potential for further development in life science.

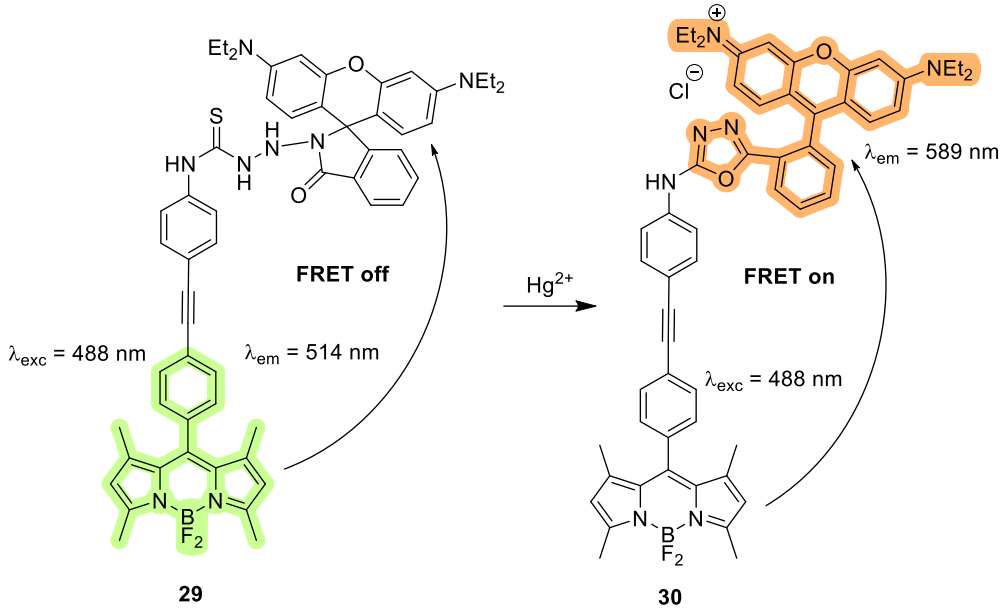

Figure 21 FRET pair formation after mercury induced ring-opening reaction.

Novel Eu^{3+} and Au^{3+} Bodipy-based transition metal complexes for the micromolar fluorogenic detection of V-type nerve agents were reported by Barba-Bon and coworkers.[80] The molecular structure of the developed chemosensor is based on the conjugated Bodipy dye with N-methyl-N-(2-hydroxyethyl)phenyl subunit as a coordination site and signalling unit that was previously applied in metal ion sensing by the same working group.[81] Moreover, fluorogenic probe **31** has an intense absorbance band at 600 nm and exhibited weak fluorescence (λ_{em} = 570 nm, Φ = < 0.001) due to the efficient ICT quenching of the Bodipy electronic excited state by electron-donating aniline subunit. Formation of **32**-Eu^{3+} and **32**-Au^{3+}, metal complexes inhibit ICT quenching efficiency of non-emissive Bodipy-chelating ligand **31** and lead to hypsochromic shifts of the absorbance band (λ_{abs} = 553 nm) with a strong increase of the fluorescence quantum yield of both complexes (Φ (**32**-Eu^{3+}) = 0.22, Φ (**32**-Au^{3+}) = 0.28). Displacement of the Bodipy ligand was observed upon addition of demeton-S to both fluorophore-metal complexes **32**-Eu^{3+} and **32**-Au^{3+}, resulting significant decrease of the fluorescence emission at 572 nm and non-emissive Bodipy chromophore **31** (Figure 22). This transformation is easily detectible and shifts the color of the solution from pink to blue, which can be observed by "naked eye". Due to the specificity of mono and bidentate coordinative ligands to form stable complexes with V-nerve agents,[82] this working group provided novel fluorogenic dosimeters based on Eu^{3+} and Au^{3+} metal complexes for the selective detection warfare chemical.

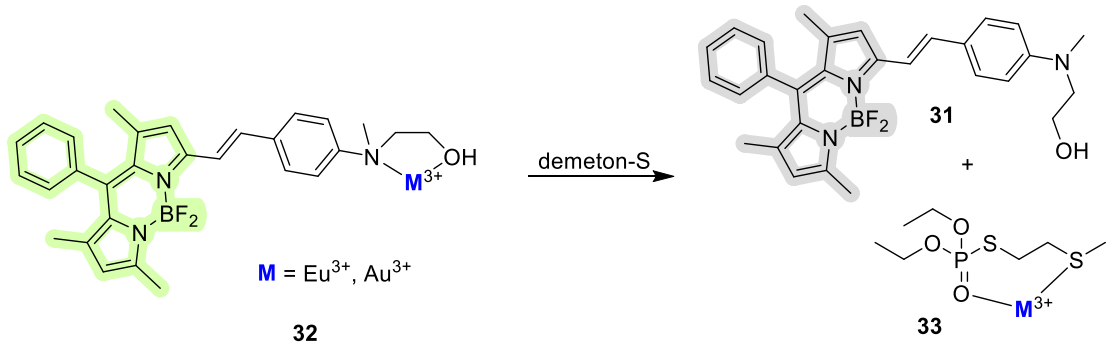

Figure 22 Demeton-S sensing approach by Barba-Bon *et al.*

N-heterocyclic carbenes (NHC) are a well-known type of ligand for the complexation with various transition metals and are widely used in organometallic chemistry.[83] NHC ligands provide strong σ-donor properties and result formation of the robust M-C_{NHC} metal-ligand bond with a strong covalent character.[84,85] In addition to the general stability of NHC transition-metal complexes,[84] this ligand offers versatility toward structural modification, which can be applied in developing novel fluorogenic metal complexes to detect different target analytes. Substantial contribution to the investigation of NHC-tagged Bodipy metal complexes in the field of molecular sensing was performed by Plenio *et al*.

In 2015 Kos and Plenio reported the synthesis of a Crabtree-type Ir(I) complex with connected Bodipy unit **35** for the fluorogenic detection of H_2 gas.[86,87] Fluorescent molecular probe for the detection of hydrogen was based on the PET-quenched Ir(I) complex **34** (Φ = 0.022), which upon reaction of oxidative addition H_2 resulted in the formation of the strong emitting Ir(III) complex **35** (Φ = 0.51) (Figure 23). This observation can be explained by the formal increase in the oxidation state of iridium (from Ir^{1+} to Ir^{3+}) and the corresponding reduction of the electronic density on the metal center after the addition of hydrogen, leading to inhibited efficiency of acceptor-PET quenching. Simple impregnation of the paper strip with a solution of Ir(I) complex provides the ability to detect hydrogen under low concentration.

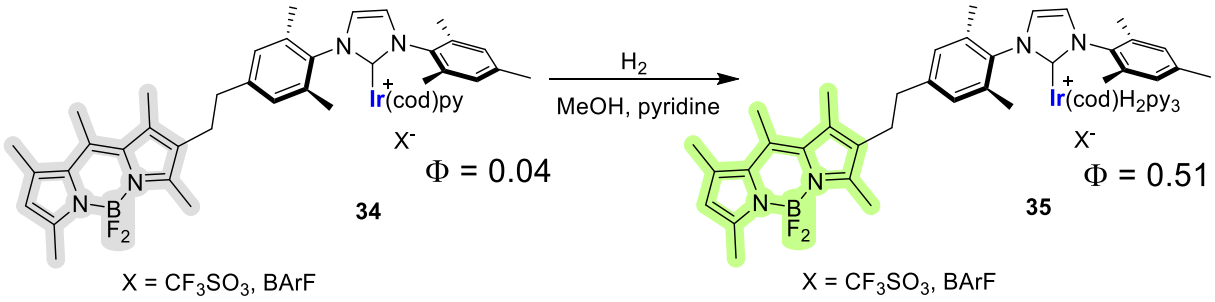

Figure 23 Fluorescence chemosensor for H_2 detection.

The authors also have published studies about similar fluorescent molecular probes for carbon monoxide detection.[86] Like in the previous example, Bodipy-moiety was covalently connected to the NHC complexes **36** (M = Rh, Ir; X = Cl, I), which exhibit low fluorescence emission (Φ = 0.008 – 0.016) due to the significant contribution of the acceptor-PET quenching mechanism. Both weakly fluorescent Bodipy-tagged iridium and rhodium cyclooctadiene complexes were converted to the highly emitting fluorescence complexes **37** (M = Rh, Ir; X = Cl, I) (Φ = 0.53–0.70) after reaction with carbon monoxide. The consequence of such transformation appears to be an outcome of the decreased electron density on the metal centers of the carbonyl complexes. The absence of major differences in fluorescence quantum yield of the chloro and iodo cyclooctadiene complexes suggests that the quenching contribution was mainly done by PET without involvement of intersystem crossing mechanism. Change of electronic density on the metal center through the ligand exchange reaction was estimated by cyclic voltammetry measurements of corresponding complexes ([(**36**)RhI(cod)] $E_{1/2}$ = 0.84 V; [(**37**)RhI$(CO)_2$] $E_{ox}(Ir^{I/II})$ = 1.39 V) where redox potential provides evidence of electron-deficient nature of the metals in the carbonyl complexes which inhibits efficiency of acceptor-PET.

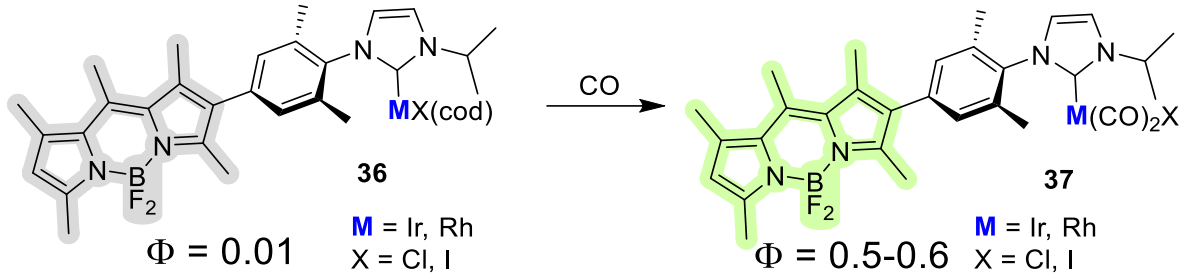

Figure 24 Fluorescence chemosensor for CO detection.

Regardless of the complexity in the development of such systems, highly sensitive Bodipy-based chemosensors can be applied to detect transition metals and combine the advantages of versatile chemistry of different transition metals in Bodipy-tagged complexes toward the development of diverse types of luminescent detectors.

1.4.2. Triplet photosensitizers

Triplet photosensitizers (PS) are molecules that form a triplet excited state after photon absorbance (photoexcitation) and usually can be characterized by strong light harvesting ability, high intersystem crossing yield and long-lifetime of the triplet state.[88–90] All PS share a general concept of photoinduced triplet energy or electron transfer mainly through the intramolecular processes and found broad application in areas such as photocatalysis[91], photodynamic therapy (PDT)[88], photovoltaics[92], photon upconversion[93], *etc*. The applicability of these compounds is generally based on the ability to undergo ISC, which includes heavy atom effect, charge recombination, exciton coupling, spin converters and radical-enhanced ISC.[89,90] In this respect, it is crucial to find a suitable fluorophore that can be easily used for the development of a variety of triplet photosensitizers with a desired application. The combination of organic chromophores with transition metal complexes is a common approach to obtain efficient photosensitizers. The typically low molar absorption coefficients of the metal complexes are enhanced by the attachment of a light-harvesting fluorophore, such as Bodipy, due to its appealing photophysical and chemical properties.[88,89] However, general strategies for designing efficient photosensitizers remain challenging and predicting ISC properties might be elusive from the organic chemist (or molecular structure) point of view.

Photodynamic therapy is a non-invasive photo-treatment of cancerous diseases using three key components: photosensitizing materials, visible or near-infrared radiation and molecular oxygen that generates various reactive oxygen species (ROS) leading to the cytotoxic damage of the unwanted cells and tissues. The process of generation of ROS species is illustrated in the modified Jablonski diagram (Figure 25).[94] Here, photosensitizer generates a singlet electronic excited state PS_1 upon absorbance of the light with appropriate wavelength and then undergoes intersystem crossing where the spin of the excited electron is inverted, forming a triplet excited state PS_3. The long lifetime of the triplet state is an important parameter for efficient therapy implementation, as the photosensitizer is more likely to encounter another molecule during its excited state, resulting in more efficient ROS generation.[95]

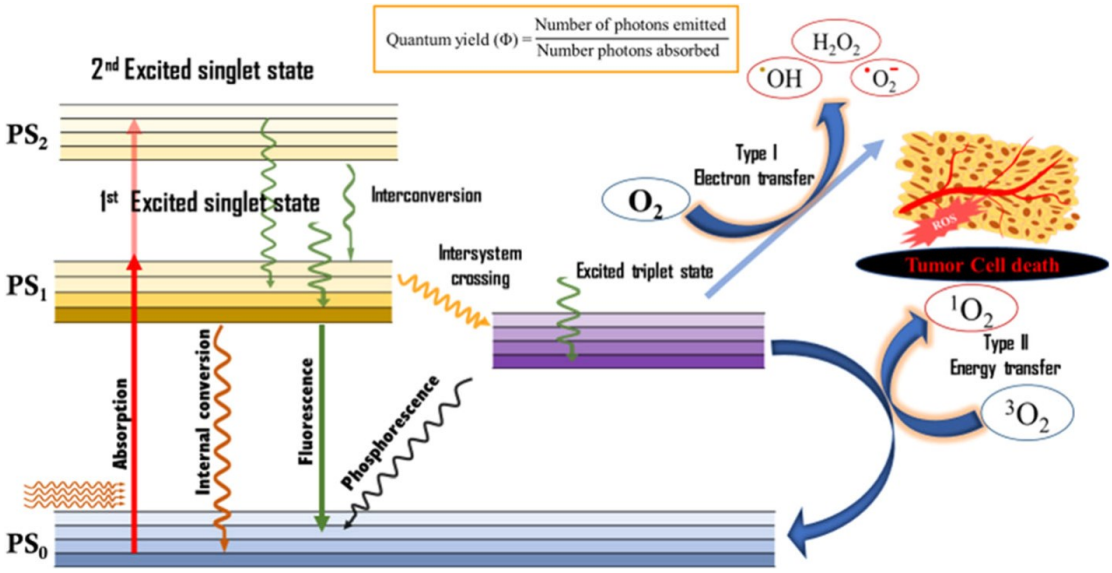

Figure 25 Jablonski diagram for the representation of principle generation of ROS by photosensitizer. Figure was adapted according to the reference R. Baskaran, J. Lee, S.-G. Yang, *Biomater. Res*. **2018**, *22*, 25.[94]

The non-modified Bodipy molecule typically lacks significant triplet-populated electronic states. However, it can be modified to become an effective photosensitizer for PDT by introducing heavy atoms to the boron dipyrromethene structure such as bromine, iodine, and transition metals.[90,96] Another heavy atom free approach[53] is the formation of orthogonal Bodipy dimers.[90,97] Bodipy-based metal-organic frameworks[98] and nanoparticles[99] are also applicable options for modification.

Hybrid metal-organic complexes with Bodipy chromophores are very good systems for application in photodynamic therapy. Yuksel *et al*.[100] have developed new Bodipy-based Ru(II) **38** and Ir (III) **39** complexes for therapeutical use to cure such diseases as myeloid leukaemia and cervical cancer (Figure 26). Structure of the novel photosensitizer is based on the substituted 4,7-phenanthroline metal complex and red-emitting styryl Bodipy (579 – 629 nm), providing applicable for the PDT range of the wavelength and high molar extinction coefficients. Ru-**38**, in comparison to Ir-**39**, has shown higher efficiency of the singlet oxygen generation and *in vivo* activity leading to cell death. Interestingly, the addition of ruthenium to the structure provides a more substantial spin-orbit coupling rate than adding iridium and correspondingly leads to a more favorable formation triplet excited state and singlet oxygen quantum yield. These results highlight a difficulty in the correlation of molecular structure and intersystem crossing, even when iridium (III) complexes are usually considered efficient triplet photosensitizers.[101] Despite the low rate of singlet oxygen generation (0.6%) for Ir-**39** in contrast to Ru-**38** (20%), both novel photosensitizers resulted in cell death without observing typical dark toxicity for the transition metal-based PS.

Another example of the highly effective Ru(II)-Bodipy bioconjugate material for PDT was presented by Chao *et al*.[102] Similarly to the previous example, distyryl-Bodipy structure was π-conjugated at 8-position with 2,2´-bipyridine and reacted with $Ru(bpy)_2Cl_2$ providing the desired complex **40** (Figure 27). Material **40** has absorbance at the red/NIR region with the corresponding peak at 652 nm, high molar absorbance coefficient ($\varepsilon = 1.2 \times 10^5$ M^{-1} cm^{-1}), high singlet oxygen quantum yield (77%), good stability in aqueous solutions and cellular uptake making this material suitable for

biological applications. This compound has shown good *in vitro* tests in photosensitizing efficiency to inhibit the ability of malignant melanoma cells to grow.

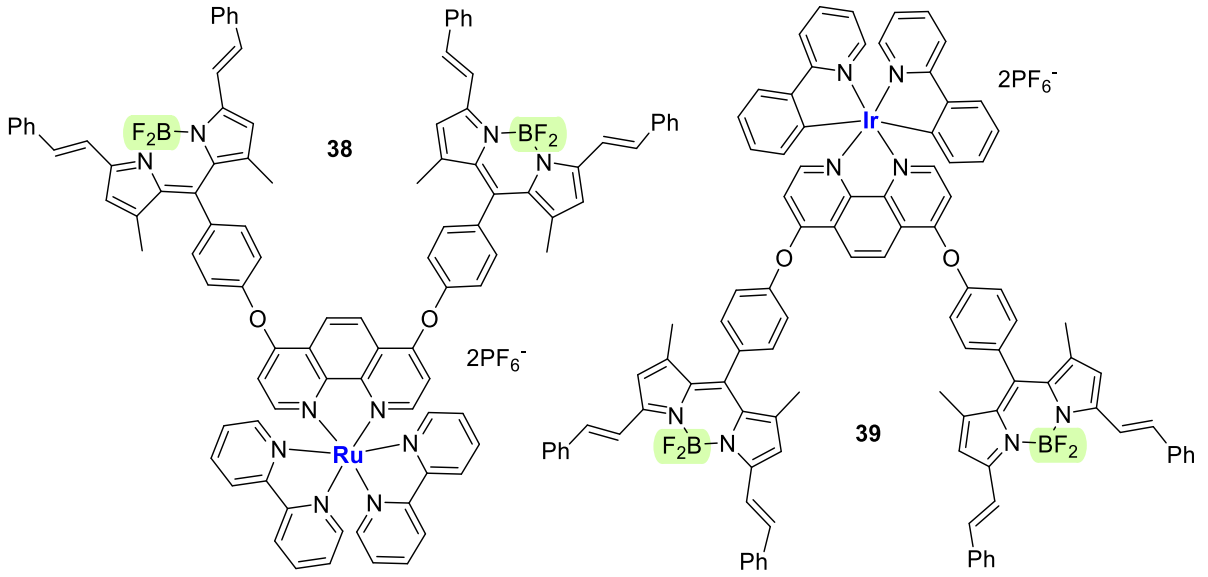

Figure 26 Hybrid metal-organic theranostic reagents Ru-**38** and Ir-**39** with attached Bodipy chromophores.

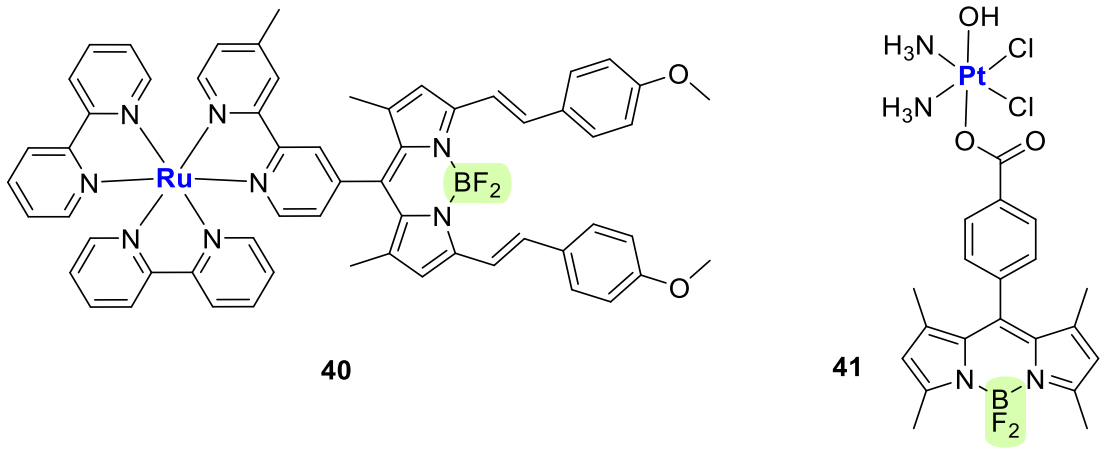

Figure 27 New ruthenium **40** and platinum-based **41** photosensitizers.

Platinum-based anticancer materials represent broad applications and importance in the current treatment of cancer diseases.[103] Chakravarty and coworkers[104] provided a new cisplatin-derivative of platinum(IV)-Bodipy **41** (Figure 27) with fascinating phototherapeutic activity for the various cancer cells using green light and negligible dark toxicity. This complex shows strong absorbance at 500 nm and fluorescence emission at 515 nm ($\varepsilon = 4.34 \times 10^4$ M^{-1} cm^{-1}), high fluorescence quantum yield (64%), and descent singlet oxygen quantum yield (29%) making this compound suitable for the cellular localization study. **41** is an excellent example of a combination of photo-induced cytotoxicity against human breast cancer and the availability of confocal imagining for tracing platinum content that provides additional interest for designing and applying platinum-based organic photosensitizers.

Based on the extensive works for Ir(III) triplet photosensitizers containing Bodipy moiety Ortiz and co-workers[105] have developed efficient PDT-imagining agents based on biscyclometalated Ir(III) complexes with attached ancillary Bodipy ligands through

acetylacetonate (acac) **42**, **43** and bipyridine-based unit for **44** at the *meso*-position (Figure 28). Both **42** and **43** complexes provide high molar absorbance coefficients (ε = 4.46 × 10^4 M^{-1} cm^{-1} and 3.38 × 10^4 M^{-1} cm^{-1} respectively) and singlet oxygen quantum yields 86% and 59%, respectively. Attachment of thienyl groups at 2 and 6 positions of the Bodipy core Ir-2 provides important for therapeutic window fluorescence and absorbance red-shift (λ_{abs} = 594 nm, λ_{em} = 652 nm). However, **44** complex shows strong absorbance only at UV region and lacks the ability to generate $^1O_2$ efficiently under visible light (only 51% under UV light), which does not make this material well-suitable for PDT. In vitro photodynamic therapy studies have shown high efficiency of **42** and **43** against cancerous HeLa cells, performing low dark and strong phototoxicity at low PS concentrations within a cell.

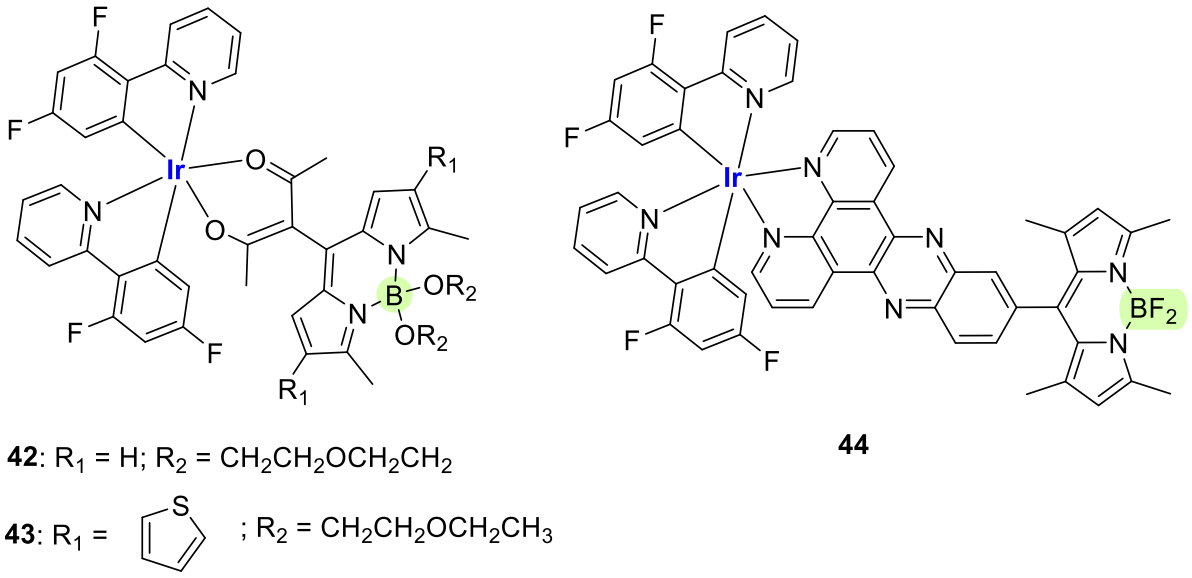

42: R_1 = H; R_2 = $CH_2CH_2OCH_2CH_2$

43: R_1 = ; R_2 = $CH_2CH_2OCH_2CH_3$

44

Figure 28 Iridium(III)-Bodipy photosensitizers for the PDT application reported by Ortiz and coworkers.

An example of Bodipy scaffold combination with gold transition-metal complex in the application in PDT was performed by Emrullahoglu *et al.*[106] Simple synthesis of acetylene-Bodipy derivative **46** and following complexation with AuCl(PPh_3) provides an alternative efficient photosensitizer **47** (Figure 29) which undergoes photophysical transformation such as a drop in the fluorescence quantum yield (from 58% to 6%) and increases the yield of singlet oxygen generation up to 84% in comparison to starting acetylene-Bodipy derivative **46**.

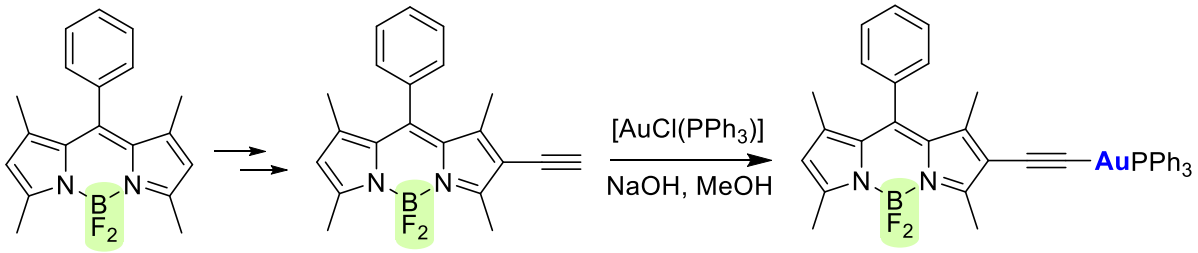

45 **46** **47**

Figure 29 Highly cytotoxic novel Bodipy-tagged gold acetylide photosensitizer.

Activity of this compound was investigated against A549 cells by using MTT assay providing high cytotoxic efficiency (EC_{50} = 2.5 nM) during green light irradiation and maintaining the cell line with low dark toxicity.

Provided examples of the combined Bodipy scaffold with transition-metal based ligands highlight the importance of the further investigation and development of novel photosensitizers for the application of photodynamic therapy.

Photocatalysis has become widely popular in the past decade, offering various synthetic modifications under mild conditions to chemists using redox[107] and energy transfer catalysis[91,108]. Numerous transition-metal based complexes like Ir[109], Ru[110], Fe[111], Cr[112], Co[113] play crucial roles in such photoinduced transformations due to the ability of efficient singlet-electron transfer and energy transfer processes. In recent years, modified Bodipy photosensitizers have turned out to be also an attractive photoorganocatalyst for different chemical transformations and further modulations of Bodipy scaffold are expected to bring promising results in photocatalysis.[54,89,114]

The combination of transition metal complexes and photocatalysts is a modern approach to discover new reactivities and investigate the potential of dual catalytic systems. In general, chemistry of transition metal-photocatalyst is well-established and efficiently used for various synthetic transformations. However, reported strategies rely mainly on combinations of individual catalysts which are usually not combined into one molecular structure.[115] Messerle *et al*. have established several Bodipy-based transition metal complex systems for dual catalysis applications.[116–118] They reported the synthesis of tethered Pd-Bodipy type of catalyst **48** which resulted in high performance palladium-catalyzed Suzuki-Miayura cross-coupling reaction and increased photocatalytic activity of thioanisole oxidation in comparison to the standard unsubstituted Bodipy fluorophore (Figure 30). Substitution of the Bodipy core with $Pd(PPh_3)_2I$ moiety leads to the bathochromic shift in the absorbance and emission bands, long-lived triplet state formation with high phosphorescence life-time (2037 μs) and effective singlet oxygen generation quantum yield 64% against 1.1% in comparison to the unsubstituted Bodipy molecule. Such combination of Bodipy-based palladium catalyst and photosensitizer allows performing sequential photocatalytic oxidation−cross-coupling reaction avoiding application of mixture individual catalysts.

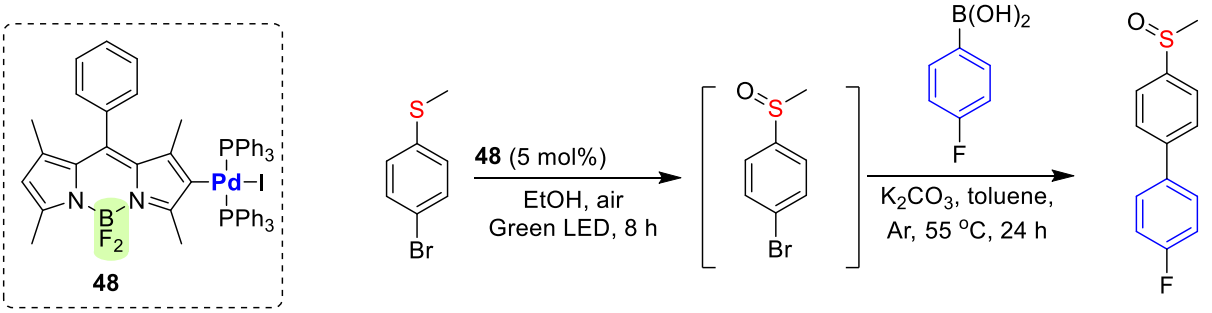

Figure 30 Pd-Bodipy tethered dual catalyst reported by Messerle *et al.*

In another work, this group synthesized different tethered Ir(I) complexes **49-51** with Bodipy scaffold (Figure 31).[117] Similarly to the previous approach, bifunctional catalyst was modified through classical functionalization of Bodipy core through the attachment of bis(pyrazole)methane ligand with the following complexation using $[Ir(cod)Cl]_2$ metal precursor and formation of cationic derivatives after addition of NaBArF. Catalyst **49** has provided the highest value of singlet oxygen quantum yield in the corresponding group of compounds, probably, due to the covalent attachment of Ir(I) to the chromophore unit providing stronger intersystem crossing. Synthesized complexes

were probed in photocatalytic oxidation reaction of benzylamine or thioanisole and iridium-catalyzed dihydroalkoxylation where complex **49** performed reaction of photooxidation more efficiently in comparison to other compounds.

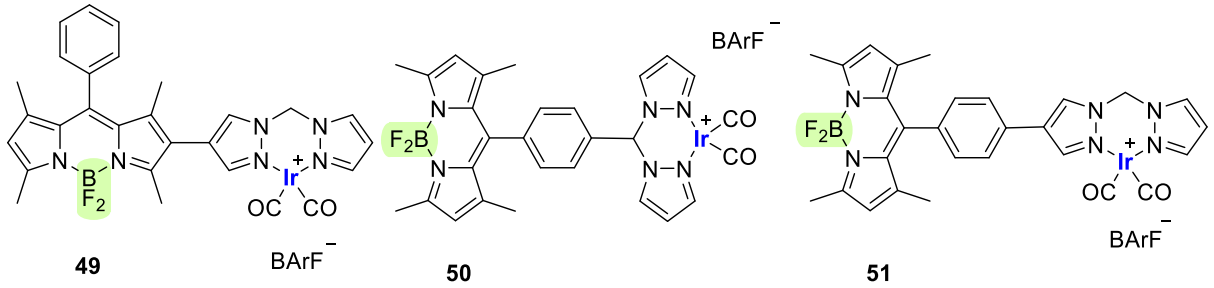

Figure 31 Various dual-catalyst systems based on Bodipy and iridium metal complex.

More importantly, dual catalytic system was tested for hydroamination-oxidation response with sequential transformation to the corresponding lactam (Scheme 6). These results represented a novel tethered photo-transition metal dual catalyst approach in studying and investigating cooperative chemical reactivity.

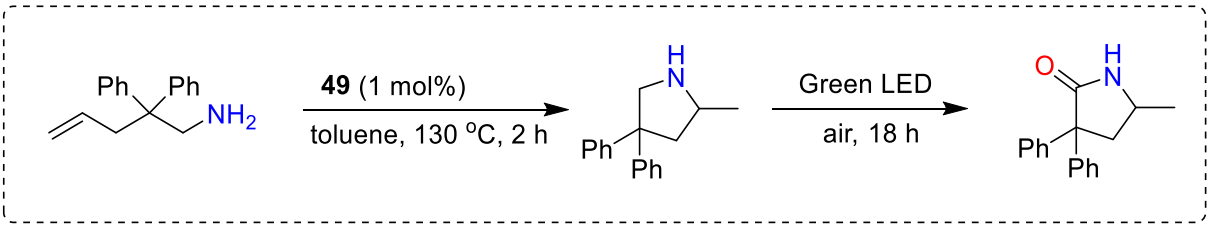

Scheme 6 Sequential hydroamination – photooxidation reaction for the lactam production

He and coworkers reported palladium(II)-Bodipy complex **52** for the application in the photoredox Sonogashira cross-coupling reactions.[119] The structure of the photocatalyst was based on the core of dichloro(1,10-phenanthroline)palladium(II) complex with attached Bodipy fluorophore and completely quenched fluorescence, indicating a high yield of the triplet state. It was observed that the performance of dichloro(1,10-phenanthroline)palladium(II) complex **53**, as a catalyst for the reaction between iodobenzene and phenylacetylene, after 24 h at room temperature was much lower than for the Bodipy-metal complex **52** (17% and 92%, respectively). Interestingly, even simple addition of a catalytic amount of non-modified Bodipy dye **54** into the reaction mixture boosted the catalytic activity of the system without a direct connection of Bodipy unit to phentanthroline complex. In this work, researchers suggested that such high catalytic performance is likely based on the photoinduced energy transfer mechanism, which enables efficient reductive elimination.

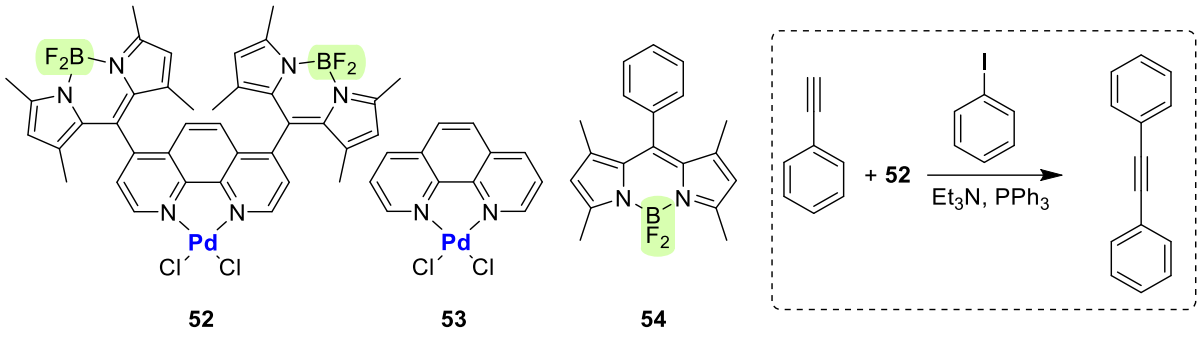

Figure 32 Bodipy-functionalized Pd(II) photoredox catalyst for Sonogashira C–C cross-coupling reactions.

Alternatively to the costly noble metal complexes version, earth-abundant copper-based photosensitizer was established in 2020 by Guo *et al.*[120] using connected Bodipy core to the copper (I) phenanthroline complexes **55** and **56** (Figure 33). Novel complex **56** has provided high aerobic photooxidation activity of formation phenols from the boronic acids under LED light and outperformed in this aspect $Ru(bpy)_3^{2+}$ and $Ir(ppy)_3^{+}$ noble metal complexes. The reaction mechanism involves the formation of singlet oxygen and superoxide anion radicals which play a central role in the oxidation of aromatic boronic acids. Transient absorbance and DFT investigations have provided information about through-bond energy transfer (TBET) and triplet-triplet energy transfer (TTET) mechanisms that facilitate Bodipy triplet excited state formation. Synthesized complex showed high molar absorbance coefficients of 1.62×10^5 M^{-1} cm^{-1} at 518 nm with singlet oxygen quantum yield value of 85%.

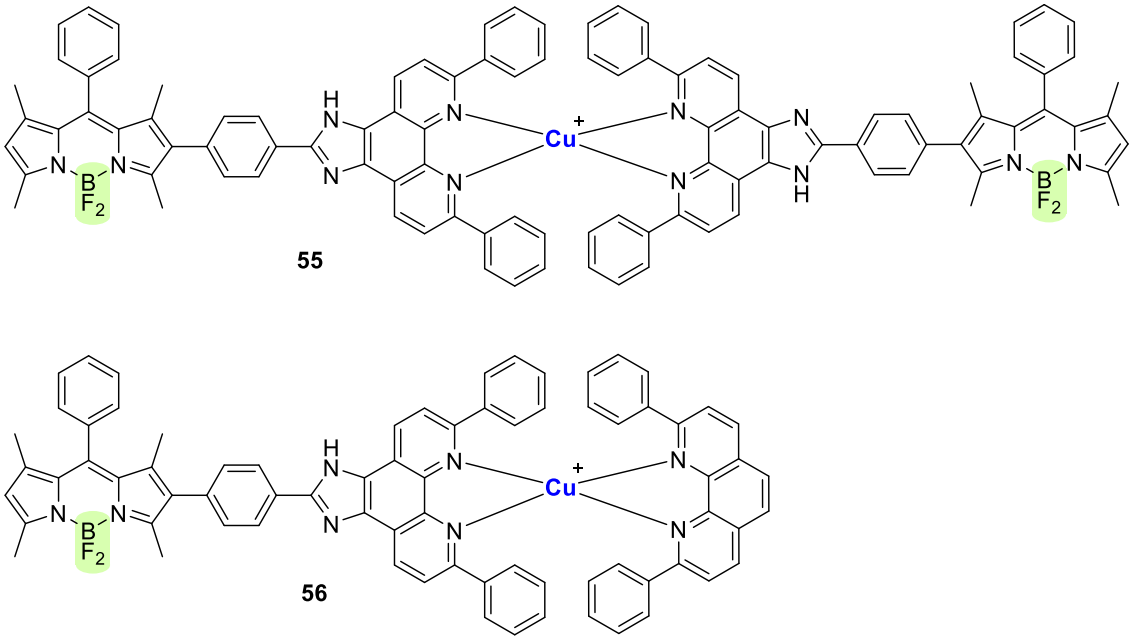

Figure 33 Earth-abundant Bodipy photosensitizers reported by Zhang *et al.*

Another application of copper-based trinuclear photosensitizer scaffold was presented by Li and coworkers (Figure 33).[121] Complex **57** was synthesized using Bodipy-pyrazolyl core structure in contrast to typical cuprous photosensitizers based on phenanthroline ligands or bisphosphine ligands. This compound demonstrated efficient intersystem crossing with formation of a long-living triplet state allowing generation of reactive oxygen species under visible-light irradiation. Complex **57** was successfully

applied in photoinduced oxidation reaction of phenylboronic acids and aromatic sulfides. Studies of such copper-based metal-organic photosensitizers allow researchers to alternatively extend the range of promising materials to expensive noble metal derivatives.

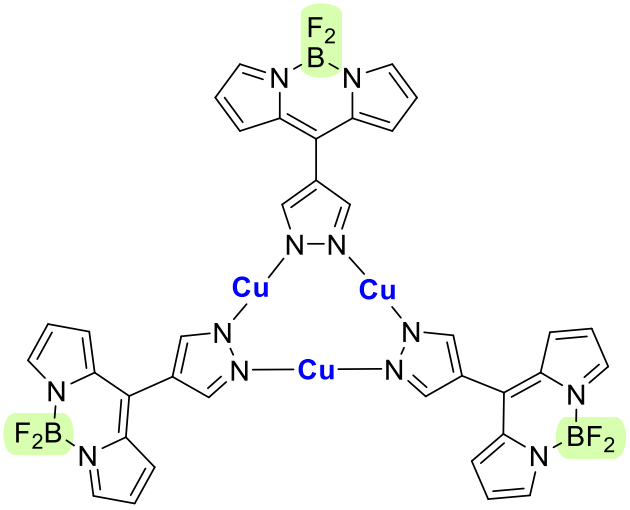

57

Figure 34 Copper-based trinuclear photosensitizer reported by Li and coworkers.

1.5. Application of fluorophores in catalytic experiments

Understanding the mechanisms of chemical transformations catalyzed by organometallic systems is essential for developing sustainable catalytic processes. However, the complexity of these reactions often makes it challenging to describe them mechanistically using traditional analytical tools. Direct observation of intermediate formation is often not possible, which leads to missing information about the competing pathways in the catalytic cycle. Therefore, to better interpret catalysis, it is necessary to isolate and analyze intermediate compounds using different analytical methods, which may not always be possible due to the sensitivity and instability of the studied materials. These challenges narrow the practical setup of a unified analytical approach for mechanistic characterization experiments and are often limited to the investigation of individual catalytic systems.[122]

Recently, fluorescence spectroscopy has emerged as an alternative technique for mechanistic studies of catalytic processes due to its non-invasive nature, high sensitivity, and the ability to observe intermediate formation in real-time. The design of such fluorescence-based mechanistic probes must follow specific requirements to avoid false signals and information. Synthetic chemists must evaluate all potential participants of the chemical reaction and build the system accordingly to account for all interfering parameters for accurate probe design. The development of fluorescent probing/sensing can be divided into two main categories: "participant" and "observer". In the participant approach, the system is designed such that the chemical reaction occurs directly on the designed fluorophore probe, resulting in changes in fluorescence signal due to the nature of various photochemical and photophysical interactions. The observer approach is based on the remote location of the fluorophore, which avoids direct interaction with the catalytic center and provides information about processes in the location of interest.[7]

In line with the aforementioned perspective, Bodipy fluorophore is an excellent candidate for the design of fluorophore probes due to the great potential of core

functionalization, tunable photophysical characteristics and lack of potentially invasive functional groups that may coordinate to the metal center of transition-metal based catalytic complexes. Over the years, new conjugated ligands for organometallic chemistry with Bodipy were established and transition metal-based complexes were developed. In this research field, a significant contribution to the study of transition metal complexes using fluorescence spectroscopy was made by the working group of Herbert Plenio. In such systems, photophysical properties of the fluorophore can be modified *via* chemical reactions and electronic interactions with the coordination sphere of the transition metal center. Ligand-exchange response in fluorophore-labelled transition-metal complexes can help monitor characteristic changes in the formation of catalytically active species during cross-coupling reactions and on the initiation of olefin metathesis catalyst.[123]

The first representative work on fluorophore-tagged transition-metal complexes was done by Sashuk and Plenio in 2009.[123] They synthesized dansyl fluorophore tagged [(NHC)Pd(allyl)Cl] complex **58** where fluorescence intensity was monitored with the course of Suzuki cross-coupling reaction between 3-trifluoromethyl-iodobenzene and phenyl boronic acid (Figure 35).

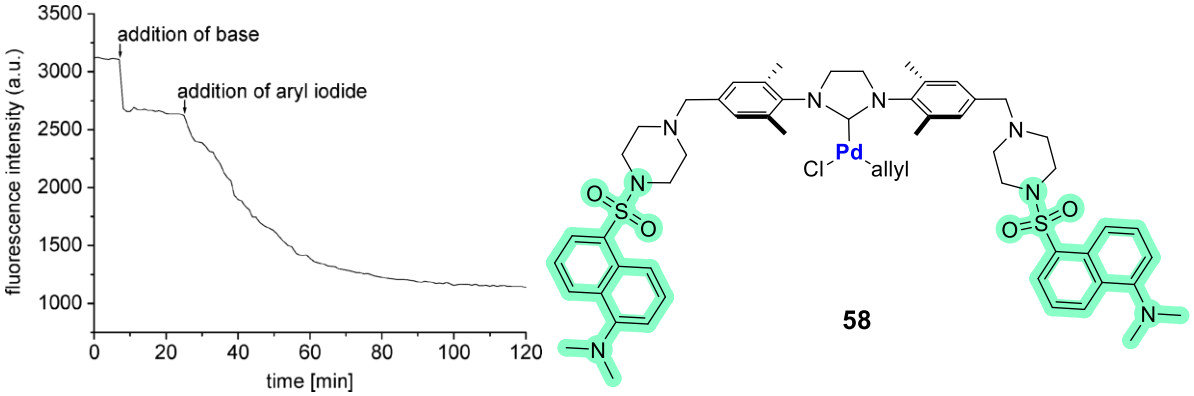

Figure 35 Fluorescence monitored Suzuki coupling reaction using dansyl fluorophore tagged complex **58**.

During the catalytic transformation, the fluorescence signal at 532 nm was observed. The fluorescence intensity of a mixture of palladium(II) precatalyst **58** and phenylboronic acid remains stable until the addition of KO*t*Bu, which leads to the formation of catalytically active palladium(0) species and an immediate drop in fluorescence intensity. The addition of the aryl halide substrate resulted in much more pronounced fluorescence intensity decay, which correlated with the GC conversion-time curve of the Suzuki coupling reaction (Figure 35). In the presented system, heavy atom quenching effect of iodide is found to be responsible for the strong decay of fluorescence emission during the coupling of 3-trifluoromethyl-iodobenzene. For control experiment of iodine quenching effect, stoichiometric amounts of KI were added to the reaction mixture and a drop of fluorescence was observed. It was shown that detecting even small concentrations (ca. $2 \cdot 10^{-7}$ mol/L) is possible where firmly attached dansyl group to NHC ligand experiences characteristic fluorescence changes on formation of the catalytically active species during the actual cross-coupling reaction.

In 2010 Plenio and Vorfalt reported study on the fluorogenic initiation of olefin metathesis reaction using Hoveyda-type precatalyst with fluorophore-tagged benzylidene ether ligand.[124] Initially, the fluorescence intensity of precatalyst **59** was tested in a toluene solution in absence of RCM substrate, and showed only low fluorescence signal. The addition of ethyl vinyl ether to the reaction mixture initiated RCM

reaction and fluorescence emission strongly increased (Figure 36). The subsequent formation of metallacyclobutane intermediate led to the dissociation of the dansyl-tagged styrene ligand **60** from the fluorescence quenching ruthenium center and resulted in a corresponding increase of the fluorescence signal. In conclusion, the reported studies have generated research interest in developing and investigating new catalytically active systems using fluorophore-tagged transition metal complexes.

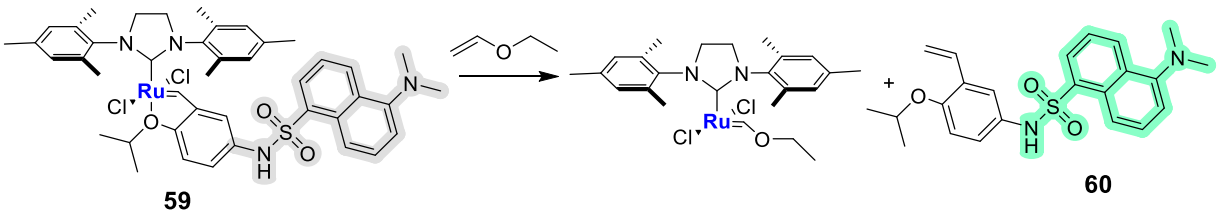

Figure 36 Fluorogenic initiation of the RCM reaction with ethyl vinyl ether.

The research group of Suzanne Blum utilized Bodipy dye in the investigation of organometallic systems using single molecule fluorescence microscopy (SMFM), a technique previously used to gain insight into numerous biological systems[125] and individual copper chelate complexes[126]. Through the use of SMFM, Blum's group was able to study a range of organometallic transformations, including single ligand exchange for molecular complexes,[127] Ru polymerization reactions,[128,129] formation of organometallic intermediate in LiCl/organozinc systems[130], *etc.* [7,131]

The initial focus of their work was on incorporating palladium(II)-Bodipy tagged metal complex **61** through covalent bonding to the hydroxyl groups presented on the glass surface (Figure 37), leading to the formation of material **62**. This study initiated research interest in application of SMFM methodology to directly observe of fluorophore-tagged metal complexes at the single molecular level outside the scope of typical biological applications.

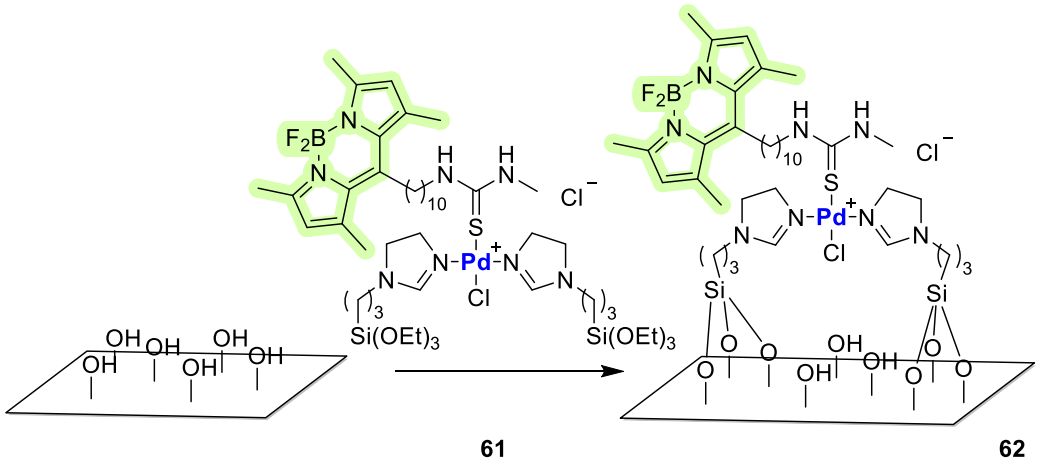

Figure 37 First reported example of Bodipy-tagged metal complexes for SMFM-based investigations by Blum and coworkers.

In the subsequent study using the same SMFM technique, they could obtain information about platinum ligand exchange reaction under real-time conditions on the modified glass surface with N,N′-[3-(triethoxysilyl)propyl]thiourea.[127] Since the fluorophore does not undergo chemical modification during reaction, its characteristic fluorescence signal remained unchanged. Using total internal reflection fluorescence microscopy (TIRF) they could observe consequence of formation surface immobilized

platinum-sulfur complex **64** resulted from the corresponding ligand exchange reaction of diethylenetriamine platinum-aqua based complex **63** (Figure 38). This method allowed determination of only molecules that bonded to the glass surface avoiding detection of the residual signal from unreacted fluorogenic material due to the fast rate of molecular diffusion in comparison to the imagining rate of TIRF.[132]

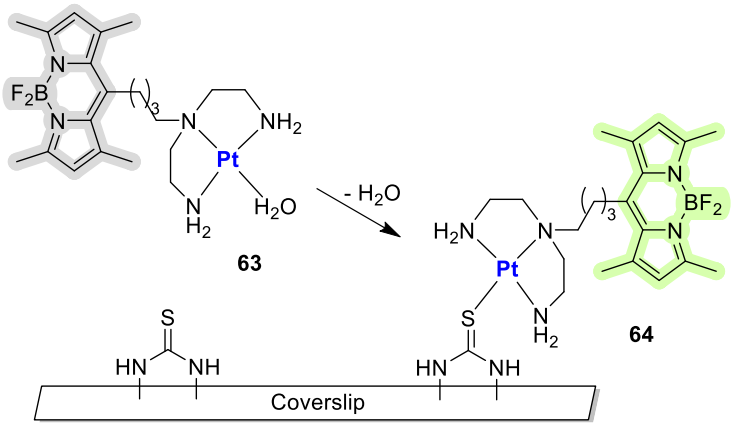

Figure 38 Fluorogenic platinum ligand-exchange reaction om the modified glass surface.

The next step of their mechanistic investigations was ring-opening polymerization reaction (ROMP) using signal-forming Bodipy-olefin fluorophore **65** and cyclopentadiene catalyzed ruthenium complex **66**. This research provided the first report of a fluorescence-based method for differentiation between homogeneous and heterogeneous metathesis polymerization catalysis, which could be helpful in understanding the nature of an active catalyst.[128] Using SMFM they observed surface polymerization reactivity and determined the formation of green polymers **67** in the solution rather than on the solid catalyst surface **66.** The absence of the formation of fluorogenic polymers on the catalyst surface was an indicator of homogeneous nature of catalytic process. Such results have followed further scientific development and similar imagining strategy was applied by Scaiano *et al*. for the characterization of copper-catalyzed click reaction on the surface of catalyst.[133]

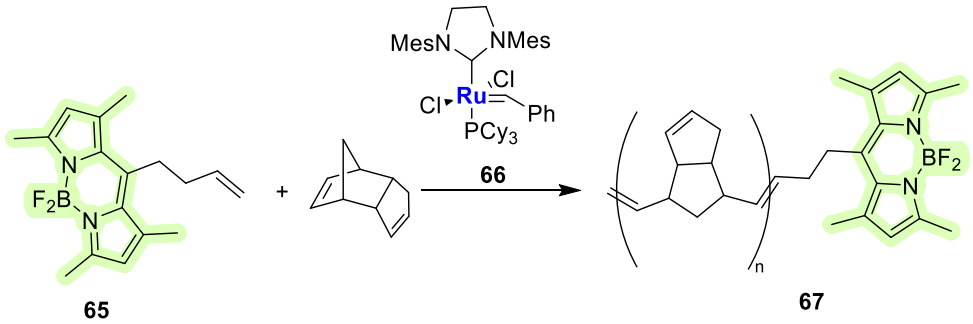

Figure 39 Studying ring-opening polymerization reaction using Bodipy-olefin fluorophore.

Surface-supported catalysts are very important in the development of sustainable recyclable catalytic systems. Interpretation of mechanisms and kinetics of various stages of catalytic transformations is not often oblivious to perform due to heterogeneity, lower reaction selectivity compared to homogeneous catalysis and existence of biphasic interaction in the surface-supported molecular catalysis. In 2016 working group of Goldsmith reported investigation of heterogeneous initiation kinetic mechanism for

PEPPSI type of palladium catalyst through SMFM approach (TIRF excitation mode similar to Blum *et al.*).[134,135] In this work, they synthesized PEPPSI type of palladium complex incorporated on the glass surface with attached to the metal center red-emitting Bodipy unit through pyridine ligand **68** (Figure 40). The choice of such exotic fluorophore was motivated by significant contraction of background signal from solvent Raman scattering, reduction of n-π* transition impurities and high fluorescence quantum yield compared to other red-fluorophores. Generally, for the PEPPSI type precatalyst, the pyridine ligand cleavage results in an active catalyst.[136] In this scenario, a bright red signal of complex **69** upon loss of pyridine unit leads to the disappearance of the fluorescence signal, indicating the process of active surface-supported catalyst formation. Correspondingly, initiation kinetic of individual complexes can be determined relatively to the kinetic of pyridine-fluorophore ligand loss *via* addition of base.

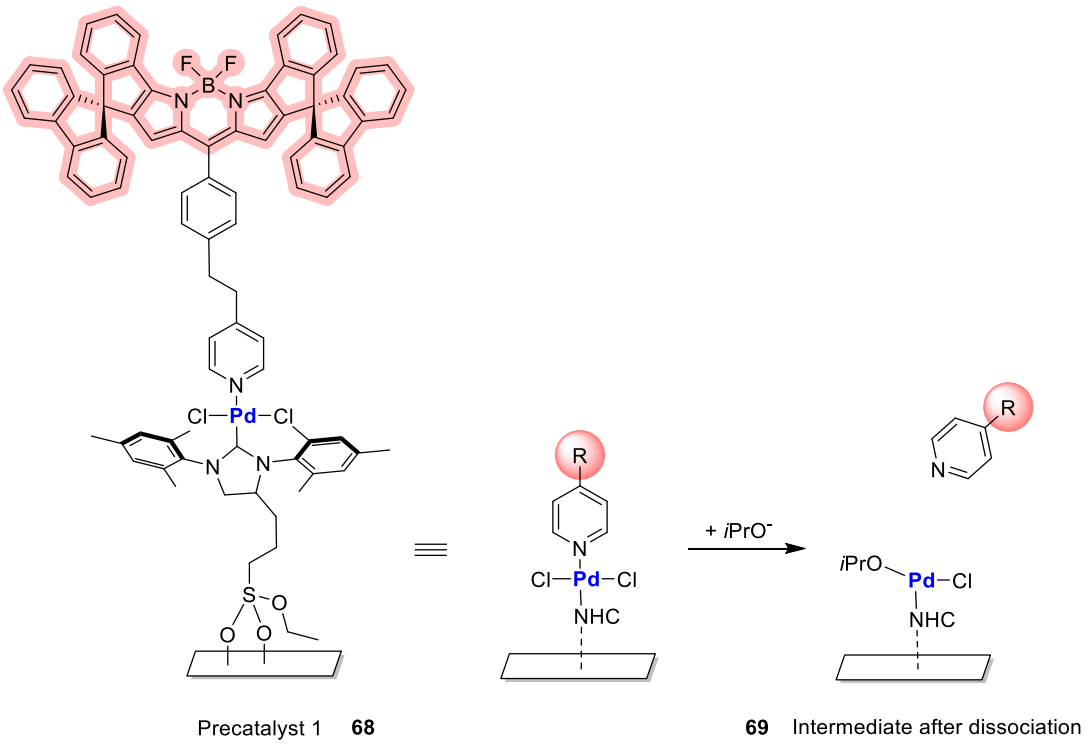

Precatalyst 1 **68** **69** Intermediate after dissociation

Figure 40 Initiation kinetic studies for PEPPSI type of palladium catalyst **68** reported by Goldsmith using SMFM approach.

Lin and Blum provided an interesting method to understand palladium-catalyzed intermediate formation during ligand exchange reaction using FRET-based fluorogenic system.[137] In this research, Bodipy dyes were chosen as a main signalling component for the formation of a two-fluorophore based FRET-pair during the exchange reaction on the palladium complex **73** (Figure 41). In this transformation, red allyl chloride Bodipy-derivative **70** played the role of substrate in oxidative addition to $Pd_2(dba)_3$ catalyst resulting formation of π-allylpalladium intermediate dimer **71** with a corresponding increase of the total fluorescence intensity under real-time measurements. In the next step, a simple addition of green Bodipy-tagged phosphine ligand **72** resulted in formation of the green-red palladium-phosphine FRET pair, which was observed and quantitively characterized *via* drop of the individual fluorescence of the donor **72** and the corresponding increase of the acceptor **70** fluorophore intensity in respect to reaction conversion. For instance, the standard analytical methods like NMR spectroscopy did not show detectable signals of intermediate formation for characterization, while

fluorescence-based methodology provided low concentration detection range low as $1 \cdot 10^{-6}$ M. Based on this data, such fluorescence technique can be suitable for mechanistic studies of catalyzed organometallic transformations which usually occur at very low concentrations in the reaction media.

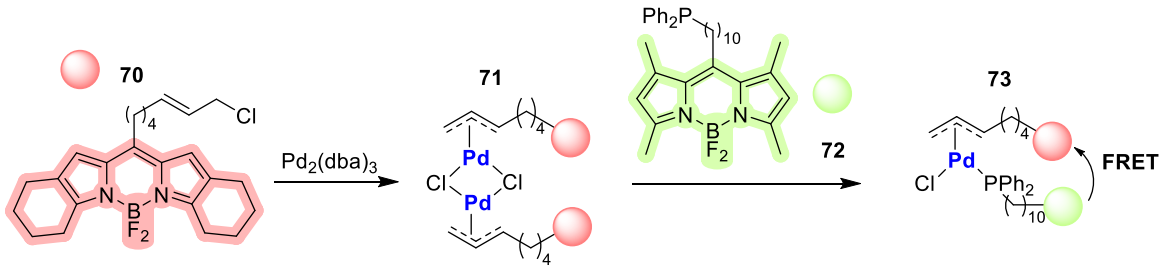

Figure 41 Formation of two-fluorophore based FRET-pair after the exchange reaction on the palladium complex reported by Blum *et al*.

Motivated by previous results from the investigation of transition metal complexes with attached fluorophores, Plenio and co-workers have systematically studied the modulation of fluorescence brightness in Bodipy-tagged N-heterocyclic carbene NHC-gold halide complexes.[138] Several highly fluorescent NHC-gold complexes were synthesized and studied in the substitution reaction of the halide ligand by 4-substituted aryl thiolates (Figure 42). Such ligand exchange reaction resulted in a decrease (up to 65-fold) of the fluorescence signal and appeared to have a significant dependence on the electronic nature of the thiols and the distance between the sulfur atom and the Bodipy moiety (up to 1.0 nm). Changes in the electronic density at the thiolate ligands through variation of substituents on the aryl ring allow modulation of the fluorescence brightness due to the photoinduced electron transfer quenching mechanism. DFT calculations suggested that the fluorescence quenching occurs predominantly by the a-PET mechanism, despite the presence of 5d transition metal and heavy atom halides. This work has established that Bodipy dyes are useful tools for determining the changes in electronic density for the transition metal complexes used in homogeneous catalysis.

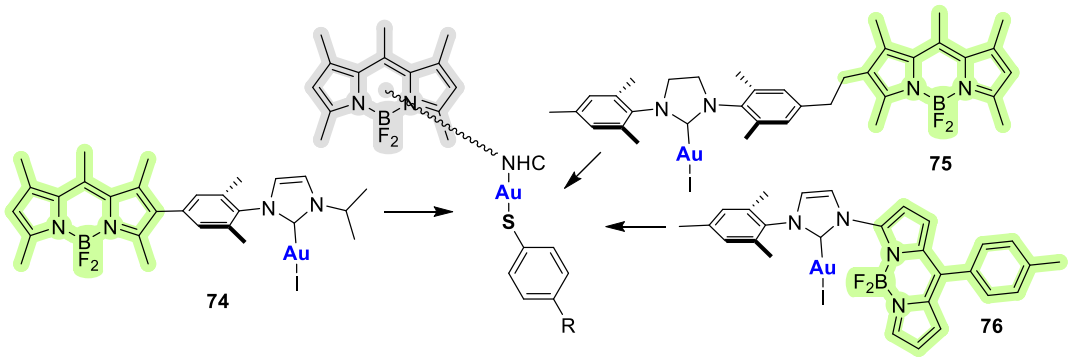

Figure 42 Reaction of Bodipy tagged [AuCl(NHC)] complexes with thiophenol to the respective [Au(SC_4H_6R)(NHC)] complexes.

In the following study, Vasiuta and Plenio reported the synthesis of Bodipy-tagged phosphine–gold complex for investigation of gold-catalyzed alkyne transformations and real-time monitoring of ligand substitution reactions on the metal center (Figure 43).[139] Novel Bodipy-gold complexes **77** and **78** were synthesized based on the aryl and cyclohexyl substituted-phosphine ligands which provided low fluorescence intensity (Φ = 0.087 and 0.096 respectively). The decrease of electron density at the gold-metal center

via chloride substitution by weakly coordinating anion (nonaflate) **79** resulted in the increase of the fluorescence quantum yield (Φ= 0.11).

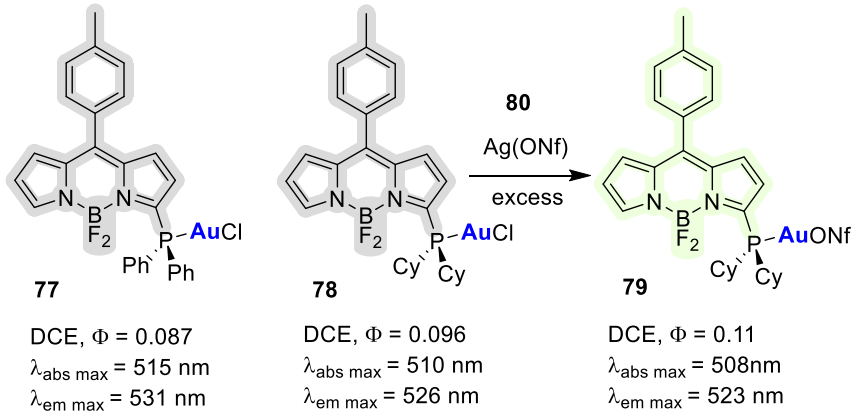

Figure 43 Application Bodipy-tagged phosphine–gold complex for catalytic investigations.

Similarly to the fluorogenic chlor-thiolate ligand exchange reaction of the Bodipy-NHC gold[86,87,138] complex, the replacement of chloride by stronger donating thiolate for BODIPY-tagged phosphine ligand leads to analogous inhibiting of the emission efficiency as in the previous example. This work presented high sensitivity to electronic changes at the metal center *via* chloride displacement by weakly coordinative anion. Real-time observation of increased fluorescence intensity indicates the generation of the catalytically active "cationic" gold complex, which plays a crucial role in the catalyzed alkyne transformations. Provided studies revealed new strategies for investigating transition metal-based complexes for understanding chemical transformation on the metal center applying fluorescence spectroscopy.

In 2019 Halter and Plenio studied ligand substitution reaction in the alternative catalytically active (cationic) metal complex systems based on the Bodipy-tagged diimine ligands. Activation of the palladium-diimine complex **81** with NaBArF, resulted in formation of the corresponding competent catalyst for ethylene polymerization **82** (Figure 44).

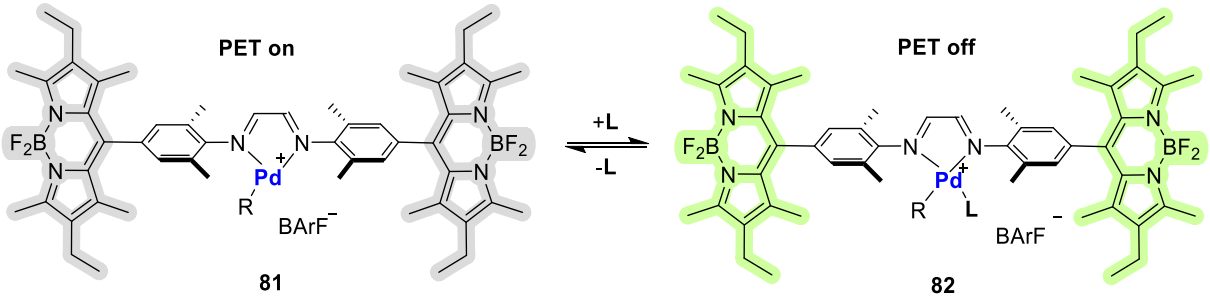

Figure 44 Fluorogenic ligand substitution reaction based on the palladium-diimine complex reported by Halter and Plenio.

In comparison to the prevalent acceptor-PET quenching for NHC-metal complexes, diimine-metal complexes provide opposite donor-PET quenching. Hence, a corresponding gain of fluorescence intensity is observed upon the increase of electronic density on the metal center due to the much weaker donicity of diimine compared to NHC ligand. Monitoring of fluorescence signal change could be observed through manipulation of metal-ligand interactions and efficiency of photoinduced electron transfer quenching *via* addition of different coordinative ligands (pyridine, acetonitrile, carbon monoxide,

olefins) to the activated complex. Characteristic changes in fluorescence provided information about association constants of the coordinative donor molecules to the cationic palladium complex demonstrating usefulness of fluorescence spectroscopy in the evaluation of chemistry of the metal center in the corresponding catalytic concentration range.

2. Scope of the dissertation

Fluorescence spectroscopy is a highly sensitive tool for the characterization of molecular interactions and events. Therefore, fluorophore-tagged molecules can be suitable for the elucidation of reaction mechanisms in homogeneous catalysis. The efficiency of the fluorescence signal can be modulated through various processes, including fluorescence quenching and resonance energy transfer. These changes can provide valuable information about the structural and electronic molecular parameters which are crucial for understanding and developing catalytic transformations based on transition metal complexes. The objective of this dissertation is to develop new Bodipy-labeled NHC-transition metal complexes for studying organometallic systems and transformations.

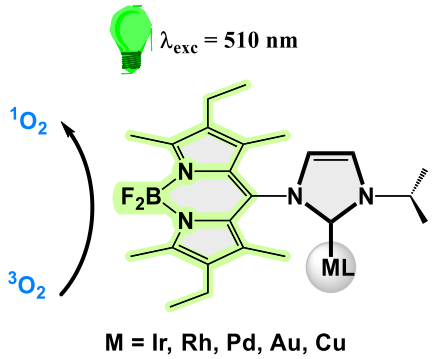

• **Part 1** *Ligand Exchange Triggered Photosensitizers – Bodipy-tagged NHC metal complexes*. (S. Popov and H. Plenio, *Eur. J. Inorg. Chem.* **2022**, *27*, e202200335)

The observation of fluorescent and non-fluorescent fluorophore-labelled metal complexes prompts the question: what happens to the excitation energy that is not converted into fluorescence? It was previously reported that Bodipy-tagged transition metal complexes can undergo fluorescence quenching predominantly due to PET mechanism despite the presence of heavy halide atom and 5d transition metal. We carried out additional investigation of this question and included published earlier NHC-Bodipy tagged metal complexes to obtain information about the impact of structural modification on photophysical characteristics. This chapter presents the synthesis and characterization of new NHC-tagged Bodipy transition metal complexes (Au, Cu, Pd, Rh, Ir), including characterization of their photophysical properties. The obtained results show how the nature of transition metal in NHC-tagged Bodipy ligand can influence fluorescence quenching through photo-induced electron transfer and heavy atom effect.

• **Part 2** *Determination of stereoelectronic properties of NHC-ligands via ion pairing and fluorescence spectroscopy.* (S. Popov and H. Plenio, *Eur. J. Inorg. Chem.* **2021**, *22*, 3708)

Quantification of steric and electronic parameters of ligands is often necessary for understanding metal-mediated catalysis. Among various methods for the determination of stereoelectronic properties of NHC ligands, account of the structural dynamics of metal complexes in solution remains limited. For these reasons, we introduce an approach based on the equilibrium of ion-paired cationic NHC-iridium complex and a fluorescent anionic Bodipy dye. 26 different NHC ligands with varying steric and electronic properties are probed and examined through established electronic descriptors (redox potential and ν(CO)).

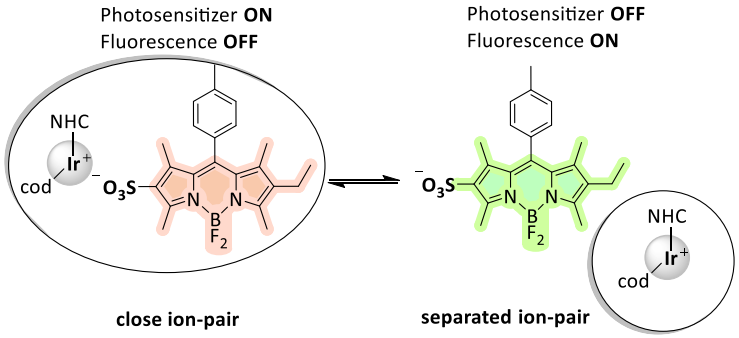

• **Part 3** *Switched fluorescence and photosensitization based on reversible ion-pairing.* (S. Popov and H. Plenio, *Chem. Commun.*, **2022**, *58*, 12669)

Based on the prior information of our research, we raised the question if modulation in photosensitizing ability can be feasible in the system of ion-paired cationic NHC-iridium complex and anionic Bodipy dye. For this purpose, we want to investigate how the electronic nature of the NHC-ligands and degree of ion association/dissociation affects the photosensitizing activity in the generation of singlet oxygen.

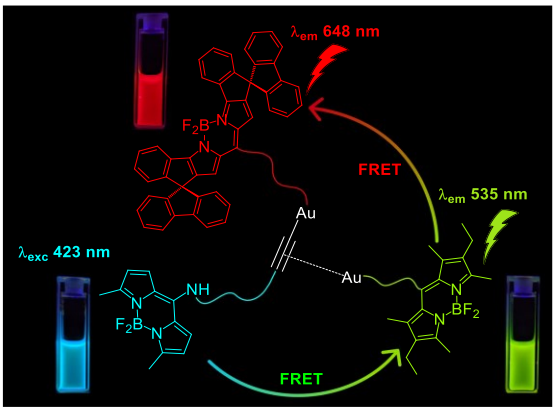

• **Part 4** *Fluorescent organometallic dyads and triads*. (Y. Shinozaki*, S. Popov* and H. Plenio, *Chem. Sci.*, **2023**, *14*, 350. *Both authors contributed to the work equally)

In non-covalent ensemble interactions, it can be challenging to identify the species responsible for fluorescence signals because measurements are taken for the sum of all fluorescent species. More precise measurement techniques and further analyses may be required to address this issue and to identify the individual species contributing to the signal. Hence, we apply the FRET-based approach to establish spatial vicinity between different molecular fragments within organometallic systems. Despite a few examples of FRET pairs based on Bodipy dyes, they still pose significant problems for practical implementation and limit availability of this method. In this work, we present the synthesis of three types (blue, green, red) of stable Bodipy-based fluorescent dyes that are linked to the organometallic complexes and result in new blue-green/green-red FRET pairs. Application of two different FRET systems involving NHC-metal complexes were demonstrated in binuclear Widenhoefer type gold complexes and in an organometallic ion pair.

3. Results and discussion

3.1. **Bodipy tagged NHC transition metal complexes** (*Part 1*)

The results in this chapter are included in the following open-access publication: S. Popov and H. Plenio, "*Ligand Exchange Triggered Photosensitizers – Bodipy-tagged NHC metal complexes*", *Eur. J. Inorg. Chem.* **2022**, *27*, e202200335. *https://doi.org/10.1002/ejic.202200335*.

Based on the observation of fluorescent and non-fluorescent complexes, the question arises as to what is happening, when the excitation energy is not converted into fluorescence. Obviously, numerous quenching pathways[1] can lead to the radiationless decay of the excited state,[138,140] but especially in the presence of heavy transition metals with strong spin-orbit coupling intersystem crossing to generate triplet states poses a feasible alternative.[15] The introduction of heavy atoms to organic compounds is the most popular method to enhance intersystem crossing, and this approach has also been applied to numerous Bodipy derivatives (Scheme 7). The derived photosensitizers utilize the triplet state energy for the generation of $^1O_2$ from $^3O_2$.[141] Some important (including transition metal-based) Bodipy-based examples of photosensitizers are shown in Scheme 7 for compounds A,[142] B,[143] C,[144] D,[106,145] E,[146] F,[116,117] and G[147]. Other than using heavy atoms (iodine, transition metals),[148] more recently additional strategies such as orthogonal π-systems including Bodipy dimers [143,149] have evolved, which also lead to efficient photosensitizers useful in photodynamic therapy.[150]

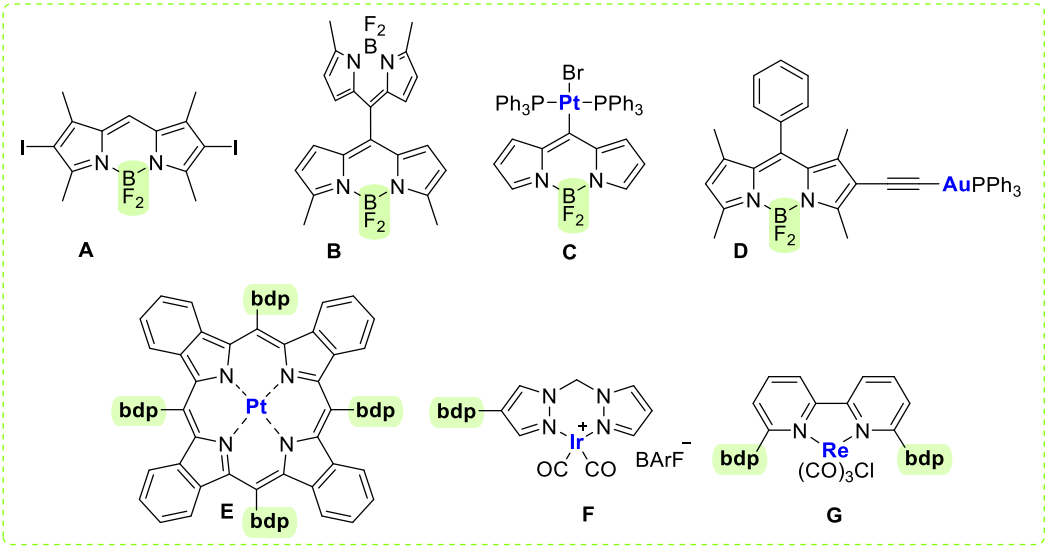

Scheme 7 Efficient (transition metal) Bodipy photosensitizers.

Nonetheless, the modulation of the intersystem crossing and the photosensitizing ability normally relies on a modification of the covalent framework, which requires significant synthetic effort. It appears to be a more flexible approach to link the fluorophore to a ligand to which a number of different metals with variable ligand spheres can be coordinated and to monitor their influence on the photosensitizing properties. To maximize the impact of the metal center, the metal binding unit should be attached close to the fluorophore (Bodipy). Consequently, in this chapter the synthesis of complexes will be reported in which the imidazolylidene-metal complexes are directly attached to the

Bodipy core and the suitability of the respective complexes as photosensitizers for $^1O_2$ generation studied.

3.1.1. Synthesis of Bodipy NHC tagged metal complexes

Numerous transition-metal complexes can be easily prepared due high ability of NHC ligands for their high coordinating ability, stability and chemical functionalization.[151] Therefore N-heterocyclics carbenes were chosen for establishment of a stable linker between the Bodipy fluorophore and a number of different transition metals for monitoring metal-fluorophore interactions and photosensitizing properties. In order to maximize potential impact of the metal center on the fluorophore, the metal binding unit should be attached directly to the Bodipy core.

We chose 8-chloro Bodipy fluorophore for the establishment of connection to NHC ligand. Such Bodipy can be easily functionalized avoiding additional steps using the Lindsey approach.[26] The reaction of *meso*-chloro Bodipy **83** with imidazole provides the respective Bodipy-substituted imidazole in 91 % yield (Scheme 8). Alkylation of **84** with 2-iodopropane results the imidazolium salt HI · **85**, which serves as a precursor for the synthesis of NHC-metal-complexes (Scheme 9).

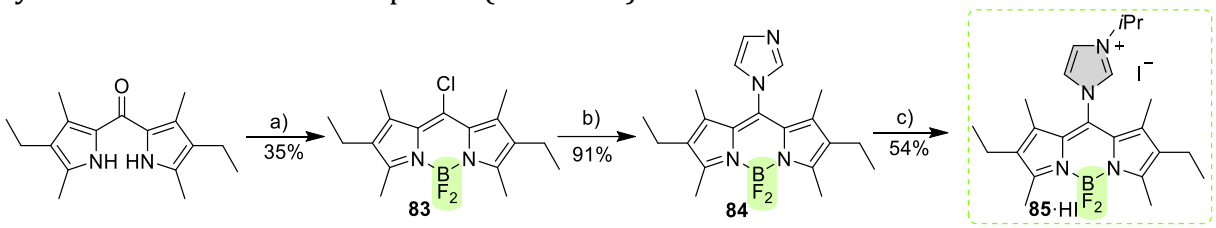

Scheme 8 Synthesis of Bodipy imidazolium salt **85**·HI. Reagents and conditions: (a) $POCl_3$, DCE, T = 80°C, 3 h; then, Et_3N, $BF_3{\cdot}OEt_2$, CH_2Cl_2, rt, 6 h (b) potassium carbonate, imidazole, CH_2Cl_2, rt, 16 h; (c) 2-iodopropane, acetone, T = 70 °C, 24 h.

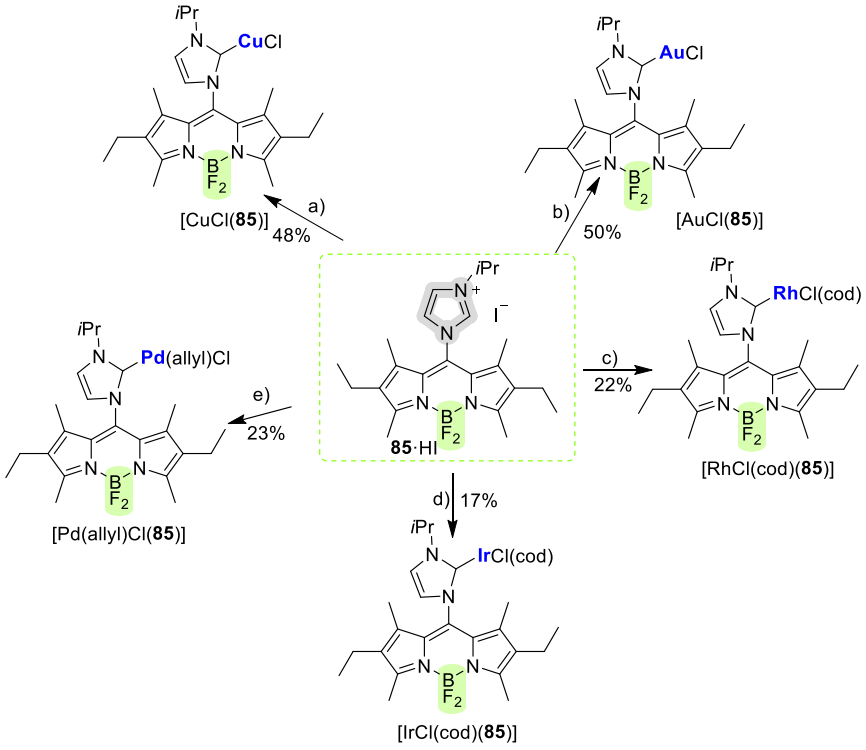

Scheme 9 Synthesis of Bodipy NHC metal complexes. Reagents and conditions: a) Ag_2O, DCE, T = 55°C, 60 min; then CuCl, DCE, T = 60°C, 1 h; b) Ag_2O, DCE, T = 55°C, 90 min; then

[AuCl(Me_2S)], DCE, *T* = 60°C, 2 h; c) Ag_2O, DCE, *T* = 55°C, 90 min; then [RhCl(cod)]$_2$, DCE, *T* = 60°C, 1.5 h; d) Ag_2O, DCE, *T* = 55°C, 90 min; then [IrCl(cod)]$_2$, DCE, *T* = 60°C, 1 h min; e) Ag_2O, DCE, *T* = 55°C, 90 min; then [PdCl(allyl)]$_2$, DCE, *T* = 60°C, 1.5 h.

There are three commonly employed approaches for the synthesis of such complexes:[152] a) *in-situ* synthesis of [AgX(NHC)] and transfer of the NHC from Ag^+ to a metal halide with precipitation of silver halide; b) deprotonation of an azolium salt to the respective carbene and approach[153] with the direct formation of NHC-metal complex from an azolium salt and metal complexes. For the synthesis of NHC-metal complexes utilizing carbene **85** both approaches b) and c) failed, probably since the basic reaction conditions led to the decomposition of the Bodipy subunit of the imidazolium salt **85**·HI. Method a) was successful even though several of the respective NHC-metal complexes were isolated in modest yields only.

Complexes [(MCl(cod)(**85**)] (M = Rh, Ir) can be easily converted to the corresponding carbonyl complexes by substitution of 1,5-cyclooctadiene ligand by two carbon monoxide *via* simple bubbling CO gas through the respective methylene chloride solutions within 30 minutes (Figure 45).

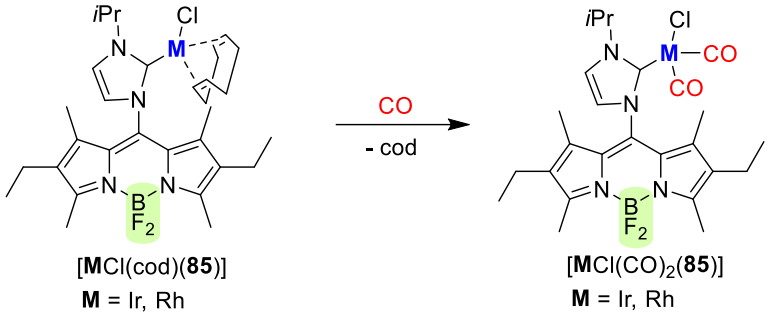

Figure 45 Synthesis of [MCl(CO)$_2$(**85**)] (M = Ir, Rh) carbonyl metal complexes.

The analysis of the IR spectra, specifically of the respective *ν*(CO), provides information on the donor properties of the respective NHC. In order to allow the comparison of the ATR data to the transmission IR data,[154] the data for the reference complex [IrCl(CO)$_2$(IMes)] (ν_{av}(CO) =2017 cm^{-1}) were also recorded using the same ATR-IR spectrometer.[155] The ν_{av}(CO) for [IrCl(CO)$_2$(**85**)] (2013 cm^{-1})(Figure S51 in SI) are shifted by 4 cm^{-1} relative to those of the reference complex. Based on these data, NHC **85** appears to be more electron-donating than the reference carbene IMes. With a view to the electron-accepting properties of the Bodipy unit this is unexpected.[156] Furthermore replacing the N-mesityl group by an *i*Pr group was shown to have very little influence on the donation of the respective NHC ligand.[157] Alternatively, the redox potential Ir(I/II) in [IrCl(cod)(**85**)] also provides information on the donor ability of the NHC ligands. [IrCl(cod)(**85**)] is characterized by a reversible cyclic voltammogram with $E_{1/2}$ = +0.811 V for Ir(I/II). This redox potential indicates that NHC **85** is significantly less electron-releasing than the reference NHC in [IrCl(cod)(IMes)] ($E_{1/2}$ = + 0.759 V). Obviously this result is not in accord with the IR data. However, based on the ewg nature of the Bodipy group, it was expected that NHC **85** is less donating than IMes. We also observed that for the related N,N'-dialkyl-substituted NHC [IrCl(CO)$_2$(NHC)] the *ν*(CO) data also deviated from the electronic information obtained *via* redox potentials.[157]

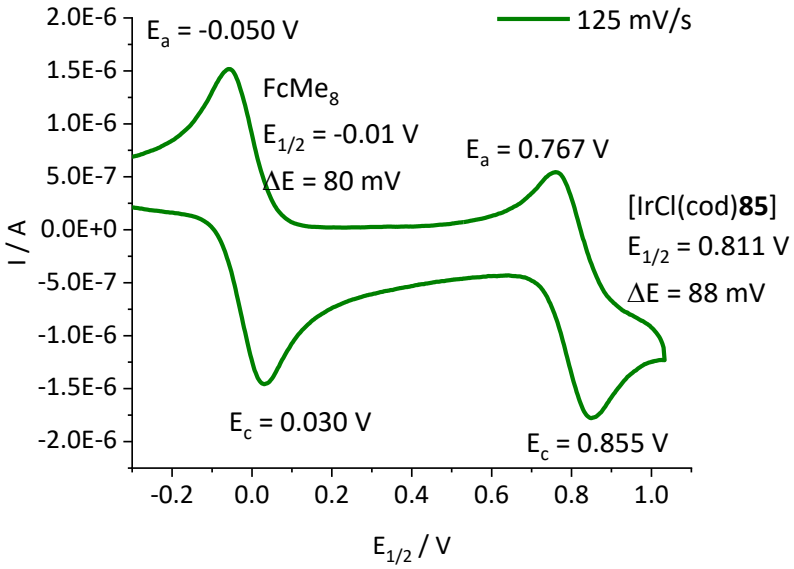

Figure 46 Cyclic voltammogram of [IrCl(cod)(**85**)] was recorded in dry methylene chloride under an atmosphere of argon, supporting electrolyte N*n*Bu$_4$PF$_6$ (c = 0.1 mol/L) at 125 mV/s scan rate referenced *vs.* FcMe$_8$. Reproduced from Ref. 265 according to CC BY-NC-ND 4.0 license *(https://creativecommons.org/licenses/by-nc-nd/4.0/).*

X-ray crystal structure of [IrCl(CO)$_2$(85)]

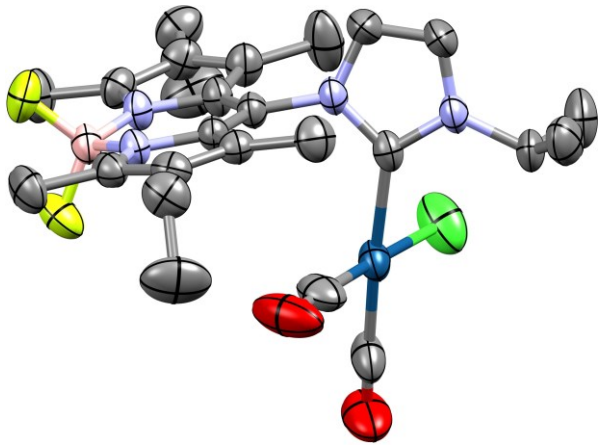

Figure 47 Crystal structure of [IrCl(CO)$_2$(**85**)] (ORTEP plot, hydrogen atoms omitted, CCDC-2174553). Relevant bond lengths (pm) and angles (°): Ir-C(NHC) 206.3(4), Ir-CO (186.6(5), 181.4(6), Ir-Cl (234.7(1), C(NHC)-Ir-C 178.2 (1), 93.4(2), C(NHC)-Ir-Cl 88.5(1), B-F (137.1(5), 138.9(5). Reproduced from Ref. 265 according to CC BY-NC-ND 4.0 license *(https://creativecommons.org/licenses/by-nc-nd/4.0/).*

In order to probe the structure of [IrCl(CO)$_2$(**85**)] in more detail and to potentially resolve the inconsistency in the ν(CO) data, single crystals of [IrCl(CO)$_2$(**85**)] were grown by cooling a pentane/CH_2Cl_2 solution of the complex (Figure 47). The crystal structure was solved and refined with SHELXT[158] within the OLEX2 shell.[159] The Ir(I) displays the typical square-planar coordination sphere consisting of two *cis*-CO-ligands, chloride and the carbene carbon. Both the imidazolylidene and the Bodipy are planar units and as a consequence of the methyl groups in the 1,7-position of Bodipy the planes of the Bodipy

and the imidazolylidene are orthogonal. Bond lengths and angles are in the typical range observed for such complexes.[160] The Ir-C(NHC) bond is on the shorter side of the typical distances which range from 206 -211 pm. Boron resides in an almost ideal tetrahedral environment and the respective angles of boron, nitrogen and fluorine are within two degrees of 109°. A slightly unusual structural feature is the ca. 20° deviation from perfect orthogonality of the square-planar Ir environment and the imidazolylidene plane.[161] The origin of this tilting appears to be the larger steric bulk of the chloride compared to the carbonyl ligand. The rotation of the square-planar unit around the Ir-C(NHC) axis relieves the close contact of the chloride with the 1,7-Bodipy methyl groups, which are shielding the space on both sides of the imidazolylidene unit.

3.1.2. Evaluation of photophysical properties

In general, photoinduced electron transfer (PET) and heavy atom effect (HAE) have been widely studied to comprehend quenching and develop new photosensitizers. In the context of earlier results two pathways are conceivable – either the excitation energy is lost *via* PET-quenching[138] or the close vicinity of heavy transition metals with strong spin-orbit coupling and the fluorophore facilitates intersystem crossing and a significant transfer of the excitation energy into the triplet state.[15] Quenching of fluorescence by HAE and PET are not mutually exclusive, and some researchers have shown evidence that this process may include a combination of two mechanisms.[3] Hence in this work we have presented evidence of the existence of two fluorescence quenching mechanisms based on the experimental data in comparison to previously reported Bodipy-based organometallic complexes (Scheme 10).[86,87,138,139,162]

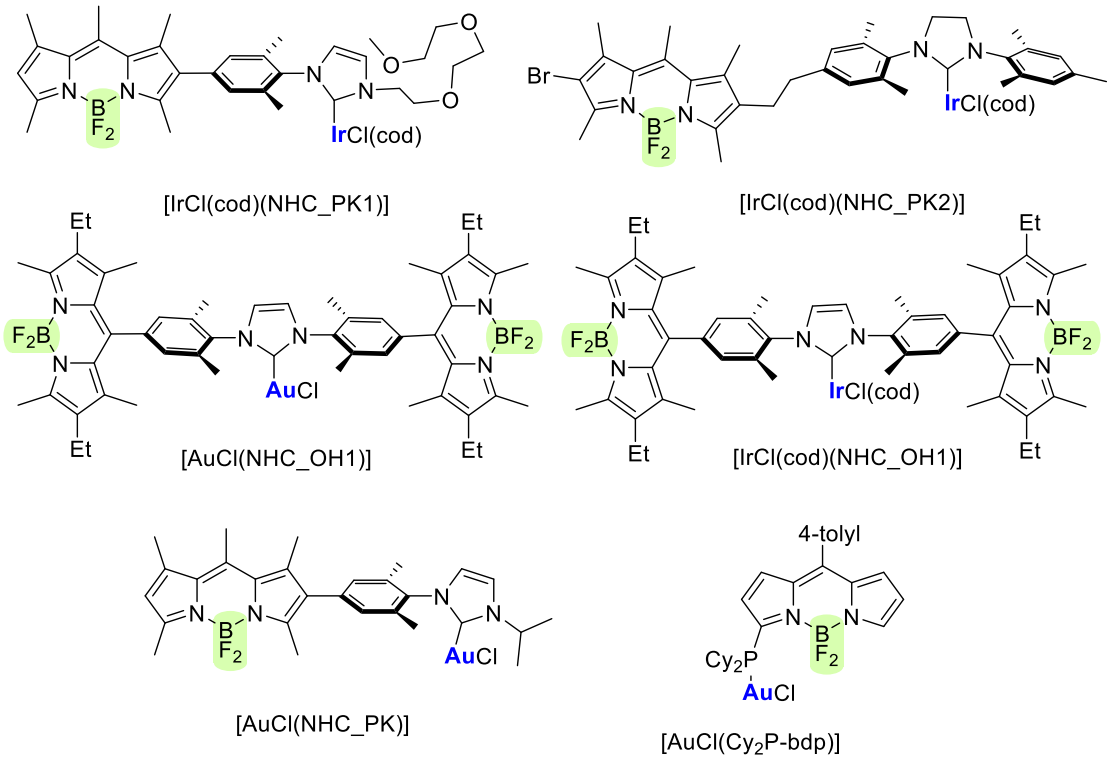

Scheme 10 Previously reported complexes included in the present studies. Reproduced from Ref. 265 according to CC BY-NC-ND 4.0 license *(https://creativecommons.org/licenses/by-nc-nd/4.0/).*

We examined the fluorescence quenching hypothesis for our Bodipy-tagged organometallic system where changes in electron density at the transition metal leads to transformations of the BODIPY fluorescence intensity *via* ligand substitution reactions in the stable and fluorescent [AuCl(**85**)] complex. Based on the systematic study of our working group it was reported that the fluorescence intensity during the reaction of [AuCl(NHC_PK)], [AuCl(bdpPCy$_2$)] and [Pd(allyl)Cl(NHC_OH1)] complex with dodecanethiol or aromatic thiols forms M-SR derivatives, for which a significant drop in fluorescence is observed due to PET-quenching (electron-transfer from the Bodipy excited state to the metal center followed by non-radiative recombination of the charges).

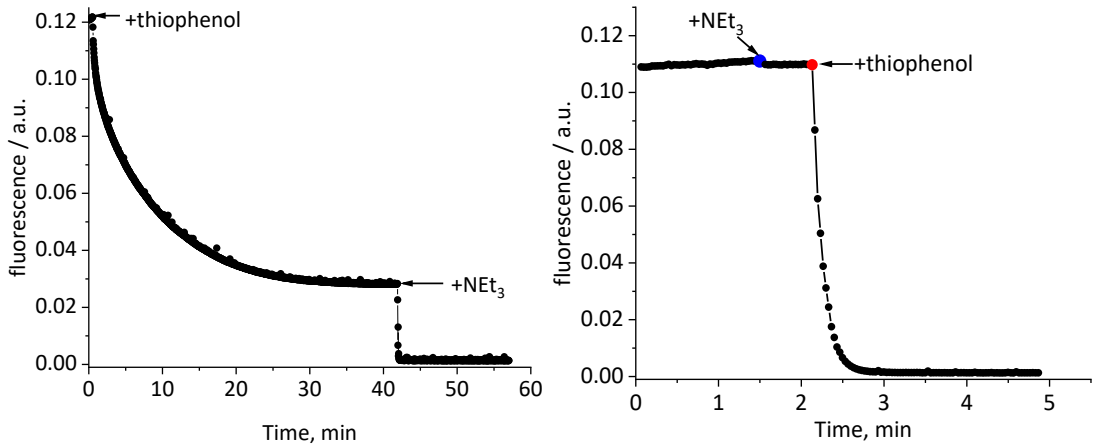

Figure 48 Fluorescence intensity *vs*. time plot for the reaction of thiophenol with [AuCl(**85**)] in 1,2-dichloroethane (c = 1.0·10^{-6} mol/L) and base (Et$_3$N). Order of addition of reactants: Left [AuCl(**85**)] + thiophenol then Et$_3$N; Right [AuCl(**85**)] + Et$_3$N then thiophenol.

The addition of thiophenol to [AuCl(**85**)] leads to a significant drop in brightness due to the partial formation of a gold-thiolate complex (even in the absence of base) (Figure 48). The addition of Et$_3$N leads to full quenching of the fluorescence signal and to the complete formation of the gold thiolate complex. It appears that acidity of the thiol plays an important role for the *in-situ* generation of the gold thiolate metal complex where electron-rich thiols react slowly in comparison to the electron-deficient derivatives. Alternatively, addition of Et$_3$N to the gold complex doesn´t affect fluorescence intensity and significantly improves reaction time of the thiophenol with [AuCl(**85**)] (Figure 49).

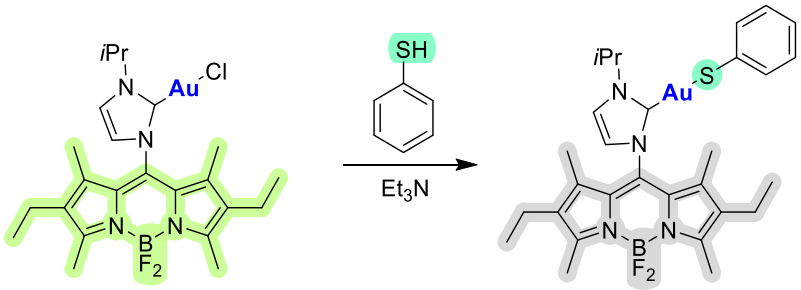

Figure 49 Ligand-exchange reaction with formation of NHC-gold thiolate complex.

The emission of photons in fluorescent molecules can be dramatically compromised when electrons of the excited singlet state S$_1$ undergo intersystem crossing to the long-lived triplet state T$_1$ which results in the decrease of fluorescence brightness.

Relatively long life times and high energy of triplet state can be involved in generation of other transient chemically active species. Once excited to the triplet state, photosensitizer is prone to the production of singlet oxygen by an energy transfer after collision of excited photosensitizer and triplet oxygen. Generation of $^1O_2$ is a simple and controllable procces which requires only light source and a photosensitizer capable to be excited by specific wavelength. Hence, using the simple experiment where the generated triplet state of the fluorophore decays *via* singlet oxygen production with following photooxidation of 1,3-Diphenylisobenzofurane (DPBF) can be a useful tool for the evaluation validity of the hypothesis of fluorescence quenching.

Important spectroscopic data like absorption and emission maxima, fluorescence quantum yield (Φ_{em}), $^1O_2$ quantum yields ($\Phi_{s.o.}$) and extinction coefficients for the newly synthesized complexes as well as for other complexes from previous studies [86,87,138,139,162] are summarized in Table 1. The UV/Vis spectra of the new transition metal complexes are dominated by the Bodipy absorption at around 540 nm. Relative to the imidazolium salt **85**·HI (λ_{max}= 545 nm) the absorption maxima experience a modest hypsochromic shift of between 4 – 7 nm depending on the metal. The extinction coefficients of the metal complexes range from 23.000 M^{-1} cm^{-1} up to 75.000 M^{-1} cm^{-1}. The two [$MCl(CO)_2$(**85**)] (M= Ir, Rh) complexes have the lowest value of extinction coefficients while the three gold complexes display the highest value. The emission wavelengths also experience a small hypsochromic shift relative to **85**·HI (λ_{em}= 558 nm) ranging between 549 – 554 nm for the different metal complexes. Among the recently reported complexes, those with two Bodipy units display the highest extinction coefficients.

Compound	$\lambda_{abs,max}$	$\lambda_{em,\ max}$	Φ_{em}	$\Phi_{s.o.}$	ε
85·HI[a]	545	558	0.45	0.11	64
[AuCl(**85**)][a]	538	549	0.28	0.43	75
[Pd(allyl)Cl(**85**)][a]	536	549	0.23	0.46	59
[CuCl(**85**)][a]	535	554	0.025	0.11	51
[$RhCl(CO)_2$(**85**)][a]	540	554	0.009	0.12	33
[$IrCl(CO)_2$(**85**)][a]	540	554	0.017	0.63	23
[IrCl(cod)(**85**)][a]	541	-	<0.01	0.09	39
[RhCl(cod)(**85**)][a]	541	-	<0.01	0.26	56
[IrCl(cod)(NHC_PK1)]	506	530	0.008	0.18	67
[IrCl(cod)(NHC_PK2)]	510	524	0.022	0.035	85
[AuCl(NHC_PK)]	506	529	0.70	0.051	65
[AuCl(NHC_OH1)]	526	538	0.67	0.065	95
[IrCl(cod)(NHC_OH1)]	526	538	0.060	0.074	94
[$AuCl(Cy_2P$-bdp)]	510	526	0.096	0.022	44

Table 1 Photophysical and photochemical parameters for the photosensitizers. Singlet oxygen quantum yield ($\Phi_{s.o.}$) was determined in CH_3CN solution by monitoring the decay of DPBF (c_0 =90 μM) in a presence of the corresponding PS (c = 1.0 μM) using 2,6-diiodo-Bodipy as a reference ($\Phi^{st}_{s.o.}$ = 0.75). [a] Value of fluorescence quantum yield was determined in CH_3CN solution using rhodamine 6G as a standard fluorophore (Φ_{st} = 0.95 in EtOH). Absorption (λ_{abs}) and emission (λ_{em}) maxima and fluorescence quantum yield (Φ_{em}) are given according to the previously reported complexes. The molar absorption coefficients (ε 10^3 M^{-1} cm^{-1}) were determined for the respective photosensitizers in

CH_3CN solution (c = 1.0 μM). Reproduced from Ref. 265 according to CC BY-NC-ND 4.0 license *(https://creativecommons.org/licenses/by-nc-nd/4.0/).*

The differences in fluorescence quantum yields for the compounds reported here are much more pronounced. While the two [MCl(cod)(**85**)] (M = Ir, Rh) complexes display negligible fluorescence, the related [MCl$(CO)_2$(**85**)] (M = Ir, Rh) show stronger emissions with Φ_{em} = 0.17 and 0.09. This fluorescence gain is typical for such complexes upon replacement of a 1,5-cyclooctadiene ligand by two carbonyls and this fluorogenic reaction has been used for the detection of CO.[86,163,164] The remaining complexes with NHC **85** display quantum yields in the narrow range between 0.21 – 0.28. Compared to related metal complexes reported previously (the complexes listed in the bottom half of Table 1 serve as an example),[86] the fluorescence quantum yields of the metal complexes with NHC **85** are significantly lower and it is interesting to learn why this is the case.

The generation of $^1O_2$ was quantified using the cycloaddition reaction with 1,3-Diphenylisobenzofurane (DPBF)[165] by monitoring the decrease of the 410 nm DPBF absorbance with time *via* UV/Vis-spectroscopy (Figure 50, left). A typical linear plot of absorbance *vs.* Time is shown in (Figure 50, right) as an example of the corresponding zero-order reaction and the slope is used to calculate the singlet oxygen quantum yield $\Phi_{s.o.}$.[165–167] The respective $\Phi_{s.o.}$ was determined for all complexes listed in Table 1. The expectation is that the proximity of a heavy atom and the fluorophore increases the likelihood of photosensitizer ability – the closer the contact the higher intersystem crossing.

There is no evidence for the oxidation of transition metal (complexes) by $^1O_2$ during the photosensitizing experiments in any of the studied complexes. While this appears to be difficult for the Au(I) and the Pd(II) complexes anyway, it might be possible for [IrCl(cod)(**85**)] with an Ir(I/II) redox potential of +0.84 V. The redox potential of the electron-deficient [IrCl$(CO)_2$(**85**)] cannot be easily determined due to the lability of the oxidized species (CO dissociation), but should be approx. +500 mV anodic of the Ir(I/II) redox potential for [IrCl$(CO)_2$(**85**)].[86] However, even for the Ir complexes, the UV/Vis and the fluorescence spectra of the metal complexes remain unchanged during the singlet oxygen generation, and based on this oxidation of the metal complexes is unlikely.

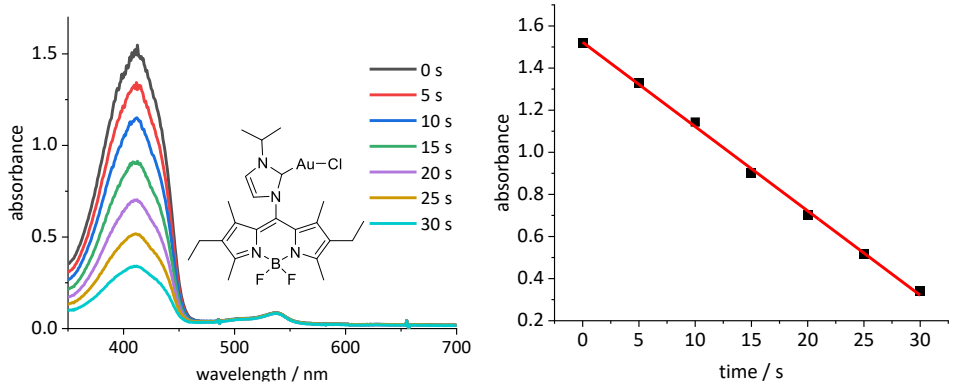

Figure 50 Decay of the 410 nm absorbance of DPBF (c_0 = 90 μM) in the presence of [AuCl(**85**)] (c = 1.0 μM) in CH_3CN and irradiation with a green LED and plot of absorbance *vs.* Time. Reproduced from Ref. 265 according to CC BY-NC-ND 4.0 license *(https://creativecommons.org/licenses/by-nc-nd/4.0/).*

With a single exception, all complexes in which the Bodipy unit is spatially separated from the transition metal are poor photosensitizers with an inefficient $^1O_2$ formation. The only exception is complex [IrCl(cod)(NHC_PK1)] with $\Phi_{s.o.}$= 0.18. Despite

small $\Phi_{s.o}$ several of the complexes in Scheme 10 also display modest fluorescence quantum yields and it is thus likely, that the excitation energy is lost *via* PET quenching.[138] Interestingly, in complex [AuCl(bdpPCy$_2$)] the gold is bonded very close to the Bodipy core, but both fluorescence and $^1O_2$ quantum yields are poor. Again it seems that the excitation energy is predominantly channeled into PET quenching, which also appears to be the case for [MCl(cod)(**85**)] (M= Rh, Ir). The remaining complexes with NHC **85** (Table 1) display modest Φ_{em} of below 0.30, but at the same also act as efficient photosensitizers – depending on the nature of the transition metal. The gold complex is more efficient than the lighter copper complex, and the same applies to the iridium relative to the lighter rhodium complex. The iridium complex is useful for the generation of $^1O_2$ and at $\Phi_{s.o.}$= 0.63 rivals the performance of the 2,6-diiodo-Bodipy. It is very interesting, that a simple ligand exchange reaction replacing the 1,5-cyclooctadiene ligand in [IrCl(cod)(**85**)] with two CO ligands generates the efficient photosensitizer [IrCl(CO)$_2$(**85**)]. Based on the recent concept of S_1-T_1 tuning,[168] it is assumed that a smaller energy difference between the S_1 and the T_1 state in [IrCl(CO)$_2$(**85**)] enables facile intersystem crossing in this complex. Nonetheless, the singlet oxygen quantum yield depends on numerous factors, not just the rate of the intersystem crossing k_{isc} but also the rates of radiative and non-radiative decay of excited states relative to k_{isc} and the thermal accessibility of excited d-states enabling non-radiative deactivation pathways[169] and the efficient transfer of the T_1 energy to $^3O_2$.[165] In this complicated interplay of different factors minor changes in the molecular setup can result in significant changes of the properties.

The cod-to-CO ligand exchange reaction is very fast even at a very low concentration of the complexes and tends to be virtually quantitative.[86,170] Previously, this reaction was identified as a fluorogenic reaction.[86] For [IrCl(cod)(**85**)] the cod-to-CO ligand exchange triggers the photosensitizer. A poor $^1O_2$ generating complex ($\Phi_{s.o.}$= 0.09) is converted into an efficient photosensitizer ($\Phi_{s.o.}$= 0.63) following the addition of two equivalents of CO to [IrCl(cod)(**85**)].

3.1.3. Catalytic investigations of photosensitizing properties

Finally, we were interested whether good photosensitizing properties of the respective transition metal complexes translate into good photocatalytic properties. The photooxidation of *p*-bromothioanisole to the respective sulfoxide was chosen as an exemplary reaction and substrate conversions determined by NMR spectroscopy (Figure 51).[171]

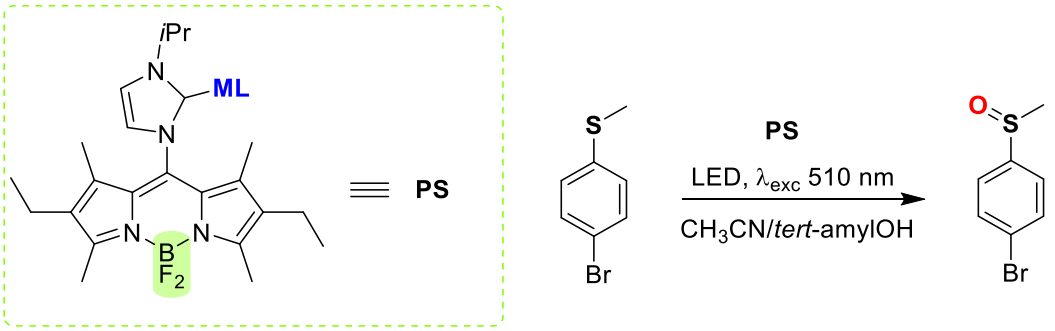

Figure 51 Photooxidation of thioethers to the respective sulfoxides. Reagents and conditions: a) *t*-amyl alcohol, acetonitrile (1 : 1), green LED, photosensitizer.

The photoreactor for the generation of $^1O_2$ was also used in the photocatalytic reactions and all reactions were carried out at 1mol% loading of the metal complex (20 h reaction time). Surprisingly, the poor photosensitizer [IrCl(cod)(**85**)] produced modest amounts of the sulfoxide (35% after 20 h), while the very efficient photosensitizer [IrCl(CO)$_2$(**85**)] provides substantially more product >99% after 20 h (40% after 8 h). At 66% conversion the gold complex [AuCl(**85**)] is reasonably efficient. Based on these results we reasoned that the catalytic role of the metal in such oxidation reactions is not limited to $^1O_2$ generation, since the higher affinity of gold towards sulfur might be one reason for better substrate conversion. Based on this argument, the accessibility of gold will be much better when the strongly coordinating chloride is replaced by a weakly coordinating bis-triflimidate NTf_2^- and consequently the catalytic efficiency should increase. [Au(NTf$_2$)(**85**)] turns out to be much more active and provides virtually quantitative substrate conversion of >99% after only 9 h reaction time. These experiments clearly support the hypothesis by Messerle *et al*.[116] that the transition metal also promotes the catalytic transformation of the thioanisole *via* metal-(O_2) or metal-S interactions. Reactions of $^3O_2$ and $^1O_2$ with iridium complexes have been reported,[172] however, such Ir(I) complexes, appear to be significantly more electron-rich than [IrCl(CO)$_2$(**85**)] and there is no evidence (vide supra), that $^1O_2$ reacts with the complexes reported here.[173] Gold complexes are better known for their interaction with sulfur than with oxygen and the role of gold is likely twofold: spin-orbit coupling leads to efficient $^1O_2$ generation and coordination of substrate stabilizes the sulfur-containing species (intermediates).

3.2. **Bodipy ion paired N-heterocyclic carbene complexes** (*Part 2*)

The results in this chapter are included in the following open-access publication: S. Popov and H. Plenio, "*Determination of stereoelectronic properties of NHC-ligands via ion pairing and fluorescence spectroscopy.*" *Eur. J. Inorg. Chem.* **2021**, *22*, 3708. *https://doi.org/10.1002/ejic.202100510*.

Most organometallic systems have numerous inter- and intra- molecular characteristics for the specification and direction of the catalytic transformation. For a chemist, this is always a challenge to select the ligand with suitable properties for application in homogeneous catalysis. In such systems, usefulness of the transition metal-based catalyst often depends on the core structure of ligand, which can be characterized by steric and electronic properties. Therefore, the nature of ligands in transition metal-catalyzed systems is an important parameter in the evaluation of ligand-ligand and ligan-substrate noncovalent interactions such as hydrogen and coordinative bonding, formation of ion pairs, π-π interactions, and host-guest complex formation.[174] Among intermolecular aspects in development of organometallic systems, studying of ion pairing is vital for understanding of noncovalent interactions and outcomes within catalytic processes.[175] The nature of ion pairing[175,176] has a crucial influence on the activity[177] and regio-, and stereo- selectivity of various transition metals-based catalytic reactions.[178]

This chapter present an experimental method, which provides information on the steric and electronic properties of ligands in metal complexes. This approach is based on the equilibrium of ion pairing of a cationic $[Ir(cod)(NHC)]^+$ complex and anionic bodipysulfonate ($bdpSO_3^-$) fluorophore. Electron-rich iridium in [IrCl(cod)(NHC)] complexes is known in PET-quenching (photoinduced electron transfer) of the fluorescence of a fluorophore bonded to this complex.[86,87,162,163] This quenching is distance-dependent and it is dominant at iridium-fluorophore distances smaller than 1 nm.[138] In previously synthesized complexes the nature of the covalent linker connecting NHC ligand and fluorophore determines the average distance between the fluorophore and the iridium quencher and it also determines the brightness of the fluorophore. In this work we present complexes in which the distance between fluorophore (anion) and quencher (cation) is variable and in which the degree of ion-pairing depends not only on the solvating nature of the solvent, but also on the stereoelectronic properties of anion and cation. For complexes of the general type $LM^+ X^-$ dissolved in a defined solvent and with variable L this approach provides a convenient handle to probe the stereoelectronic properties of ligand L.

3.2.1. Establishment of NHC-iridium based Bodipy-tagged complex system

Synthetic flexibility for the chemical functionalization and diversification of NHC ligands allows us to encompass stereoelectronic variation of derived iridium-based complexes via ion pairing. In this work, we studied over 26 NHC ligands with sterically and electronically various substituents on the nitrogen atoms and imidazole backbones. The series of [IrCl(cod)(NHC)] complexes were synthesized from the corresponding azolium salts using three commonly established approaches.[154,179–181] a) One step reaction between the azolium salt and in the presence of $[IrCl(cod)]_2$ metal precursor after deprotonation to the respective carbene using strong non-nucleophilic base (Ko*t*Bu

or KHMDS) in THF solution. b) Application of the weak base approach with direct formation of NHC-metal complex in acetone solution. c) Transmetallation from the *in-situ* synthesized [AgX(NHC)] complex and transfer of the NHC to a metal precursor in DCM solution.

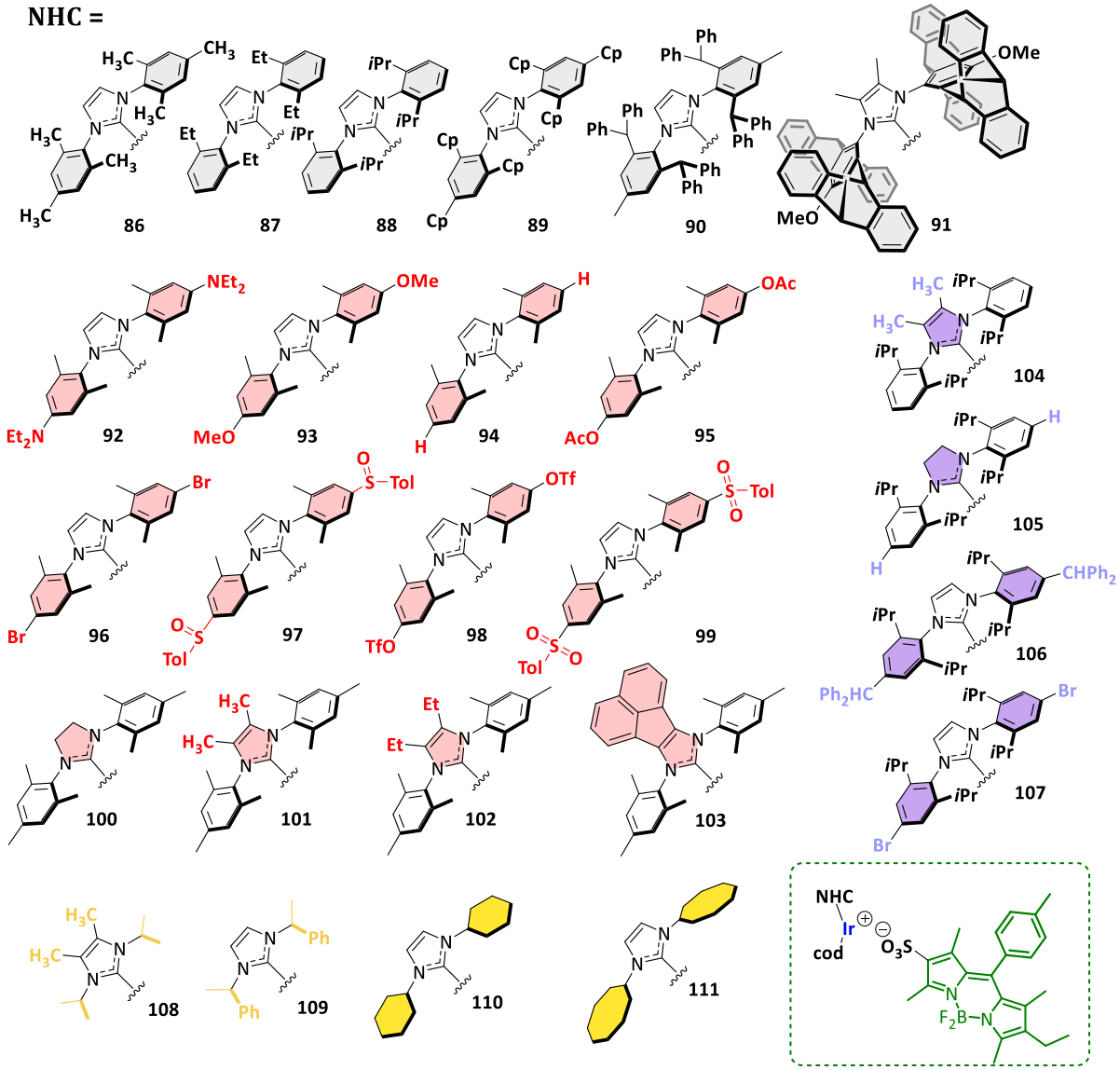

Scheme 11 List of (NHC) iridium complexes employed for the analysis of stereoelectronic properties.

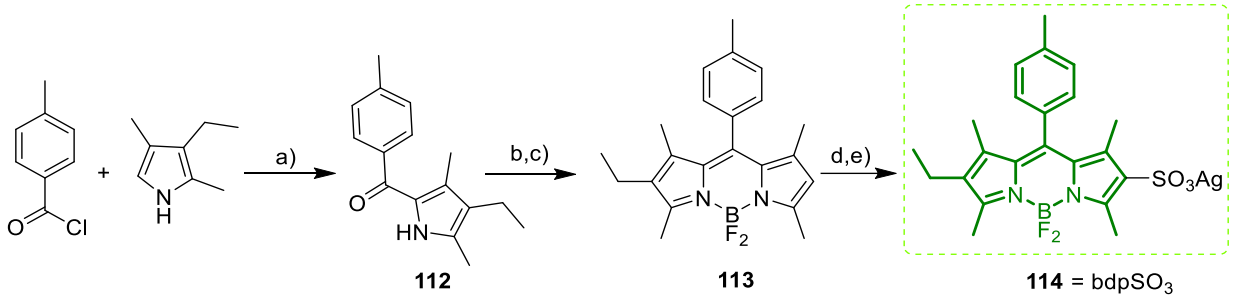

Figure 52 Synthesis of the Bodipysulfonate **114**. Reagents: (a) Et_3N, THF, reflux, 8 h; (b) 2,4-dimethylpyrrole, $POCl_3$, rt, 2 h; c) Et_3N, $BF_3{\cdot}Oet_2$, CH_2Cl_2, rt, 4 h; (d) $ClSO_3H$, CH_3CN, *T* = -40 °C, 30 min; (e) Ag_2CO_3, rt, 12 h.

The Bodipysulfonate **114** was synthesized *via* sulfonation of Bodipy **113** by chlorosulfonic acid to avoid a potential disulfonated product formation.[47] "Fully blocked" Bodipy **113** was synthesized according to the adopted general procedure[182]. 2-ketopyrrole **112** was obtained *via* Fried-Crafts acylation of 3-ethyl-2,4-dimethylpyrrole using Et_3N as a nucleophilic catalyst. Followed by $POCl_3$-mediated condensation of **112** with 2,4-dimethylpyrrole of the resulted in Bodipy **113**. Electrophilic sulfonation of **113** with chlorosulfonic acid and quenching of the *in-situ* formed sulfonic acid with Ag_2CO_3 provides the respective silver sulfonate **114** (Figure 52).

The Bodipy sulfonate metal complexes were synthesized in virtually quantitative yield according to Dorta *et al.*, who had studied in detail the reactions of [IrCl(cod)(NHC)] complexes with different silver salts containing weakly coordinating anions in CH_2Cl_2/CH_3CN solution (Figure 53).[183]

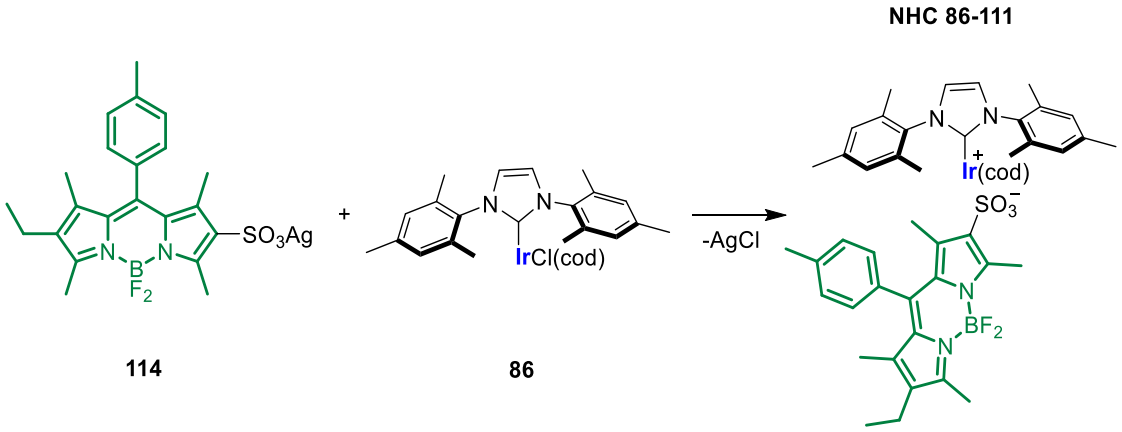

Figure 53 Synthesis of [Ir(bpdSO_3)(cod)(NHC)]. Reagents and conditions: [Ag(bdpSO_3)] (**114**), CH_2Cl_2/CH_3CN.

In non-polar solvents the sulfonate complex forms close ion pairs[175] and due to the short distance between fluorophore and iridium the fluorophore is quenched – presumably *via* a PET mechanism.[138] The fluorescence is restored in slightly more polar solvents, since solvent separated ions are formed for which the distance between quencher and fluorophore is too large to significantly influence the fluorescence properties. Consequently, monitoring the fluorescence of such complexes under various conditions is going to provide information on the degree of ion-pairing in such complexes.

3.2.2. Monitoring of fluorescence emission in ion paired complexes

The fluorescence of complex [Ir(bdpSO$_3$)(cod)(**88**)] (c =1.0 · 10^{-6} mol/L) was determined in four different solvent (mixtures): toluene, toluene – 1,2-DCE (1 : 1 vol.), toluene – 1,2-DCE (1 : 2 vol.) and in 1,2-DCE solution where intensity increase in the same order (Figure 54). Various complexes **86**–**111** have shown significant difference in values of the initial fluorescence intensities in 1,2-DCE solution. To minimize small weighing and pipetting errors as well as changes in the intensity of the excitation light source, the fluorescence intensities are always given relative to the values for the fully separated ion pairs. This is easily achieved by adding a very small amount of NBu$_4$Br -solution at the end of each experiment. The strongly coordinating bromide quantitatively displaces the bdpSO$_3^-$ from the iridium coordination sphere, which is resulting in the spatial separation of quencher and fluorophore. The fluorescence of the solutions of the different complexes (c =1.0 · 10^{-6} mol/L) is in the ideal range of ca. 10 %–90 % of the maximum fluorescence.

Complex	Toluene	1,2-DCE
86 *(IMes)*	3.3	16.2
87 *(IEt)*	3.2	17.9
88 *(IPr)*	4.4	70.7
89 *(2,4,6-Cp)*	7.0	64.6
90 *(2,6-CHPh$_2$)*	9.5	88.0
91 *(N,N-Pentiptycenyl)*	20.5	84.1
92 *(p-NEt$_2$)*	3.9	58.1
93 *(p-OMe)*	3.0	26.7
94 *(p-H)*	2.0	16.5
95 *(p-OAc)*	3.7	14.8
96 *(p-Br)*	3.4	10.8
97 *(p-SOTol)*	4.5	11.4
98 *(p-OTf)*	4.2	8.8
99 *(p-SO$_2$Tol)*	3.6	8.3
100 *(SIMes)*	1.7	22.3
101 *(Me bb)*	2.5	30.5
102 *(Et bb)*	2.9	33.2
103 *(1,8-naphtadiyl bb)*	2.4	17.3
104 *(IPr (Me bb))*	12.6	81.1
105 *(SIPr)*	8.7	71.7
106 *(IPr (p-CHPh$_2$))*	4.3	66.5
107 *(IPr (p-Br))*	5.2	57.9
108 *(N-iPrMe)*	5.5	15.9
109 *(N-EtPh)*	7.0	14.6
110 *(N-Cyclohexyl)*	4.4	14.2
111 *(N-Cyclooctyl)*	5.2	12.0

Table 2 Relative fluorescence intensities (I_{end}/I_{start}, %) for [Ir(bdpSO$_3$)(cod)(NHC)] (c = 1.0 · 10^{-6} M) complexes. Reproduced from Ref. 157 according to CC BY-NC-ND 4.0 license (*https:/creativecommons.org/licenses/by-nc-nd/4.0/)* using fluorescence intensities only for the toluene and 1,2-DCE solution.

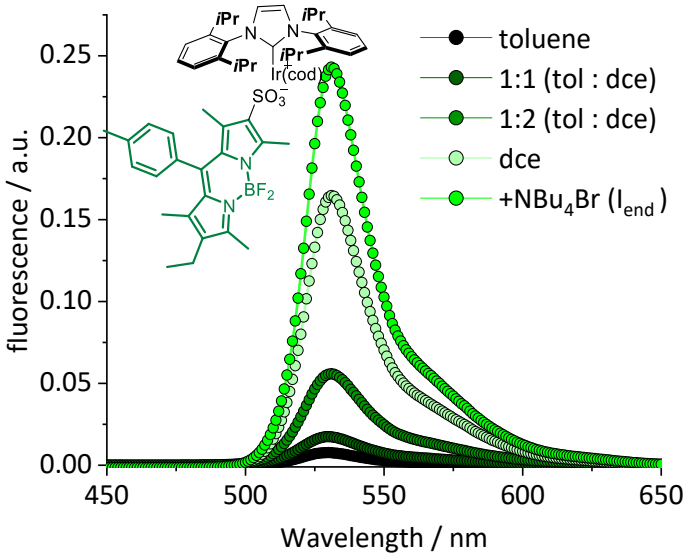

Figure 54 Fluorescence emission spectra of [Ir(bdpSO$_3$)(cod)(**88**)] complex (c = 1.0 · 10^{-6} M) in different solvent mixtures.

Consequently, the apparent equilibrium constant according to the simplest equilibrium reaction MX = M$^+$(solv) + X$^-$(solv) describing the dissociation of the close ion-pair, has to be in the range of the inverted concentration of the initial complex. Based on this, the highly sensitive fluorescent based method is ideal for investigating ion dissociation of the [Ir(bdpSO$_3$)(cod)(NHC)] with variable NHC ligands. However, care needs to be exercised concerning the aforementioned equilibrium constants. As pointed out by Gibson *et al.*[184] such ionic equilibria in non-polar solvents are not as simple as for polar solvents. Due to the poorly solvating nature of the non-polar solvents, aggregates such as M$_2$X$^+$ or MX$_2^-$ with modulated fluorescence or different types of solvent-shared ion pairs complicate the simplistic approach.[175,185] More importantly, the activity coefficients of ions in non-polar solvents with low dielectric constants are exponentially related to the inverse 3/2 power of the permittivity and because of this, the activity coefficient is extremely sensitive to ionic strength in such solvents.[186] In line with this we have observed a concentration dependence of the apparent equilibrium constants in our experiments, when studying ion separation at different concentrations to determine equilibrium constants. Therefore, evaluation of the stereoelectronic properties of the NHC ligands, was done at a constant concentration of the salt.[187]

3.2.3. Evaluation of steric NHC ligand properties *via* fluorescence ion pairing

Methods for the determination of the steric properties of NHC ligands are much less common than for electronic properties.[188] The simple Tolman approach based on CPK-models is not applicable to NHC ligands, due to the primarily C$_2$-symmetric shape of such ligand. Cavallo *et al*. developed the buried-volume approach, which provides a good description of the steric properties of NHC ligands and relies on solid state coordinates obtained from X-ray crystal structure analysis, for which single crystals of the respective complex are needed.[189] In this concept the metal is located at the center of a sphere (default radius 350 pm) and is coordinated by an NHC ligand (metal-C(NHC) =200 or 228 pm reflecting the size of different metals).[190] The buried volume (%V$_{bur}$) is the fraction of the volume of the sphere, which is occupied by the atoms of the NHC ligands (excluding the hydrogen atoms).[191] A detailed analysis of the scope and the limitations of the buried-volume method was provided by Gomez-Suarez, Nelson and Nolan.[192] A significant problem of this approach is the treatment of conformationally flexible molecules, since

the buried volume provides data only for the conformation observed in the solid state and does not take into account the conformational degrees of freedom of a molecule in solution.

In a refined approach Cavallo *et al*. Later introduced topographic steric maps which contain altimetric isocontour lines offering a quantitative description of the catalytic pocket[193] to account for variable steric effects in different areas around the metal center. This approach is applicable to a wide range of different metal-ligand complexes and is aiming at the computer-aided design of catalytic pockets.[194] Despite the huge success of this approach, the analysis of the steric environment of the metal center still relies on the static coordinates typically obtained from X-ray crystal structure analysis or DFT. Molecular dynamics, leading to changes in the shape and the accessibility of the pocket are not taken into account. In an attempt to consider conformative flexibility for metal-ligand design Patton *et al*. Recently reported on Boltzmann-weighted Sterimol parameters useful in multivariate models of enantioselectivity.[195] Alternatively, Gusev developed a parameter *r* as a measure of the direct repulsive interactions between a NHC ligand and CO ligands in [Ni(CO)$_3$(NHC)]. Such parameters are also needed to analyze and predict ligand and catalyst effects in organometallic catalysis.[196]

[IrCl(cod)(NHC)]	$\Delta E_{1/2}$ [V]	E_a-E_c [mV]	ν_{av} [cm^{-1}]	I_{rel} %	V_{bur} %
86 *(IMes)*	0.765	80	2023.3	16.21	36.5^{Au}
87 *(IEt)*	0.748	76	2023.4	17.87	31.7^{Ir}
88 *(IPr)*	0.762	82	2023.8	70.71	45.4^{Au}
89 *(2,4,6-Cp)*	0.737	66	2021.3	64.56	
90 *(2,6-CHPh$_2$)*	0.863	75	2026.0	87.98	50.4^{Au}
91*(N,N-Pentiptycenyl)*	0.804	81	2024.3	84.07	48.8^{Ag}
92 *(p-NEt$_2$)*	0.648	80	2021.0	58.10	31.6^{Ir}
93 *(p-OMe)*	0.757	96	2022.8	26.74	
94 *(p-H)*	0.786	78	2024.0	16.52	31.6^{Ir}
95 *(p-OAc)*	0.793	92	2025.1	14.78	31.7^{Ir}
96 *(p-Br)*	0.862	78	2025.5	10.83	31.7^{Ir}
97 *(p-SOTol)*	0.870	72	2028.5	11.4	
98 *(p-OTf)*	0.903	88	2027.4	8.77	31.8^{Ir}
99 *(p-SO$_2$Tol)*	0.920	80	2029.5	8.26	
100 *(SIMes)*	0.735	76	2024.5	22.31	36.9^{Au}
101 *(Me bb)*	0.692	83	2020.3	30.52	31.4^{Ir}
102 *(Et bb)*	0.681	95	2021.1	33.20	31.6^{Ir}
103 *(1,8-naphtadiyl bb)*	0.770	73	2022.8	17.25	
104 *(IPr (Me bb))*	0.720	96	2021.3	81.11	44.8^{Au}
105 *(SIPr)*	0.744	81	2024.9	71.66	47.0^{Au}
106 *(IPr (p-CHPh$_2$))*	0.777	64	2023.3	66.50	
107 *(IPr (p-Br))*	0.870	96	2025.8	57.92	
108 (*N-iPrMe)*	0.754	75	2020.8	15.88	38.5^{Au}
109 *(N-EtPh)*[(a)]	0.821	93	2026.3	14.56	36.4^{Au}
110 *(N-Cyclohexyl)* [(a)]	0.785	123	2022.3	14.20	27.5^{Au}
111 *(N-Cyclooctyl)* [(a)]	0.831	117	2021.3	12.00	

Table 3 Redox potentials of [IrCl(cod)(NHC)] complexes in 1,2-dichloroethane (rt, supporting electrolyte NnBu$_4$PF$_6$ 0.1 M) and referenced against the formal potential of

octa-methylferrocene ($FcMe_8$ $E_{1/2}$ = -0.01 V) and rel. fluorescence intensities I_{rel} =I/I_{end}. The $\nu(CO)_{av}$ from $[IrCl(CO)_2(NHC)]$ complexes and fluorescence from $[Ir(bdpSO_3)(cod)(NHC)]$. Literature source for the buried volumes (experimental and DFT), redox potentials and carbonyl frequences[151,157,179,192]. For the buried volume data Au =[AuX(NHC)], Ir =[IrCl(cod)(NHC)] and Ag =[AgCl(NHC)]. (a) CV is not fully reversible. Reproduced from Ref. 157 according to CC BY-NC-ND 4.0 license *(https://creativecommons.org/licenses/by-nc-nd/4.0/).*

Based on the analysis of initial fluorescence intensities in toluene and 1,2-DCE solution for set of sterically modified NHC ligands, it is possible to evaluate the steric properties in corresponding complexes. The Ir complexes **90** and **91** with two bulkiest NHC ligands display the most intense toluene fluorescence and 1,2-DCE intensity (Figure 55). It seems that even in non-polar toluene complexes are characterized by a different degree of anion-cation contacts.[197] Based on fluorescence and V_{bur} data the **90** and **91** based NHC ligand is the bulkiest ligand studied here (Table 3).The steric data set contains interesting subsets. The series of complexes **86** and **87** are IMes type complexes, which are characterized by the different *ortho*- substituents R = Me and Et. The fluorescence of **86** and **87** are virtually identical (after correction according to linear fit curve),[198] meaning that the steric effect of the ethyl group relative to the methyl group is negligible. This may explain, why the *ortho*-ethyl substituted NHC ligands are rarely used in catalysis.

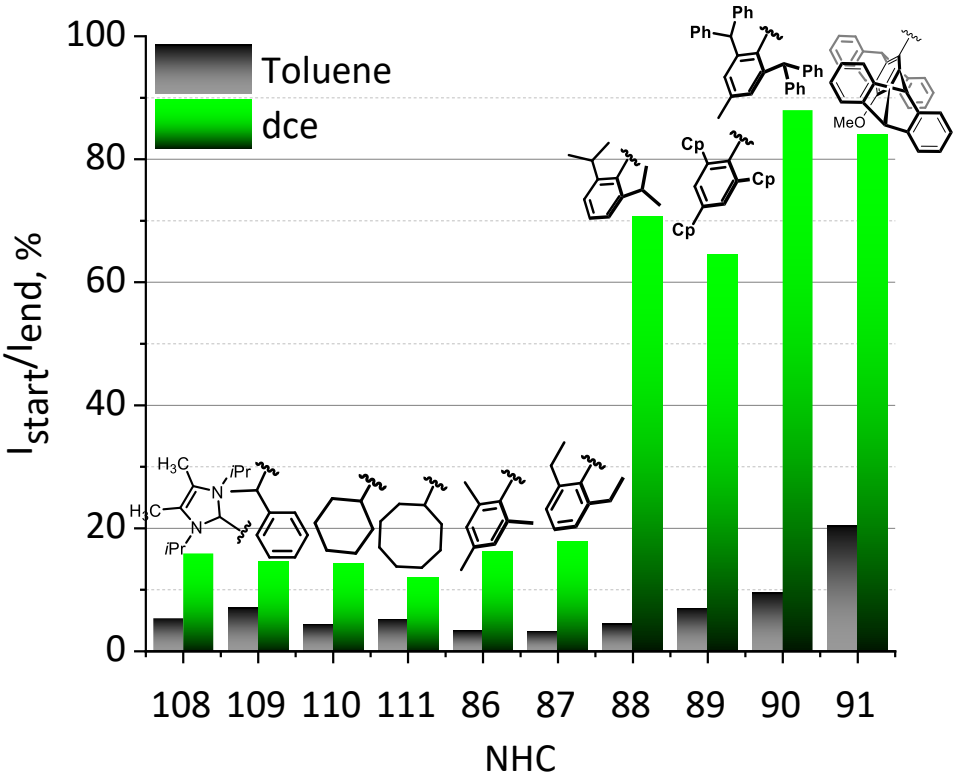

Figure 55 Plot of the relative fluorescence (I_{rel} =I_{start}/I_{end}) for the complexes $[Ir(bdpSO_3)(cod)(NHC)]$ in two different solvents. In black color are initial intensities in toluene and in 1,2-dichloroethane (green). Reproduced from Ref. 157 according to CC BY-NC-ND 4.0 license *(https:/creativecommons.org/licenses/by-nc-nd/4.0/)* using fluorescence intensities only for the toluene and 1,2-DCE solution.

It is difficult to compare to literature data, since crystal structure and DFT-derived differ significantly.[179] In the solid state this buried volume will depend very much on the orientation of the terminal -CH_3 group relative to the metal center. For the ion pairing the

orientation of this -CH_3 groups close to the metal center appears to play only a very minor role. The four complexes with N-alkyl substituents (**108**, **109**, **110**, **111**) are characterized by modest levels of fluorescence ranging from 12.0–15.9 %. This series of complexes is interesting, since significant discrepancies of the buried volume approach and the ion-pair dissociation approach become apparent. Based on the fluorescence (Figure 55) and based on the buried volumes, the NHC ligands in complex **109** and **86** display similar size. The buried volume provided in Table 3 (entry **109**) was determined for the imidazolin-2-ylidne ligands, but it is known, that imidazol-2-ylidene and imidazolin-2-ylidne display very similar buried volumes, which normally differ by less than 1 %.[192] Both NHC in complex **110** (N-Cy^6) and complex **111** (N-Cy^8) are smaller than the NHC in complex **86**, with the N-cyclooctyl NHC being slightly larger than the N-cyclohexyl NHC according to the fluorescence data. Complex **108** with (N-isopropyl and two backbone methyl groups) is interesting since the observed fluorescence intensity is weak (I_{rel} =11.4 %) and the steric demand of this NHC appears to be much lower than for NHC ligands of the IMes series. This is in stark contrast to the buried volume of this NHC ligand, which is given as V_{bur} =38.5 %, while the related complex without backbone methyl groups has V_{bur} =28.2 %. The reason for the huge buried volume of complex **108** is the solid state structure in which both methyl groups of isopropyl point towards the gold, while H of isopropyl points towards the backbone substituents.[199] The large buried volume of this NHC ligand was discussed by Truscott *et al*.[200] and according to DFT calculations (B3LYP/6-31 +G*) the isomer with the two methyl groups of the isopropyl group pointing towards the backbone methyl was calculated to be approx. 7 kcal/mol less stable than the 180°-rotamer with the isopropyl hydrogen pointing towards the backbone methyl groups.[201] Based on the fluorescence data reported here it seems, that for the [Ir(bdpSO_3)(cod)(NHC)] complexes the rotamer with the methyl groups pointing towards the metal center does not contribute significantly and that the buried volume of NHC **108** is much smaller than previously believed.

Solvent titration experiments. Fluorogenic titration experiments can be a useful approach for the investigation of the effects of coordinative ligands in ion pairing ligand-substrate interactions. Initially, toluene solutions of different [Ir(bdpSO_3)(cod)(NHC)] complexes (c =1.0 · 10^{-6} mol/L) were titrated with DMAc and the fluorescence determined after each addition (Figure 56). The initial fluorescence (without any added DMAc) is weak, since anion and cation form close ion-pairs in which iridium quenches the fluorophore. Nonetheless, even the toluene solutions show slightly different fluorescence levels, which appear to be sorted according to the steric bulk of the respective NHC ligand. The addition of polar solvent (DMAc) to a toluene solution leads to an up to 12-fold increase in fluorescence (Figure 56). The final intensity corresponds to the fluorescence of the fully separated ion-pair, which is the same regardless of the nature of the initial complexes. The effect of steric bulk on the ion pairing is again visible, since complexes with bulky NHC ligands (**90** and **91**) reach the maximum fluorescence much earlier - *i. e*. upon addition of less polar DMAc than complexes with less bulky NHC ligands (**86** and **88**).

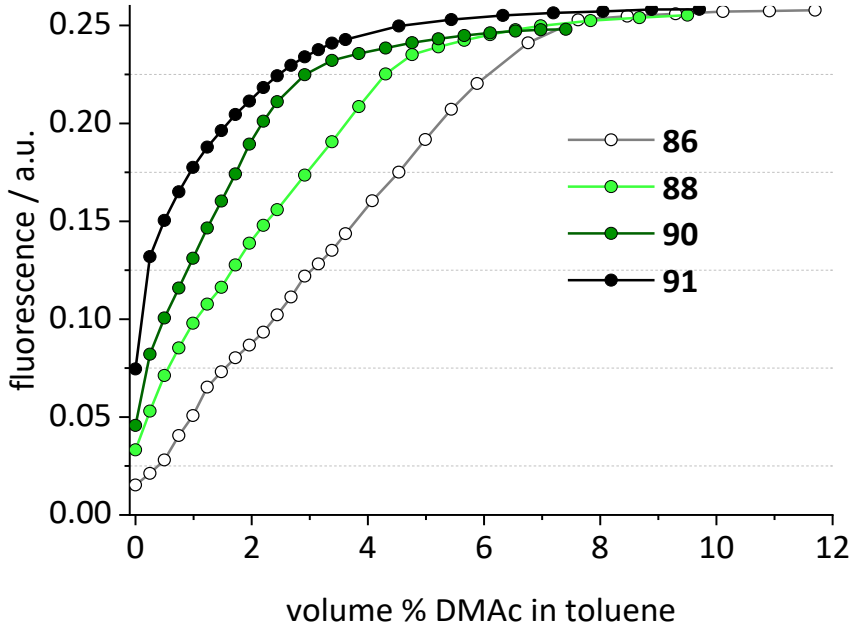

Figure 56 Fluorescence of complexes [Ir(bdpSO$_3$)(cod)(NHC)] (NHC =**86**, **88**, **90** and **91**) (c = 1.0 · 10^{-6} mol/L) in toluene with addition of DMAc (fluorescence dilution corrected). Reproduced from Ref. 157 according to CC BY-NC-ND 4.0 license *(https://creativecommons.org/licenses/by-nc-nd/4.0/).*

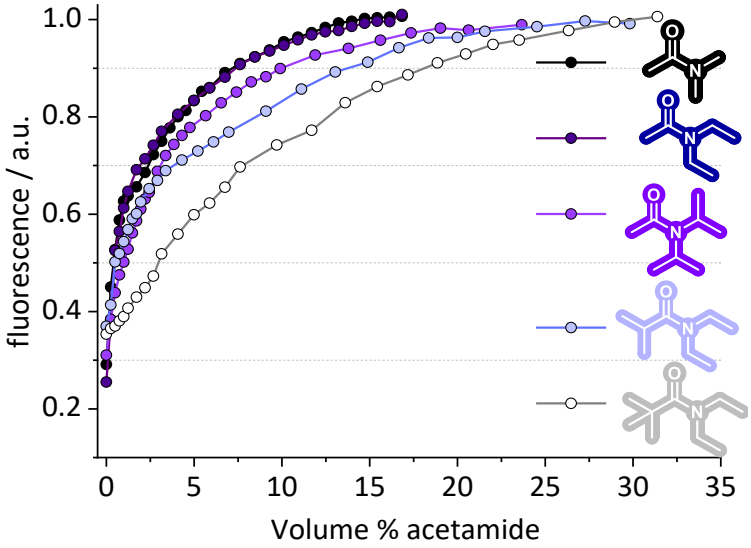

Figure 57 Plot of fluorescence change for complex [Ir(bdpSO$_3$)(cod)(**91**)] (c =1.0 · 10^{-6} mol/L) in toluene *vs.* added volume-% of acetamide (fluorescence dilution corrected).

[Ir(bdpSO$_3$)(cod)(**91**)] complex based on the bulky pentiptycene NHC ligand was used to examine the impact of steric bulk of the coordinative acetamides to the metal centre with modified acetyl- and amine- substituents (Figure 57). The addition of 5 different acetamides to a toluene solution with the corresponding metal complex leads to a different increase in the fluorescence signal where the effect of steric nature of coordinative ligand (acetamide) in ion separation is visible. Such titration experiment shows that acetamides with bigger alkyl groups reach the maximum fluorescence much later.

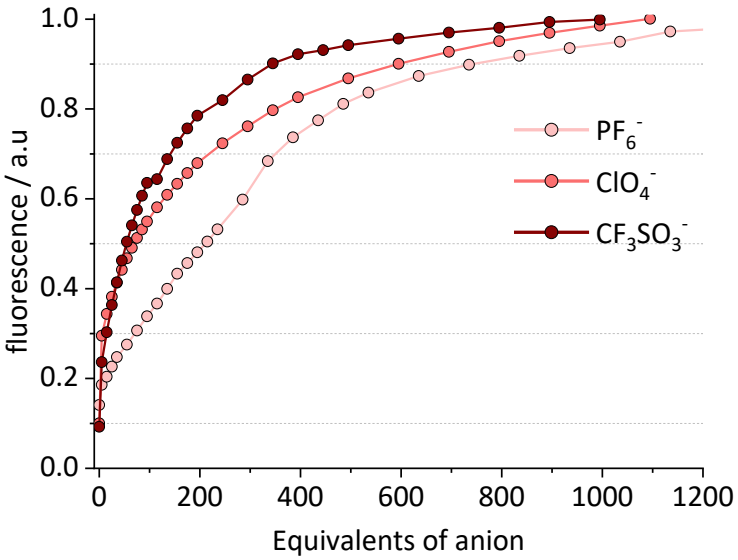

Figure 58 Plot of fluorescence change for complex [Ir(bdpSO$_3$)(cod)(**88**)] (c =1.0 · 10^{-6} mol/L) in toluene *vs*. added amount equivalents of NBu$_4$X salt (X = $CF_3SO_3^-$, ClO_4^-, PF_6^-) (fluorescence dilution corrected).

A similar approach using [Ir(bdpSO$_3$)(cod)(**88**)] was applied for the investigation of ion exchange reactions by addition of weakly coordinative anions that can bind to strongly electrophilic metal centres (Figure 58). Understanding of anion/catalyst interactions is crucial aspect in understanding and development of successful catalytic systems.[202] As shown above, the steric character of ligand is essential in directing of ligand/substrate interactions. We decided to study the ion exchange reaction by the addition of weakly coordinating anions $CF_3SO_3^-$, ClO_4^-, PF_6^- (as NBu_4^+ salts) to a toluene solution of the corresponding metal complex. According to the data from the titration experiment we obtained different fluorescence trends of anion exchange at the metal centre. Anions with higher coordinating tendency to the metal centre reach higher fluorescence intensity faster in order $CF_3SO_3^-$ > ClO_4^- > PF_6^- where hexafluorophosphate is the weakest coordinative ion.[203] These preliminary experiments illustrate the sensitivity of the fluorescence signal with respect to the nature of the NHC ligand.

3.2.4. Evaluation of electronic NHC ligand properties *via* fluorescence ion pairing

Numerous experimental and theoretical methods are used for the determination of the electronic properties of N-heterocyclic carbenes ligands to transition metals.[151,192,204,205] The classic Tolman approach based on [Ni(CO)$_3$(NHC)] complexes utilizing ν(CO) is still valuable and provides information on the net electron density transferred from the NHC ligand to the metal center. This approach is less convenient with a view to the extreme toxicity of Ni(CO)$_4$[206] and has largely been replaced by a closely related method based on work by Crabtree *et al*. utilizing other carbonyl complexes [M(CO)$_2$X(NHC)] (M =Rh, Ir and X = Br, Cl).[207] This approach was later unified by Nolan *et al*. enabling the correlation of the Ni- and the Rh-carbonyl scale,[160] while Plenio and Wolf linked the Rh- and Ir-based scales to the Tolman parameters.[208] However, the choice of the metal carbonyl was believed to be arbitrary, but Belpassi *et al*. Showed recently, that for [Au(CO)(NHC)]$^+$ complexes the ν(CO) primarily depends on the metal-to-ligand π back-donation.[209]

The redox potentials of [IrCl(cod)(NHC)] complexes are another useful parameter for the determination of electronic properties of NHC ligands.[154,210] Even though the Ir(I/II) redox potential primarily probes the ability of the ligand to stabilize higher oxidation states at the metal center, this parameter was shown to reflect the respective ν(CO) data.[204,208] NMR spectroscopy has also been employed to better understand the electronic properties of NHC ligands. The use of ^{13}C chemical shift of the carbene carbon atom in palladium(II)-benzimidazolylidene complexes were suggested by Huynh *et al*.,[211] while Ganter *et al*. showed the respective azolium ^{13}C-^{1}H coupling constants to be a measure of the donor capacity of the respective NHC ligands.[212] ^{13}C-NMR was proposed by Tarantelli, Belpassi *et al.* to measure σ-donor properties of NHC ligands in gold(I) complexes.[213]

The NMR shifts of the ^{31}P NMR resonances in phosphinidene complexes and of the ^{77}Se resonances in selenoureas were proposed by Bertrand *et al*.[214] and Ganter *et al*.[215] as a measure of the π-accepting abilities of the respective NHC ligands. DFT calculations by Cavallo *et al*. support the usefulness of this method,[216] while Huynh points to some inconsistencies, possibly due to the interference of steric effect on the ^{77}Se NMR shifts.[151] Bond dissociation energies of carbonyl gold complexes have also been proposed as a measure for ligand effects including NHC ligands.[217]

Based on the knowledge that several methods for the determination of the electronic properties of NHC ligands utilize [IrCl(cod)(NHC)] and the closely related [IrCl(CO)$_2$(NHC)] complexes.[192] It appears that the fluorescence method described here also relies on [IrCl(cod)(NHC)] complexes for which the weakly coordinating bdpSO$_3^-$ simply replaces the chloride ligand.

For the characterization of electronic dependencies in ion separation for modified NHC ligands complexes **92–103** were synthesized (Figure 59). We decided to use structurally very similar materials and only differ with respect to the nature of the *p*-substituent at the N-aryl rings (*p*-R =NEt$_2$, OMe, H, Br, OAc, SOtol, OTf, SO$_2$tol) of the imidazolylidene. Most complexes of the IMes series display only weak fluorescence in toluene than pure 1,2-DCE.

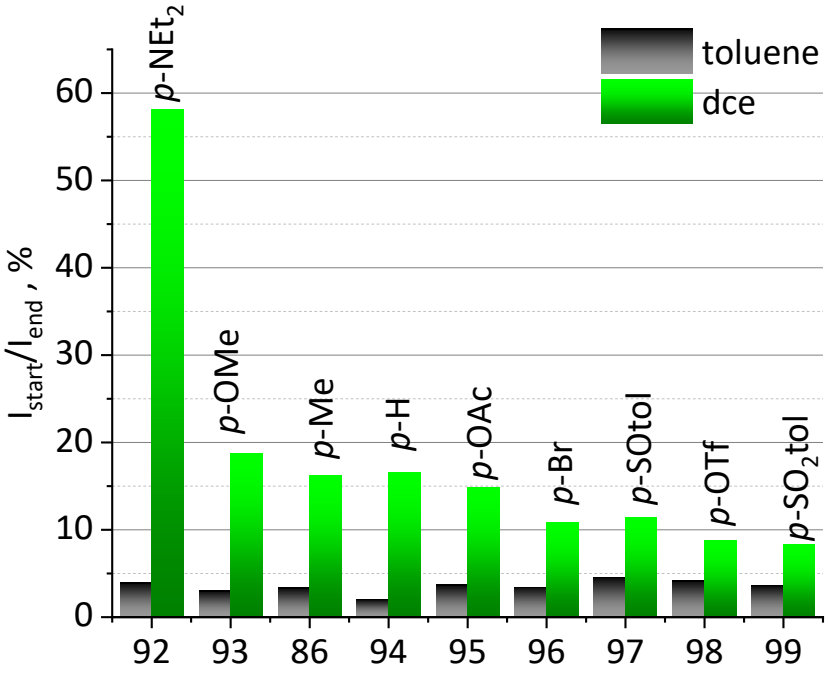

Figure 59 Plot of the relative fluorescence (I_{rel} =I_{start}/I_{end}) for the complexes [Ir(bdpSO$_3$)(cod)(NHC)] (NHC =**86, 92–103**) of the IMes series in two different solvents.

In black color are initial intensities in toluene and in 1,2-dichloroethane (green). Reproduced from Ref. 157 according to CC BY-NC-ND 4.0 license (*https:/creativecommons.org/licenses/by-nc-nd/4.0/)* using fluorescence intensities only for the toluene and 1,2-DCE solution.

The dissociation of the complexes into separated ion pairs is not pronounced due to the moderate steric bulk of the NHC ligands – with the exception of the most electron-rich complex **92**. Since the steric bulk of the different NHC ligands in the IMes series is very similar, the fluorescence modulation is predominantly caused by the different donation of the IMes-type NHC ligands. Obviously, in the more electron-rich complexes the dissociation into solvent-separated ions is facilitated, since electron-rich NHC substituents stabilize the respective cationic iridium complex.

Probing the Ir(I/II) redox potentials. In order to distinguish between steric and electronic effects of the NHC ligands on ion-pairing, the electronic properties of all NHC ligands employed in this study need to be determined. The M(I/II) redox potentials of [MCl(cod)(NHC)] (M = Ir, Rh) were previously established to be a measure of the electron donating ability of the respective NHC ligands.[154,208] The respective Ir(I/II) redox potentials of all [IrCl(cod)(NHC)] complexes (Scheme 11) were measured or taken from the literature (Table 3).

With the exception of three N-alkyl NHC complexes (**109**, **110**, **111**), the electrochemistry of the iridium complexes is well-behaved. The complexes are characterized by reversible redox waves with oxidation/reduction wave separations in the range of 64–96 mV. In the full data set, several subsets can be identified (*e.g.* IMes series and IPr series), in which substituents at certain positions are changed in a systematic manner, to change NHC donation while the steric bulk of the NHC ligand remains constant. The influence of the various *p*-R substituents in the N-aryl NHC complexes on the Ir(I/II) redox properties is pronounced. This is evidenced by the almost 300 mV range of the redox potentials depending on the nature of the substituents – despite the fact, that the N-aryl rings are orthogonal to the respective central imidazolylidene ring. There is considerable evidence in the literature, that the N-aryl rings are able to directly interact with the metal center *via* π-face interactions[210,218] leading to an efficient transfer of electronic information between the N-aryl ring and the metal center.

For complexes **92–103**, an excellent correlation of Hammett parameters of the nature of the *p*-R substituents and redox potentials was observed (Figure 60). The closely related IPr-series of complexes (**88, 104, 105, 106**) display analogous changes in the redox potentials. A note concerning the Hammett constant of OC(O)Me is required. The tabulated value for this group is σ_p =0.31,[219] which would make it an outlier in Figure 60. But this value may not be correct since it is unlikely, that the acetoxy group is more electron withdrawing than the closely related OC(O)Ph substituent (σ_p =0.13). This peculiarity concerning the acetoxy substituent was noted previously by Papp *et al.* and a revision of the respective Hammett constant suggested;[220]their value (σ_p = 0.08) is used in Figure 60.

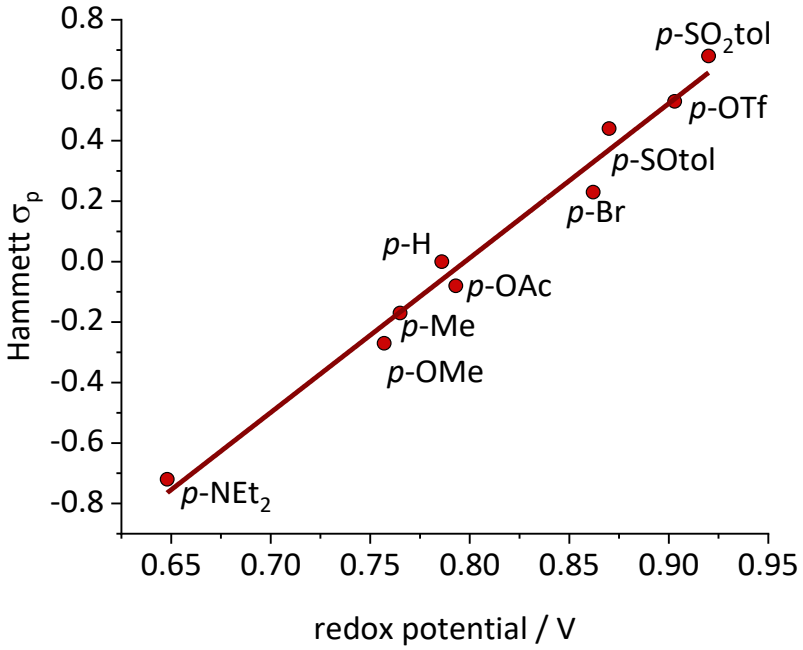

Figure 60 Plot of the Hammett constants of the respective *p*-R substituents and the redox potentials for [IrCl(cod)(NHC)] (NHC = **92–103**). Reproduced from Ref. 157 according to CC BY-NC-ND 4.0 license *(https://creativecommons.org/licenses/by-nc-nd/4.0/).*

The redox potentials are sensitive to small changes of the N-aryl substituents: Complexes **86** ($E_{1/2}$ =0.765 V), **87** ($E_{1/2}$ =0.748 V) and **88** ($E_{1/2}$ =0.762 V) serve as an instructive example: Complex **86** has three methyl groups on each N-aryl ring, complex **87** has two ethyl groups and complex **88** has two isopropyl groups on each N-aryl ring.

Consequently, the steric bulk of the NHC ligands in complexes **92–103, 101** and **102** is very similar and the NHC ligands primarily differ with respect to the electronic properties. The remaining complexes in Table 3 show less variation in the electronic properties and more steric variations. Most redox potentials are within expectations based on the nature of the NHC-substituents. For a few complexes significant deviations from the expected redox potentials were observed (complex **90** and **91**), which will be discussed later in the context of infrared spectroscopy-based determinations of NHC electronic parameters.

The cyclic voltammograms of the N-alkyl NHC complexes **109, 110** and **111** are not fully reversible, thus the Ir(I/II) redox potentials lack precision. The redox potential of those N-alkyl NHC complexes show nearly the same redox potentials. Complex **108** is oxidized at considerably more cathodic redox potential ($E_{1/2}$ = 0.754 V)—again the effect of the two backbone methyl groups on the redox potential is significant.

Correlation of fluorescence data and redox potentials. In order to resolve the combined influence of sterics and electronics on the fluorescence of the respective [IrCl(cod)(NHC)] complexes, the Ir(I/II) redox potential (as a descriptor of the electronic properties of NHC ligands) and the fluorescence are correlated. The plot of redox potentials $\Delta E_{1/2}$ and the relative fluorescence intensities (I_{rel}) for complexes of the electronic subset (Figure 61, red data set for IMes-type complexes and blue data set for IPr-type complexes) can both be fitted with simple exponential functions.[221] Alternatively, based on ln(K) ≈ ΔE, a linear plot is shown in Figure 62.[222]

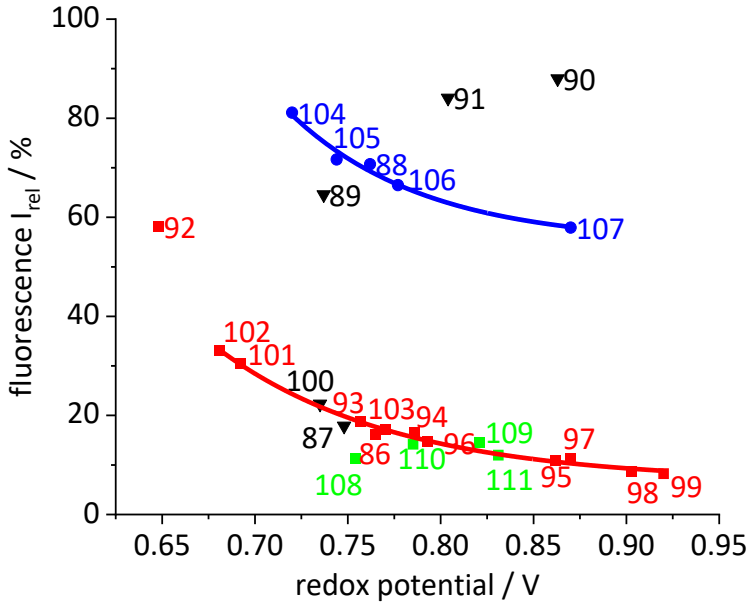

Figure 61 Relative fluorescence intensity of [Ir(bdpSO$_3$)(cod)(NHC)] *vs.* redox potential plot for all [IrCl(cod)(NHC)] complexes in 1,2-dichloroethane. Reproduced from Ref. 157 according to CC BY-NC-ND 4.0 license *(https:/creativecommons.org/licenses/by-nc-nd/4.0/)* with addition of non-linear fit for the IPr-type complexes.

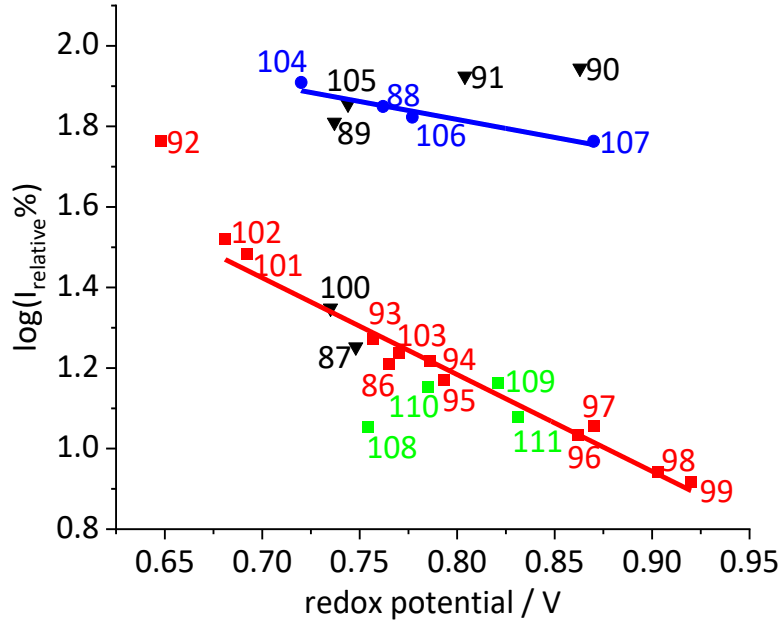

Figure 62 log($I_{relative}$%) of [Ir(bdpSO$_3$)(cod)(NHC)] complexes in 1,2-dichloroethane *vs.* redox potential plot for all [IrCl(cod)(NHC)] complexes in 1,2-dichloroethane. Reproduced from Ref. 157 according to CC BY-NC-ND 4.0 license *(https:/creativecommons.org/licenses/by-nc-nd/4.0/)* with addition of linear fit for the IPr-type complexes.

The only outlier in the red series of complexes is complex **92**. We consider it less likely, that the higher-than-expected fluorescence is caused by the interaction of the cationic Ir with the weakly coordinating aryl-NEt$_2$ substituent. In the various solvent titration experiments with acetamides the addition of such small amounts of donating ligand has no measurable influence on the fluorescence (Figure 56). Eventually, the basic

nitrogen atom is partially protonated by adventitious acid (CO_2/H_2O) and the derived counter anion interferes with the $bdpSO_3^-$ coordination. Such contamination cannot be excluded with certainty, since the experiments are done in very dilute (micro-molar) solutions.

Based on the analysis of red set of metal complexes containing ligands with variable donicity but similar sterics, it is possible to deconvolute the steric and the electronic influence of NHC ligands in the respective metal complexes. The vertical distance ($\Delta\log I_{rel}\%$) between the red linear fit curve (Figure 62) may be used as a relative steric denominator termed Fluobulk (fluorescence bulk) given relative to the IMes series of complexes. For example, for complexes **88** (Fluobulk = +1.28), **89** (Fluobulk = +1.03), **90** (Fluobulk = +1.17) and **91** (Fluobulk = +1.34). Therefore, pentiptycene based NHC ligand is by far the bulkiest NHC ligand studied here.

Correlation of fluorescence and carbonyl frequencies data. The influence of the electronic properties of the NHC ligands on the ion pairing can also be evaluated using the established Tolman electronic parameter or as an equivalent the average of the respective symmetric and antisymmetric ν(CO) in [IrCl(CO)$_2$(NHC)] complexes (Figure 63). This is also helpful, since the electrochemistry of three N-alkyl complexes displays only partial reversibility. In order to obtain a consistent data set minimizing the effect of IR measurements conditions on the ν(CO) no spectroscopic data from the literature were used – except for a few complexes reported by Duckett *et al.*,[179] whose IR data for similar complexes are virtually identical to the data measured by us. The data used were taken from our previous reports, missing IR spectra for known or for new complexes were measured under the same conditions to obtain a uniform data set.

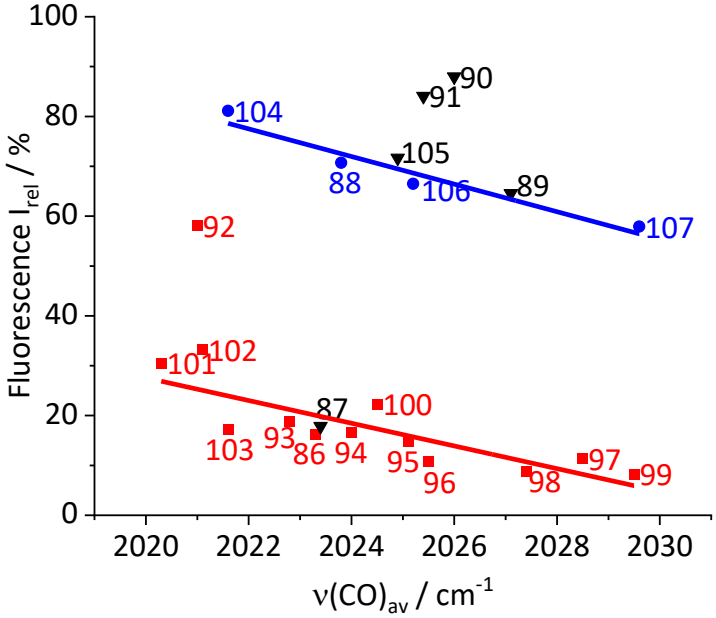

Figure 63 Relative fluorescence intensity ($I_{relative}\%$) of [Ir(bdpSO$_3$)(cod)(NHC)] complexes in 1,2-dichloroethane *vs.* the average of $\nu(CO)_{av}$ for [IrCl(CO)$_2$(NHC)] in CH_2Cl_2. Reproduced from Ref. 157 according to CC BY-NC-ND 4.0 license (*https:/creativecommons.org/licenses/by-nc-nd/4.0/)*with addition of linear fit for the IPr-type complexes.

Again, the data set is split up into four different subunits: IMes series (**red**), IPr series (**blue**), and other complexes (**black**). The systematic change of NHC donation in the IMes and the IPr series can be fitted with linear functions. As evidenced by the systematic

changes in the IMes and IPr series of complexes, this approach appears equally valid – even though the correlation coefficient of the linear fit is significantly smaller than for the redox potential fit. However, it should also be taken into account, that the experimental error of the ν(CO) accounts to at least 1 cm^{-1}.[223] This is significant compared to the signal dispersion, while the error of the redox potential determination relative to the dispersion of the redox potentials is below 10 mV for reversible voltammograms. The next question concerns the validity of the determined redox potentials. The redox potentials of a few complexes show unexpected values. The redox potential of complex **90** was determined as $E_{1/2}$ = +0.863 V, which is much more anodic than what might be expected based on the four *ortho*-$CHPh_2$ of the N-aryl ring. Based on the redox potential of complex **106** (containing two *para*-$CHPh_2$ substituents the -$CHPh_2$ substituent can be considered to be a very weakly electron withdrawing group since the redox potential is shifted by only 29 mV relative to that of complex **105** (has two *para*-H instead of two *para*-$CHPh_2$).

The redox potential of complex **91** ($E_{1/2}$ = +0.804 V) is also observed at much higher redox potential than expected –based on the substituents at the N-aryl rings (each N-aryl groups has four donating alkyl substituents and a donating *para*-OMe group) and the redox potential could have been expected to be at least 100 mV more cathodic. Based on this, one might argue that the redox potentials of [IrCl(cod)(NHC)] complexes with sterically highly demanding NHC ligands are shifted as a result of the encumbered geometry at the metal center, *i. e.* that the redox potential depends on the steric bulk of the NHC ligands.

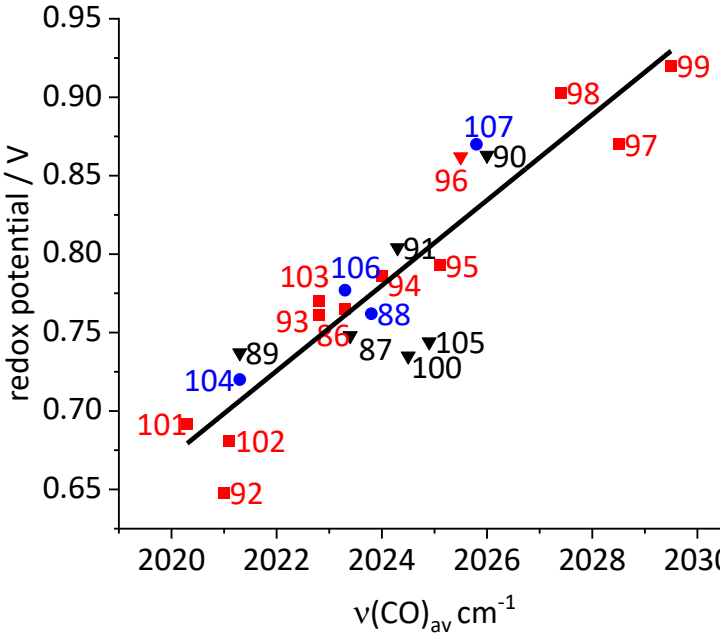

Figure 64 Redox potential of [Ir(bdpSO_3)(cod)(NHC)] complexes *vs.* averaged carbonyl wavenumbers $\nu(CO)_{av}$. Reproduced from Ref. 157 according to CC BY-NC-ND 4.0 license *(https://creativecommons.org/licenses/by-nc-nd/4.0/).*

In order to resolve such issues a correlation of the Ir(I/II) redox potentials of [IrCl(cod)(NHC)] complexes and the $\nu(CO)_{av}$ /cm^{-1} of [IrCl$(CO)_2$(NHC)] was done (Figure 64). The linear fit in the plot relies on the red, blue and black data set. For the data points close to the linear fit, the IR spectroscopic data and the redox potentials appear to be correlated and are thus considered valid. Especially the data points for the aforementioned complexes **90** and **91** are very close to the linear fit and the two redox potentials are thus considered to be representative of the "true" NHC donation.

3.2.5. **Photosensitising activity of Bodipy ion paired NHC-iridium complexes** (*Part 3*)

This chapter has been published in: S. Popov, H. Plenio, *"Switched fluorescence and photosensitization based on reversible ion-pairing", Chem. Commun.,* **2022**, *58,* 12669. *https://doi.org/10.1039/D2CC05195H*.

In this chapter presented a novel general concept for tunable photosensitizers, which relies on variable ion-pairing of a cationic NHC-iridium complex and an anionic fluorescent dye. As was shown above, ion-pairing of [Ir(cod)(NHC)]$^+$ complexes and Bodipy-sulfonate **114** (bdpSO$_3^-$) in solvents of low polarity (toluene) leads to the fquenching of the fluorescence, which is restored upon spatially separating the anion and the cation. This observation leads to the question of whether the excitation energy in the close ion-pair is lost or whether the 5d-metal iridium in close vicinity to the dye enables intersystem crossing leading to a PS that enables the formation of singlet oxygen $^1O_2$.[117]

First, the PS properties of the close ion-pair of [Ir(bdpSO$_3$)(cod)(**86**)] in toluene solution were studied. The generation of $^1O_2$ was quantified utilizing the cycloaddition reaction with 1,3-Diphenylisobenzofurane (DPBF)[165] and by monitoring the decrease of the 410 nm DPBF absorbance with time *via* UV/Vis-spectroscopy. The linear plot of absorbance *vs.* time corresponds to a zero-order reaction and the slope indicates the rate of photooxidation, which corresponds to the rate of $^1O_2$ generation.[166,224] [Ir(bdpSO$_3$)(cod)(**86**)] was found to be highly active in the generation of $^1O_2$ and k(po)= 0.048 s^{-1} is close to that of 2,6-diiodobodipy benchmark k(po)= 0.081 s^{-1}. The background activity of the fluorescent dye in the absence of a 5d-metal in the respective silver salt [Ag(bdpSO$_3$)] **114** is negligible at k(po)= 0.002 s^{-1}.

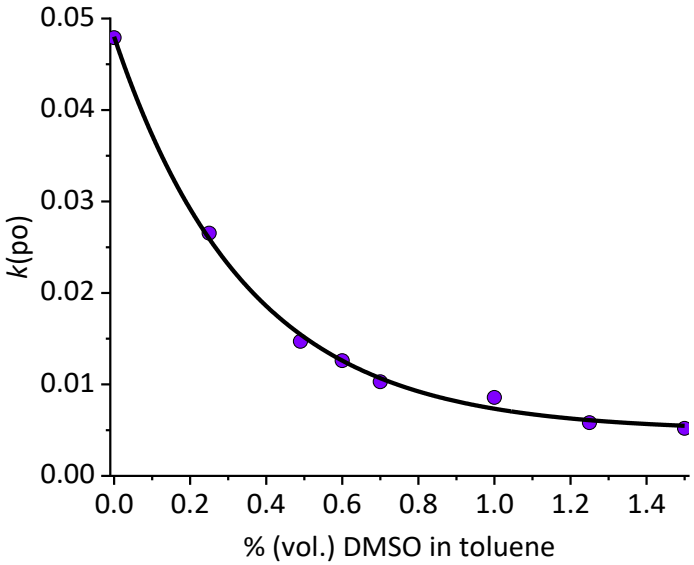

Figure 65 Rate of photooxidation k(po) by [Ir(bdpSO$_3$)(cod)(**86**)] in toluene solution (c = 1.0 μM) containing different amounts of DMSO upon irradiation at 510 nm (exponential fit R^2= 0.999). Reproduced from Ref. 266 according to CC BY-NC 3.0 license *(https://creativecommons.org/licenses/by-nc/3.0/)*.

Next, was tested how the anion-cation interactions affect k(po). To a toluene solution of [Ir(bdpSO$_3$)(cod)(**86**)] aliquots of DMSO were added and the rate of photooxidation was determined (Figure 65). Obviously, the addition of DMSO enhances

the separation of the ion pair and the increased distance between the fluorescent dye and the triplet sensitizer decreases the efficiency of photooxidation since the excitation energy remains in the singlet states. The PS activity of the complex can thus be tuned to any desired value between the activity of the close ion-pair and almost zero for the separated ion-pair.

The fluorescence of the solution increases upon addition of DMSO, since the probability of intersystem crossing decreases with increasing distance of fluorophore and 5d metal ion. Based on this, the $^1O_2$ generation is switched-off in polar solar solvents and switched-on in non-polar solvents.

The next question concerns the fate of the excitation energy. For toluene solutions of [Ir(bdpSO$_3$)(cod)(**86**)] containing variable amounts of DMSO (0 - 1.5 %-vol.) with different cation-anion interactions, the fluorescence was correlated with the rate of photooxidation (Figure 66). The linear relationship displayed shows, that in the solvent-separated ions the 510 nm light excitation populates the S_1 state and that upon increasing association of anion and cation this excitation energy is gradually transferred into the T_1 state - as evidenced by the PS properties. It can be concluded, that the population of the excited singlet state for the close ion pair is primarily converted into the respective triplet state.

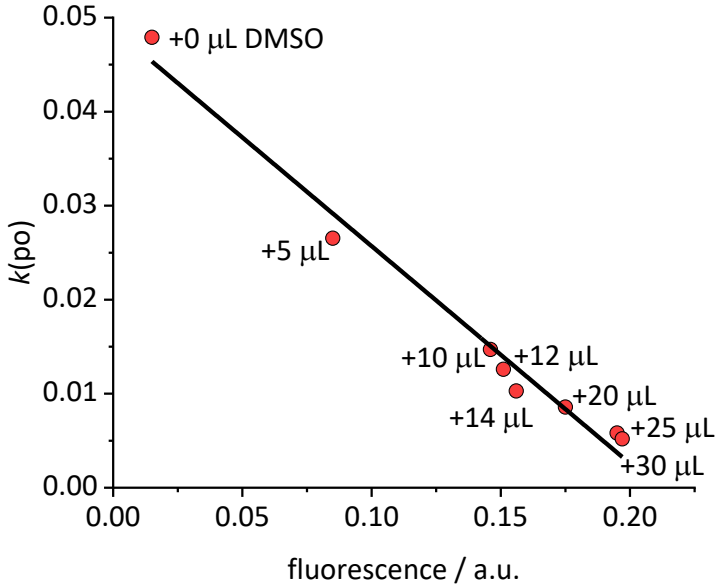

Figure 66 Plot of the rates of photooxidation *k*(po) (corresponding to the generation of singlet oxygen $^1O_2$) by [Ir(bdpSO$_3$)(cod)(**86**)] complexes in toluene solution (*c* = 1.0 µM) *vs*. the fluorescence after addition of designated aliquots of DMSO to the initial toluene solution (linear fit R^2= 0.98) upon irradiation at 510 nm. Reproduced from Ref. 266 according to CC BY-NC 3.0 license *(https://creativecommons.org/licenses/by-nc/3.0/)*.

An ideal switch is characterized by repeated on-off events. This was demonstrated for the model complex [Ir(bdpSO$_3$)(cod)(**86**)]. The separation-recombination of anion and cation was observed *via* monitoring the fluorescence signal (Figure 67). A solution of this complex in toluene (PS = on, fluorescence = off) was treated with one equivalent of a NBu$_4$Br solution. Since the bromide coordinates strongly to the cationic iridium complex, the close ion-pair of [Ir(cod)(NHC)]$^+$ and bdpSO$_3^-$ is separated and [IrBr(cod)(**86**)] is formed (off state = fluorescent and negligible $^1O_2$ formation). Reversibility of the switching process is demonstrated by adding one equivalent of NaBArF (sodium tetrakis[(3,5-trifluoromethyl)phenyl]borate) - a salt with a weakly coordinating anion.[225] Addition of NaBArF induces formation and precipitation of NaBr from the

toluene solution, which appears to be the driving force of this reaction.[226] Since $bdpSO_3^-$ is more strongly coordinating than $BArF^-$ the initial close ion-pair is re-formed. This on-off sequence was repeated five times and each time the fluorescence was restored to its initial value. However, we also observed that after switching off the PS, it cannot be switched on again. Additional experiments were carried out and even the addition of NaBArF to a toluene solution of [Ir($bdpSO_3$)(cod)(**86**)] shuts-down $^1O_2$ production. To rule out interference of the anion, $KCTf_3$ was tested and again the PS effect disappeared. The anion does not seem to be responsible[227] and instead Na^+ appears to be the culprit. Crown ether (18-crown-6) was added to the reaction mixture containing [Ir($bdpSO_3$)(cod)(**86**)] and NaBArF and the PS activity is recovered. It is now assumed, that the addition of NaBArF leads to the formation of an electron-deficient [Ir($bdpSO_3^-$)Na]$^+$ subunit with a bridging sulfonate group, which is inactive as a photosensitizer. This hypothesis led us to study the effect of electron density on the PS properties.

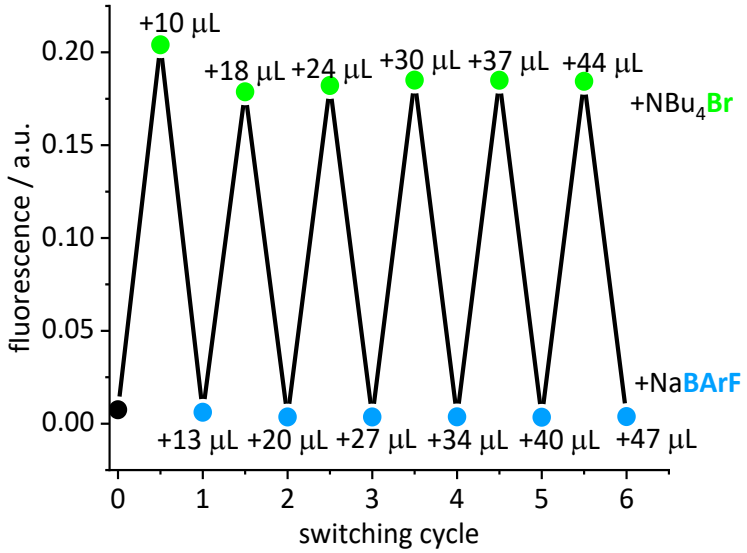

Figure 67 Switched fluorescence for [Ir($bdpSO_3$)(cod)(**86**)] complex (c = 1.0 µM) in toluene after addition of NBu_4Br (c = 0.2 mM) and NaBArF (c = 0.2 mM) solution. Reproduced from Ref. 266 according to CC BY-NC 3.0 license *(https://creativecommons.org/licenses/by-nc/3.0/)*.

Recently, the concept of tuning the energy gap between the lowest singlet excited state S_1 and the lowest triplet state T_1 (ΔE_{ST}) to efficiently utilize the excitation energy has been introduced.[228] We now assume, that by systematically changing the donation of the NHC ligand in the respective [Ir($bdpSO_3$)(cod)(NHC)] complexes, the energies of respective S_1 and T_1 levels can be systematically shifted relative to each other.[229] Consequently, a number of complexes (Scheme 12) with electron donating or electron-withdrawing groups attached to the NHC ligand were studied in $^1O_2$ generation. The donation of the NHC ligands was quantified by determining the Ir(I/II) redox potential of the respective [Ir($bdpSO_3$)(cod)(NHC)] complexes.[154] The modulation of NHC donicity leads to very significant changes in the PS ability. [Ir($bdpSO_3$)(cod)(NHC)] with strongly donating NHC ligands are even more efficient photosensitizers than [Ir($bdpSO_3$)(cod)(**86**)] and the most electron-rich complex p-NEt_2 is the best PS in this series. Related complexes with poorly donating NHC ligands (m-NO_2 **115**) are poor photosensitizers. This observation also explains the behavior of the electron-deficient [Ir($bdpSO_3^-$)Na]$^+$ subunit. It is not obvious, how the Ir(I/II) redox-potentials are correlated with the energy difference between S_1 and T_1 state, but nonetheless a linear

correlation (R^2 = 0.95) of the redox potentials and the rate of photooxidation of the respective complexes is observed over a wide range of redox potentials (Figure 68).

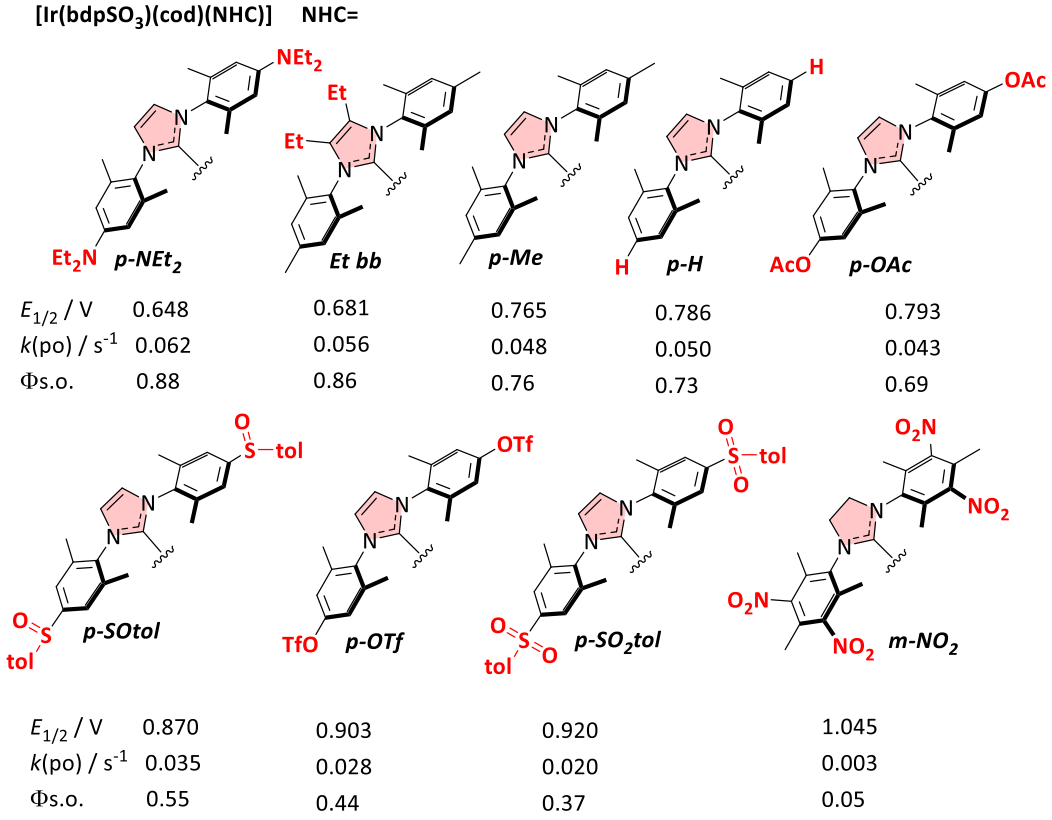

Scheme 12 [Ir(bdpSO$_3$)(cod)(NHC)] complexes studied in the $^1O_2$ generation. The respective redox potentials Ir(I/II) (CH_2Cl_2/NBu_4PF_6 (0.1 M)) and the rates of photooxidation of DPBF are listed below.

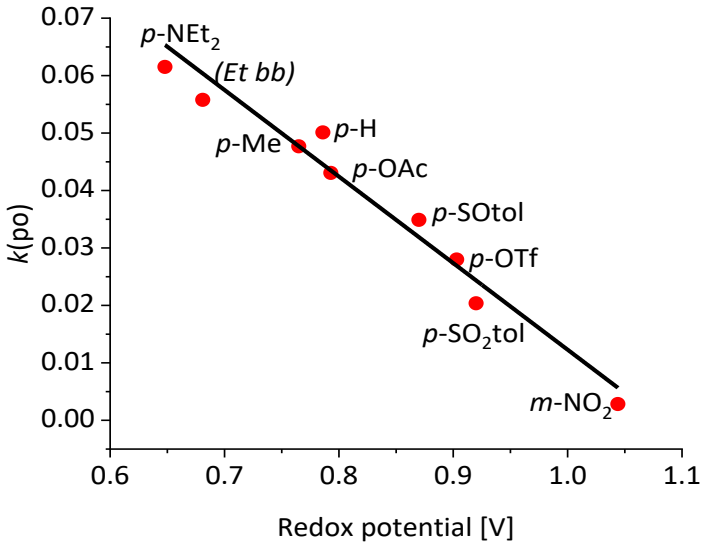

Figure 68 Rate of $^1O_2$ generation *k*(po) by [Ir(bdpSO$_3$)(cod)(NHC)] complexes in toluene solution *vs.* redox potential for [IrCl(cod)(NHC)] complexes in 1,2-dichloroethane. Reproduced from Ref. 266 according to CC BY-NC 3.0 license *(https://creativecommons.org/licenses/by-nc/3.0/)*.

3.3. **Fluorescent Organometallic Dyads and Triads** (*Part 4*)

This chapter has been published in: Y. Shinozaki, S. Popov (shared first author), H. Plenio, "*Fluorescent organometallic dyads and triads: establishing spatial relationships*", *Chem. Sci*., **2023**, *14*, 350. https://doi.org/10.1039/D2SC04869H.

My own contributions to this work are the following:

- involvement in conceiving the project;
- design of the experiments (ion pairing via FRET, formation of triad, blue-red-green FRET evaluation, *etc.*);
- performing the experiments and formal analysis (i.e., NMR, MS, fluorescence, and UV/Vis measurements);
- synthesis of the studied compounds (red *meso*-alkyl Bodipy, blue Bodipy, FRET metal complexes for triad and ion pairing experiments, *etc.*).
- Writing the supporting information.

Linking molecular fragments through chemical bonds to generate more complex species defines synthetic chemistry.[230–232] Isolation of newly generated molecules allows their identification using established physical techniques, like NMR spectroscopy. In a non-covalent setting the species generated are characterized by significant dynamics and the rapid interconversion of numerous species may preclude the isolation of a single reaction product whose formation is governed by numerous equilibria involving the individual building blocks.[230,231] In such cases it may be difficult to establish connectivities between the different molecular fragments. FRET is a potential tool to study molecular interactions and dynamic changes. Primarily in biochemistry, biology and medicine the use of fluorescent dyes utilizing FRET (fluorescence or Förster resonance energy transfer) is ubiquitous[11] and known to provide information about conformational changes involving proteins and DNA[233] or intracellular dynamics,[234] but also in polymer chemistry[235] and supramolecular chemistry.[236] FRET is a non-radiative process in which an excited donor dye transfers energy to an acceptor dye in the ground state through long-range dipole/dipole interactions.[1,237] This approach relies crucially on suitable fluorescent dyes (FRET pairs) developed in the last couple of decades, and which are characterized by proper functional groups to enable bioconjugation and compatibility with typical biochemical environments and aqueous solutions.[238]

Organometallic chemistry mostly takes place in a non-aqueous environment, rendering fluorophores used in biochemistry less suitable. Lewis basic heteroatoms are undesirable in organometallic chemistry, since they potentially coordinate the metal centers. Bodipy based dyes[29,239] are proving to be very useful in organometallic chemistry.[86,87,139,162] Numerous applications of this dye for mechanistic studies of chemical reactions involving single molecules or single particles utilizing fluorescence microscopy have been reported[240]– with major contributions by the Blum group.[130,131,241]

However, only a few FRET pairs based on Bodipy dyes have been reported in the literature.[242] Diederich *et al*. reported on a FRET pair composed of a green and a red Bodipy FRET pair, which were attached to a resorcin[4]arene cavitand. A Förster radius of approx. 3.7 nm was determined, which is huge compared to the size of typical organometallic complexes.[243] Conceptual work from Lim and Blum[137] reports on a

palladium complex incorporating an allylic ligand tagged with a green fluorophore and a phosphine ligand tagged with an orange fluorescent dye in the coordination sphere. Upon green excitation the close vicinity of the two dyes leads to efficient resonance energy transfer evidenced by an orange fluorescence upon excitation of the green Bodipy. Plenio *et al*. utilized the Diederich FRET pair in NHC-metal complexes to achieve large virtual Stokes shifts for CO detection.[163] The same group showed for closely related fluorophores, that FRET is also observed upon dimerization of NHC-gold complexes.[244] However, significant problems for practical applications remain. The synthesis of the previously used red Bodipy is cumbersome and furthermore the chemical stability of the Diederich red Bodipy in an organometallic environment is rather limited and significantly improved red fluorophores are clearly needed.

This chapter is devoted to the synthesis of organometallic complexes utilizing a stable and readily available red fluorophore with convenient linker groups, and demonstrate organometallic chemistry applications of a new green-red FRET pair with excellent chemical and photochemical stability as well as a related blue-green dyad. The newly established dyad is extended by a blue Bodipy[245] to provide a useful triad, in which the blue excitation energy is transferred to the green fluorophore, followed by transfer to the red fluorophore whose emission is observed when spatial vicinity between the three dyes is given.

3.3.1. Synthesis of red and green NHC-metal complexes

Red Bodipy-substituted azolium salts were synthesized as outlined in Scheme 13. The literature procedure for the cyclization of the tosylated pyrrole **116**[246] to the spiro-Bodipy was modified. In our hands the original procedure for the Pd/phosphine catalyzed ring-closing reaction generates significant amounts of the undesired β-isomer instead of the desired α-isomer (Scheme 13), whose separation is difficult.

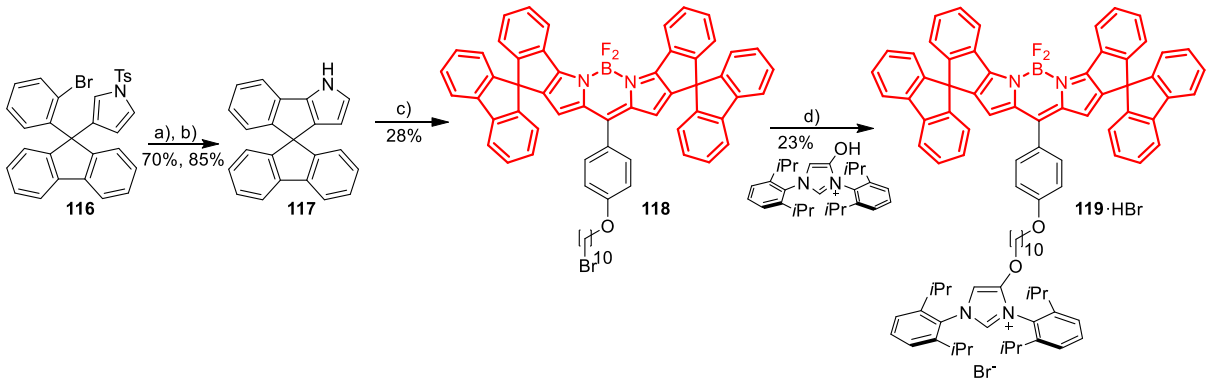

Scheme 13 Synthesis of red imidazolium salts. Reagents and conditions: a) $Pd(OAc)_2$, DMF, K_2CO_3, 100 °C, 20 h; b) Cs_2CO_3, THF/MeOH, rt, 24 h; c) alkylation with 1,4-(CHO),(O$(CH_2)_{10}$Br)C_6H_4, followed by addition of TFA, CH_2Cl_2, 3 h then DDQ, 1 h then $BF_3{\cdot}Et_2O$, Et_3N, 3 h; d) K_2CO_3, KI, acetone, reflux, 12 h. Reproduced from Ref. 249 according to CC BY-NC 3.0 license *(https://creativecommons.org/licenses/by-nc/3.0/)*.

Since it is known, that direct arylation reactions do not necessarily require additional phosphine ligands, ligand-free approaches for the cyclization were tested and optimized.[246,247] Using $Pd(OAc)_2$ in DMF in the absence of phosphine provides the α-isomer as the predominant cyclization product in 70% yield (β-isomer <1%). The detosylation of spiro-pyrrole was done by simply stirring the protected pyrrole with Cs_2CO_3 base in THF/MeOH and gave spiro-pyrrole **117** in 85% yield. The reaction of spiro-

pyrrole **117** with benzaldehydes provides the respective Bodipy derivatives **118** and **119**·HBr following established procedures for related compounds.[163] The alkylation of the phenolic hydroxy-imidazolium salt with **118** provides azolium salt **119**·HBr tagged with a red spiro-Bodipy.[138] This ether forming reaction requires very long alkyl chains (here -$(CH_2)_{10}$Br), since for shorter linkers, like (-$(CH_2)_6$Br) significant product formation was not observed. Comparable observations were made before and the lack of reactivity for the shorter linkers is attributed to the steric bulk of the two building blocks (spiro-Bodipy and imidazolium salt).[86]

The red *meso*-aryl Bodipy **118** turns out to be highly stable towards the basic reaction conditions and the same holds true for the green *meso*-alkyl Bodipy **122**. In stark contrast, the red *meso*-alkyl Bodipy **120** (Figure 69) is highly sensitive towards the basic reagents used in metal complex synthesis and not suitable for the synthesis of NHC-metal complexes.

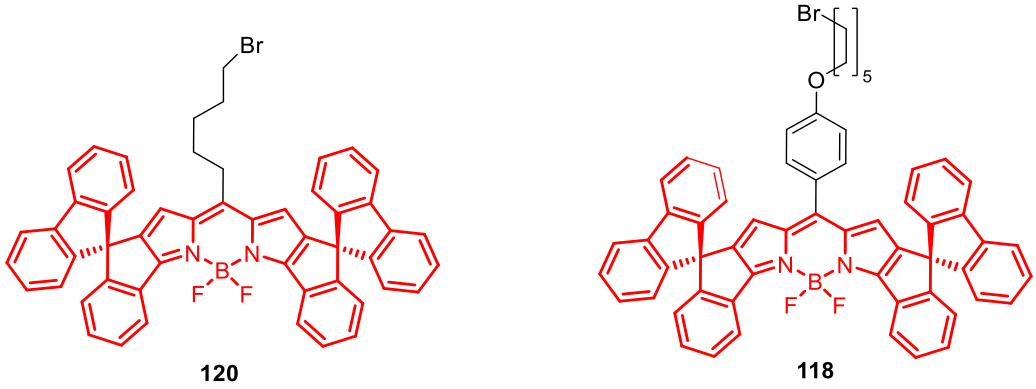

Figure 69 Initially used red *meso*-alkyl Bodipy **120** and *meso*-aryl Bodipy **118** in this work.

3.3.2. Evaluation of the red-green FRET

To enable the fine tuning of FRET design a simple green-red dyad was synthesized, in which the respective fluorophores are connected by a short linker (Scheme 14).

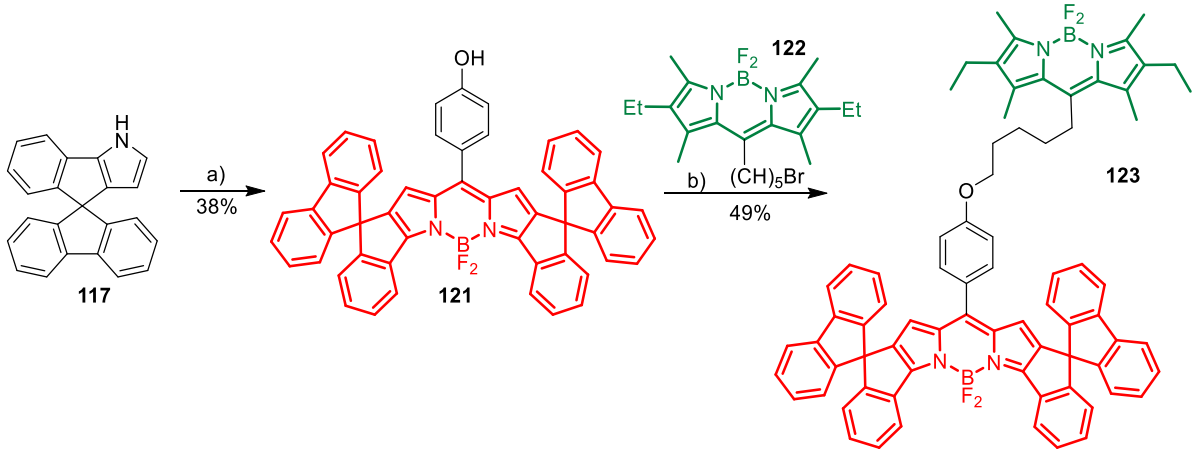

Scheme 14 Synthesis of basic red/green dyad. Reagents and conditions: a) 1,4-hydroxybenzaldehyde, TFA, CH_2Cl_2, 3 h followed by DDQ, 1 h followed by BF_3·Et_2O, Et_3N, 3 h; b) K_2CO_3, KI, acetone, reflux, 12 h. Reproduced from Ref. 249 according to CC BY-NC 3.0 license *(https://creativecommons.org/licenses/by-nc/3.0/)*.

Initial experiments were done to establish the best parameters for FRET measurements, utilizing the simple dyad **123** and related compounds with the respective green and red

fluorophores **122** and **118**. First the most useful excitation wavelength for the green-red dyad was determined. Ideally, the excitation of the green donor fluorophore does not lead to excitation of the red fluorophore (cross-talk).[248] However, in real systems the excitation of the green fluorophore inevitably leads to some excitation of the red fluorophore, since the absorbance of the red dye in the 500 nm region is small, but different from zero (Figure 70). The absorption spectrum of dyad **123** is a nearly perfect superposition of the individual spectra of the green and the red Bodipy **122** and **118** suggesting no interaction between the two fluorophores in the respective ground states.

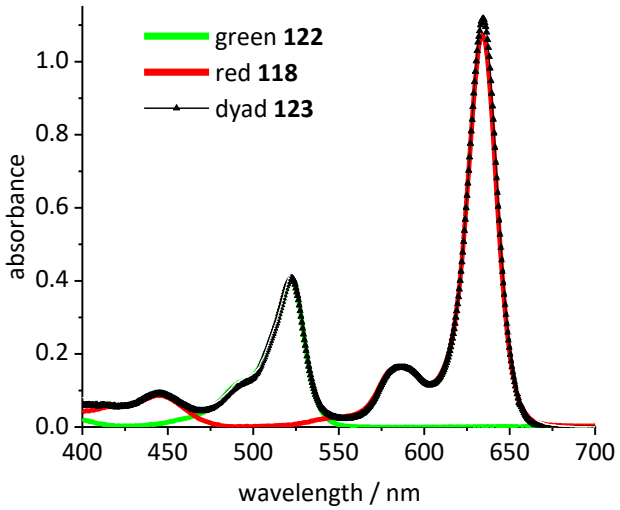

Figure 70 Absorbance spectra of green Bodipy **122** (λ_{max} = 523 nm) and red Bodipy **118** (λ_{max} = 634.5 nm) and dyad **123** in CH_2Cl_2 (c= 5.0·10^{-6} mol/L). Reproduced from Ref. 249 according to CC BY-NC 3.0 license *(https://creativecommons.org/licenses/by-nc/3.0/)*.

Next, the two individual fluorophores **118** and **122** were probed at different excitation wavelengths and the ratio of the respective emission intensities was determined. The highest I_{535} / I_{648} value is 37 at 505 nm excitation corresponding to a cross-talk intensity of approx. 2.7% (Figure 71).

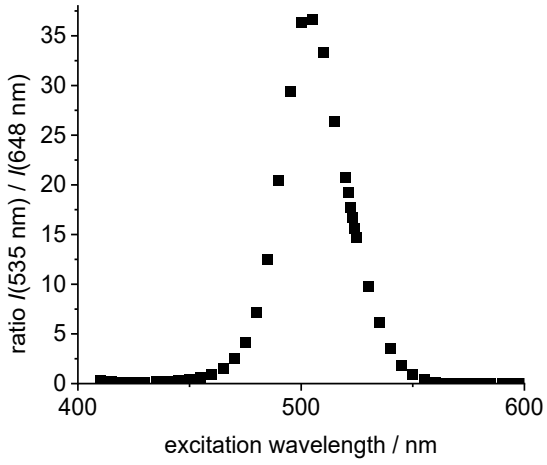

Figure 71 Plot of excitation wavelength *vs.* ratio of emission intensities of the individual green Bodipy **122** ($\lambda_{em,max}$ = 535 nm) and the individual **118** ($\lambda_{em,max}$ = 648 nm) in DCE (c= 5.0·10^{-6} mol/L). Reproduced from Ref. 249 according to CC BY-NC 3.0 license *(https://creativecommons.org/licenses/by-nc/3.0/)*.

In dyad **123** (Scheme 14) the excitation energy is transferred from the green donor fluorophore to the red acceptor fluorophore. Consequently, the excitation of the dyad at 505 nm leads to insignificant emission at 535 nm, and full emission at 648 nm. This is indicative of virtually complete energy transfer from the green to the red fluorophore, which is not surprising with a view to the short distance between the green and the red fluorophore.

The formation of dinuclear species from two individual species containing fluorophores for FRET experiments depends on the concentration of the reactants. Obviously, the position of the equilibrium as well as the rate for such reactions are more favorable at higher concentrations. However, due to the small Stokes shift the emission wavelength is close to the maxima of the absorption of the respective fluorophore and at higher concentration of the fluorophore a significant portion of the emitted light is reabsorbed. Based on experiments at different concentrations of fluorophore **118** and **122** (c= 1 – 50 ·10^{-6} mol/L) the brightest fluorescence is observed between c= 5 – 10 ·10^{-6} mol/L. However, already at c= 5 ·10^{-6} mol/L significant self-absorbance occurs and the molar emission for the green fluorophore is attenuated by ca. 20% (based on the extrapolated emission at c= 1.0·10^{-6} mol/L), and by ca. 50% for the red fluorophore (extrapolated from c= 1.0·10^{-6} mol/L). When measuring the FRET at higher concentrations the 648 nm emission intensity at c= 10.0·10^{-6} mol/L is lower than at c= 5.0·10^{-6} mol/L and at c= 50·10^{-6} mol/L the absolute fluorescence intensity is less than 10% of the emission intensity at c= 5.0·10^{-6} mol/L. However, despite significant signal attenuation, fluorescence can be easily determined due to the excellent brightness of the Bodipy fluorophore. Based on this, FRET measurements over a wide concentration range are possible.

3.3.3. FRET studies on green-red NHC-gold complexes

In this work we also tested, whether the red azolium salt **119**·HBr and the green **124**·HBr[244] salt are suitable for the synthesis of a wide range of NHC-metal complexes (see supporting information).[249] Green fluorescent metal complexes with [(NHC)ML] with ML= AuCl, RhCl(cod), IrCl(cod) and Pd(allyl)Cl and red fluorescent metal complexes [(NHC)ML] with ML= CuBr, AuCl, RhCl(cod), IrCl(cod) and Pd(allyl)Cl were obtained using the weak base approach. The red *meso*-aryl Bodipy turns out to be highly stable towards the basic reaction conditions and the same holds true for the green *meso*-alkyl Bodipy. In stark contrast, the red *meso*-alkyl Bodipy is highly sensitive towards the basic reagents used in metal complex synthesis and not suitable for the synthesis of NHC-metal complexes.[135]

The fluorescence properties of the respective red and green metal complexes [(NHC)ML] with ML= AuCl, Pd(allyl)Cl, RhCl(cod) and IrCl(cod) are identical, since the distance metal-bodipy is far too large to exert any significant influence on the fluorophore and for the same reason the properties of the metal complexes are not influenced by the nature of the fluorophore. The fluorophores can be considered as remote labels not affecting the metal to any significant degree. The stability of a palladium-pyridine complexes tagged with a related spiro-Bodipy in an organometallic setting was previously demonstrated by Goldsmith *et al*.

The reaction of [Au(CCPh)(NHC)] with [Au(NTf$_2$)(NHC)] is known to provide the respective digold-acetylide complex with a σ- and a π-bound NHC-gold complex (Widenhoefer dimer).[250] The analogous reaction is reported here using the green and red fluorescent gold complexes [Au(CCPh)(**124**_green)] and [Au(NTf$_2$)(**119**_red)] to provide the dinuclear complex **125** (Scheme 15).

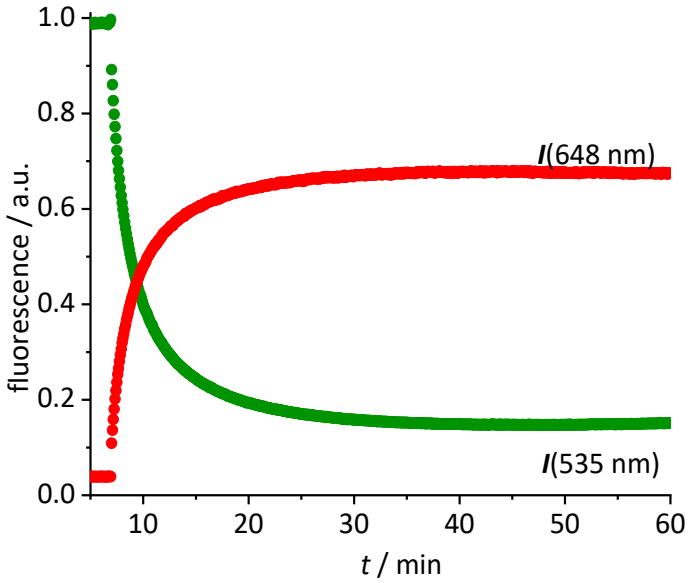

Figure 72 Time-dependent evolution of the fluorescence (green fluorescence renormalized to 1.0) for the reaction of [Au(CCPh)(**124**_green)] with [Au(NTf$_2$)(**119**_red)] in 1,2-DCE (c= 5.0·10^{-6} mol/L). Reproduced from Ref. 249 according to CC BY-NC 3.0 license *(https://creativecommons.org/licenses/by-nc/3.0/)*.

A solution of the red gold complex [Au(NTf$_2$)(**119**_red)] in 1,2-dichloroethane was added to a solution of the green gold complex [Au(CCPh)(**124**_green)] in the same solvent in a fluorescence cuvette at t = 7 min. The reaction mixture was irradiated with 505 nm light and the fluorescence in the red channel (648 nm) and in the green channel (535 nm) was observed (Figure 72). The reaction ensues after mixing both reactants and the formation of the dimeric gold complex is evidenced by a pronounced decrease in the green 535 nm emission and a corresponding increase in the red 648 nm emission due to FRET (Figure 72). The green emission decreases to 14% of the initial value.[251] In contrast to dyad **123** the resonance energy transfer is not quantitative, which is hardly surprising, because the distance between the green and the red fluorophore is much larger.[252] Considering the flexibility of the red and green subunits of the molecules it is likely, that the FRET is isotropic and orientation factors need not be considered. Because of this flexibility it is also difficult to obtain precise information on the average distance between the green and the red fluorophore. Based on the observed FRET the distance between the red and the green Bodipy in **125** is estimated to be at least 25% shorter than the Förster radius of the green/red FRET pair.[253] Obviously, the interaction between the two fluorophores is sufficiently long range to be suitable for the observations of FRET in molecules of this size. The chemical transformation appears to be complete within ca. 30 min and after that both emission signals in the red and in the green channel remain constant - despite continuous irradiation - thus providing evidence for the photostability of the respective fluorophores. In order to verify this approach, the complex **125** was also synthesized (Scheme 15), isolated and fully characterized by NMR-spectroscopy and high-resolution mass spectrometry.

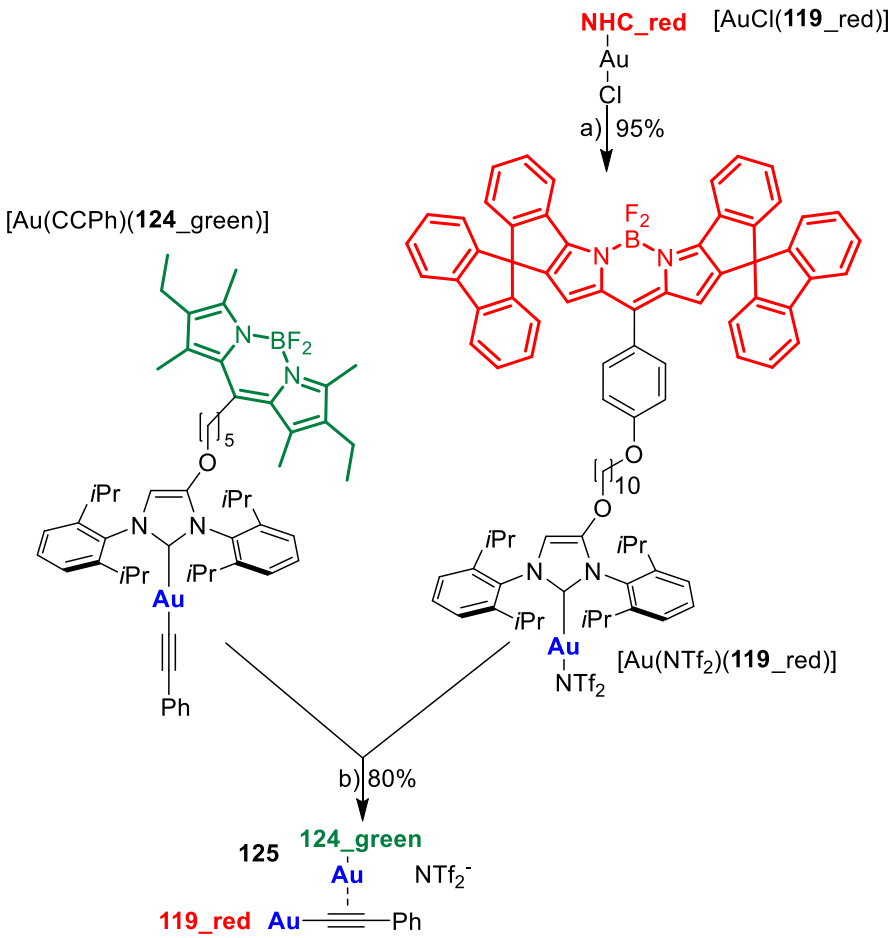

Scheme 15 Synthesis of two red-green dinuclear gold complexes. Reagents and Conditions: a) [Ag(NTf_2)], CH_2Cl_2, rt, 30 min, b) CH_2Cl_2, rt, 40 min. Reproduced from Ref. 249 according to CC BY-NC 3.0 license *(https://creativecommons.org/licenses/by-nc/3.0/)*.

3.3.4. Monitoring ion pairing/ion separation using green-red FRET

Dissociation of close ion pairs in solution leads to spatial separation of the respective anions and cations. It should be possible to monitor this process *via* FRET if appropriate fluorescent labels are used. In previous section was shown general application of ion pairing/dissociation processes based on changes in fluorescence of the anion, but this approach only works in a specific setting because it relies on the quenching effect of the transition metal (iridium) cation towards the anionic Bodipysulfonate **114** ($bdpSO_3^-$). Consequently, close ion pairs are characterized by weak fluorescence and separated ion pairs by strong fluorescence. Here presented a general approach independent of specific properties of metals, in which both the anion and the cation are labeled with red and green fluorescent dyes, respectively. This should lead to a pronounced FRET signal for close ion pairs. A salt consisting of a Bodipy-labeled NHC gold cation and a Bodipysulfonate anion was synthesized in the reaction of [AuCl(**119**_red)] with the silver salt of Bodipysulfonate **114** (Scheme 16). A solution of complex **126** in toluene displays a strong FRET signal, indicating the presence of close ion pairs in the weakly solvating aromatic solvent (excitation spectra red and green circles, figure 73). The close ion pairs can be separated by addition of a polar solvent, such as DMAc (excitation spectra red and green triangles, figure 73).

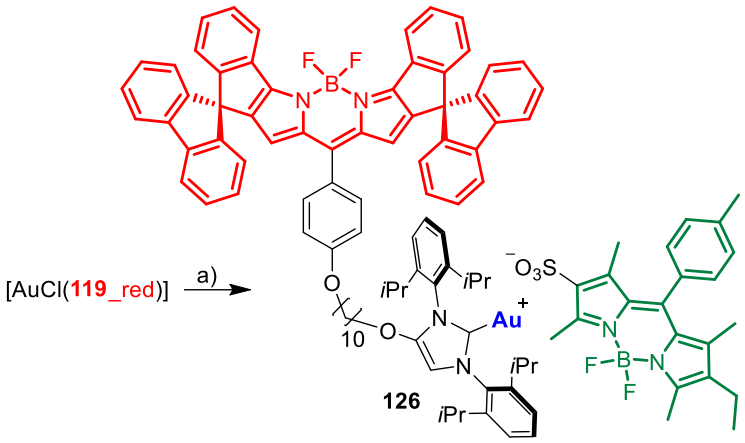

Scheme 16 Synthesis of [Au(bpdSO$_3$)(**119**_red)] (**126**). Reagents and conditions: a) [Ag(bdpSO$_3$)] (**114**), CH_2Cl_2. Reproduced from Ref. 249 according to CC BY-NC 3.0 license *(https://creativecommons.org/licenses/by-nc/3.0/)*.

The increase in the dielectric constant of the solvent mixture and the weak interaction of DMAc with gold lead to solvent-separated ion pairs,[175,254] which are characterized by a weak 648 nm signal (red triangles, Figure 73) and a strong 535 nm signal upon excitation at 500 nm. Following the addition of DMAc to the toluene solution (1.4%-vol. DMAc) of **126** the average distance between the fluorophores corresponds to the Förster radius of the green/red pair. Upon formation of the close ion pair the intensity of the 648 nm signal increases 21-fold while the green signal decreases by a factor of 6.6. The close ion pair can be disconnected by addition of a ligand to gold, such as phenyl acetylene. At c = 1.0·10^{-6} mol/L of the salt in toluene approx. 10^4 equivalents of phenyl acetylene are needed to fully separate the ion pair. The method presented here is fairly general and allows the investigation of ion pairing in different settings. Understanding ion pairing is highly relevant for catalytic olefin polymerization using cationic transition metal complexes[255] or for cationic gold catalyzed hydration and alkoxylation of alkynes[256] and the methodology presented here should be highly useful.

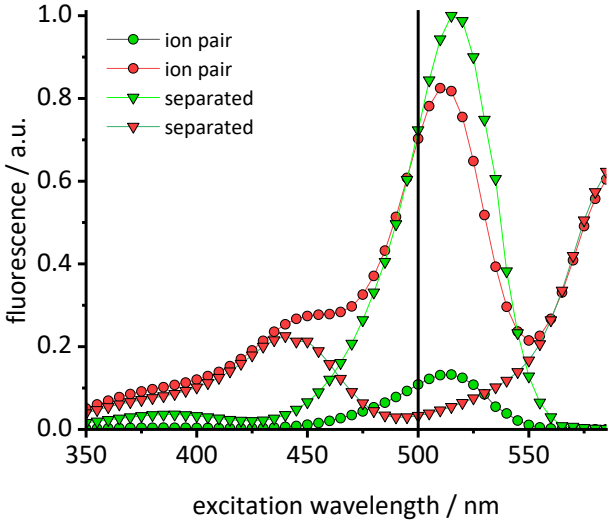

Figure 73 Excitation spectra of Bodipy ion pair dyad **126** in toluene (c= 2.0 · 10^{-6} mol/L) (green dots = 535 nm emission, red dots = 648 nm emission, green fluorescence renormalized to 1.0) and of the separated dyad in toluene solution (c= 2.0 · 10^{-6} mol/L) (green triangles = 535 nm emission, red triangles = 648 nm emission) after addition of concentrated NBu_4Br solution (vertical black line denotes preferred excitation

wavelength 500 nm). Reproduced from Ref. 249 according to CC BY-NC 3.0 license *(https://creativecommons.org/licenses/by-nc/3.0/)*.

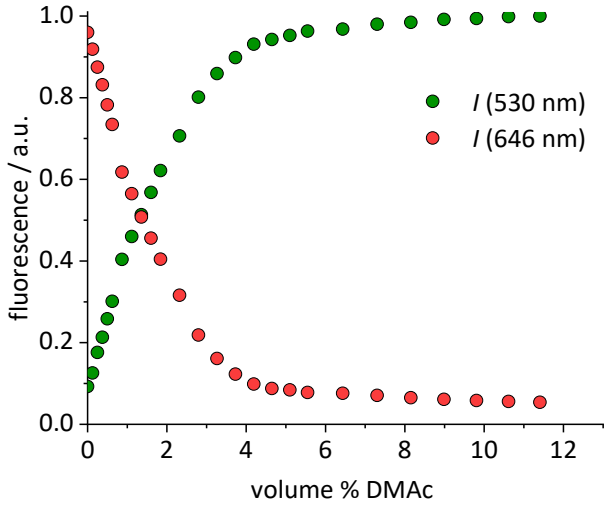

Figure 74 Plot of the fluorescence of red/green (acceptor/donor) (fluorescence renormalized to 1.0) for complex **126** *vs.* volume-% of DMAc in toluene solution (c= 1.0 · 10^{-6} mol/L) upon 500 nm excitation. Reproduced from Ref. 249 according to CC BY-NC 3.0 license *(https://creativecommons.org/licenses/by-nc/3.0/)*.

3.3.5. Evaluation of the blue-green dyad

Prior the construction of the triad, we tested, whether it is possible to synthesize NHC-gold complexes incorporating a blue Bodipy. This may not be straightforward, since the NH-unit attached directly to the Bodipy-core is slightly acidic and may react with the base needed for the formation of the carbene from the imidazolium salt. Nonetheless, a blue imidazolium salt **127**·HCl was synthesized as described in Scheme 17. For the synthesis of the NHC-gold complex different approaches were tested (weak base approach, *via* free carbene, NHC-Ag as NHC transfer reagent) and only the latter approach turned out to be successful. The NHC-Ag complex was *in-situ* generated from the imidazolium salt using Ag_2O and used directly for the reaction with [AuCl(Me_2S)]. The conversion appears to be near quantitative, but due to the small scale on which the synthesis was done, the isolated yield of pure material is only 55%.

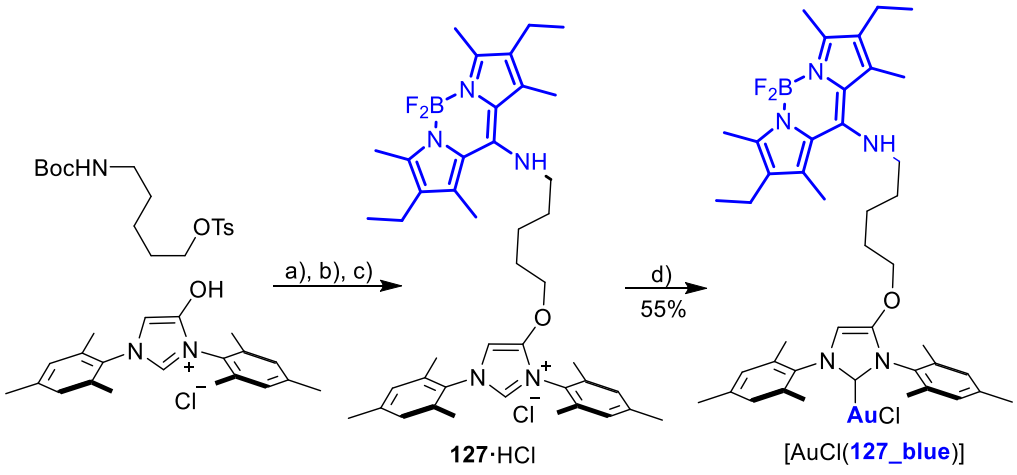

Scheme 17 Synthesis [AuCl(**127**_blue)]. Reagents and conditions: a) K_2CO_3, KI, acetone, reflux, 12 h; b) HCl in dioxane, CH_2Cl_2, overnight; c) *meso*-Cl-Bodipy, Et_3N, CH_3CN/CH_2Cl_2,

12 h; d) Ag_2O, 1,2-DCE, *T*= 60°C, 60 min then [AuCl(SMe_2)], 12 h. Reproduced from Ref. 249 according to CC BY-NC 3.0 license *(https://creativecommons.org/licenses/by-nc/3.0/)*.

To form a triad involving three different components each molecule requires an individual fluorescent tag and the FRET conditions need to be fulfilled to enable the efficient blue → green → red energy transfer. The green/red dyad has already been established and the next step is to extend the established dyad by a third dye to a triad. To retain the emission of the triad in the visible region of the spectrum, the third dye should be on the short-wave side of the established dyad.[257] *Meso*-amino substituted Bodipy constitute a synthetically variable and easily available group of fluorophores, [25,145,258] which display absorption/emission properties in the 400 – 450 nm region and which appear to be suitable for a Bodipy triad. In order to select the most appropriate dye the absorption and emission spectra of four different amino-Bodipy **128**, **129**, **130** and **131** were measured (Scheme 18). The initial aim of the selection process was to find a blue Bodipy with a suitable excitation spectrum with minimal cross-talk concerning the green dye **132**, which serves as a simple model compound for the green complexes synthesized.

The NMR spectra of blue series compounds **128**, **129**, **130** and **131** display interesting features. In **128** the six protons attached to Bodipy display unique (slightly broadened) signals in the ^{1}H-NMR and nine distinct ^{13}C signals for the Bodipy unit plus three signals for the propyl chain. Based on this observation, the C-N(propyl) bond appears to have significant double bond character with inhibited rotation, decreasing the symmetry of the molecule and leading to two different Bodipy sides. In **129** this partial double bond character appears to be reduced (probably due to the slightly electron-richer Bodipy unit due to the two electron-releasing methyl groups) since fewer signals in the ^{13}C-NMR are observed, some of which are severely broadened. In **130** and **131** the alkyl groups on both sides of the N-propyl chain prevent the planarization of the propyl nitrogen atom and a symmetric NMR spectrum is observed.

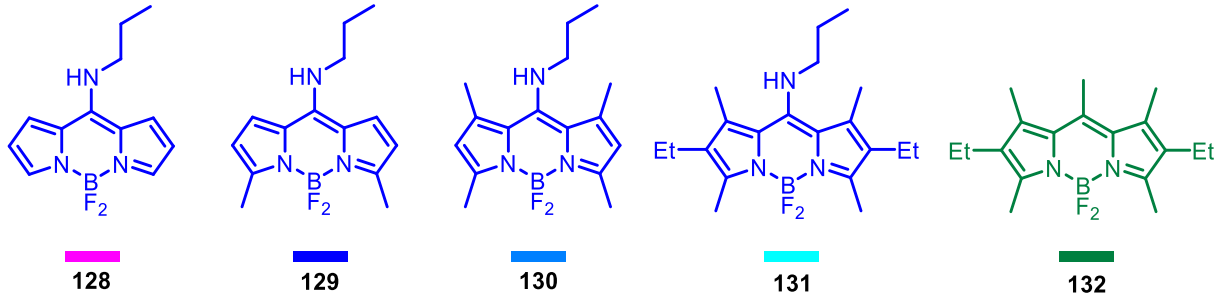

Scheme 18 List of blue Bodipy dyes tested with green Bodipy **132**. Reproduced from Ref. 249 according to CC BY-NC 3.0 license *(https://creativecommons.org/licenses/by-nc/3.0/)*.

The absorption maxima of the blue Bodipy **128**, **129**, **130** and **131** are 413 nm, 422 nm, 426 nm and 431 nm, respectively (Figure 75). The four blue fluorophores possess the same backbone but the additional alkyl substituents attached to the Bodipy core shift the absorbance towards the longer wavelengths, while the extinction of the dyes remains nearly constant. The absorption spectrum of the green dye displays a 523 nm absorbance and another (weaker) one at 375 nm, while the 415 – 435 nm region between those two maxima is characterized by weak absorbance. To characterize the spectral behavior, the ratio of the absorbances for the four blue dyes relative to the green dye are shown in Figure 75. The most favorable ratio of 29 is observed for **129**, meaning that the

absorbance of **128** at 422 nm is 29 times stronger than that of **132** at the same wavelength. From a chemical point-of-view **129** is also preferred over **128**, since the two methyl groups replace two fairly acidic protons next to the NBF_2N -unit, which renders **128** (and derivatives) base-sensitive.

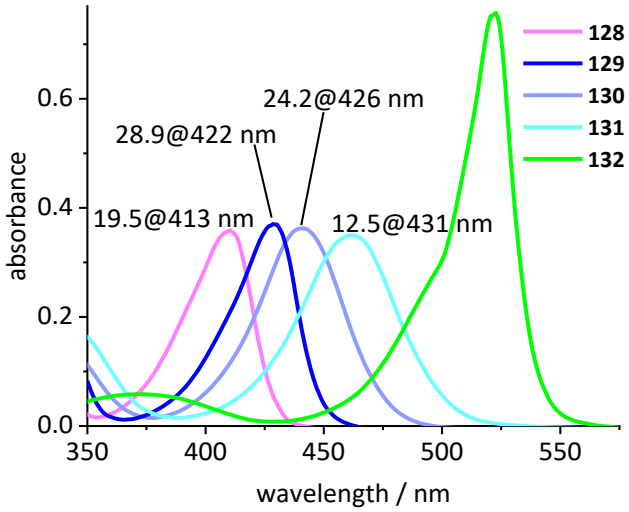

Figure 75 Absorption spectra of **128**, **129**, **130** and **131** and the green dye **132**. The numbers on top of the peaks denote the ratio of the absorption of **128**, **129**, **130** and **131**, respectively, relative to the absorbance of **132** at the given wavelengths (c= 2.0 · 10^{-6} mol/L). Reproduced from Ref. 249 according to CC BY-NC 3.0 license *(https://creativecommons.org/licenses/by-nc/3.0/)*.

To further aid the selection of a favorable dye for the blue-green FRET, the cross-talk intensities of the dyes **128**, **129**, **130** and **131** are plotted relative the fluorescence intensity of the green at the respective excitation wavelength (Figure 76). **129** turns out to be the most favorable FRET-partner for the green dye, since at 422 nm excitation the emission from the blue dye is 9.5 stronger than the emission from the green dye at the same excitation wavelength.

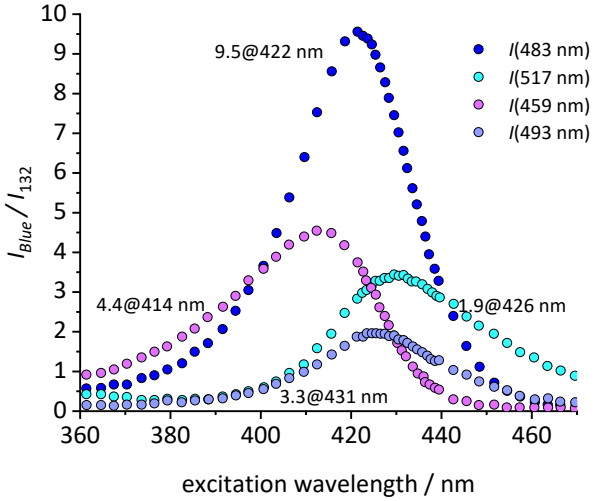

Figure 76 Plot of the ratio of fluorescence intensities (I_{Blue} / I_{132}) *vs.* the excitation wavelength for **128**, **129**, **130, 131** and **132**. 9.5 @ 422 nm denotes the best ratio I(**129**)/I(**132**) at 422 nm excitation for the 483 nm fluorescence (c= 2.0 · 10^{-6} mol/L).

Reproduced from Ref. 249 according to CC BY-NC 3.0 license *(https://creativecommons.org/licenses/by-nc/3.0/)*.

Following the selection of the blue Bodipy **133** (from **129**) the gold-acetylide complex **134** representing the respective blue-green dyads was synthesized (Scheme 19). The identity of the gold-acetylide subunit was established *via* NMR-spectroscopy and by high resolution mass spectrometry (FRET experiments, see below). The resulting material is a 1:1-mixture of [AuCl(**122**_green)] and dbu (1,8-diazabicyclo[5.4.0]undec-7-ene used as the base for alkyne deprotonation and gold-acetylide formation). This adduct could not be separated since the material decomposes upon attempted purification. In the ^{1}H NMR spectrum of **134**·dbu the NH-proton of the blue Bodipy unit cannot be observed and based on this it is assumed that the dbu closely interacts with the NH -unit and the respective proton is shared by the nitrogen atom attached to Bodipy and the nitrogen atom of dbu enhancing adduct formation. The dbu molecule is also observed in the mass spectrum of **134**·dbu.

3.3.6. Evaluation of the blue-green-red FRET triad

The three fluorophores in the potential triad **135** enable multiple fluorescence information channels reporting on the status of the molecule during the triad forming reaction. The respective signals either the blue, the green or the red fluorescence from 423 nm excitation of the blue fluorophore or alternatively from 500 nm excitation of the green fluorophore.

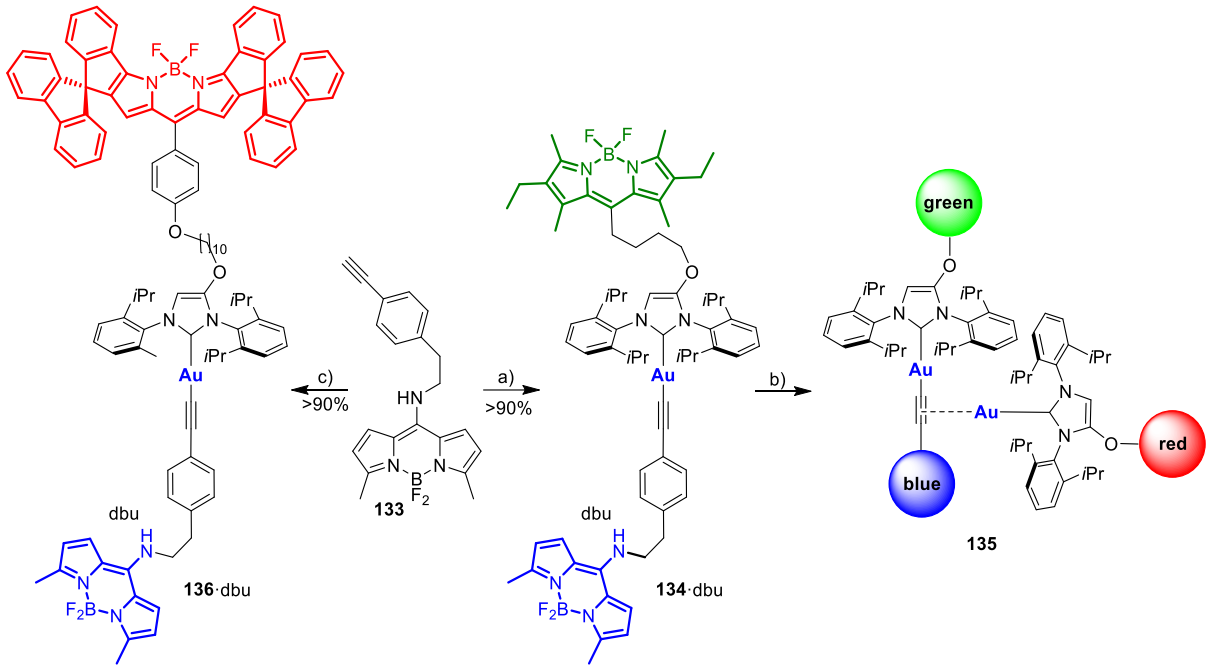

Scheme 19 Synthesis of the blue-green dyad and the blue-green-red triad. Reagents and conditions: a) [AuCl(**122**_green)], dbu, CH_2Cl_2; b) + [Au(NTf_2)(**119**_red)] in 1,2-dichlorethane; c) [AuCl(**119**_red)], dbu, CH_2Cl_2. Reproduced from Ref. 249 according to CC BY-NC 3.0 license *(https://creativecommons.org/licenses/by-nc/3.0/)*.

A solution of **134**·dbu in 1,2-dichloroethane in a fluorescence cuvette was converted into the triad **135** by adding a solution of [Au(NTf_2)(**119**_red)] and the fluorescence changes are monitored. Based on the design of the triad, irradiation at 423 nm should give rise to the efficient energy transfer from the blue Bodipy to the green Bodipy and then to the red Bodipy in a cassette type fashion.[242] The individual emission spectra of the blue, the

green and the red Bodipy (Figure SI S9[249]), show that 423 nm excitation also leads to significant direct excitation of the red Bodipy and consequently to red cross-talk emission, while the excitation of the green Bodipy at 423 nm gives rise to a weak cross-talk fluorescence signal. This blue-red cross-talk occurs because the red Bodipy displays a significant absorbance in the 400 – 450 nm region. The only visible spectral region in which the red Bodipy displays only weak absorbance is between 480 – 530 nm but irradiation in this spectral region leads to some direct excitation of the green fluorophore.

A solution of **134**·dbu (c= 5.0 · 10^{-6} mol/L) was treated with one equivalent of [AuCl(**119**_red)] and irradiated at 423 nm (Figure 77). This leads to an instantaneous increase of the red emission,[259] but it does not produce a significant change in the green emission. Obviously, the 423 nm light leads to the excitation of the blue Bodipy and the excitation energy is then transferred to the green dye *via* FRET. However, since the green emission experiences only small changes after addition of the first equivalent of [Au(NTf_2)(**119**_red)], it can be concluded that FRET to the red Bodipy does not occur to a significant extent. Consequently, the addition of one equiv. of [Au(NTf_2)(**119**_red)] does not lead to the formation of the triad. The observed red fluorescence originates from the direct excitation of the red Bodipy at 423 nm (cross-talk). Additional evidence for this interpretation comes from the fact that this red fluorescence intensity is virtually the same as the one produced by a c= 5.0 · 10^{-6} mol/L solution of [Au(NTf_2)(**119**_red)] in 1,2-dichloroethane.[260] Consequently, in the cross-talk and self-absorbance corrected data set, the red emission is almost unchanged (Figure SI S28[249]). To better understand the absence of triad formation after addition of one equiv. of [Au(NTf_2)(**119**_red)], the reaction of [Au(NTf_2)(IPr)] with a single equivalent of dbu was probed by ^{1}H-NMR spectroscopy. Upon addition of one equivalent of dbu to a solution of [Au(NTf_2)(IPr)] in $CDCl_3$ several ^{1}H- and ^{13}C-NMR signals of the dbu experience significant shifts. Based on this, it is concluded that dbu forms a complex with the cationic gold, which explains why the triad is not formed after addition of one equivalent of complex [Au(NTf_2)(**119**_red)].

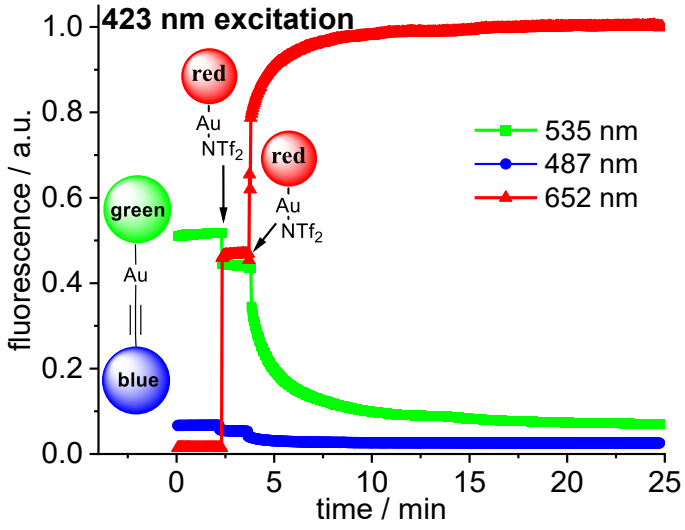

Figure 77 Plot of the time-dependent fluorescence intensities for the blue Bodipy ($\lambda_{em,max}$ = 487 nm), green Bodipy ($\lambda_{em,max}$ = 535 nm) and red Bodipy ($\lambda_{em,max}$ = 652 nm) at λ_{exc} = 423 nm within the blue-green-red acetylide triad with addition of n equiv. (n= 1, 2) of [Au(NTf_2)(**119**_red)] leading finally to the formation of **135**. Initial concentration of complexes in 1,2-dichloroethane c= 5.0·10^{-6} mol/L (uncorrected data, red fluorescence

renormalized to 1.0). Reproduced from Ref. 249 according to CC BY-NC 3.0 license (https://creativecommons.org/licenses/by-nc/3.0/).

Addition of a second equivalent of [Au(NTf$_2$)(**119**_red)] (resulting in c= 10.0 · 10^{-6} mol/L of the red fluorophore) leads to a pronounced, but slow change in the fluorescence during the following minutes both upon 423 nm excitation (Figure 77) and upon 500 nm excitation (Figure 78). The slow change in the red fluorescence indicates a chemical reaction with a corresponding reaction rate. This is in contrast to the immediate change in fluorescence after addition of the first equivalent of [Au(NTf$_2$)(**119**_red)]. The addition of the second equivalent of [Au(NTf$_2$)(**119**_red)] now also leads to a very pronounced drop in the green fluorescence. Obviously, the triad is formed and the 423 nm excitation energy is predominantly (SI 56[249]) transferred from the blue to the green and finally to the red Bodipy. The formation of the triad can also be followed, by switching to 500 nm excitation of the green fluorophore. As shown before, 500 nm light does not lead to a significant cross-talk with the red fluorophore. Therefore, the observation of red fluorescence upon 500 nm excitation is primarily the result of resonance energy transfer from the green to the red Bodipy (Figure 78) providing additional evidence for triad formation.

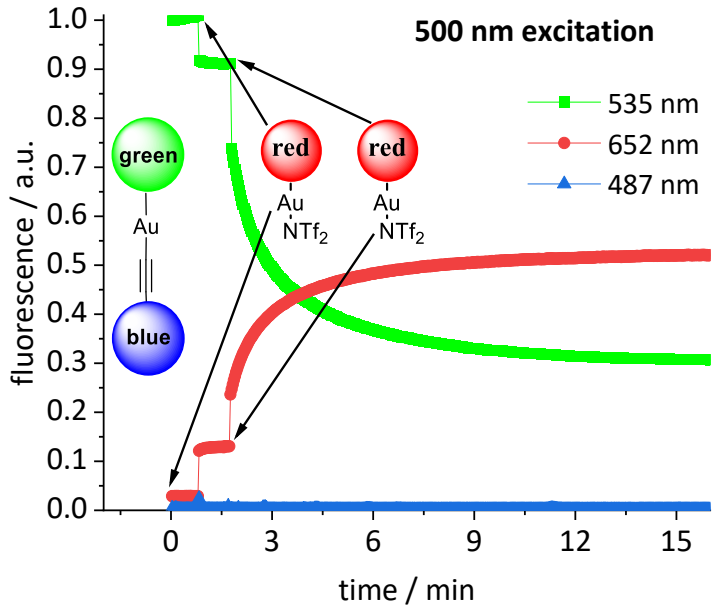

Figure 78 Plot of the time-dependent fluorescence intensities for the blue Bodipy ($\lambda_{em,max}$ = 487 nm), green Bodipy ($\lambda_{em,max}$ = 535 nm) and red Bodipy ($\lambda_{em,max}$ = 652 nm) at λ_{exc} = 500 nm within the blue-green-red acetylide triad with addition of n eq. (n= 1,2) of [Au(NTf$_2$)(**119**_red)] leading finally to the formation of **135**. Initial concentration of complexes is (c= 5.0·10^{-6} mol/L) in 1,2-dichloroethane (green fluorescence renormalized to 1.0). Reproduced from Ref. 249 according to CC BY-NC 3.0 license (https://creativecommons.org/licenses/by-nc/3.0/).

Based on highly sensitive fluorescence spectroscopy FRET pairs are shown to be a powerful tool to establish connectivities. This will also be useful for the detection of dinuclear intermediates or dinuclear decomposition products in homogeneous catalysis, which likely occur in several very important transition metal catalyzed reactions: For the copper-catalyzed click reactions Fokin *et al.*[261] demonstrated the intermediate formation of dinuclear copper complexes. In olefin metathesis Grubbs *et al.*[262] were able to identify a dinuclear ruthenium complex as a catalyst decomposition product and bimolecular

decomposition appears to be a major catalyst decomposition pathway in olefin metathesis.[263] In Pd-catalyzed cross coupling reactions di- and polynuclear precatalysts and intermediates appear to be highly significant.[264] The small amount of catalyst used in such reactions and/or the small amount of binuclear species formed, renders their direct observation difficult – especially in the absence of a unique spectroscopic signature of such bimetallic species. The methodology presented here, should enable the direct observation of such intermediates *via* FRET and should facilitate the determination of the respective kinetics.

4. Summary and conclusions

The primary aim of this thesis was to develop and study novel Bodipy-tagged NHC transition metal complexes using fluorescence spectroscopy. It was shown that connecting Bodipy and transition metal complexes can result in specific photophysical transformations of fluorescence emission providing information about steric and electronic properties of NHC ligands and insights into the assembly/disassembly of organometallic complexes.

Part 1. *Ligand Exchange Triggered Photosensitizers – Bodipy-tagged NHC metal complexes*.[265]

Complexes in which different transition metals and the fluorophore are in close vicinity can exhibit significantly reduced fluorescence emission. Previously this phenomenon has been attributed exclusively to PET quenching, even for complexes containing heavy atoms like iodine and 5d transition metals.[138] In this work, we asked whether intersystem crossing quenching pathway can contribute to fluorescence attenuation for complexes with heavy transition metals closely attached to the fluorophore moiety.

1. We synthesized the new imidazolium salt **85**·HI with 8-Bodipy to prepare various NHC-metal complexes [CuCl(**85**)], [AuCl(**85**)], [Pd(allyl)Cl(**85**)], [MCl(cod)(**85**)] and [MCl(CO)$_2$(**85**)] (M = Rh, Ir) (Figure 79). We determined the electron donation of NHC **85** *via* IR spectroscopy (carbonyl group frequencies) and cyclic voltammetry (Ir(I/II) redox potential).

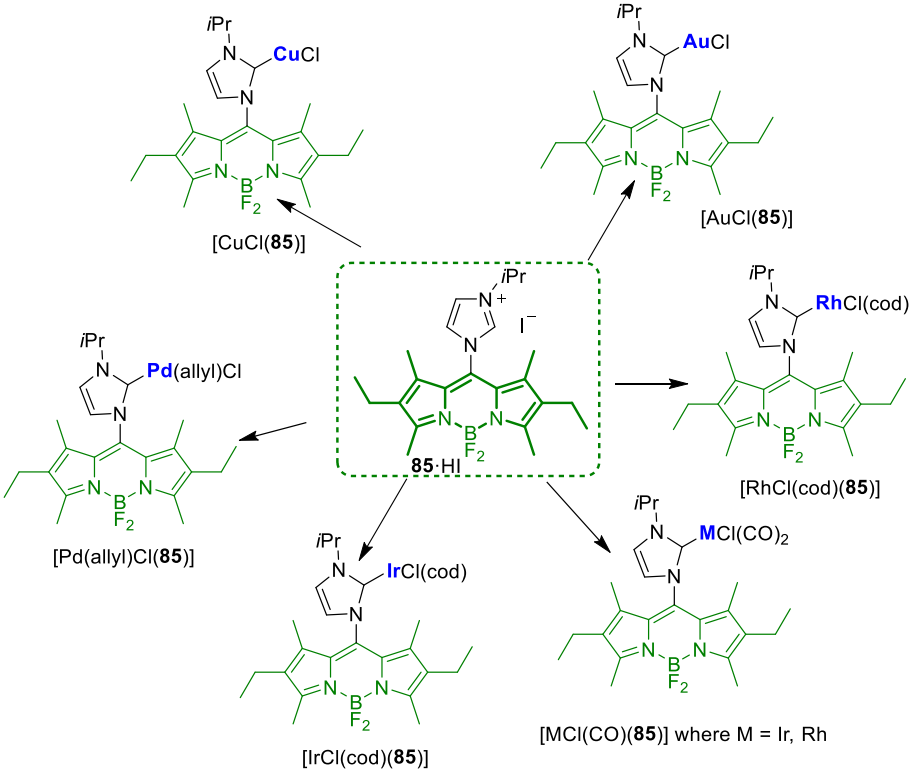

Figure 79 Novel transition metal complexes containing Bodipy-tagged NHC ligand.

2. The newly synthesized complexes are characterized by different fluorescence properties. Strong fluorescence quenching was observed in the complexes with Rh and Ir (Φ_{em} = <0.01), while complexes with Au (Φ_{em} = 0.28) and Pd (Φ_{em} = 0.23) exhibited significant emission quenching. We investigated the radiationless channelling of

excitation energy in Bodipy-based transition metal complexes by utilizing the photosensitizing properties to generate singlet oxygen. The photosensitizing activity was quantified by observing singlet oxygen quantum yield of up to $\Phi_{s.o.}$ = 0.63.

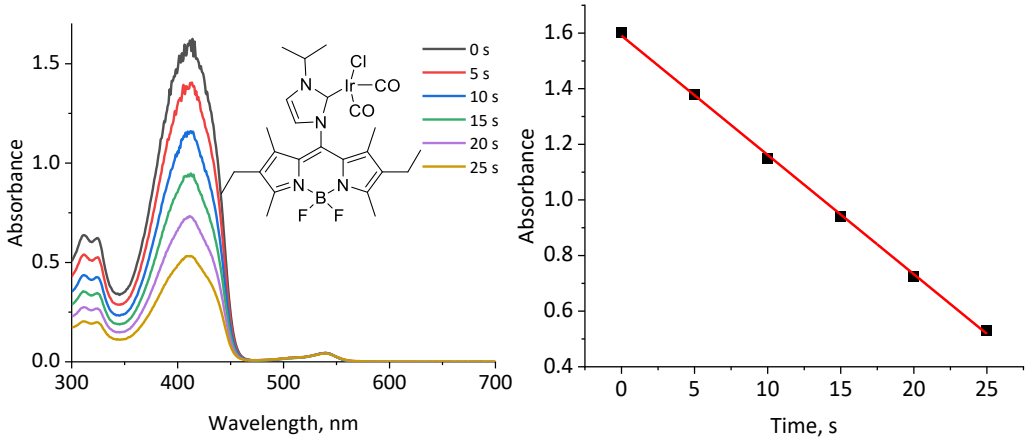

Figure 80 Measuring of photosensitizing activity: Photooxidation of DPBF in the presence of [IrCl(CO)$_2$(**85**)] photocatalyst. Reproduced from Ref. 265 according to CC BY-NC-ND 4.0 license *(https://creativecommons.org/licenses/by-nc-nd/4.0/).*

3. Following a simple ligand exchange reaction of cod by two CO [IrCl(CO)$_2$(**85**)], a pronounced increase to $\Phi_{s.o.}$ = 0.63 is observed, while [IrCl(cod)(**85**)] displayed poor $\Phi_{s.o.}$ = 0.09 (Figure 81). It was shown that the modification of metal complex fragments bonded to an NHC ligand results in channelling of the activation energy from the S_1 level into the T_1 level providing efficient photosensitizers for singlet oxygen generation.

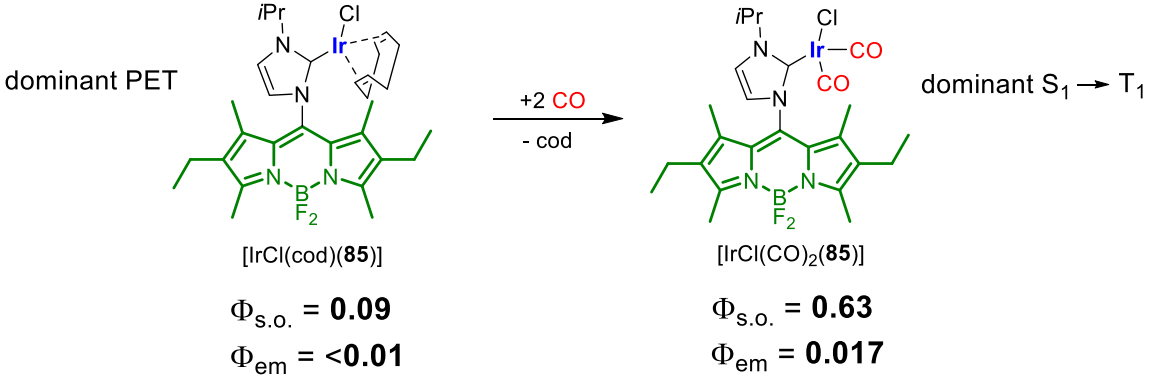

Figure 81 Ligand exchange reaction of [IrCl(cod)(**85**)] complex with CO and photophysical properties of corresponding complexes.

4. NHC-metal complexes with 3d- or 4d-metals (Cu, Rh) and weak spin-orbit coupling provide photosensitizers with modest activity, while complexes of 5d-metals (Ir, Au) with NHC ligand **85** can provide efficient photosensitizers for the generation of $^1O_2$. Based on the reported results, the electronic structure of the transition metal also influences the ability to act as a photosensitizer. The electron-rich [IrCl(cod)(**85**)] turns out to be a less efficient photosensitizer than [IrCl(CO)$_2$(**85**)], which is synthesized in virtually quantitative yield by a simple cod-to-CO ligand exchange (Figure 81).

The interplay of minor changes in the molecular setup can result in significant tunability of the photophysical properties in fluorophore-tagged complexes where the transition metal is in close proximity to the fluorophore. It was shown that the simple modification of metal complex fragments bonded to the NHC ligand allows the modification of the fluorescence and singlet oxygen quantum yield. In such systems,

excitation energy can be lost not only by photoinduced electron transfer, but also by the radiationless transition from the S_1 to the T_1 excited electronic state.

Part 2. *Determination of Stereoelectronic Properties of NHC Ligands via Ion Pairing and Fluorescence Spectroscopy.*[157]

XRD analysis of solid state structures is influenced by packing effects and normally a single conformer is presented in a "frozen out" state. In solution often an ensemble of different conformers exists simultaneously, consequently a solution-based approach can provide valuable data for sterically flexible molecules. Electron-rich iridium [IrCl(cod)(NHC)] complexes are known for their ability to quench the fluorescence of a fluorophore bonded to this complex. This quenching helps determine average iridium-fluorophore distances utilizing the corresponding increase of the fluorophore brightness due to greater fluorophore-quencher distances. In this work, we synthesized ion paired salts of cationic [IrCl(cod)(NHC)] complexes and anionic fluorophore. We questioned if in such systems sterically demanding ligands can promote the formation of solvent-separated ion pairs resulting in different spatial separation of iridium (fluorescence quencher) and fluorophore (anion).

1. 26 different iridium complexes were synthesized that contain NHC ligands with varying steric and electronic properties (Figure 82). Electronic descriptors of corresponding iridium complexes were evaluated (redox potential and ν(CO)).

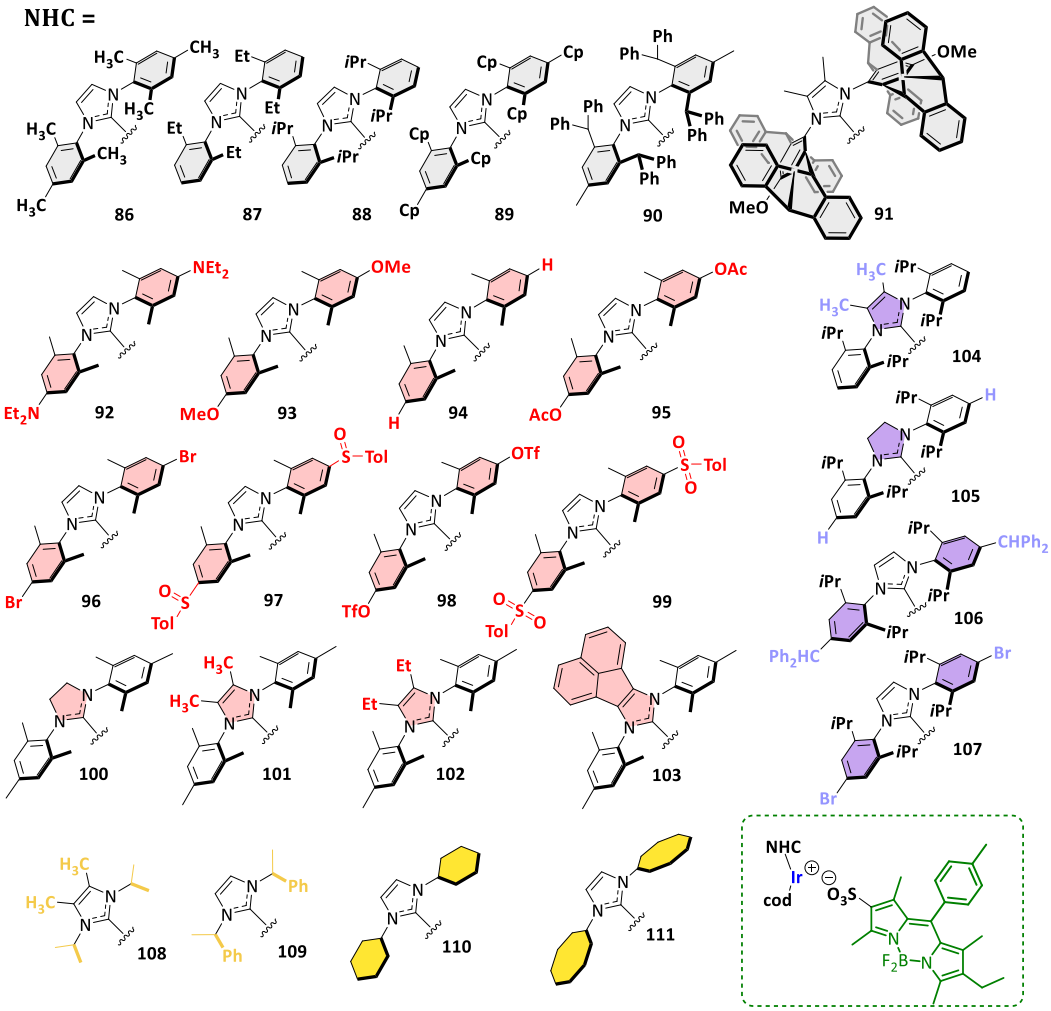

Figure 82 26 iridium complexes with varying steric and electronic NHC ligand properties were synthesized.

2. The respective fluorescence intensity for the corresponding [Ir(bdpSO$_3$)(cod)(NHC)] complexes was determined in dce solution. Electron-donating and sterically demanding ligands facilitate the formation of solvent-separated ion pairs, which results in the spatial separation of cation and anion (Figure 83). The enlarged distance between the fluorophore and the Ir quencher leads to a pronounced fluorescence signal increase.

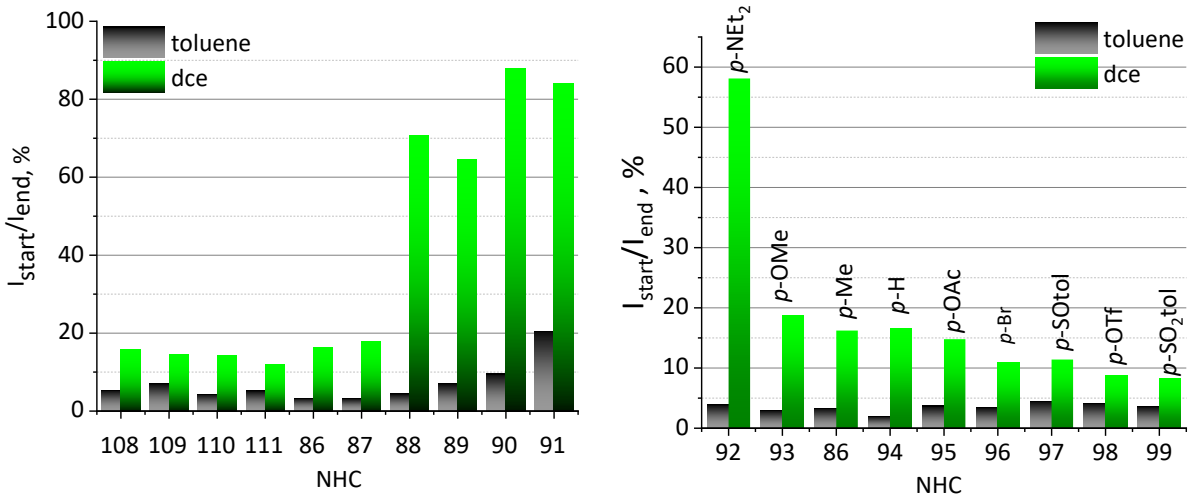

Figure 83 Fluorescence intensity in toluene/dce solution for the respective [Ir(bdpSO$_3$)(cod)(NHC)] complexes (numbering of the NHC ligands is according to Figure 82). Reproduced from Ref. 157 according to CC BY-NC-ND 4.0 license *(https://creativecommons.org/licenses/by-nc-nd/4.0/).*

3. The electronic properties of the ligands were examined *via* the established electronic descriptors (redox potential and ν(CO)) (Figure 84). The linear relationship of redox potential and carbonyl frequencies allows the correction of the fluorescence data according to the different donicity of NHC ligands and reveals the steric bulk of NHC ligands.

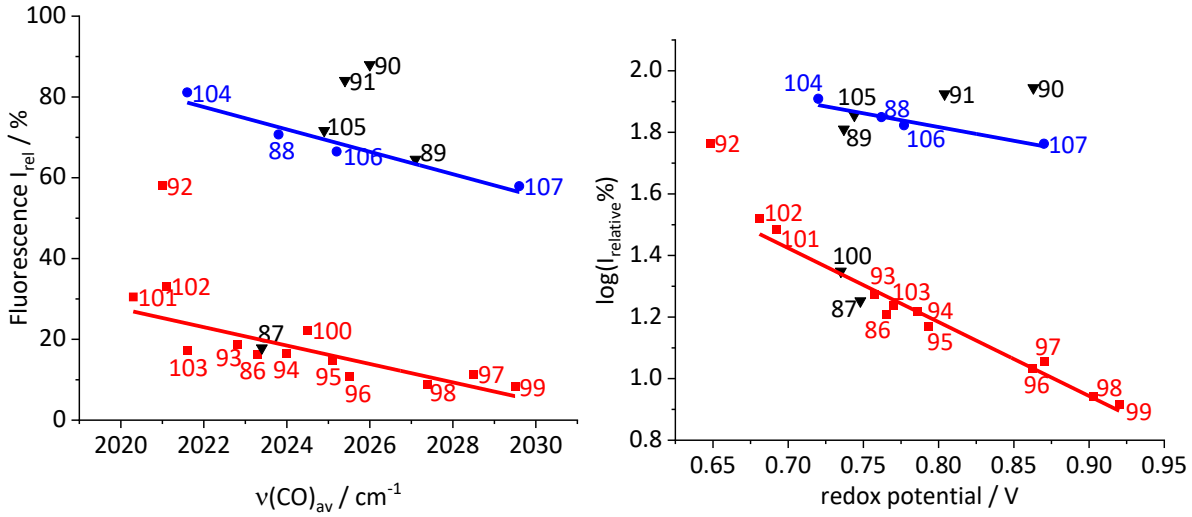

Figure 84 Correlation of fluorescence data *via* established electronic descriptors (redox potential and ν(CO)). Reproduced from Ref. 157 according to CC BY-NC-ND 4.0 license *(https://creativecommons.org/licenses/by-nc-nd/4.0/).*

The ion pairing approach provides information on the determination of both steric and electronic properties of NHC ligands which influence the formation of solvent-

separated ion pairs. Correlation of the fluorescence data *via* electronic descriptors (redox potential and ν(CO)) allows the deconvolution of the combined influence of electronic and steric contributions of the respective NHC ligands. The determination of the steric properties of ligands should not be limited to NHC ligands – in principle the steric bulk and the electronic properties of any type of ligand can be studied using a similar approach.

Part 3. *Switched fluorescence and photosensitization based on reversible ion-pairing.* [266]

Based on the preliminary information, fluorescence emission can be quenched when the transition metal is in the close proximity to the fluorophore. In such systems, excitation energy can be lost *via* photoinduced electron transfer and the radiationless transition from the S_1 to T_1 excited electronic state. In this work, we asked what is the predominant fluorescence quenching pathway for an ion paired cationic NHC-iridium complex and anionic Bodipy. We wanted to investigate how the degree of ion pairing can influence the switching of fluorescence properties and photosensitizing efficiency depending on the equilibrium of ion association/dissociation.

1. We found that the close ion-pair of [Ir(bdpSO$_3$)(cod)(**86**)] is an efficient photosensitizer for the generation of singlet oxygen, while the solvent-separated ion pair (after addition of DMSO) is highly fluorescent (Figure 85). Consequently, controlling ion association governs the path of the excitation energy which is channelled either to the S_1 state or *via* intersystem crossing into the T_1 state.

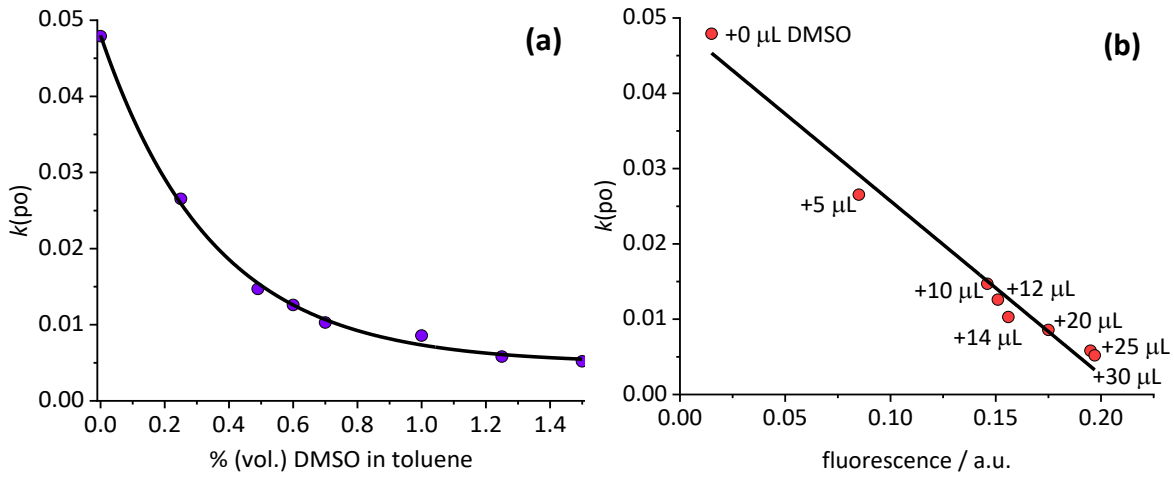

Figure 85 Correlation of the rate (k(po)) of $^1O_2$ generation (a) and fluorescence intensity (b) by [Ir(bdpSO$_3$)(cod)(**86**)] in toluene solution containing different amounts of DMSO.

2. It was established that modulation of NHC donation affects the photosensitizing properties. Only electronically rich NHC provide highly efficient photosensitizers, according to singlet oxygen quantum yield of up to $\Phi_{s.o.}$ = 0.88. The donation of the NHC ligands was correlated by using the Ir(I/II) redox potential of the respective [Ir(bdpSO$_3$)(cod)(NHC)] complexes (Figure 86). Reproduced from Ref. 266 according to CC BY-NC 3.0 license *(https://creativecommons.org/licenses/by-nc/3.0/)*.

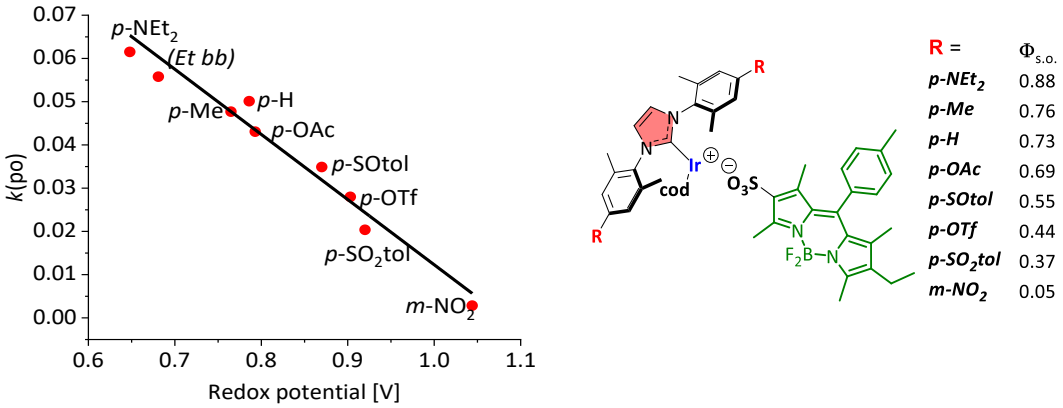

Figure 86 Correlation of rate (k(po)) of $^1O_2$ generation for various eletronic [Ir(bdpSO$_3$)(cod)(NHC)] complexes *vs.* redox potential for [IrCl(cod)(NHC)] complexes in dce. Reproduced from Ref. 266 according to CC BY-NC 3.0 license (*https://creativecommons.org/licenses/by-nc/3.0/*).

3. The use of reversible association/dissociation between ions in ion paired complexes can be used to develop various types of molecular switches. We introduced a novel switch based on complex [Ir(bdpSO$_3$)(cod)(**86**)]. The separation-recombination of anion and cation was observed *via* monitoring the fluorescence signal (Figure 87). The reversibility of ion paired complex in toluene solution was demonstrated by adding one equivalent of NBu$_4$Br salt with strongly coordinating bromide anion (BdpSO$_3^-$ is separated from the metal quencher, fluorescence = on) and NaBArF with a weakly coordinating anion (BdpSO$_3^-$ is more strongly coordinating to the metal quencher than BArF$^-$, fluorescence = off).

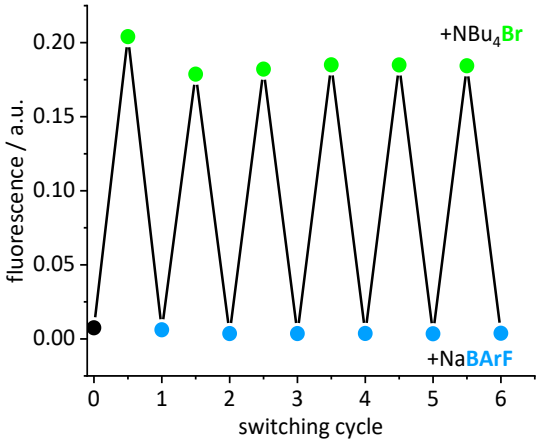

Figure 87 Switched fluorescence for [Ir(bdpSO$_3$)(cod)(**86**)] complex after addition of 1 eq. of NBu$_4$Br and NaBArF solution. Reproduced from Ref. 266 according to CC BY-NC 3.0 license (*https://creativecommons.org/licenses/by-nc/3.0/*).

In conclusion, switched fluorophores/photosensitizers are presented, whose activity can be modulated depending on the interaction between anion and cation controlled by solvent composition. Accordingly, in a close ion pair the activation energy in the S_1 level can be channelled into the T_1 level providing efficient photosensitizers for singlet oxygen generation. The basic principle presented in this work can be adapted for specific applications by choosing other ion pairs with weaker, stronger and even selective interactions, whose separation can be induced by different chemical or physical stimuli.

Part 4. *Fluorescent organometallic dyads and triads: establishing spatial relationships.*[249]

Identification of assembly/disassembly transformations in organometallic systems using single type of fluorescent tag is a challenging task. The use of fluorescence resonance energy transfer (FRET) is an alternative strategy to improve detectability. Application of the FRET method with suitable fluorescent tags allows observation of spatial connectivities in organometallic complexes and elucidation of specific interaction between acceptor and donor fluorophore molecules which are placed in the close vicinity or presented as a part of the same molecule.

1. Azolium salts tagged with blue, green and red fluorescent Bodipy were synthesized and used to prepare various NHC metal complexes (Figure 88). The designed dyes are chemically and photochemically stable, characterized by the absence of Lewis basic heteroatoms, equipped with convenient functional groups for conjugation and form efficient FRET pairs with minimal cross-talk.

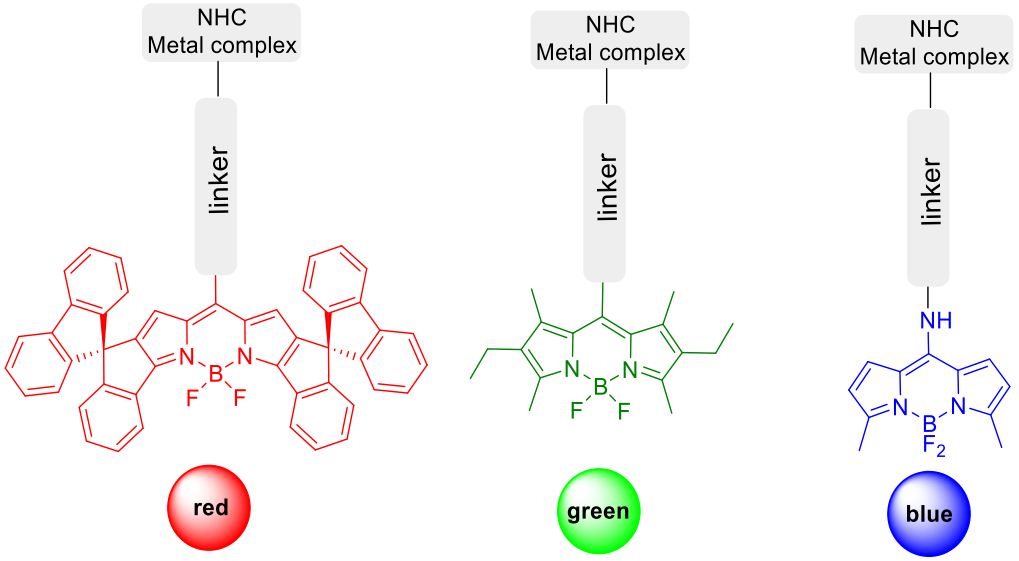

Figure 88 Fluorophore (blue, green, red) tagged NHC metal complexes.

2. Organometallic dyads **125** and **126** based on the green and red emission provide two data channels on the formation of complexes, which were demonstrated for alkyne bridged digold species (Figure 89a) and for ion pairing of the red fluorescent cation and the green fluorescent anion (Figure 89b). The excitation of both dyads at 500 nm leads to insignificant emission at 535 nm, and full emission at 648 nm due to FRET. This indicates a virtually complete energy transfer from the green to the red fluorophore, which occurs due to the short distance between the green and the red fluorophore. For complex **126,** the increase of the dielectric constant of the solvent mixture after the addition of DMAc and the weak interaction of DMAc with gold lead to solvent-separated ion pairs, which are characterized by a weak 648 nm signal and a strong 530 nm signal.

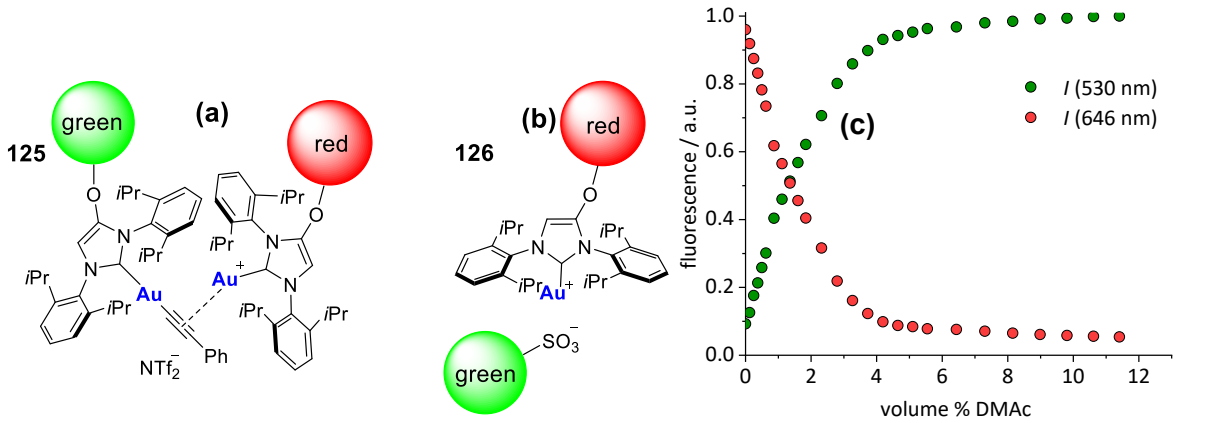

Figure 89 Formation of organometallic dyads for alkyne bridged digold species (a) and ion paired cationic iridium complex and anionic Bodipy fluorophore (b). (c) Titration of ion paired [Au(bpdSO$_3$)(**119**_red)] complex solution with DMAc. reproduced from Ref. 249 according to CC BY-NC 3.0 license *(https://creativecommons.org/licenses/by-nc/3.0/)*.

3. The two fluorophore dyad approach was extended to probe the assembly of three different subunits, each of them was synthesized using different tagged Bodipy dyes (blue, green, red). The excitation of the blue dye initiates energy transfer in the sequence blue /green /red, proving the assembly of the three different tagged subunits (triad) in a single molecule **135**.

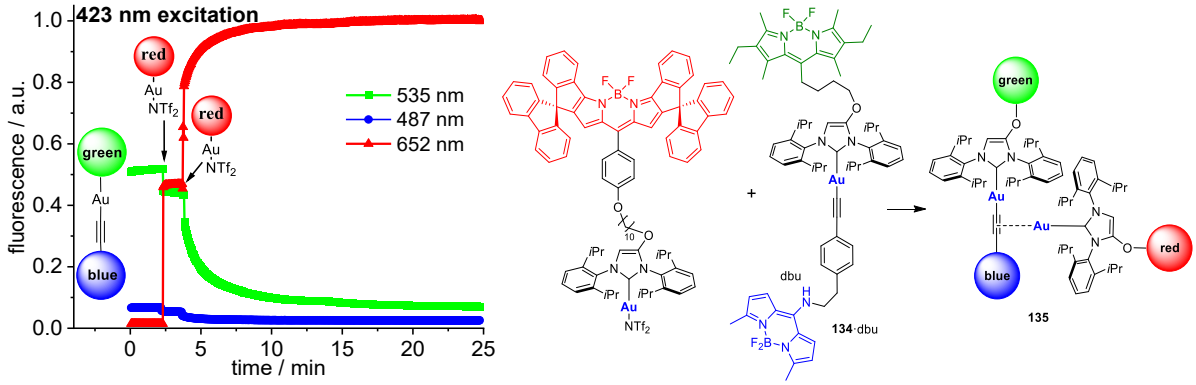

Figure 90 Triad formation for a Widenhoefer dimer with Bodipy-tagged complexes. reproduced from Ref. 249 according to CC BY-NC 3.0 license *(https://creativecommons.org/licenses/by-nc/3.0/)*.

The tagging of molecular components with robust fluorophores can be a general strategy in (organometallic) chemistry to establish connectivities for binuclear catalyst resting states and binuclear catalyst decomposition products in homogeneous catalysis. This methodology opens the doors for a better understanding of dynamic interactions in solution organometallic chemistry – in a concentration range less easily available to many other spectroscopic techniques.

5. Zusammenfassung der Ergebnisse

Das Hauptziel dieser Arbeit war die Entwicklung und Untersuchung neuartiger Bodipy-markierter NHC-Übergangsmetallkomplexe. Mit Hilfe der Fluoreszenzspektroskopie wurde gezeigt, dass die Bindung von Bodipy an Übergangsmetallkomplexe zu spezifischen photophysikalischen Veränderungen der Fluoreszenzemission führen kann. Diese Veränderungen liefern Informationen über die sterischen und elektronischen Eigenschaften der NHC-Liganden und Einblicke über den Annbau/Aufbau der Organometallkomplexe.

Teil 1. *Ligandenaustausch-ausgelöste Photosensibilisatoren mit Bodipy-markierten NHC-Metallkomplexen*.[265]

Komplexe, in denen sich verschiedene Übergangsmetalle und das Fluorophor in unmittelbarer Nähe befinden, können eine deutlich reduzierte Fluoreszenzemission aufweisen. Dieses Phänomen wurde bisher ausschließlich auf PET-Löschung zurückgeführt, und zwar auch bei Komplexen, die schwere Atome enthalten, wie z. B. Jod und 5d-Übergangsmetalle.[138] In dieser Arbeit wurde untersucht, ob ein intersystem crossing Quenching-Prozess die Fluoreszenzabschwächung von Komplexen mit schweren Übergangsmetallen, die direkt an den Fluorophorteil gebunden sind, beeinflussen kann.

1. Wir synthetisierten das neue Imidazoliumsalz **85**·HI mit 8-Bodipy zur Herstellung verschiedener NHC-Metallkomplexe [CuCl(**85**)], [AuCl(**85**)], [Pd(allyl)Cl(**85**)], [MCl(cod)(**85**)] and [MCl(CO)$_2$(**85**)] (M = Rh, Ir) (Abbildung 91). Wir bestimmten die Donorstärke von NHC **85** mittels IR-Spektroskopie (Carbonylgruppenfrequenzen) und zyklischer Voltammetrie (Ir(I/II)-Redoxpotential).

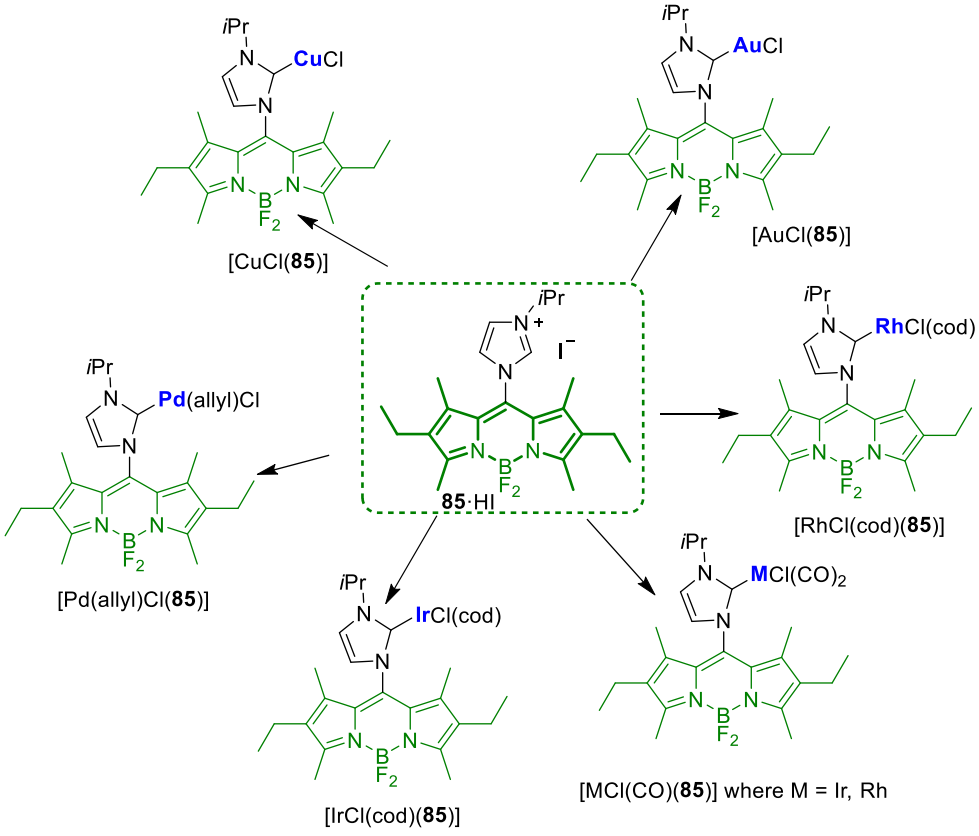

Abbildung 91 Neue Übergangsmetallkomplexe, die mit Bodipy markierte NHC-Liganden enthalten.

2. Die neu synthetisierten Komplexe zeichnen sich durch unterschiedliche Fluoreszenzeigenschaften aus. Bei den Komplexen mit Rh und Ir (Φ_{em} = <0.01), wurde eine starke Fluoreszenzabschwächung beobachtet, während die Komplexe mit Au (Φ_{em} = 0.28) und Pd (Φ_{em} = 0.23) eine deutliche Emissionsabschwächung zeigten. Wir untersuchten die strahlungslose Übertragung von Anregungsenergie in Bodipy-basierten Übergangsmetallkomplexen. Dabei nutzten wir die photosensibilisierenden Eigenschaften zur Erzeugung von Singulett-Sauerstoff. Die photosensibilisierende Aktivität wurde durch Ermittlung der Singulett-Sauerstoff-Quantenausbeute bis zu $\Phi_{s.o.}$ = 0.63 quantifiziert.

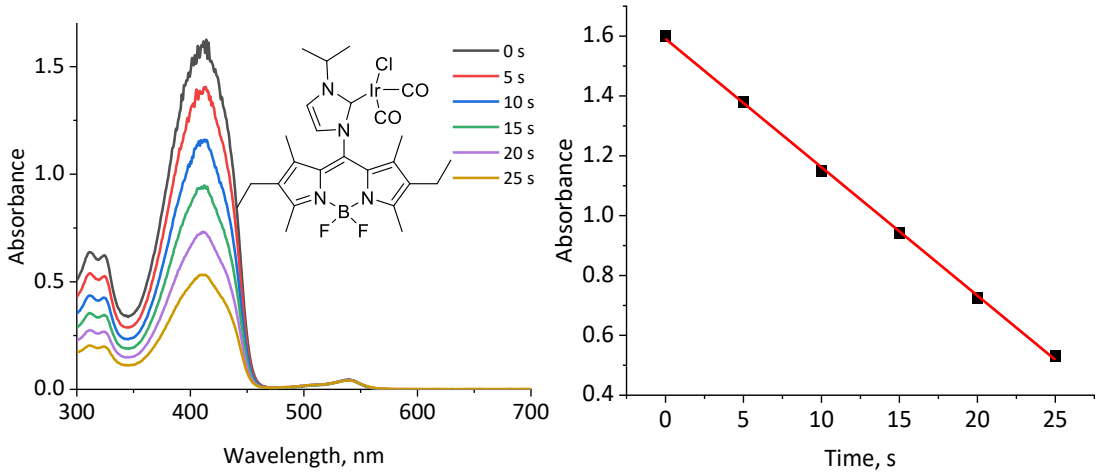

Abbildung 92 Messung der Photosensibilisierungsaktivität: Photooxidation von DPBF mit Photokatalysator [IrCl(CO)$_2$(**85**)]. Reproduziert aus Ref. 265 gemäß der CC BY-NC-ND 4.0 Lizenz (*https://creativecommons.org/licenses/by-nc-nd/4.0/*).

3. Nach einer erfolgreichen Ligandenaustauschreaktion von cod durch zwei CO [IrCl(CO)$_2$(**85**)] wird ein deutlicher Anstieg auf $\Phi_{s.o.}$ = 0.63 beobachtet, während [IrCl(cod)(**85**)] ein schwaches $\Phi_{s.o.}$ = 0.09 zeigt (Abbildung 93). Es wurde gezeigt, dass die Modifikation von Metallkomplexfragmenten, die an einen NHC-Liganden gebunden sind, zu einer Verschiebung der Aktivierungsenergie vom S_1 zum T_1 Niveau führt, wodurch effiziente Photosensibilisatoren für die Erzeugung von Singulett-Sauerstoff entstehen.

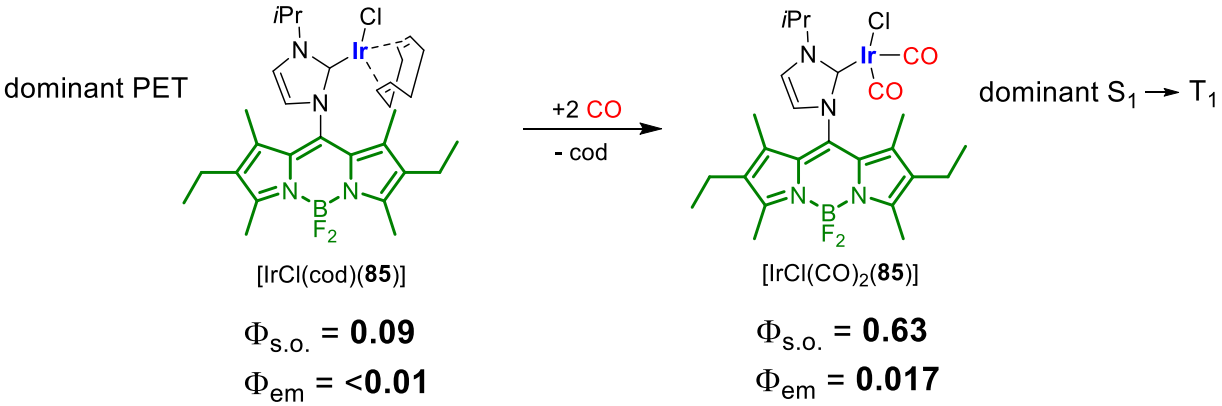

Abbildung 93 Ligand exchange reaction of [IrCl(cod)(**85**)] complex with CO and photophysical properties of corresponding complexes.

4. NHC-Metallkomplexe mit 3d- oder 4d-Metallen (Cu, Rh) und schwacher Spin-Orbit-Kopplung führen zu Photosensibilisatoren mit geringer Aktivität, während Komplexe von 5d-Metallen (Ir, Au) mit NHC-Ligand **85** effiziente Photosensibilisatoren für die Generierung von $^1O_2$ ergeben können. Ausgehend der berichteten Ergebnisse beeinflusst die elektronische Struktur des Übergangsmetalls auch die Fähigkeit, als Photosensibilisatoren zu wirken. Der elektronreiche [IrCl(cod)(**85**)] Komplex erweist sich als weniger effizienter Photosensibilisator als [IrCl(CO)$_2$(**85**)], das durch einen einfachen cod-zu-CO-Ligandenaustausch in nahezu quantitativer Ausbeute synthetisiert werden kann (Abbildung 93).

Das Zusammenwirken kleiner Änderungen im molekularen Aufbau kann zu einer erheblichen Variabilität der photophysikalischen Eigenschaften von Fluorophoren markierten Komplexen führen, bei denen sich das Übergangsmetall in unmittelbarer Nähe zum Fluorophor befindet. Es wurde gezeigt, dass die Veränderung von Metallkomplexfragmenten, die an den NHC-Liganden gebunden sind, die Modifizierung der Fluoreszenz und der Singulett-Sauerstoff-Quantenausbeute ermöglicht. In solchen Systemen kann die Anregungsenergie nicht nur durch den photoinduzierten Elektronentransfer verloren gehen, sondern auch durch den strahlungslosen Übergang vom elektronischen Zustand S_1 zum T_1.

Teil 2. *Bestimmung der stereoelektronischen Eigenschaften von NHC-Liganden durch Ionenpaarung und Fluoreszenzspektroskopie.*[157]

Die XRD-Analyse von Festkörperstrukturen wird durch Packungseffekte beeinflusst, und normalerweise wird ein einziger Konformer in einem "eingefrorenen" Zustand dargestellt. In Lösung existiert oft ein Ensemble verschiedener Konformer gleichzeitig, so dass ein lösungsbasierter Ansatz wertvolle Daten für sterisch flexible Moleküle liefern kann. Elektronenreiche Iridium [IrCl(cod)(NHC)]-Komplexe sind für ihre Fähigkeit bekannt, die Fluoreszenz eines an diesen Komplex gebundenen Fluorophors zu quenchen. Diese Fähigkeit hilft bei der Bestimmung der durchschnittlichen Iridium-Fluorophor-Abstände unter Verwendung der entsprechenden Zunahme der Fluorophor-Helligkeit aufgrund größerer Fluorophor-Quencher-Abstände. In dieser Arbeit synthetisierten wir Ionenpaarsalze aus kationischen [IrCl(cod)(NHC)]-Komplexen und anionischen Fluorophoren. Wir fragten uns, ob in solchen Systemen sterisch komplexe Liganden die Bildung von durch Lösungsmittel getrennten Ionenpaaren fördern können, was zu einer unterschiedlichen räumlichen Trennung von Iridium (Fluoreszenzquencher) und Fluorophor (Anion) führt.

1. 26 verschiedene Iridiumkomplexe wurden synthetisiert, die NHC-Liganden mit unterschiedlichen sterischen und elektronischen Eigenschaften enthalten (Abbildung 94). Die elektronischen Parameter der entsprechenden Iridiumkomplexe wurden ausgewertet (Redoxpotential und ν(CO)).

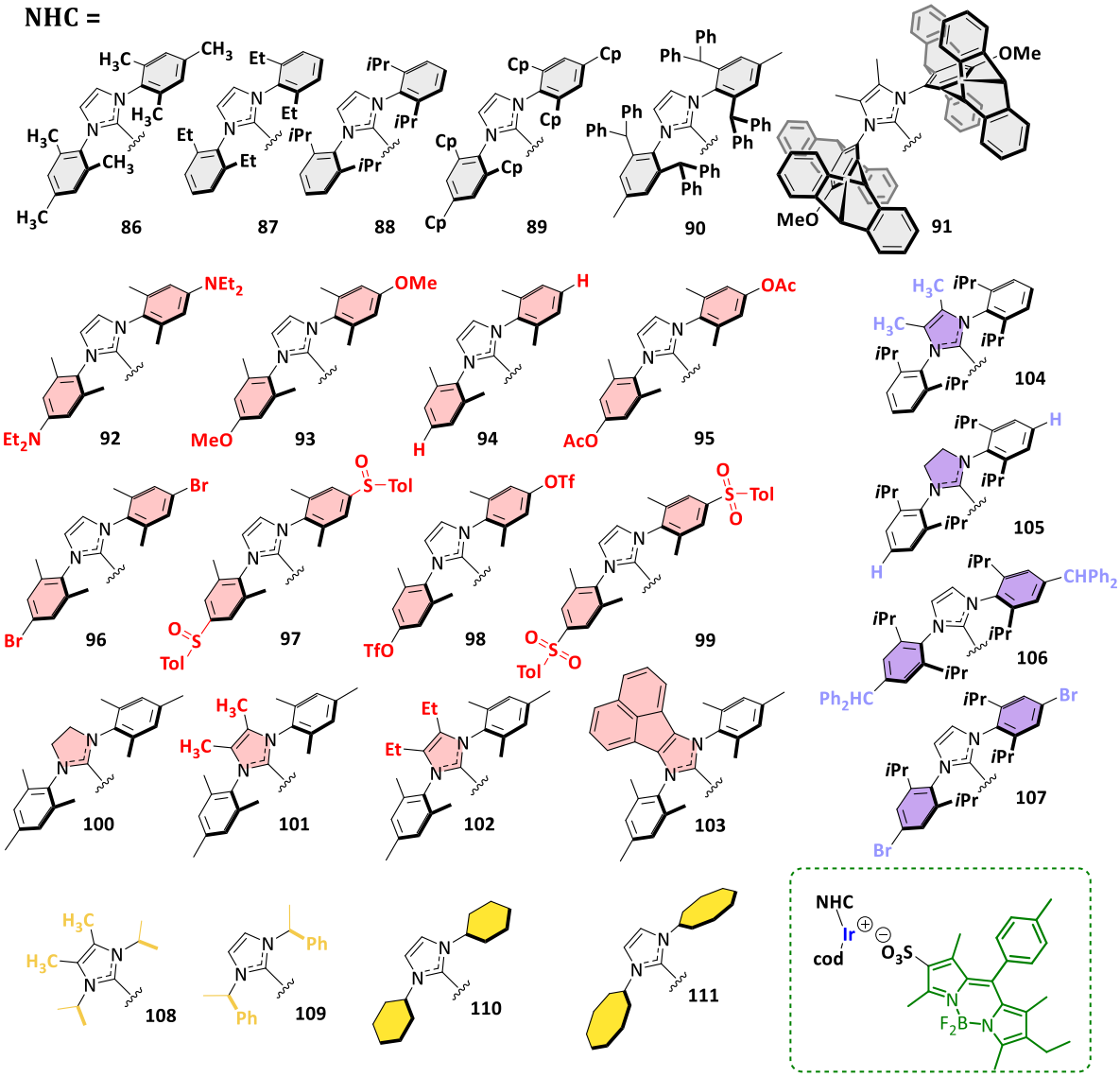

Abbildung 94 Es wurden 26 Iridiumkomplexe mit unterschiedlichen sterischen und elektronischen NHC-Ligandeneigenschaften synthetisiert.

2. Die jeweilige Fluoreszenzintensität für die entsprechenden [Ir(bdpSO_3)(cod)(NHC)]-Komplexe wurde in dce-Lösung bestimmt. Elektronendonierende und sterisch belastende Liganden erleichtern die Bildung von Lösungsmittel getrennten Ionenpaaren, die zu einer räumlichen Trennung von Kation und Anion führt (Abbildung 95). Der vergrößerte Abstand zwischen dem Fluorophor und dem Ir-Quencher führt zu einer deutlichen Zunahme des Fluoreszenzsignals.

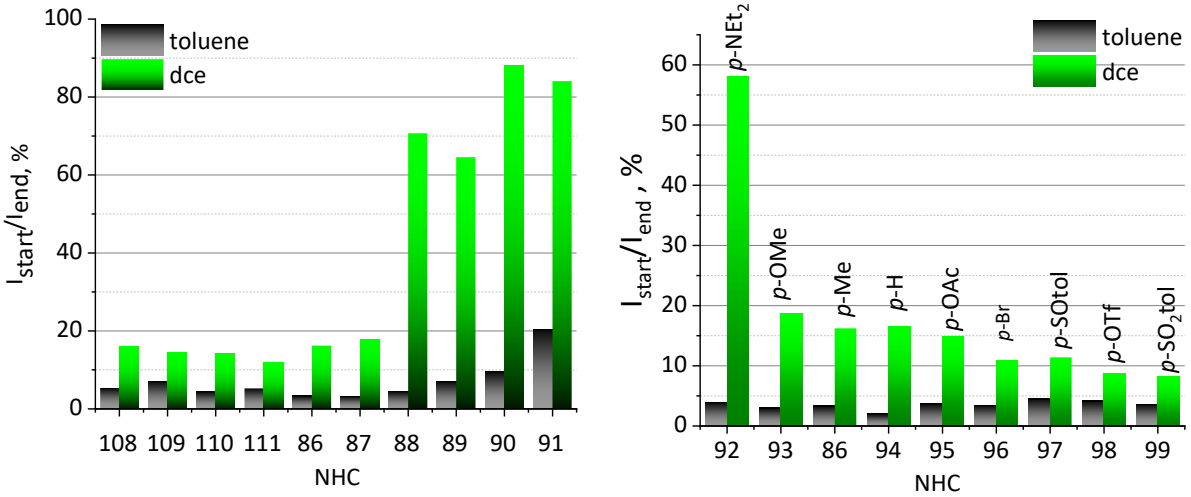

Abbildung 95 Fluoreszenzintensität in Toluol/dce-Lösung für die entsprechenden [Ir(bdpSO$_3$)(cod)(NHC)]-Komplexe (die Nummerierung der NHC-Liganden entspricht der Abbildung 94). Reproduziert aus Ref. 157 gemäß der CC BY-NC-ND 4.0 Lizenz *(https:/creativecommons.org/licenses/by-nc-nd/4.0/)*.

3. Die elektronischen Eigenschaften der Liganden wurden anhand der etablierten elektronischen Deskriptoren (Redoxpotential und ν(CO)) untersucht (Abbildung 96). Die lineare Beziehung zwischen Redoxpotential und Carbonylfrequenzen ermöglicht die Korrektur der Fluoreszenzdaten entsprechend der unterschiedlichen Donorfähigkeit der NHC-Liganden und zeigt die sterische Größe der NHC-Liganden.

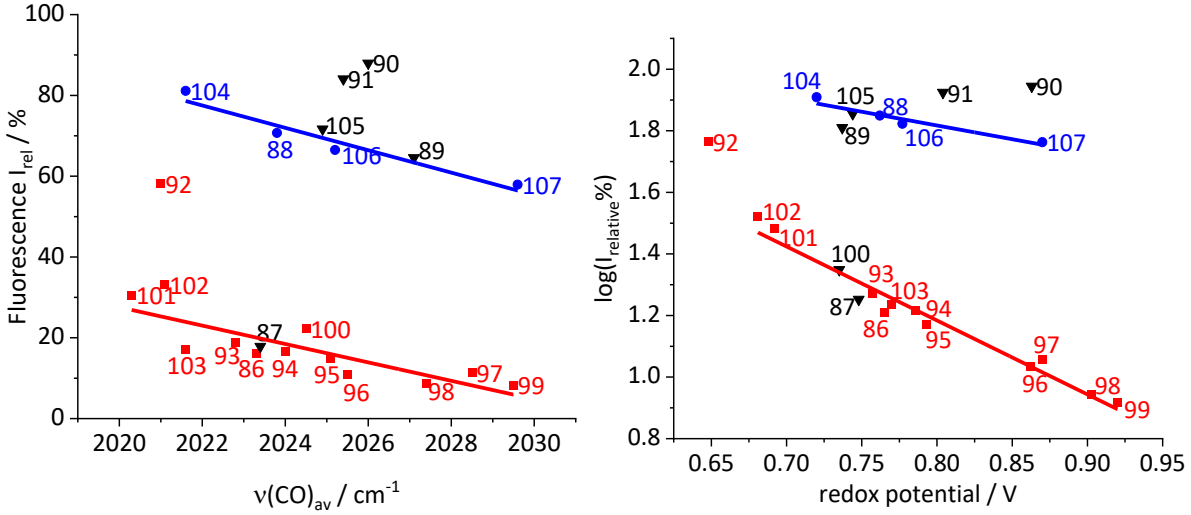

Abbildung 96 Korrelation der Fluoreszenzdaten über etablierte elektronischen Deskriptoren (Redoxpotential und ν(CO)). Reproduziert aus Ref. 157 gemäß der CC BY-NC-ND 4.0 Lizenz *(https:/creativecommons.org/licenses/by-nc-nd/4.0/)*.

Der Ionenpaarungsansatz liefert Informationen zur Bestimmung sowohl der sterischen als auch der elektronischen Eigenschaften von NHC-Liganden, die sich auf die Bildung von Lösungsmittel getrennten Ionenpaaren auswirken. Die Korrelation der Fluoreszenzdaten über elektronische Deskriptoren (Redoxpotential und ν(CO)) ermöglicht die Dekonvolution des kombinierten Einflusses von elektronischen und sterischen Faktoren der entsprechenden NHC-Liganden. Die Bestimmung der sterischen Eigenschaften von Liganden sollte nicht auf NHC-Liganden beschränkt sein - im Prinzip könnten die sterische Belastung und die elektronischen Eigenschaften jeder Art von Ligand mit einem ähnlichen Konzept untersucht werden.

Teil 3. *Schaltbare Fluoreszenz und Photosensibilisierung basierend auf reversibler Ionenpaarung.*[266]

Nach den vorläufigen Informationen kann die Fluoreszenzemission gequencht werden, wenn sich das Übergangsmetall in der Nähe des Fluorophors befindet. In solchen Systemen kann die Anregungsenergie durch photoinduzierten Elektronentransfer und den strahlungslosen Übergang vom angeregten elektronischen Zustand S_1 zu T_1 verloren gehen. In dieser Arbeit stellten wir uns die Frage, welches der hauptsächliche Weg der Fluoreszenzlöschung für einen ionengepaarten kationischen NHC-Iridium-Komplex und anionisches Bodipy ist. Wir wollten untersuchen, wie der Anteil der Ionenpaarung die Schaltung der Fluoreszenzeigenschaften und die Photosensibilisierungseffizienz in Abhängigkeit vom Gleichgewicht der Ionenassoziation/-dissoziation beeinflussen kann.

1. Wir haben festgestellt, dass das enge Ionenpaar von [Ir(bdpSO$_3$)(cod)(**86**)] ein effizienter Photosensibilisator für die Erzeugung von Singulett-Sauerstoff ist, während das vom Lösungsmittel getrennte Ionenpaar (nach Zugabe von DMSO) stark fluoresziert (Abbildung 97). Die Kontrolle der Ionenassoziation bestimmt somit den Weg der Exzitationsenergie, die entweder in den S_1-Zustand oder über den Intersystemübergang in den T_1-Zustand geleitet wird.

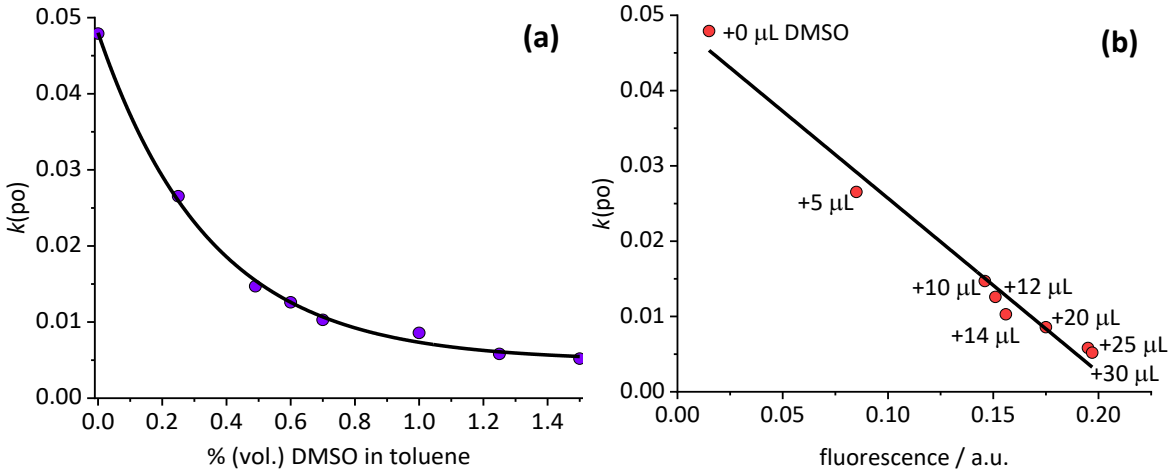

Abbildung 97 Korrelation der Geschwindigkeit (*k*(po)) der $^1O_2$-Generierung (a) und der Fluoreszenzintensität (b) durch [Ir(bdpSO$_3$)(cod)(**86**)] in einer Toluollösung, die verschiedene Mengen an DMSO enthält. Reproduziert aus Ref. 266 gemäß der CC BY-NC 3.0 Lizenz (*https:/creativecommons.org/licenses/by-nc/3.0/*)

2. Es wurde festgestellt, dass die Modulation der NHC-Donierung sich auf die Photosensibilisierungseigenschaften auswirkt. Nur elektronenreiche NHC liefern hocheffiziente Photosensibilisatoren, deren Singulett-Sauerstoff-Quantenausbeute bei bis zu $\Phi_{s.o.}$ = 0.88 liegt. Die Donorfähigkeit der NHC-Liganden wurde anhand des Ir(I/II)-Redoxpotenzials der jeweiligen [Ir(bdpSO$_3$)(cod)(NHC)]-Komplexe korreliert (Abbildung 98).

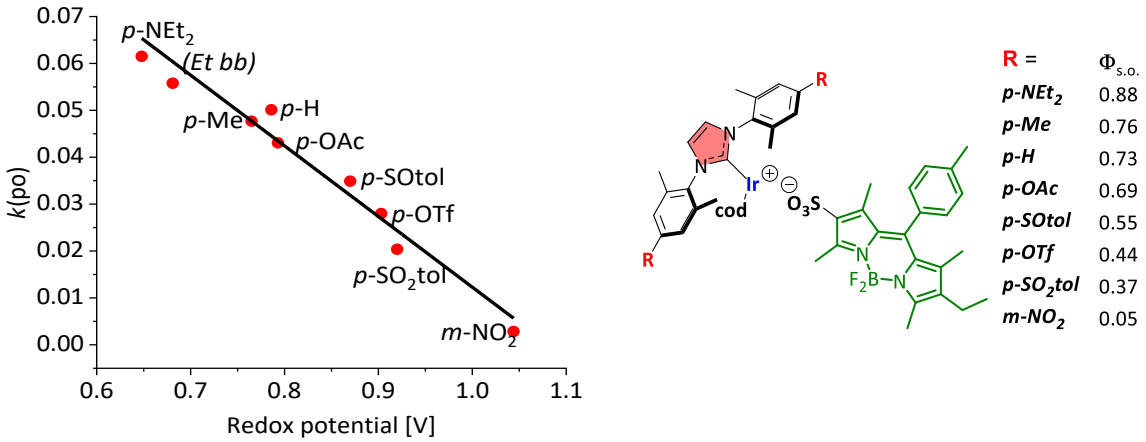

Abbildung 98 Korrelation der Geschwindigkeit (k(po)) zur $^1O_2$-Erzeugung für verschiedene elektronische [Ir(bdpSO$_3$)(cod)(NHC)]-Komplexe im Vergleich zum Redoxpotential für [IrCl(cod)(NHC)]-Komplexe in dce. Reproduziert aus Ref. 266 gemäß der CC BY-NC 3.0 Lizenz (*https://creativecommons.org/licenses/by-nc/3.0/*).

3. Die Nutzung der reversiblen Assoziation/Dissoziation zwischen Ionen in ionengepaarten Komplexen kann zur Entwicklung verschiedener Arten von molekularen Schaltern verwendet werden. Wir haben einen neuartigen Schalter auf der Grundlage des Komplexes [Ir(bdpSO$_3$)(cod)(**86**)] vorgestellt. Die Trennung-Rekombination von Anion und Kation wurde durch Überwachung des Fluoreszenzsignals beobachtet (Abbildung 99). Die Reversibilität des ionengepaarten Komplexes in Toluollösung wurde durch Zugabe eines Äquivalents NBu$_4$Br-Salzes mit stark koordinierendem Bromidanion (BdpSO$_3^-$ wird vom Metallquencher getrennt, Fluoreszenz = an) und NaBArF mit einem schwach koordinierenden Anion (BdpSO$_3^-$ ist stärker koordinierend zum Metallquencher als BArF$^-$, Fluoreszenz = aus) nachgewiesen.

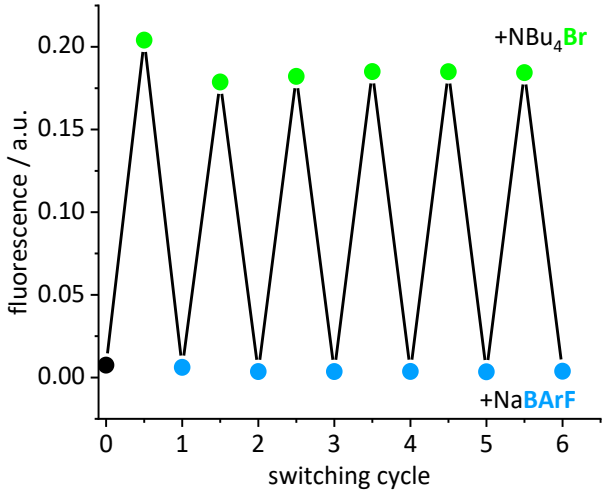

Abbildung 99 Schaltbare Fluoreszenz für den [Ir(bdpSO$_3$)(cod)(**86**)]-Komplex nach Zugabe von 1 Äq. NBu$_4$Br und NaBArF-Lösung. Reproduziert aus Ref. 266 gemäß der CC BY-NC 3.0 Lizenz (*https://creativecommons.org/licenses/by-nc/3.0/*).

Abschließend werden schaltbare Fluorophore/Photosensibilisatoren vorgestellt, deren Aktivität in Abhängigkeit von der Wechselwirkung zwischen Anion und Kation, die durch die Lösungsmittelzusammensetzung gesteuert wird, moduliert werden kann. Somit kann bei einem engen Ionenpaar die Aktivierungsenergie im S_1-Niveau in das T_1-Niveau geleitet werden, wodurch effiziente Photosensibilisatoren für die Erzeugung von

Singulett-Sauerstoff entstehen. Das in dieser Arbeit vorgestellte Grundprinzip kann für spezifische Anwendungen angepasst werden, indem andere Ionenpaare mit schwächeren, stärkeren und sogar selektiven Wechselwirkungen gewählt werden, deren Trennung durch verschiedene chemische oder physikalische Stimuli initiiert werden kann.

Teil 4. *Fluoreszierende organometallische Dyaden und Triaden: Herstellung räumlicher Beziehungen.*[249]

Die Identifizierung von Aufbau- und Abbauprozessen in metallorganischen Systemen mit Hilfe einer einzigen Art von Fluoreszenzmarkierung ist eine schwierige Aufgabe. Der Einsatz von Fluoreszenzresonanzenergietransfer (FRET) ist eine alternative Strategie zur Verbesserung der Detektierbarkeit. Die Anwendung der FRET-Methode mit geeigneten Fluoreszenzmarkern ermöglicht die Beobachtung räumlicher Verbindungen in metallorganischen Komplexen und die Aufklärung spezifischer Wechselwirkungen zwischen Akzeptor- und Donor-Fluorophormolekülen, die sich in der Nähe befinden oder als Teil des gleichen Moleküls vorliegen.

1. Azoliumsalze, die mit blau, grün und rot fluoreszierendem Bodipy markiert sind, wurden synthetisiert und zur Herstellung verschiedener NHC-Metallkomplexe verwendet (Abbildung 100). Die entwickelten Farbstoffe sind chemisch und photochemisch stabil und zeichnen sich dadurch aus, dass sie keine basischen Lewis-Heteroatome enthalten, mit geeigneten funktionellen Gruppen für die Konjugation ausgestattet sind und effiziente FRET-Paare mit minimalem Cross-Talk bilden.

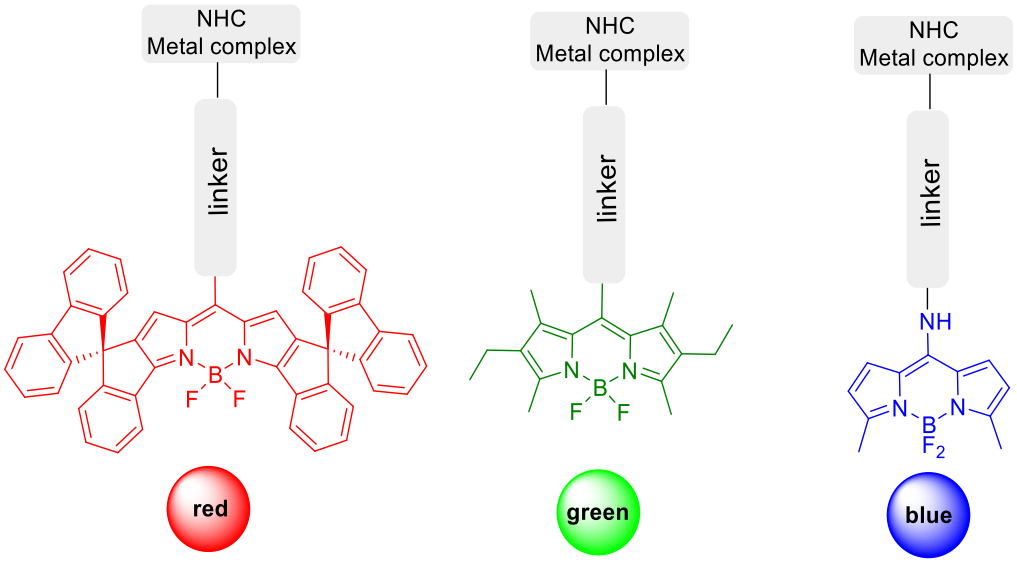

Abbildung 100 Fluorophore (blau, grün, rot) markierte NHC-Metallkomplexe.

2. Die metallorganischen Farbstoffe **125** und **126**, die auf der grünen und roten Emission basieren, liefern zwei Informationskanäle für die Bildung von Komplexen, die für Alkin-verbrückte Digoldspezies (Abbildung 101a) und für die Ionenpaarung des rot fluoreszierenden Kations und des grün fluoreszierenden Anions (Abbildung 101b) nachgewiesen wurden. Dies deutet auf einen praktisch vollständigen Energietransfer vom grünen zum roten Fluorophor hin, der aufgrund des geringen Abstands zwischen dem grünen und dem roten Fluorophor stattfindet. Bei Komplex **126** führen die Erhöhung der Dielektrizitätskonstante des Lösungsmittelgemischs nach der Zugabe von DMAc und die schwache Wechselwirkung von DMAc mit Gold zu lösungsmittelgetrennten Ionenpaaren,

die durch ein schwaches 648 nm Signal und ein starkes 530 nm Signal gekennzeichnet sind.

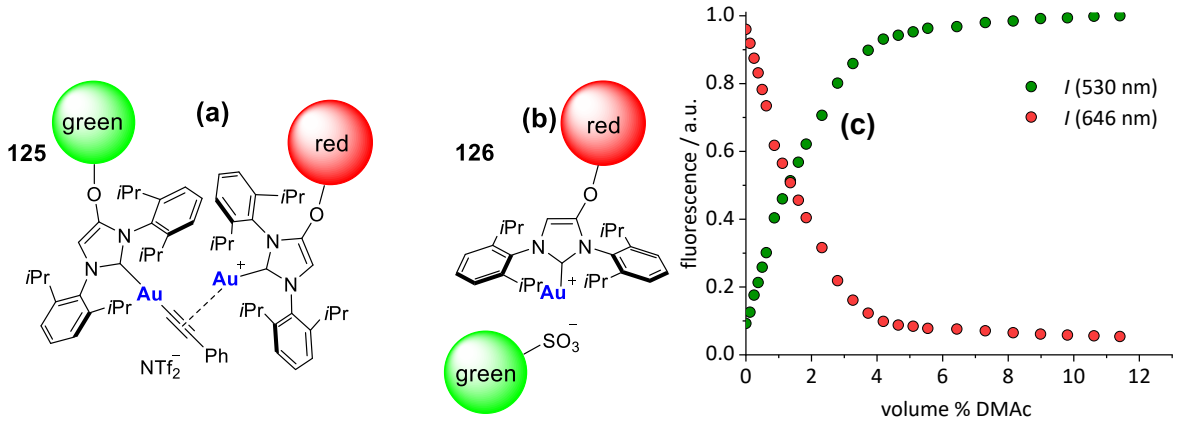

Abbildung 101 Herstellung von metallorganischen Dyaden für alkinverbrückte Digoldspezies (a) und ionengepaarte kationische Iridiumkomplexe und anionische Bodipy-Fluorophore (b). (c) Titration der ionengepaarten [Au(bpdSO_3)(**119**_red)]-Komplexlösung mit DMAc. Reproduziert aus Ref. 249 gemäß der CC BY-NC 3.0 Lizenz (*https:/creativecommons.org/licenses/by-nc/3.0/*)

3. Der Ansatz mit zwei Fluorophoren wurde erweitert, um den Zusammenbau von drei verschiedenen Subsystemen zu untersuchen, die mit unterschiedlich markierten Bodipy-Farbstoffen (blau, grün, rot) synthetisiert wurden. Die Anregung des blauen Farbstoffs löst einen Energietransfer in der Reihenfolge blau/grün/rot aus, was die Vereinigung der drei unterschiedlich markierten Untereinheiten (Triade) in einem einzigen Molekül **135** belegt (Abbildung 102).

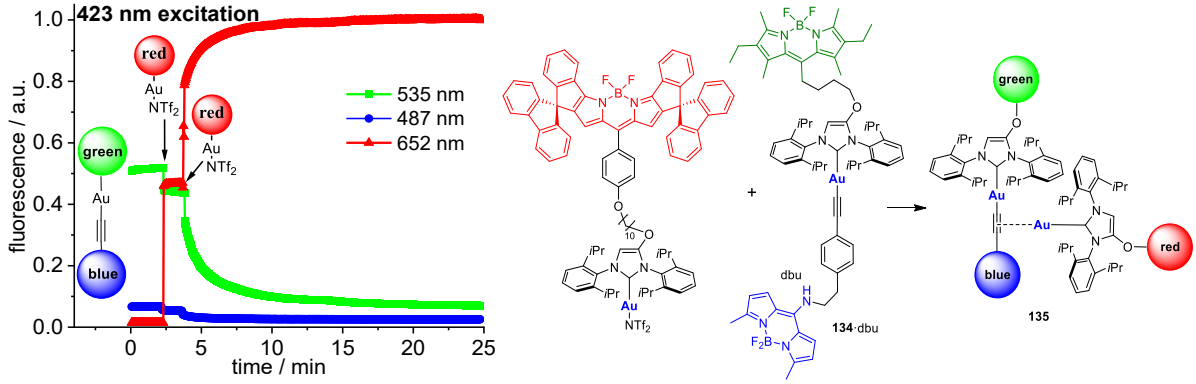

Abbildung 102 Triadenbildung für ein Widenhoefer-Dimer mit Bodipy-markierten Komplexen. Reproduziert aus Ref. 249 gemäß der CC BY-NC 3.0 Lizenz (*https:/creativecommons.org/licenses/by-nc/3.0/*).

Die Markierung molekularer Komponenten mit robusten Fluorophoren kann eine allgemeine Strategie in der (organometallischen) Chemie sein, um Zusammenhänge für binukleare Katalysatorruhezustände und binukleare Katalysatorabbauprodukte in der homogenen Katalyse herzustellen. Diese Methodik öffnet die Möglichkeiten für ein besseres Verständnis der dynamischen Wechselwirkungen in der metallorganischen Chemie in Lösung - in einem Konzentrationsbereich, der für viele andere spektroskopische Techniken weniger leicht zugänglich ist.

6. Experimental

General experimental. Synthesis was performed in pre-dried Schlenk flasks under a positive pressure of argon or nitrogen. The flasks were fitted with rubber septa and gas-tight syringes with stainless steel needles or double-cannula were used to transfer air- and moisture-sensitive liquids. All reactions involving transition metal complexes were conducted in oven-dried glassware. All solvents were dried and used after distillation: dichloromethane and 1,2-dichloroethane dried over CaH_2; THF dried over sodium, dimethylacetamide distilled over CaH_2; methanol distilled over K_2CO_3; acetone distilled over CaO. CH_2Cl_2 was obtained from Fisher Scientific and pentane was obtained from BCD Chemie GmbH in Frankfurt. Toluene from Sigma-Aldrich (Lab. Reagent grade, 99.3 %) was dried and purified.[267] After distillation, solvents were stored over molecular sieves 4Å. All reagents were used as purchased for the reactions without further purification. Column chromatography was performed on silica 60 (Machery-Nagel GmbH & Co.KG, 0.063-0.2 mm) with the indicated eluent mixtures. Filtration processes were performed using filter paper 310 with particle retention 10− 20 μm or SCHOTT-DURAN glass filter Por.4. High vacuo denotes pressure range 10 – 10^{-3} mbar. ^{1}H, ^{13}C, and ^{19}F NMR spectra were recorded on a Bruker DRX 500 or Bruker ARX 300 spectrometer. The chemical shifts are given in parts per million (ppm) on the delta scale (δ) and are referenced to tetramethylsilane (^{1}H, ^{13}C NMR = 0.0 ppm). Abbreviations for NMR data: s = singlet; d = doublet; t = triplet; q = quartet; sep = septet; m = multiplet; bs = broad signal. Mass spectra were recorded on the Bruker Impact II spectrometer using electrospray ionization (ESI) and atmospheric pressure chemical ionization (APCI). UV-Vis spectra were recorded on Analytik Jena Specord 600 UV-Vis spectrometer. Emission spectra were recorded on corrected J&M TIDAS S700/CCD UV/NIR 2098 spectrometer combined with J&M TIDAS LSM monochromator with 75 W Xenon light source. Cyclic voltammetry was performed using standard electrochemical instrumentation consisting of an EG&G 273A-2 potentiostat-galvanostat. A three-electrode configuration was employed. The working electrode was a Pt disk (diameter 1 mm) sealed in soft glass with a Pt wire as a counter electrode. The pseudo reference electrode was an Ag wire. Potentials were calibrated internally against the formal potential of ferrocene (+0.46 V *vs*. Ag/AgCl) or octamethylferrocene (-0.01 V *vs*. Ag/AgCl). All cyclic voltammograms were recorded in dry methylene chloride or 1,2-dichloroethane under an atmosphere of argon, supporting electrolyte N*n*Bu_4PF_6 (c =0.1 mol/L) at scan rate of 50-150 mV/s. The photoreactions were performed using a green LED light strip (12 V strip green light 5 m 3528 SMD 300 LED, 60 LED/m, 4.8 W per meter strips). Home-built photoreactor was made by wrapping approximately 2.3 m of the LED strips around a 600 ml glass beaker. The quartz cuvettes were placed in the middle of the photoreactor, with a bottom diameter of 9 cm for the beaker reactor. The following [IrCl(cod)(NHC)] complexes were synthesized in this work according to literature procedures; [(**86**)IrCl(cod)][181], [(**87**)IrCl(cod)][179], [(**88**)IrCl(cod)][181], [(**90**)IrCl(cod)][268], [(**91**)IrCl(cod)][269], [(**92**)IrCl(cod)][154], [(**93**)IrCl(cod)][179], [(**94**)IrCl(cod)][154], [(**95**)IrCl(cod)][179], [(**96**)IrCl(cod)][154], [(**97**)IrCl(cod)][154], [(**98**)IrCl(cod)][179], [(**99**)IrCl(cod)][154], [(**100**)IrCl(cod)][154], [(**101**)IrCl(cod)][179] [(**102**)IrCl(cod)][179], [(**104**)IrCl(cod)][270], [(**105**)IrCl(cod)][160], [(**108**)IrCl(cod)][200], [(**110**)IrCl(cod)][200], [IrCl(cod)(**115**)][271]. Compounds 9-(2-Bromophenyl)-9H-fluoren-9-ol[272], 8-Chloro Bodipy[273], 8-SMe Bodipy[25], **122**[244], [AuCCPh(**124**_green)][244], [AuCl(**124**_green)][244], **124**·HBr[244], [Au(NTf_2)(**124**_green)][244] were prepared according the reported literature procedures.

6.1.1. Experimental Procedures and Compounds Characterization

General procedure A – synthesis of 85·HI metal complexes. To a Schlenk flask equipped with a stirring bar containing **85·HI** and Ag_2O under a flow of the nitrogen gas, dry 1,2-dichloroethane was added and the flask was sealed. After 90 min of stirring in the dark at 55 °C, a metal precursor was added, and the mixture was stirred for an additional 2 h at 60 °C. The resulting suspension was filtered through a short pad of celite. The filtrate was collected and evaporated under reduced pressure. The product was purified by column chromatography (cyclohexane/ethyl acetate = 3/1).

General procedure B – synthesis of [MCl(CO)$_2$(85)] (M =Rh, Ir) metal complexes. To a Schlenk flask equipped with a stirring bar and septa, the corresponding cod-complex and CH_2Cl_2 (2 mL) was added. A balloon with CO gas was connected *via* cannula and CO was bubbled through the stirred solution for 30 min at room temperature. The volatiles were evaporated under reduced pressure, pentane (5 mL) was added, and the suspension was sonicated for 5 min. The solid material was filtered off and washed with another batch of pentane (2 × 5 mL).

General Procedure C – [IrCl(cod)(NHC)] formation. A vial was charged with the corresponding azolium salt (1.0 eq.), $[IrCl(cod)]_2$ (0.5 eq.) and K_2CO_3 (3.0 eq.). The resulting mixture was suspended in acetone (3.0 mL) and stirred for 20 h at 60 °C. After this time the solvent was removed in vacuo and dichloromethane added (3.0 mL). The mixture was filtered through a pad of silica. The residue was purified by flash chromatography (CH_2Cl_2) to afford the desired complex as a yellow microcrystalline solid.

General Procedure D – [IrCl(cod)(NHC)] formation. Azolium salt (1.8 eq.) and KO*t*Bu (2.0 eq.) were placed in a Schlenk tube, dissolved in dry THF (5 mL) under atmosphere of N_2 and stirred for 30 min at room temperature. To this mixture was added the $[IrCl(cod)]_2$ (1.0 eq.). The reaction mixture was stirred for 4 h at room temperature and the solvent was evaporated in vacuo. The mixture was dissolved in CH_2Cl_2 and filtered through a pad of silica. The residue was purified by flash chromatography (CH_2Cl_2) to afford the desired complex as yellow microcrystalline solid.

General Procedure E – [IrCl(cod)(NHC)] formation. Azolium salt (1.0 eq.) and Ag_2O (0.5 eq.) were placed in Schlenk tube and dissolved in dry CH_2Cl_2. The mixture was stirred overnight, changing color from a black slurry to a clear solution. Addition of $[IrCl(cod)]_2$ (0.5 eq.) gave a bright yellow solution. After stirring the solution for 3 h at room temperature the volatiles were evaporated *in vacuo*. The residue was purified by flash column chromatography (CH_2Cl_2) to afford the desired complex as yellow microcrystalline solid.

General Procedure F – synthesis of Bodipy derivatives. To a solution of pyrrole (0.33 mmol, 2.0 eq.) and aldehyde (0.16 mmol, 1.0 eq.) in dry CH_2Cl_2 (3.0 mL) was added a catalytic amount of TFA (1 drop), and the solution was stirred at rt for 15 h under nitrogen atmosphere. The reaction mixture was poured into 5% aq. solution of $NaHCO_3$ and extracted with CH_2Cl_2 (3 x 100 mL). The combined organic layers were washed with brine (100 mL), followed by drying of the organic layer over $MgSO_4$ and filtration over a paper filter. After evaporation of the volatiles in a rotavap, the residue was dissolved in dry CH_2Cl_2 (3.0 mL) and treated with DDQ (36 mg, 0.16 mmol). After stirring for 1 h, Et_3N (0.2 mL, 1.4 mmol) and $BF_3{\cdot}OEt_2$ (0.3 mL, 2.4 mmol) were added at 0 °C, and the resulting mixture was stirred at rt for another 15 h. The reaction mixture was poured into 5% aq. solution of $NaHCO_3$ and extracted with CH_2Cl_2 (3 x 100 mL). The combined organic layers

were washed with brine (100 mL), followed by drying over $MgSO_4$ and filtration. After evaporation of the volatiles in a rotavap, the crude product was purified by column chromatography followed by recrystallization from CH_2Cl_2 and MeOH to afford the pure product.

General procedure G – synthesis of alkoxy substituted products. A mixture of alkyl bromide (0.3 mmol, 1.5 eq.), alcohol (0.2 mmol, 1.0 eq.), K_2CO_3 (0.4 mmol, 2.0 eq.), and KI (0.6 mmol, 3.0 eq.) in dry acetone (3.0 mL) was heated to reflux for 15 h under nitrogen atmosphere. The mixture was poured into CH_2Cl_2 (200 mL) and washed with brine (100 mL). After drying over $MgSO_4$ and filtration over a paper filter the solvent was evaporated in a rotavap. The remaining solid was purified by column chromatography (silica, CH_2Cl_2 100%→ CH_2Cl_2/EtOH = 50/1).

General procedure H – synthesis of 8-Amino Bodipy derivatives. To a solution of the corresponding 8-Chloro-Bodipy[273](0.5 mmol, 1.0 eq.) in CH_2Cl_2 (5 mL) propylamine (1.0 mmol, 2.0 eq.) was added. The reaction mixture was stirred at rt for 2 h. After the addition of water (50 mL) the resulting solution was poured into CH_2Cl_2 (30 mL) and the organic layer separated. The organic solution was washed with brine (25 mL) and water, dried over $MgSO_4$, filtered over a paper filter and evaporated on the rotavap under reduced pressure. The crude product was purified by column chromatography on silica (CH_2Cl_2/MeOH = 30/1).

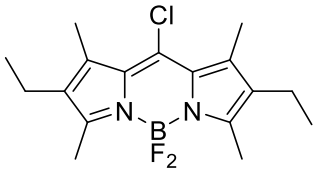

83

Synthesis of *meso*-chloro Bodipy 83.[273] 2,4-dimethyl-3-ethyl-pyrrole (2 ml, 14.8 mmol) was dissolved in 50 ml of dry Et_2O and (5.12 ml, 15.5 mmol) of 3 M EtMgBr solution in Et_2O were added dropwise at 0 °C over 1 h under nitrogen atmosphere before heating to reflux for 3 h. After cooling to rt, 15% phosgene solution in toluene (5.28 ml, 7.4 mmol) was added dropwise within 1 h and formation of a pale precipitate was observed upon addition. The reaction mixture was stirred for 48 h at rt, cooled to 0 °C and 100 ml of water was added. Phases were separated and the aqueous phase was extracted with $CHCl_3$. Combined organic phases were dried over $MgSO_4$ and all volatiles were evaporated on the rotavap under reduced pressure. Resulted crude pale-yellow product was washed with CH_2Cl_2 (15 mL) and used in further synthesis without additional purification (yield 1.24 g, 60%). In the next step, Dipyrrolyl-2-yl methanone (640 mg, 4 mmol) was dissolved in 1,2-dichloroethane (40 ml). $POCl_3$ (0.72 ml, 8 mmol) was added, and the reaction mixture was heated to reflux for 3 h, then cooled in an ice bath. Et_3N (5.6 ml, 40 mmol) was added, and the reaction was stirred at 0 °C for 20 min. $BF_3{\cdot}OEt_2$ (5.6 ml, 44 mmol) was added dropwise while maintaining the temperature at 0 °C. The reaction mixture was allowed to warm up to rt and stirred for additional 2 h. The resulting solution was poured into diethyl ether (600 ml). The organic layer was separated and was washed with water. After drying over $MgSO_4$, filtration, and evaporation, the crude product was purified using flash chromatography (CH_2Cl_2/cyclohexane = 1/1) to give product as red crystalline solid (480 mg, yield 37%).

^{1}H NMR (300 MHz, chloroform-*d*) δ / ppm = 2.49 (s, 6H), 2.40 (m, 10H), 1.05 (t, J = 7.6 Hz, 1H).

^{13}C{^{1}H} NMR (75 MHz, chloroform-*d*) δ / ppm = 153.8, 138.2, 135.3, 133.3, 129.3, 17.2, 14.9, 13.9, 12.6.

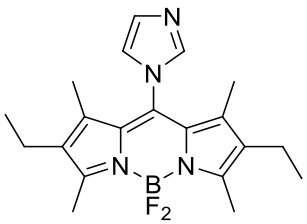

84

Synthesis of 8-Imidazolo-Bodipy (84). In a 25 mL round-bottom flask equipped with a stirring bar, imidazole (502 mg, 7.38 mmol, 10 eq.), 8-chloro-Bodipy **83** (250 mg, 0.74 mmol, 1 eq.) and K_2CO_3 (407 mg, 2.95 mmol, 4 eq.) were dissolved in CH_2Cl_2 (10 ml). The mixture was stirred in a flask at rt for 24 h. The resulting solution was poured into CH_2Cl_2 (200 mL). The organic layer was separated and washed with water. After drying over $MgSO_4$, filtration, and evaporation. The crude product was purified by column chromatography (CH_2Cl_2 / MeOH = 25/1) to the product as a microcrystalline red solid (255 mg, yield 93 %).

^{1}H NMR (300 MHz, chloroform-*d*) δ / ppm = 7.57 (s, 1H, NCHN), 7.32 (s, 1H, CH), 7.01 (s, 1H, CH), 2.53 (s, 6H, CH_3 Bodipy), 2.33 (q, *J* =7.6 Hz, 4H, CH_2CH_3 Bodipy), 1.41 (s, 6H, CH_3 Bodipy), 1.01 (t, *J* =7.6 Hz, 6H, CH_2CH_3 Bodipy).
^{13}C{^{1}H} NMR (126 MHz, chloroform-*d*) δ / ppm = 157.2, 137.5, 136.5, 134.2, 131.4, 130.8, 129.6, 119.9, 17.1, 14.6, 12.9, 8.8.
^{19}F NMR (471 MHz, chloroform-*d*) δ / ppm = -144.63 (dq, $J(^{11}B\text{-}^{19}F_a)$ =33 Hz, $J(^{19}F\text{-}^{19}F)$ =104 Hz), -145.39 (dq, $J(^{11}B\text{-}^{19}F_b)$ = 31 Hz, $J(^{19}F\text{-}^{19}F)$ = 108 Hz).
HRMS (ESI positive): m/z calcd. for $C_{20}H_{26}BF_2N_4$: 371.22131 [M +H]$^+$; found 371.22155.

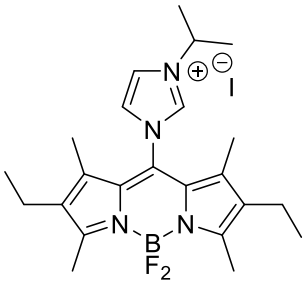

85

Synthesis of Bodipy-imidazolium salt (85·HI). To the imidazole **84** (100 mg, 0.27 mmol, 1 eq.) in 4 mL of acetone, 2-iodopropane (0.4 mL, 4 mmol, 15 eq.) was added and the mixture was stirred in the sealed flask at 70 °C overnight. The mixture was cooled to rt, after removal of the volatiles, the residue was purified by column chromatography (CH_2Cl_2 / MeOH = 10/1) to give the product as red microcrystalline solid (79 mg, 54 % yield).
^{1}H NMR (500 MHz, chloroform-*d*) δ / ppm = 10.39 (s, 1H, NCHN), 8.36 – 8.35 (m, 1H, CH), 7.43 – 7.42 (m, 1H, CH), 5.65 – 5.57 (m, 1H, CH *i*Pr), 2.49 (s, 6H, CH_3 Bodipy), 2.30 (q, *J* =7.6 Hz, 4H, CH_2CH_3 Bodipy), 1.67 (d, *J* =6.7 Hz, 6H, CH_3 *i*Pr), 1.47 (s, 6H, CH_3 Bodipy), 0.99 (t, *J* =7.6 Hz, 6H, CH_2CH_3 Bodipy).
^{13}C{^{1}H} NMR (126 MHz, chloroform-*d*) δ / ppm = 159.7, 136.2, 136.0, 135.6, 128.1, 126.2, 123.8, 122.9, 54.7, 23.5, 17.1, 14.5, 13.1, 9.7.
^{19}F NMR (471 MHz, chloroform-*d*) δ / ppm = -144.66 (dq, $J(^{11}B\text{-}^{19}F_a)$ = 33 Hz, $J(^{19}F\text{-}^{19}F)$ -=104 Hz), -145.41 (dq, $J(^{11}B\text{-}^{19}F_b)$ =31 Hz, $J(^{19}F\text{-}^{19}F)$ =108 Hz).
^{19}F {^{11}B} NMR (471 MHz, chloroform-*d*) δ / ppm = -144.38, -144.61, -145.50, -145.72.
^{11}B NMR (160 MHz, chloroform-*d*) δ 0.48.
HRMS (ESI positive): m/z calcd. for $C_{23}H_{32}BF_2N_4$: 413.26826 [M]$^+$; found 413.26888.

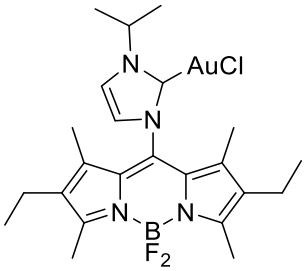

[AuCl(**85**)]

Syntheses of [AuCl(85)]. General Procedure A: **85**·HI (50 mg, 0.092 mmol), Ag_2O (10.7 mg, 0.046 mmol), [AuCl(SMe_2)] (27.1 mg, 0.092 mmol) in 1,2-dichloroethane (5 mL). Complex [AuCl(**85**)] was obtained as a red microcrystalline solid (29 mg, 48 % yield).

Synthesis of [AuNTf$_2$(**85**)]: 10 mL Schlenk flask was equipped with a stirring bar, the corresponding [AuCl(**85**)] (12.3 mg, 0.019 mmol) and [Ag(NTf$_2$)] (7.8 mg, 0.020 mmol), followed by addition of CH_2Cl_2 (2 mL). The mixture was stirred for 2 h at room temperature, protected from light. The formed precipitate of AgCl was separated by filtration over celite. The celite was washed with dichloromethane (10 mL). The combined filtrates were evaporated and dried overnight in a vacuum and obtained material was used further without additional purification.
^{1}H NMR (500 MHz, chloroform-*d*) δ / ppm = 7.32 (s, 1H, CH), 7.06 (s, 1H, CH), 5.31 – 5.22 (m, 1H, CH *i*Pr), 2.53 (s, 6H, CH_3 Bodipy), 2.33 (q, *J* =7.6 Hz, 4H, CH_2CH_3 Bodipy), 1.57 (s, 3H, CH_3 *i*Pr), 1.49 (s, 6H, CH_3 Bodipy), 1.43 (s, 3H, CH_3 *i*Pr), 1.03 (t, *J* = 7.6 Hz, 6H, CH_2CH_3 Bodipy).
^{13}C{^{1}H} NMR (126 MHz, chloroform-*d*) δ / ppm = 172.0, 158.0, 136.3, 134.5, 131.9, 129.1, 122.6, 118.1, 54.4, 23.8, 23.6, 17.2, 14.6, 9.6.
^{19}F NMR (471 MHz, chloroform-*d*) δ / ppm = -144.11 (dq, $J(^{11}B\text{-}^{19}F_a)$ =33 Hz, $J(^{19}F\text{-}^{19}F)$ =108 Hz), -146.35 (dq, $J(^{11}B\text{-}^{19}F_b)$ = 31 Hz, $J(^{19}F\text{-}^{19}F)$ =108 Hz).
HRMS (APCI): m/z calcd. for $C_{23}H_{31}AuBClFN_4$: 625.19745; found 625.19859.

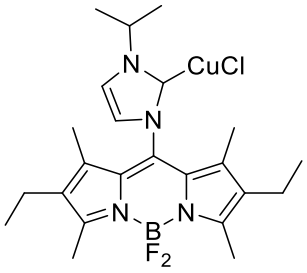

[CuCl(**85**)]

Syntheses of [CuCl(85)]. General Procedure A: **85**·HI (50 mg, 0.092 mmol), Ag_2O (10.7 mg, 0.046 mmol), CuCl (9.2 mg, 0.092 mmol) in 1,2-dichloroethane (5 mL). Complex [CuCl(**85**)] was obtained as a red microcrystalline solid (22.7 mg, 48% yield).
^{1}H NMR (500 MHz, chloroform-*d*) δ / ppm = 7.27 (s, 1H), 7.05 (s, 1H), 4.99 (p, *J* = 6.7 Hz, 1H), 2.53 (s, 6H), 2.32 (q, *J* = 7.5 Hz, 4H), 1.58 (d, *J* = 6.7 Hz, 6H), 1.45 (s, 6H), 1.02 (t, *J* = 7.5 Hz, 6H).
^{13}C{^{1}H} NMR (126 MHz, chloroform-*d*) δ / ppm = 157.82, 136.34, 134.41, 132.63, 129.13, 122.5, 118.6, 54.5, 27.0, 24.2, 17.2, 14.6, 13.0, 9.5.
^{19}F NMR (471 MHz, chloroform-*d*) δ / ppm = -144.23 (dq, $J(^{11}B\text{-}^{19}F_a)$ = 33 Hz, $J(^{19}F\text{-}^{19}F)$ = 108 Hz), -146.34 (dq, $J(^{11}B\text{-}^{19}F_b)$ = 33 Hz, $J(^{19}F\text{-}^{19}F)$ = 108 Hz).
HRMS (ESI positive) for $C_{46}H_{62}B_2CuF_4N_8$ found 887.4527.

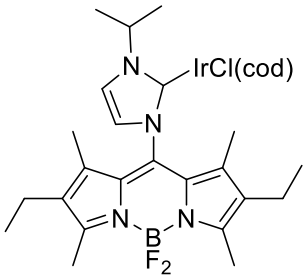

[IrCl(cod)(**85**)]

Syntheses of [IrCl(cod)(85)]. General Procedure A: **85**·HI (30 mg, 0.055 mmol), Ag_2O (6.4 mg, 0.028 mmol), $[IrCl(cod)]_2$ (18.5 mg, 0.028 mmol) in 1,2-dichloroethane (2 mL) yields the complex [IrCl(cod)(**85**)] as a dark red crystalline solid (7 mg, 17 % yield).
^{1}H NMR (500 MHz, chloroform-*d*) δ / ppm = 7.18 (d, *J* = 2.0 Hz, 1H, CH), 6.97 (d, *J* =1.9 Hz, 1H, CH), 5.85 – 5.80 (m, 1H, CH *i*Pr), 4.60 – 4.57 (m, 1H, H_{cod}), 4.31 – 4.26 (m, 1H, H_{cod}), 3.29 – 3.27 (m, 1H, H_{cod}), 2.77 – 2.73 (m, 1H, H_{cod}), 2.54 (d, *J* =9.6 Hz, 6H, CH_3 Bodipy), 2.33 (q, *J* = 8.0 Hz, 4H, CH_2CH_3 Bodipy), 2.26 – 2.15 (m, 2H, H_{cod}), 2.11 – 2.03 (m, 1H, H_{cod}), 1.96 – 1.87 (m, 1H, H_{cod}), 1.83 – 1.75 (m, 1H, H_{cod}), 1.74 (s, 3H, CH_3 *i*Pr), 1.56 (d, *J* =6.8 Hz, 3H, CH_3 Bodipy), 1.52 (d, *J* = 6.8 Hz, 3H, CH_3 Bodipy), 1.41 (s, 3H, CH_3 *i*Pr), 1.36 – 1.32 (m, 2H, H_{cod}), 1.15 – 1.05 (m, 1H, H_{cod}), 1.14 – 0.97 (m, 6H, CH_2CH_3 Bodipy).
^{13}C{^{1}H} NMR (126 MHz, methylene chloride-d_2) δ / ppm = 180.0, 158.7, 154.9, 140.7, 135.9, 134.9, 134.0, 133.6, 132.3, 130.1, 123.7, 118.3, 86.5, 83.3, 71.1, 52.2, 36.7, 31.9, 31.3, 30.3, 27.8, 24.2, 23.7, 17.6, 14.8, 13.4, 13.0, 11.3, 10.0.
^{19}F NMR (471 MHz, methylene chloride-d_2) δ / ppm = -145.50 (dq, $J(^{11}B\text{-}^{19}F_a)$ =33 Hz, $J(^{19}F\text{-}^{19}F)$ = 108 Hz), -146.03 (dq, $J(^{11}B\text{-}^{19}F_b)$ = 33 Hz, $J(^{19}F\text{-}^{19}F)$ = 108 Hz).
HRMS (ESI positive): m/z calcd. for $C_{31}H_{43}BF_2IrN_4$: 713.31726 $[M]^+$; found 713.31873.

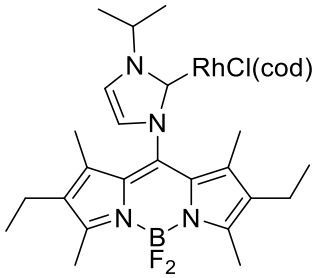

[RhCl(cod)(**85**)]

Syntheses of [RhCl(cod)(85)]. General Procedure A: **85**·HI (30 mg, 0.055 mmol), Ag_2O (6.4 mg, 0.028 mmol), $[RhCl(cod)]_2$ (13.8 mg, 0.028 mmol) in 1,2-dichloroethane (2 mL) yields the complex [RhCl(cod)(**85**)] as a dark red crystalline solid (8 mg, 22 % yield).
^{1}H NMR (500 MHz, methylene chloride-d_2) δ / ppm = 7.19 (d, *J* =1.7 Hz, 1H, CH), 7.03 (d, *J* =1.4 Hz, 1H, CH), 6.12 – 6.04 (m, 1H, CH *i*Pr), 4.75 – 4.72 (m, 1H, H_{cod}), 4.69 – 4.65 (m, 1H, H_{cod}), 3.63 – 3.60 (m, 1H, H_{cod}), 3.14 – 3.11 (m, 1H, H_{cod}), 2.56 (s, 3H, CH_3 Bodipy), 2.51 (s, 3H, CH_3 Bodipy), 2.50 – 2.43 (m, 1H, H_{cod}), 2.38 – 2.31 (m, 4H), 2.26 – 2.19 (m, 1H, H_{cod}), 2.09 – 2.02 (m, 2H, H_{cod}), 1.93 – 1.87 (m, 1H, H_{cod}), 1.82 – 1.76 (m, 1H, H_{cod}), 1.72 (s, 3H, CH_3 *i*Pr), 1.70 – 1.67 (m, 1H, H_{cod}), 1.64 – 1.59 (m, 1H, H_{cod}), 1,56 (s, 3H, CH_3 Bodipy), 1.43 (s, 3H, CH_3 Bodipy), 1.33 (s, 3H, CH_3 *i*Pr), 1.03 – 0.96 (m, 6H, CH_2CH_3 Bodipy).
^{13}C{^{1}H} NMR (126 MHz, methylene chloride-d_2) δ / ppm = 182.8 (d, *J* =52.2 Hz), 159.0, 154.7, 141.2, 135.7, 135.0, 134.3, 133.6, 132.3, 129.9, 124.1, 118.5, 99.2, 97.2, 79.2 (d, *J* = 13.9 Hz), 70.6 (d, *J* =14.4 Hz), 68.3 (d, *J* =14.0 Hz), 60.8, 35.9, 31.4, 31.2, 30.5, 27.5, 24.3, 23.7, 21.3, 17.5 (d, *J* =8.6 Hz), 14.9 (d, *J* = 7.1 Hz), 11.5, 9.8.
^{19}F NMR (471 MHz, methylene chloride-d_2) δ / ppm = -145.58 (dq, $J(^{11}B\text{-}^{19}F_a)$ =33 Hz, $J(^{19}F\text{-}^{19}F)$ =108 Hz), -145.91 (dq, $J(^{11}B\text{-}^{19}F_b)$ =33 Hz, $J(^{19}F\text{-}^{19}F)$ =104 Hz).
HRMS (ESI positive): m/z calcd. for $C_{31}H_{43}BF_2N_4Rh$: 623.25984 $[M]^+$; found 623.26046.

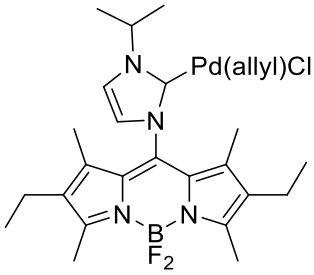

[Pd(allyl)Cl(**85**)]

Synthesis of [Pd(allyl)Cl(85)]. General Procedure A: **85**·HI (30 mg, 0.055 mmol), Ag_2O (6.4 mg, 0.028 mmol), $[Pd(allyl)Cl]_2$ (10.2 mg, 0.028 mmol) in 1,2-dichloroethane (2 mL) yields the complex [Pd(allyl)Cl(**85**)] as a dark red crystalline solid (8 mg, 25 % yield).
^{1}H NMR (500 MHz, chloroform-*d*) δ / ppm = 7.29 (d, J = 1.9 Hz, 1H, CH), 7.09 (d, J =1.9 Hz, 1H, CH), 5.57 – 5.49 (m, 1H, CH *i*Pr), 5.17 – 5.09 (m, 1H, allyl), 4.16 – 4.14 (m, 1H, allyl), 3.14 (d, J =13.5 Hz, 1H, allyl), 3.08 (d, J =6.7 Hz, 1H, allyl), 2.52 (d, J =7.1 Hz, 6H, CH_3 Bodipy), 2.42 – 2.25 (m, 4H, CH_2CH_3 Bodipy), 2.16 (d, J =12.0 Hz, 1H, allyl), 1.64 (s, 3H, CH_3 Bodipy), 1.57 – 1.50 (m, 9H, CH_3 Bodipy + CH_3 *i*Pr), 1.03 – 0.99 (m, 6H, CH_2CH_3 Bodipy).
^{13}C{^{1}H} NMR (126 MHz, chloroform-*d*) δ / ppm = 181.5, 157.0, 156.7, 137.5, 133.9, 133.7, 133.5, 129.6, 129.3, 122.0, 118.4, 115.2, 73.2, 53.0, 50.1, 26.8, 23.64, 23.57, 16.91, 16.88, 14.4, 12.69, 12.65, 9.6, 9.4.
^{19}F NMR (471 MHz, chloroform-*d*) δ / ppm = -144.50 (dq, J(^{11}B-$^{19}F_a$) =33 Hz, J(^{19}F-^{19}F) =108 Hz), -145.89 (dq, J(^{11}B-$^{19}F_b$) = 33 Hz, J(^{19}F-^{19}F) =108 Hz).
HRMS (ESI positive): m/z calcd. for $C_{26}H_{36}BF_2N_4Pd$: 559.20305 $[M]^+$; found 559.20394.

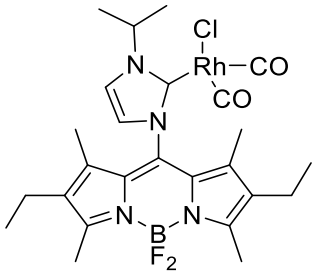

[$RhCl(CO)_2$(**85**)]

Synthesis of [$RhCl(CO)_2$(85)]. General Procedure B: [$RhCl(CO)_2$(**85**)] complex was obtained as a dark red solid from [RhCl(cod)(**85**)] (12 mg, 84 % yield).
^{1}H NMR (500 MHz, methylene chloride-d_2) δ / ppm = 7.36 (d, J =1.8 Hz, 1H, CH), 7.20 (d, J =1.7 Hz, 1H, CH), 5.52 – 5.45 (m, 1H, CH *i*Pr), 2.52 (s, 6H, CH_3 Bodipy), 2.34 (q, J =7.6 Hz, 4H, CH_2CH_3, Bodipy), 1.56 – 1.53 (m, 12H, CH_3 Bodipy +CH_3 *i*Pr), 0.98 (t, J =7.6 Hz, 6H, CH_2CH_3 Bodipy). **^{13}C{^{1}H} NMR** (126 MHz, methylene chloride-d_2) δ / ppm = 185.9, 185.5, 182.8, 182.3, 176.1, 175.7, 157.9, 134.8, 133.4, 129.9, 124.2, 119.8, 23.8, 17.5, 14.6, 13.2, 10.4.
^{19}F NMR (471 MHz, methylene chloride-d_2) δ / ppm = -144.88 (dq, J(^{11}B-$^{19}F_a$) = 31 Hz, J(^{19}F-^{19}F) =108 Hz), -145.82 (dq, J(^{11}B-$^{19}F_b$) = 33 Hz, J(^{19}F-^{19}F) = 108 Hz).
HRMS (ESI positive): m/z calcd. for $C_{26}H_{34}BF_2N_5ORh$: 584.1874 $[M + CH_3CN]^+$; found 584.1876.

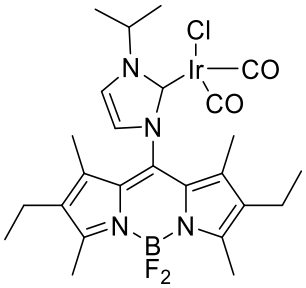

[IrCl(CO)$_2$(**85**)]

Synthesis of [IrCl(CO)$_2$(85)]. General Procedure B: [IrCl(CO)$_2$(**85**)] complex was obtained as a dark red solid from [IrCl(cod)(**85**)] (10 mg, 78 % yield).
^{1}H NMR (500 MHz, methylene chloride-d_2) δ / ppm = 7.40 (s, 1H, CH), 7.21 (s, 1H, CH), 5.50–5.45 (m, 1H, CH *i*Pr), 2.51 (s, 6H, CH_3 Bodipy), 2.33 (q, J =7.5 Hz, 4H, CH_2CH_3 Bodipy), 1.61 – 1.46 (m, 12H, CH_3 Bodipy +CH_3 *i*Pr), 0.98 (t, J =7.6 Hz, 6H, CH_2CH_3 Bodipy).
^{13}C{^{1}H} NMR (126 MHz, methylene chloride-d_2) δ / ppm = 207.1, 180.9, 174.8, 168.2, 158.1, 135.0, 133.2, 124.4, 120.0, 30.5, 23.9, 17.7, 14.8, 13.5, 10.6.
^{19}F NMR (471 MHz, methylene chloride-d_2) δ / ppm = -144.83 (dq, J(^{11}B-$^{19}F_a$) =33 Hz, J(^{19}F-^{19}F) = 108 Hz), -145.82 (dq, J(^{11}B-$^{19}F_b$) = 31 Hz, J(^{19}F-^{19}F) = 108 Hz).
HRMS (ESI positive): m/z calcd. for $C_{25}H_{31}BF_2IrN_4O_2$: 661.2132 $[M]^+$; found 661.2141. ν(CO) 1971 and 2055 cm^{-1}.

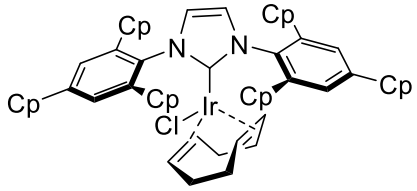

[IrCl(cod)(**89**)]

Synthesis of [IrCl(cod)(89)]. General Procedure C: 2,4,6-tricyclopentylphenyl imidazolium salt (41 mg, 0.060 mmol), Ag_2O (7 mg, 0.030 mmol), [IrCl(cod)]$_2$ (20 mg, 0.030 mmol) in CH_2Cl_2 (5 mL) yields the complex as a yellow crystalline solid (30 mg, 52% yield).
^{1}H NMR (500 MHz, chloroform-d) δ / ppm = 7.13 (d, J = 45.0 Hz, 4H), 6.95 (s, 2H), 4.15 (s, 2H), 3.46 (s, 2H), 3.05 (p, J = 8.1 Hz, 2H), 2.93 (s, 2H), 2.76 (s, 2H), 2.36 (s, 2H), 2.13 (s, 4H), 1.91 – 1.12 (m, 60H).
^{13}C{^{1}H} NMR (126 MHz, chloroform-d) δ / ppm = 181.2, 147.6, 144.8, 142.6, 135.8, 124.6, 123.2, 121.7, 82.1, 51.6, 46.4, 41.4, 37.4 (br.), 34.8, 33.7, 33.2 (br.), 28.9, 25.9 (br.).
HRMS (ESI positive): m/z: calcd. for $C_{53}H_{72}IrN_2$: 929.53193 $[M]^+$; found: 929.53195.

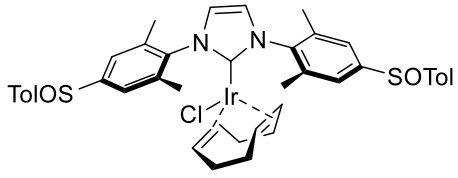

[IrCl(cod)(**97**)]

Synthesis of [IrCl(cod)(97)].[154] General Procedure C: *para*-tolylsulfinyl-imidazolium salt (56 mg, 0.095 mmol), K_2CO_3 (39 mg, 0.283 mmol), [IrCl(cod)]$_2$ (31 mg, 0.046 mmol) in acetone (3 mL) yields the complex as a yellow crystalline solid (37 mg, 44% yield).

^{1}H NMR (300 MHz, methylene chloride-d_2) δ / ppm = 7.57 (d, J = 8.2 Hz, 4H), 7.42 (d, J = 25.5 Hz, 4H), 7.30 (d, J = 7.9 Hz, 4H), 7.03 (s, 2H), 3.99 (s, 2H), 2.75 (s, 2H), 2.37 (s, 12H), 2.21 (s, 6H), 1.48 – 1.32 (m, 4H), 1.25 – 1.06 (m, 4H).
HRMS (APSI positive): m/z: calcd. for $C_{41}H_{44}IrN_2O_2S_2$: 853.2468[M]$^+$; found: 853.24663.

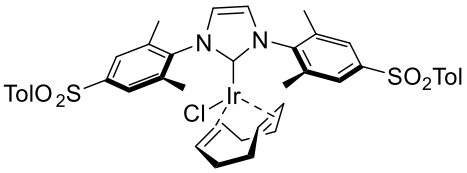

[IrCl(cod)(**99**)]

Synthesis of [IrCl(cod)(99)].[154] General Procedure C: *para*-tolylsulfonyl-imidazolium salt (70 mg, 0.113 mmol), K_2CO_3 (47 mg, 0.338 mmol), $[IrCl(cod)]_2$ (38 mg, 0.056 mmol) in acetone (3 mL) gave complex as a yellow crystalline solid (44 mg, 41% yield).
^{1}H NMR (500 MHz, methylene chloride-d_2) δ / ppm = 7.84 (d, J = 8.3 Hz, 4H), 7.75 (d, J = 15.7 Hz, 4H), 7.34 (d, J = 8.6 Hz, 4H), 7.03 (s, 2H), 3.96 (s, 2H), 2.67 (s, 2H), 2.40 (s, 12H), 2.22 (s, 6H), 1.44 – 1.33 (m, 2H), 1.28 – 1.21 (m, 4H), 1.14 – 1.03 (m, 2H).
HRMS (APSI positive): m/z: calcd. for $C_{41}H_{45}ClIrN_2O_4S_2$: 921.21331; found: 921.21167.

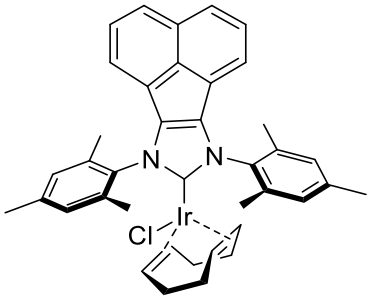

[IrCl(cod)(**103**)]

Synthesis of [IrCl(cod)(103)]. General Procedure D: imidazolium salt (70 mg, 0.150 mmol), KO*t*Bu (20 mg, 0.180 mmol), $[IrCl(cod)]_2$ (50 mg, 0.075 mmol) in THF (10 mL) yields the complex as a yellow crystalline solid (55 mg, 48% yield).
^{1}H NMR (300 MHz, chloroform-d) δ / ppm = 7.68 (d, J = 8.3 Hz, 2H), 7.42 – 7.29 (m, 2H), 7.09 (s, 4H), 6.86 (d, J = 7.0 Hz, 2H), 4.28 (s, 2H), 3.13 (s, 2H), 2.43 (s, 12H), 2.25 (s, 6H), 1.91 – 1.64 (m, 4H), 1.51 – 1.21 (m, 4H).
^{13}C{^{1}H} NMR (126 MHz, chloroform-d) δ / ppm = 187.10, 138.92, 138.65, 134.84, 129.96, 129.53, 128.53, 127.67, 126.45, 120.37, 83.94, 51.94, 33.75, 29.12, 21.43, 19.90, 18.53.
HRMS (APSI positive): m/z: calcd. for $C_{39}H_{40}IrN_2$: 729.28153 [M]$^+$; found: 729.28163.

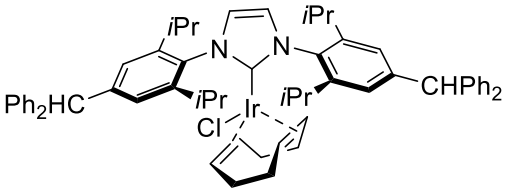

[IrCl(cod)(**106**)]

Synthesis of [IrCl(cod)(106)]. General Procedure C: imidazolium salt (50 mg, 0.066 mmol), K_2CO_3 (27 mg, 0.198 mmol), $[IrCl(cod)]_2$ (22 mg, 0.033 mmol) in acetone (3 mL) yields the complex as a yellow crystalline solid (38 mg, 55% yield).

^{1}H NMR (500 MHz, chloroform-*d*) δ / ppm = 7.31 (t, *J* = 7.5 Hz, 8H), 7.24 (t, *J* = 6.8 Hz, 4H), 7.17 (d, *J* = 7.2 Hz, 8H), 7.08 (s, 2H), 7.02 (s, 2H), 6.98 (s, 2H), 5.62 (s, 2H), 4.23 – 4.22 (m, 2H), 3.48 (s, 2H), 2.90 – 2.89 (m, 2H), 2.53 (s, 2H), 1.74 – 1.66 (m, 2H), 1.59 – 1.54 (m, 2H), 1.42 – 1.10 (m, 18H), 1.01 (d, *J* = 6.8 Hz, 12H).
^{13}C{^{1}H} NMR (126 MHz, chloroform-*d*) δ / ppm = 183.5, 145.1, 144.1, 134.3, 129.6, 128.4, 126.5, 124.7, 82.5, 57.1, 51.0, 33.7, 29.0, 26.6.
HRMS (APSI positive): m/z: calcd. for $C_{35}H_{46}Br_2ClIrN_2$: 1021.50063; found: 1021.50220.

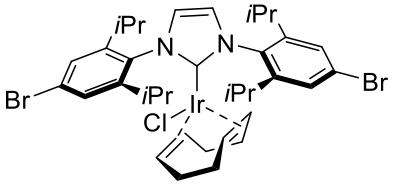

[IrCl(cod)(**107**)]

Synthesis of [IrCl(cod)(107)]. General Procedure C: imidazolium salt (40 mg, 0.069 mmol), K_2CO_3 (28 mg, 0.206 mmol), $[IrCl(cod)]_2$ (23 mg, 0.035 mmol.) in acetone (3 mL) yields the complex as a yellow crystalline solid (38 mg, 60% yield).
^{1}H NMR (500 MHz, chloroform-*d*) δ / ppm = 7.41 (d, *J* = 38.0 Hz, 4H), 6.98 (s, 2H), 4.27 (s, 2H), 3.40 (s, 2H), 2.83 (s, 2H), 2.67 (s, 2H), 1.82 – 1.67 (m, 2H), 1.65 – 1.55 (m, 2H), 1.46 – 1.23 (m, 16H), 1.09 (d, *J* = 6.3 Hz, 12H).
^{13}C{^{1}H} NMR (126 MHz, chloroform-*d*) δ / ppm = 183.12, 135.32, 128.0, 126.4, 124.51, 124.30, 84.28, 77.16, 51.78, 33.62, 29.28, 28.82, 26.34.
HRMS (ESI positive): m/z: calcd. for $C_{35}H_{46}Br_2ClIrN_2$: 886.19170 $[M]^+$; found: 886.18816.

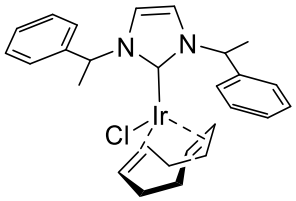

[IrCl(cod)(**109**)]

Synthesis of [IrCl(cod)(109)]. General Procedure E: 1,3-bis-phenylethyl imidazolium salt (27 mg, 0.086 mmol), Ag_2O (10 mg, 0.043 mmol), $[IrCl(cod)]_2$ (29 mg, 0.043 mmol) in CH_2Cl_2 (5 mL) yields the complex as a yellow crystalline solid (27 mg, 51% yield).
^{1}H NMR (300 MHz, chloroform-*d*) δ / ppm = 7.67 – 7.55 (m, 2H), 7.47 – 7.26 (m, 8H), 6.81 (d, *J* = 2.1 Hz, 1H), 6.78 – 6.69 (m, 2H), 6.68 (d, *J* = 2.1 Hz, 1H), 4.74 – 4.55 (m, 2H), 3.15 – 3.10 (m, 1H), 2.94 – 2.88 (m, 1H), 2.35 – 2.09 (m, 3H), 2.02 –1.95 (m, 1H), 1.92 (d, *J* = 7.1 Hz, 3H), 1.83 (d, *J* = 7.1 Hz, 3H), 1.76 – 1.34 (m, 4H).
^{13}C{^{1}H} NMR (126 MHz, chloroform-*d*) δ / ppm = 179.8, 142.1, 140.2, 128.9, 128.7, 128.1, 127.8, 127.6, 126.6, 118.7, 118.0, 84.8, 84.6, 59.5, 58.1, 52.2, 51.4, 33.9, 33.4, 29.6, 29.5, 22.7, 21.1.
HRMS (ESI positive): m/z: calcd. for $C_{27}H_{32}IrN_2$: 577.21893 $[M]^+$; found: 577.21817.

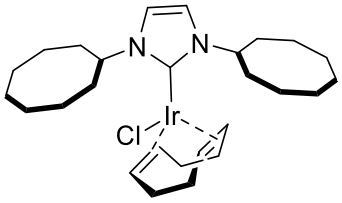

[IrCl(cod)(**111**)]

Synthesis of [IrCl(cod)(111)]. General Procedure E: N-cycloalkyl imidazolium salt (28 mg, 0.086 mmol), Ag_2O (10 mg, 0.043 mmol), $[IrCl(cod)]_2$ (29 mg, 0.043 mmol) in CH_2Cl_2 (5 mL) yields the complex as a yellow crystalline solid (26 mg, 45% yield).
^{1}H NMR (300 MHz, chloroform-*d*) δ / ppm = 6.79 (s, 2H), 5.55 – 5.48 (m, 2H), 4.69 – 4.54 (m, 2H), 3.00 – 2.85 (m, 2H), 2.35 – 2.15 (m, 4H), 2.17 – 2.02 (m, 2H), 2.01 – 1.86 (m, 4H), 1.90 – 1.45 (m, 28H).
^{13}C{^{1}H} NMR (75 MHz, chloroform-*d*) δ / ppm = 177.0, 117.3, 83.5, 59.7, 50.7, 35.3, 33.9, 29.8, 27.3, 26.28, 26.19, 25.22, 24.8.
HRMS (ESI positive): m/z: calcd. for $C_{29}H_{47}IrN_3$: 630.33938 $[M + CH_3CN]^+$; found: 630.33931.

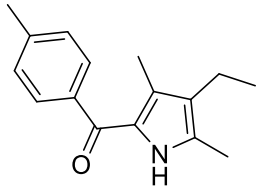

Synthesis of 112.[274] To a stirred solution of kryptopyrrole (5.0 g, 40.6 mmol) and dry Et_3N (4.11 g, 40.6 mmol) in THF (40 mL) at rt was added 4-methyl-benzoic acid chloride (6.46 g, 41.8 mmol) during 10 minutes. Next the mixture was heated under reflux for 8 h and then cooled to rt. The triethylamine hydrochloride precipitate was removed by filtration and the precipitate washed with THF. The combined filtrates were evaporated to dryness in a rotavapor and the solid residue **112** recrystallized from methanol (6.07 g, yield 62%).
^{1}H NMR (500 MHz, chloroform-*d*) δ / ppm = 9.51 (s, 1H), 7.58 (d, *J*= 8.1 Hz, 2H), 7.26 (d, *J* = 8.1 Hz, 2H), 2.44 (s, 3H), 2.41 (q, *J*= 7.6 Hz, 2H), 2.28 (s, 3H), 1.95 (s, 3H), 1.08 (t, *J*= 7.6 Hz, 3H).
^{13}C{^{1}H} NMR (126 MHz, chloroform-*d*) δ / ppm = 185.9, 141.5, 138.0, 133.2, 128.9, 128.4, 127.4, 125.5, 21.9, 17.6, 15.5, 12.2, 11.8.

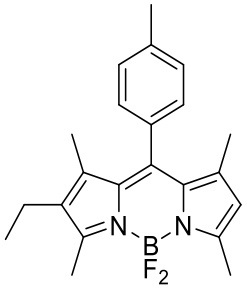

Synthesis of Bodipy 113.[182] (3,5-Dimethyl-1H-pyrrol-2-yl)(*p*-tolyl)methanone **112** (900 mg, 3.73 mmol) was dissolved in dry CH_2Cl_2 (40 mL). 3-Ethyl-2,4-dimethyl-1H-

pyrrole (0.381 mL, 3.73 mmol) and $POCl_3$ (558 µL, 6.0 mmol) were slowly added under 0°C and the resulting solution was stirred at rt for 2 h. The mixture was then neutralized by addition of dry triethylamine (4.42 mL, 31.7 mmol). The mixture was stirred for 40 min at rt, then $BF_3{\cdot}OEt_2$ (4.60 mL, 37.3 mmol) added and stirring continued for another 3 h. The crude mixture was washed with saturated aqueous solution of $NaHCO_3$ (60 ml) and then with water (100 mL). The aqueous layer was back extracted with DCM (3 · 50 mL). The combined organic layers were dried over ($MgSO_4$), filtered and the solvent removed under reduced pressure. The resulting orange crude product was purified by column chromatography (EtOAc/cyclohexane = 1/3) to provide the title compound **113** as an orange solid (505 mg, yield 37%).

^{1}H NMR (300 MHz, chloroform-*d*) δ / ppm = 7.28 (d, *J* = 8.2 Hz, 2H), 7.15 (d, *J* = 8.1 Hz, 2H), 5.93 (s, 1H), 2.54 (s, 6H), 2.44 (s, 3H), 2.31 (q, *J* = 7.6 Hz, 2H), 1.37 (s, 3H), 1.33 (s, 3H), 0.99 (t, *J* = 7.6 Hz, 3H).

^{13}C{^{1}H} NMR (126 MHz, chloroform-*d*) δ / ppm = 155.54, 154.03, 142.33, 141.69, 139.75, 139.06, 133.71, 132.73, 130.14, 128.31, 120.82, 21.78, 17.45, 14.91, 12.96, 12.16.

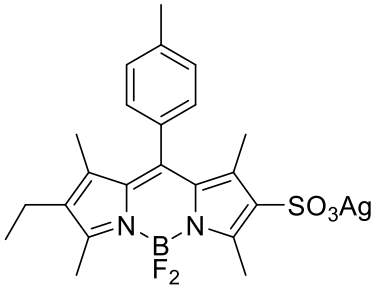

Synthesis of BodipySO_3Ag 114. A solution of chlorosulfonic acid (21 µL, 0.31 mmol) in dry acetonitrile (1 mL) was added dropwise to a solution of Bodipy **113** (121 mg, 0.33 mmol) in dry acetonitrile (12 mL) over 10 min under N_2 at -40 °C. Then the resulting solution was slowly warmed to rt. After 30 min, TLC showed that most of the starting material was consumed. Ag_2CO_3 (108 mg, 0.393 mmol) was added to neutralize the solution and stirred overnight. The reaction mixture was filtered through celite pad and the filtrate was evaporated to dryness. The formed BodipySO_3Ag was dissolved in minimum amount of DCM and precipitated by addition of excess of diethyl ether (5 mL). Precipitate was collected by filtration as an orange powder (105 mg, yield 61%). Melting point (231-234 °C).

^{1}H NMR (500 MHz, methanol-d_4) δ / ppm = 7.43 (d, *J* = 7.7 Hz, 2H), 7.23 (d, *J* = 8.0 Hz, 2H), 2.78 (s, 3H), 2.56 (s, 3H), 2.49 (s, 3H), 2.41 (q, *J* = 7.6 Hz, 2H), 1.69 (s, 3H), 1.41 (s, 3H), 1.04 (t, *J* = 7.6 Hz, 3H).

^{13}C{^{1}H} NMR (126 MHz, methanol-d_4) δ / ppm = 159.99, 151.89, 144.15, 142.39, 140.74, 139.95, 136.35, 134.05, 133.39, 131.12, 130.19, 129.22, 21.40, 17.77, 14.66, 14.02, 13.14, 12.94, 12.32.

HRMS (APCI negative): m/z calcd. for $C_{22}H_{24}BF_2N_2O_3S$ $[M]^-$: 445.15742, found 445.15861.

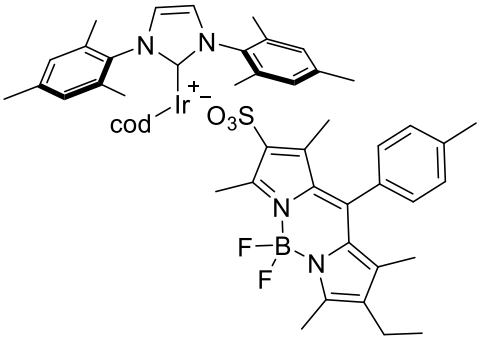

Synthesis of [Ir(bdpSO$_3$)(cod)(86)]. [IrCl(cod(**86**)] 5.12 mg ($8.00 \cdot 10^{-6}$ mol) was dissolved in CH_2Cl_2 (15 mL) and a solution of bdpSO$_3$Ag **114** 4.43 mg ($8.00 \cdot 10^{-6}$ mol) in acetonitrile (10 mL) added. The AgCl precipitate formed immediately and was separated by filtration over celite. The celite was washed with dichloromethane (10 mL). The combined filtrates were evaporated and dried overnight in vacuum (8.4 mg, quantitive).
^{1}H NMR (500 MHz, methylene chloride-d_2) δ / ppm = 7.34 (d, J = 7.7 Hz, 2H), 7.18 (d, J = 7.9 Hz, 2H), 7.01 (s, 2H), 6.94 (s, 4H), 4.88 (s, 2H), 2.88 (s, 2H), 2.55 (d, J = 6.3 Hz, 6H), 2.47 (s, 3H), 2.36 (s, 8H), 2.18 (s, 6H), 1.98 (s, 6H), 1.79 (s, 2H), 1.64 (d, J = 13.8 Hz, 2H), 1.42 (s, 3H), 1.35 (s, 3H), 1.32 (s, 2H), 1.20 – 1.09 (m, 2H), 1.01 (t, J = 7.6 Hz, 3H).
^{13}C{^{1}H} NMR (126 MHz, methylene chloride-d_2) δ / ppm = 178.7, 158.6, 152.7, 143.2, 141.6, 140.3, 139.8, 139.4, 137.5, 136.2, 135.4, 134.7, 132.7, 130.5, 130.0, 128.9, 128.6, 124.1, 83.1, 48.8, 33.4, 30.3, 29.3, 21.8, 21.4, 19.1, 18.6, 17.6, 14.8, 14.4, 13.2, 12.4.
^{19}F NMR ((471 MHz, chloroform-d) δ / ppm = -144.12 (m, 2F).
HRMS (ESI negative): m/z calcd. for $C_{22}H_{24}BF_2N_2O_3S$: 445.15742 $[M]^-$; found 445.15818.
HRMS (ESI positive): m/z calcd. for $C_{29}H_{36}IrN_2$: 605.25023 $[M]^+$; found 605.24963.

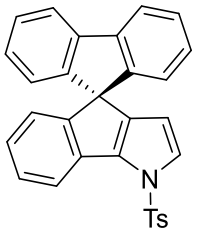

Synthesis of pyrrole 117-Tos.[272] A mixture of 9-(2-bromophenyl)-9H-fluoren-9-ol (14.6 g, 27.0 mmol), Pd(OAc)$_2$ (1.0 g, 4.5 mmol), and K_2CO_3 (7.8 g, 56.4 mmol) in dry DMF (150 mL) was stirred at 100 °C for 20 h. After the solvent was distilled off under low vacuum, the residue was dissolved in CH_2Cl_2 (150 mL) and washed with brine (100 mL) and water (150 mL). The organic layer was separated, dried over $MgSO_4$, and filtered. Evaporation of the solution in a rotavap gave the product as a brown solid. The crude product was slurried with a mixture of CH_2Cl_2 and cyclohexane (ca. 20 mL, 1:1), and the resulting precipitate was collected by suction filtration to provide **117-Tos** as a white solid (8.7 g, 18.9 mmol, 70%). The characterization data of **117-Tos** match with literature data.[272]
^{1}H NMR (500 MHz, chloroform-d) δ / ppm = 8.15 (d, J = 7.7 Hz, 1H), 7.83 (d, J = 8.4 Hz, 2H), 7.79 (d, J = 7.6 Hz, 2H), 7.36 – 7.27 (m, 5H), 7.22 (d, J = 3.2 Hz, 1H), 7.08 (td, J = 7.5, 1.0 Hz, 2H), 6.93 (td, J = 7.5, 1.0 Hz, 1H), 6.63 (d, J = 7.6 Hz, 2H), 6.53 (d, J o= 7.4 Hz, 1H), 5.87 (d, J = 3.2 Hz, 1H), 2.43 (s, 3H).
^{13}C{^{1}H} NMR (126 MHz, chloroform-d) δ / ppm = 152.7, 146.6, 145.2, 142.0, 140.1, 138.5, 136.2, 134.2, 130.2, 128.0, 127.9, 127.8, 127.0, 127.0, 125.9, 123.8, 123.7, 120.2, 119.7, 108.7, 21.8.

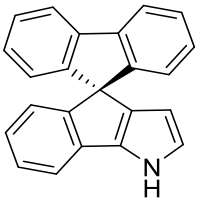

Synthesis of pyrrole 117.[272] A mixture of **117-Tos** (4.2 g, 9.0 mmol) and Cs_2CO_3 (9.1 g, 27.8 mmol) in THF/MeOH (3:1, 145 mL) was stirred for 24 h. After evaporation of the solvent, the residue was dissolved in CH_2Cl_2 (50 mL). The organic layer was washed with H_2O, dried over $MgSO_4$, filtered over a paper filter and evaporated in a rotavap to provide a dark orange solid. Recrystallization from CH_2Cl_2 and cyclohexane afforded **117** as a white crystalline solid (2.4 g, 7.7 mmol, 85 %). The characterization data of **117** match with literature data.[272]

^{1}H NMR (500 MHz, chloroform-*d*) δ / ppm = 8.44 (s, 1H), 7.82 (d, *J* = 7.6 Hz, 2H), 7.39 – 7.29 (m, 3H), 7.23 – 7.17 (m, 1H), 7.12 (td, *J* = 7.5, 1.0 Hz, 2H), 6.89 – 6.79 (m, 4H), 6.55 (d, *J* = 7.5 Hz, 1H), 5.86 – 5.76 (m, 1H).

^{13}C{^{1}H} NMR (126 MHz, chloroform-*d*) δ / ppm =153.1, 148.5, 141.7, 135.4, 133.8, 127.6, 127.4, 127.1, 124.4, 123.9, 123.7, 121.9, 119.9, 115.9, 104.0, 60.8.

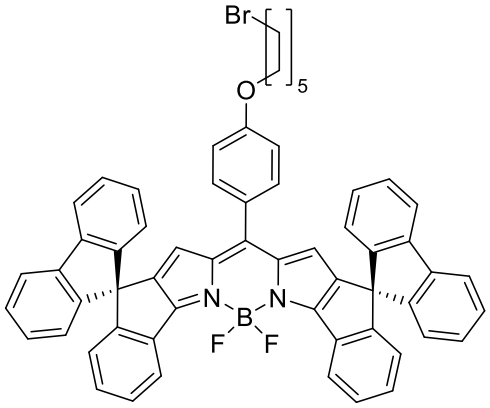

Synthesis of 118. General Procedure G: Bodipy **121** (153 mg, 0.2 mmol, 1 eq.), 1,10-Dibromodecane (90 mg, 0.3 mmol, 1.5 eq.), K_2CO_3 (55 mg, 0.4 mmol, 2 eq.), KI (100 mg, 0.6 mmol, 4 eq.) were placed in 10 mL round flask and dissolved in dry acetone (3.0 mL). The crude red product was purified by column chromatography (EtOAc/cyclohexane = 1/4) and gave **118** as a dark red powder (55 mg, yield 28%).

^{1}H NMR (500 MHz, chloroform-*d*) δ / ppm = 8.52 (d, *J* = 7.7 Hz, 2H), 7.82 (d, *J* = 7.6 Hz, 4H), 7.53 (td, *J* = 7.6, 1.1 Hz, 2H), 7.39 (td, *J* = 7.5, 1.1 Hz, 4H), 7.34 – 7.29 (m, 2H), 7.21 (dtd, *J* = 15.1, 7.5, 1.1 Hz, 6H), 6.98 (d, *J* = 7.6 Hz, 4H), 6.77 (d, *J* = 8.7 Hz, 2H), 6.67 (d, *J* = 7.7 Hz, 2H), 3.86 (t, *J* = 6.5 Hz, 2H), 3.41 (t, *J* = 6.9 Hz, 2H), 1.85 (p, *J* = 6.9 Hz, 2H), 1.76 – 1.67 (m, 2H), 1.44 – 1.34 (m, 4H), 1.28 (d, *J* = 2.4 Hz, 8H).

^{13}C NMR (75 MHz, chloroform-*d*) δ / ppm = 161.2, 160.6, 156.6, 148.3, 142.9, 142.3, 141.3, 141.1, 132.6, 131.9, 130.4, 128.7, 127.97, 127.93, 126.2, 124.29, 124.23, 124.20, 120.7, 120.1, 114.2, 68.0, 59.8, 34.0, 32.8, 29.38, 29.30, 29.2, 29.0, 28.7, 28.1, 25.9.

HRMS (ESI positive): *m/z* calcd. for $C_{63}H_{51}BBrF_2N_2O$ $[M+H]^+$ 981.32254, found 981.32330, calcd. for $C_{63}H_{50}BBrF_2N_2NaO$ $[M+Na]^+$ 1003.30449, found 1003.30674, calcd. for $C_{63}H_{50}BBrFN_2O$ $[M-F]^+$ 961.31631, found 961.31873.

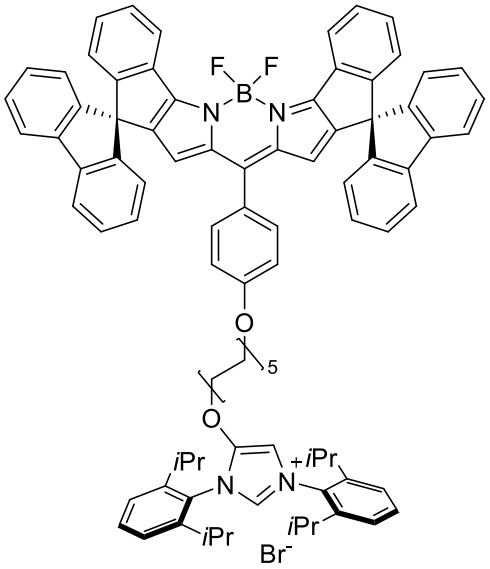

Synthesis of 119·HBr. General Procedure G: 1,3-bis(2,6-diisopropylphenyl)-4-hydroxy-1H-imidazol-3-ium chloride (97 mg, 0.2 mmol, 1 eq.), Bodipy **118** (294 mg, 0.3 mmol), K_2CO_3 (55 mg, 0.4 mmol, 2 eq.), KI (100 mg, 0.6 mmol, 4 eq.) were placed in 10 mL round flask and dissolved in dry acetone (3.0 mL). The crude red product was purified by column chromatography (MeOH/CH_2Cl_2 = 1/20) and gave **119·HBr** as a dark red powder (64 mg, yield 23%).

^{1}H NMR (500 MHz, chloroform-*d*) δ / ppm = 8.90 (dt, *J* = 4.6, 2.1 Hz, 1H), 8.52 (d, *J* = 7.6 Hz, 2H), 7.98 (dq, *J* = 7.4, 2.4 Hz, 1H), 7.82 (d, *J* = 7.6 Hz, 4H), 7.59 (q, *J* = 7.6 Hz, 2H), 7.53 (t, *J* = 7.6 Hz, 2H), 7.42 – 7.32 (m, 8H), 7.30 (d, *J* = 8.6 Hz, 2H), 7.20 (dt, *J* = 17.5, 7.5 Hz, 6H), 6.98 (d, *J* = 7.5 Hz, 4H), 6.79 – 6.73 (m, 2H), 6.66 (d, *J* = 7.7 Hz, 2H), 6.25 (s, 2H), 4.52 (t, *J* = 6.3 Hz, 2H), 3.84 (t, *J* = 6.4 Hz, 2H), 2.57 (hept, *J* = 6.9 Hz, 2H), 2.46 (hept, *J* = 7.0 Hz, 2H), 1.70 (ddt, *J* = 21.5, 14.2, 6.6 Hz, 4H), 1.40 (d, *J* = 6.8 Hz, 6H), 1.37 – 1.15 (m, 30H).

^{13}C{^{1}H} NMR (126 MHz, chloroform-*d*) δ / ppm = 161.3, 160.6, 156.6, 148.5, 148.3, 145.7, 145.1, 142.9, 142.3, 141.3, 141.1, 132.6, 132.31, 132.21, 132.0, 130.5, 130.4, 130.2, 128.8, 128.0, 127.9, 126.3, 126.1, 124.8, 124.7, 124.3, 124.3, 124.2, 120.7, 120.1, 114.2, 104.3, 75.9, 68.1, 59.8, 29.41, 29.32, 29.25, 29.23, 29.18, 29.12, 29.01, 28.6, 25.9, 25.5, 25.0, 24.37, 24.14, 23.5.

HRMS (ESI positive): *m*/*z* calcd. for $C_{90}H_{86}BF_2N_4O_2$ $[M\text{-}Br]^+$ 1303.68119, found 1303.68127.

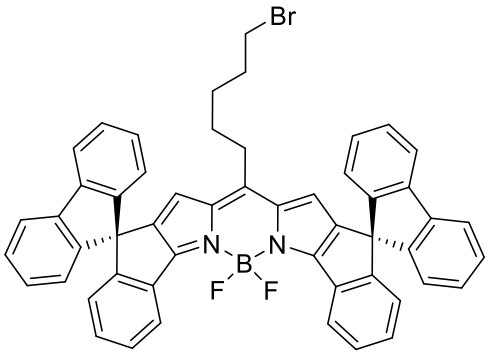

Synthesis of 120. General Procedure F: Pyrrole **117** (100 mg, 0.33 mmol), 6-bromohexanal (29 mg, 0.16 mmol), DDQ (36 mg, 0.16 mmol), Et_3N (0.2 mL, 1.4 mmol), BF_3OEt_2 (0.3 mL, 2.4 mmol) were placed in 25 mL Schlenk flask and dissolved in dry CH_2Cl_2 (5.0 mL). The crude red product was purified by column chromatography

(EtOAc/cyclohexane = 1/7) and gave Bodipy **120** as a dark red powder (46 mg, yield 38%).

^{1}H NMR (500 MHz, chloroform-*d*) δ / ppm = 8.46 (d, *J* = 7.7 Hz, 2H), 7.85 (dd, *J* = 7.7, 0.9 Hz, 4H), 7.49 (td, *J* = 7.6, 1.0 Hz, 2H), 7.41 (td, *J* = 7.5, 1.1 Hz, 4H), 7.20 (td, *J* = 7.5, 1.1 Hz, 6H), 6.98 (dd, *J* = 7.6, 0.9 Hz, 4H), 6.69 – 6.61 (m, 2H), 6.56 (s, 2H), 3.23 (t, *J* = 6.7 Hz, 2H), 2.64 – 2.52 (m, 2H), 1.78 – 1.68 (m, 2H), 1.67 – 1.56 (m, 2H), 1.42 – 1.32 (m, 2H).

^{13}C{^{1}H} NMR (126 MHz, chloroform-*d*) δ / ppm = 161.5, 156.9, 148.4, 143.9, 142.8, 141.5, 141.2, 132.6, 130.5, 128.9, 128.20, 128.14, 124.37, 120.2, 117.4, 33.4, 32.6, 32.3, 30.5, 28.8.

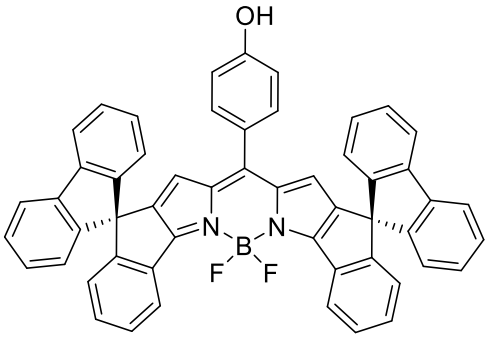

Synthesis of 121. General Procedure F: Pyrrole **117** (100 mg, 0.33 mmol), 4-Hydroxybenzaldehyde (20 mg, 0.16 mmol), DDQ (36 mg, 0.16 mmol), Et_3N (0.2 mL, 1.4 mmol), BF_3OEt_2 (0.3 mL, 2.4 mmol) were placed in 25 mL Schlenk flask and dissolved in dry CH_2Cl_2 (5.0 mL). The crude red product was purified by column chromatography (EtOAc/cyclohexane = 1/4) and gave Bodipy **121** as a dark red powder (46 mg, yield 38%).

^{1}H NMR (500 MHz, chloroform-*d*) δ / ppm = 8.51 (d, J = 7.7 Hz, 2H), 7.82 (dt, *J* = 7.7, 0.9 Hz, 4H), 7.52 (td, *J* = 7.6, 1.1 Hz, 2H), 7.39 (td, *J* = 7.5, 1.1 Hz, 4H), 7.28 – 7.24 (m, 2H), 7.20 (dtd, *J* = 11.1, 7.5, 1.2 Hz, 6H), 6.97 (dt, *J* = 7.6, 1.0 Hz, 4H), 6.73 – 6.69 (m, 2H), 6.64 (d, *J* = 7.7 Hz, 2H), 6.23 (s, 2H), 4.99 (s, 1H).

^{13}C{^{1}H} NMR (126 MHz, chloroform-*d*) δ / ppm = 161.4, 157.1, 156.7, 148.2, 143.0, 142.0, 141.3, 141.1, 132.5, 132.2, 130.5, 128.8, 128.0, 127.9, 126.7, 124.3, 124.3, 124.2, 120.6, 120.1, 115.1, 59.7, 53.4.

HRMS (ESI positive): *m/z* calcd. for $C_{53}H_{32}BF_2N_2O$ $[M+H]^+$ 761.25758, found 761.25657, calcd. for $C_{53}H_{31}BF_2N_2NaO$ $[M+Na]^+$ 783.23952, found 783.24024, calcd. for $C_{53}H_{31}BFN_2O$ $[M-F]^+$ 741.25135, found 741.25217.

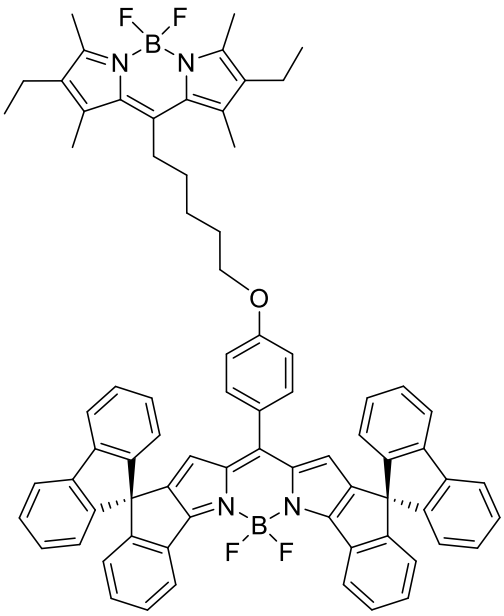

Synthesis of 123. General Procedure G: Bodipy **121** (153 mg, 0.2 mmol, 1 eq.), Bodipy **122** (136 mg, 0.3 mmol, 1.5 eq.), K_2CO_3 (55 mg, 0.4 mmol, 2 eq.), KI (100 mg, 0.6 mmol, 4 eq.) were placed in 10 mL round flask and dissolved in dry acetone (4.0 mL). The crude red product was purified by column chromatography (EtOAc/cyclohexane = 1/4) and gave **123** as a dark red powder (110 mg, yield 49%).

^{1}H NMR (500 MHz, chloroform-*d*) δ / ppm = 8.52 (d, *J* = 7.7 Hz, 2H), 7.82 (d, *J* = 7.8 Hz, 4H), 7.53 (td, *J* = 7.6, 1.1 Hz, 2H), 7.40 (td, J = 7.5, 1.1 Hz, 4H), 7.35 – 7.29 (m, 2H), 7.23 (dd, *J* = 7.5, 1.2 Hz, 2H), 7.19 (td, *J* = 7.5, 1.2 Hz, 4H), 6.98 (d, *J* = 7.6 Hz, 4H), 6.80 – 6.75 (m, 2H), 6.66 (d, *J* = 7.7 Hz, 2H), 6.25 (s, 2H), 3.89 (t, *J* = 6.2 Hz, 2H), 2.98 (t, *J* = 7.8 Hz, 2H), 2.49 (s, 6H), 2.34 (p, *J* = 7.7 Hz, 4H), 2.29 (s, 6H), 1.80 (q, *J* = 6.3 Hz, 2H), 1.64 (t, *J* = 6.1 Hz, 3H), 0.97 (t, *J* = 7.6 Hz, 6H).

^{13}C{^{1}H} NMR (126 MHz, chloroform-*d*) δ / ppm = 161.3, 160.4, 156.6, 152.1, 148.3, 144.4, 142.9, 142.1, 141.3, 141.1, 135.6, 132.6, 132.0, 130.8, 130.4, 128.8, 128.0, 127.9, 126.5, 124.3, 124.2, 124.2, 120.6, 120.0, 114.1, 67.4, 59.8, 53.4, 31.2, 28.7, 28.4, 26.5, 17.1, 14.8, 13.3, 12.4.

HRMS (ESI positive): *m/z* calcd. for $C_{75}H_{63}B_2F_4N_4O$ $[M+H]^+$ 1133.51241, found 1133.51382, calcd. for $C_{75}H_{62}B_2F_3N_4O$ $[M-F]^+$ 1113.50618, found 1113.50802, calcd. for $C_{75}H_{62}B_2F_4N_4NaO$ $[M+Na]^+$ 1155.49436, found 1155.49631.

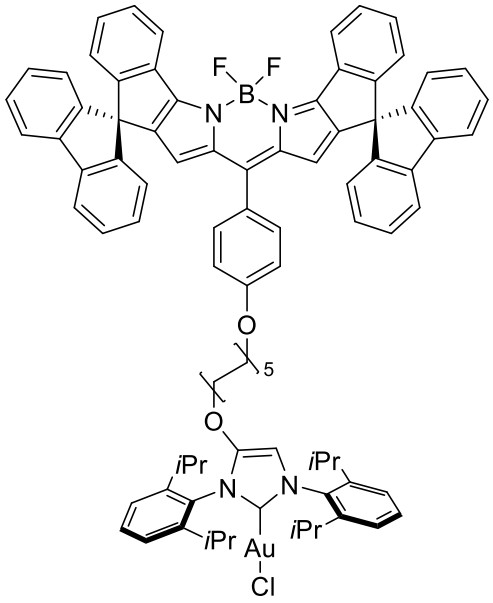

Synthesis of [AuCl(119_red)]. A mixture of imidazolium salt **119·HBr** (83 mg, 0.06 mmol, 1 eq.), K_2CO_3 (25 mg, 0.18 mmol, 3 eq.) and [AuCl(SMe_2)] (17.7 mg, 0.06 mmol, 1 eq.) were placed in dried 5 mL Schlenk flask and dissolved in dry acetone (2.0 mL). Reaction mixture was heated to reflux for 15 h under nitrogen atmosphere. CH_2Cl_2 (ca. 10 mL) was added to the reaction mixture and the solution filtered through a celite plug. The crude mixture obtained after evaporation of the volatiles was purified by column chromatography (EtOAc/cyclohexane = 1/5) and gave [AuCl(**119**_red)] as a microcrystalline dark red powder (54 mg, yield 59%).

^{1}H NMR (500 MHz, methylene chloride-d_2) δ / ppm = 8.48 (d, J = 7.7 Hz, 2H), 7.87 (dd, J = 7.6, 1.0 Hz, 4H), 7.62 – 7.51 (m, 4H), 7.42 (td, J = 7.5, 1.1 Hz, 4H), 7.39 – 7.31 (m, 6H), 7.28 (td, J = 7.6, 1.1 Hz, 2H), 7.21 (td, J = 7.5, 1.1 Hz, 4H), 6.98 (d, J = 7.6 Hz, 4H), 6.82 – 6.77 (m, 2H), 6.67 (d, J = 7.7 Hz, 2H), 6.47 (s, 1H), 6.31 (s, 2H), 4.02 (t, J = 6.5 Hz, 2H), 3.87 (t, J = 6.5 Hz, 2H), 2.72 (h, J = 6.7 Hz, 2H), 2.63 (h, J = 6.9 Hz, 2H), 1.73 – 1.64 (m, 4H), 1.37 (dd, J = 13.1, 6.9 Hz, 12H), 1.34 – 1.25 (m, 12H), 1.23 (q, J = 5.7, 5.1 Hz, 12H).

^{13}C{^{1}H} NMR (126 MHz, methylene chloride-d_2) δ / ppm = 179.4 (C_{NHC}), 161.1, 160.8, 156.8, 148.5, 148.1, 146.4, 145.9, 143.0, 142.5, 141.4, 141.0, 134.7, 132.6, 132.00, 130.55, 130.47, 130.44, 130.36, 128.7, 128.0, 127.9, 126.1, 124.15, 124.12, 124.04, 123.98, 120.6, 120.1, 114.2, 99.2, 72.8, 68.2, 59.8, 29.26, 29.22, 29.20, 29.00, 28.99, 28.70, 28.58, 25.8, 25.6, 24.4, 23.86, 23.84, 23.3, 0.8.

HRMS (ESI positive): m/z calcd. For $C_{90}H_{86}BF_2N_4O_2$: 1303.68064 $[M\text{-}AuCl]^+$; found 1303.68222.

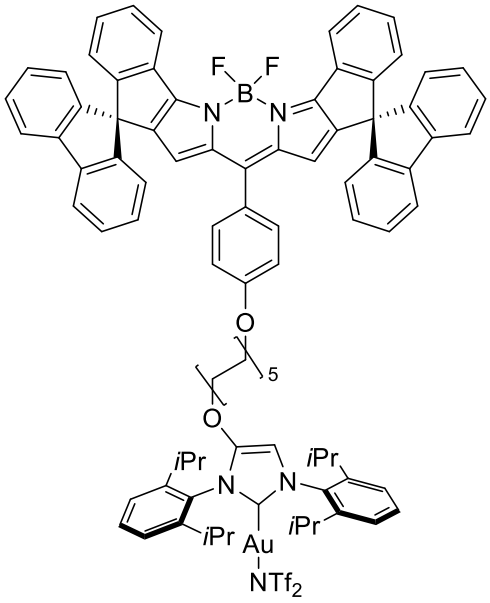

Synthesis of [AuNTf$_2$(119_red)]. A mixture of [AuCl(**119**_red)] complex (20 mg, 0.013 mmol, 1.0 eq.) and Ag(NTf$_2$) (5.4 mg, 0.014 mmol, 1.05 eq.) were dissolved in dry CH_2Cl_2 (1.5 mL), and reaction mixture was stirred for 30 min in the dark at rt under nitrogen atmosphere. The mixture was filtered *via* celite, and the filtrate was evaporated on the rotavap under reduced pressure. The crude material was rinsed with pentane (1 mL), dried in vacuum and gave [AuNTf$_2$(**119**_red)] as a dark red solid (22 mg, yield 95%).
^{1}H NMR (500 MHz, methylene chloride-d_2) δ / ppm = 8.49 (d, *J* = 7.7 Hz, 2H), 7.87 (d, *J* = 7.6 Hz, 4H), 7.57 (qd, *J* = 7.8, 1.7 Hz, 4H), 7.42 (td, *J* = 7.6, 1.1 Hz, 4H), 7.35 (dd, *J* = 7.9, 6.1 Hz, 6H), 7.28 (td, *J* = 7.5, 1.1 Hz, 2H), 7.21 (td, *J* = 7.6, 1.1 Hz, 4H), 6.99 (d, *J* = 7.6 Hz, 4H), 6.79 (d, *J* = 8.5 Hz, 2H), 6.67 (d, *J* = 7.7 Hz, 2H), 6.57 (s, 1H), 6.31 (s, 2H), 4.06 (t, *J* = 6.5 Hz, 2H), 3.86 (t, *J* = 6.5 Hz, 2H), 2.64 (p, *J* = 6.8 Hz, 2H), 2.56 (h, *J* = 6.8 Hz, 2H), 1.75 – 1.66 (m, 4H), 1.34 (dd, *J* = 11.3, 6.9 Hz, 14H), 1.29 (d, *J* = 6.9 Hz, 10H), 1.23 (d, *J* = 6.9 Hz, 12H).
^{13}C{^{1}H} NMR (126 MHz, methylene chloride-d_2) δ / ppm = 162.0, 161.1, 160.8, 156. 8, 149.0, 148.1, 146.3, 145.9, 142.9, 142.5, 141.4, 141.0, 134.4, 132.6, 132.0, 130.7, 130.6, 130.5, 130.1, 128.7, 128.0, 127.9, 126.1, 124.16, 124.10, 124.03, 123.98, 120.6, 120.1, 117.6, 114.2, 100.0, 73.0, 68.2, 59.8, 29.36, 29.28, 29.23, 29.21, 29.08, 29.01, 28.99, 28.77, 28.58, 25.8, 25.6, 24.1, 23.9, 23.6, 23.3.

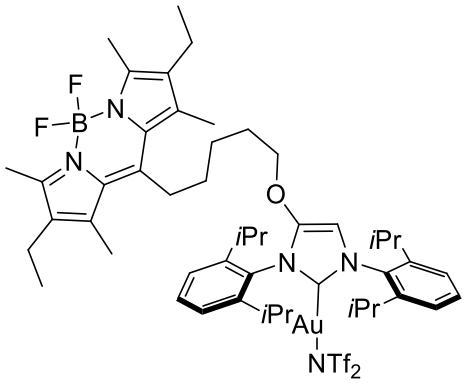

Synthesis of [Au(NTf$_2$)(124_green)].[244] A mixture of [AuCl(**124**_green)][244] complex (13 mg, 0.013 mmol, 1.0 eq.), and Ag(NTf$_2$) (5.4 mg, 0.014 mmol, 1.05 eq.) were dissolved in dry CH_2Cl_2 (1.0 mL), and reaction mixture was stirred for 30 min in the dark at rt under nitrogen atmosphere. The mixture was filtered through a celite plug, and the filtrate evaporated on the rotavap under reduced pressure. The crude material was rinsed with pentane (1 mL), dried in high vacuum and gave [Au(NTf$_2$)(**124**_green)] as an orange solid (15 mg, yield 91%).

^{1}H NMR (500 MHz, methylene chloride-d_2) δ / ppm = 7.55 (dt, J = 11.5, 7.8 Hz, 2H), 7.35 (t, J = 8.4 Hz, 4H), 6.60 (s, 1H), 4.11 (t, J = 6.3 Hz, 2H), 2.96 (dd, J = 10.7, 5.8 Hz, 2H), 2.58 (dt, J = 13.8, 7.2 Hz, 2H), 2.49 (s, 3H), 2.45 (q, J = 7.5 Hz, 6H), 2.29 (s, 6H), 1.82 (p, J = 6.6 Hz, 2H), 1.63 – 1.53 (m, 4H), 1.35 (d, J = 6.9 Hz, 6H), 1.33 (d, J = 6.8 Hz, 6H), 1.29 (d, J = 6.9 Hz, 6H), 1.24 (d, J = 6.9 Hz, 6H), 1.09 (t, J = 7.6 Hz, 6H).

^{13}C{^{1}H} NMR (126 MHz, methylene chloride-d_2) δ / ppm = 162.2, 152.1, 148.8, 146.2, 145.9, 144.3, 135.8, 134.4, 132.8, 130.7, 130.6, 130.0, 124.1, 124.0, 122.7, 120.2, 117.6, 115.0, 100.1, 72.6, 31.3, 29.7, 29.1, 28.8, 28.7, 28.2, 26.31, 24.1, 23.9, 23.6, 23.3, 17.1, 14.6, 13.2, 12.2.

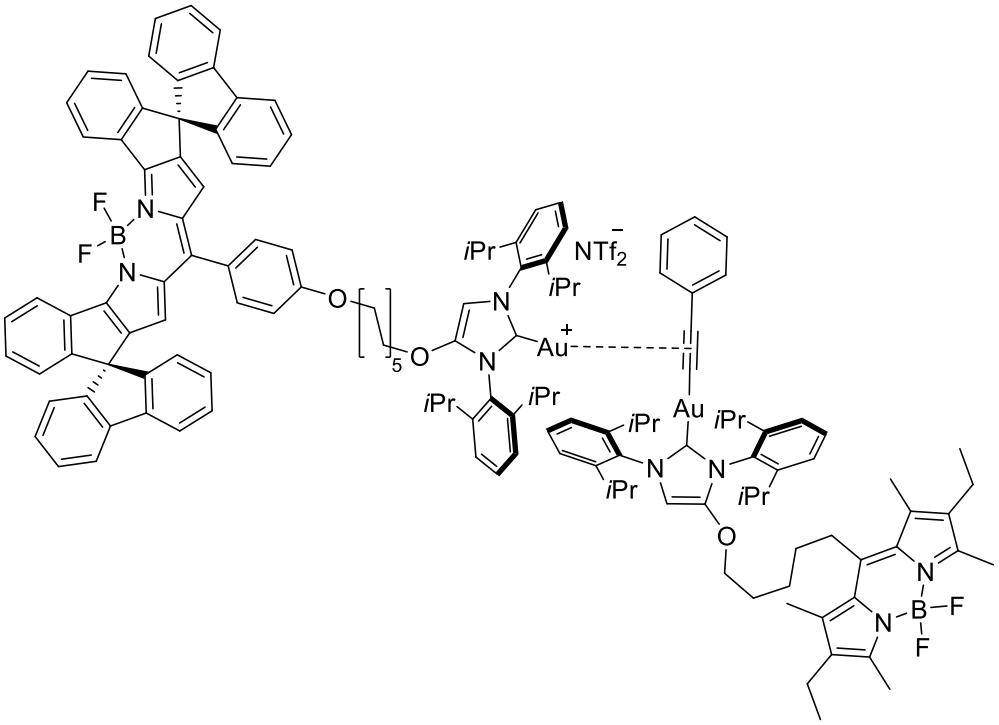

Synthesis of 125. A solution of [AuCl(**124**_green)] (16.4 mg, 0.015 mmol, 1 eq.) and [$AuNTf_2$(**119**_red)] (27.1 mg, 0.015 mmol, 1 eq.) in dry CH_2Cl_2 (1.5 mL) was stirred for 40 min in the dark. After the solvent was evaporated on the rotavap under reduced pressure, the resulting solid was rinsed with Et_2O (ca. 1 mL) and pentane (ca. 1.5 mL) and dried in high vacuum to give a dark violet solid **125** (34.6 mg, 0.012 mmol, 80%).

^{1}H NMR (500 MHz, methylene chloride-d_2) δ / ppm = 8.48 (d, *J* = 7.7 Hz, 2H), 7.86 (d, *J* = 7.6 Hz, 4H), 7.62 – 7.45 (m, 6H), 7.44 – 7.34 (m, 7H), 7.31 – 7.24 (m, 9H), 7.21 (tt, *J* = 7.5, 1.3 Hz, 5H), 7.15 – 7.09 (m, 2H), 6.98 (d, *J* = 7.6 Hz, 4H), 6.79 (dd, *J* = 8.6, 2.4 Hz, 2H), 6.74 – 6.69 (m, 2H), 6.67 (d, *J* = 7.7 Hz, 2H), 6.50 (d, *J* = 19.6 Hz, 2H), 6.31 (d, *J* = 1.8 Hz, 2H), 4.06 (t, *J* = 6.3 Hz, 2H), 4.00 (t, *J* = 6.5 Hz, 2H), 3.86 (td, *J* = 6.6, 2.1 Hz, 2H), 3.44 (q, *J* = 7.3 Hz, 1H), 2.97 – 2.91 (m, 2H), 2.69 – 2.55 (m, 4H), 2.49 (s, 9H), 2.45 (q, *J* = 7.6 Hz, 4H), 2.28 (s, 6H), 1.77 (p, *J* = 6.5 Hz, 2H), 1.68 (dt, *J* = 14.2, 6.7 Hz, 4H), 1.52 (d, *J* = 7.2 Hz, 4H), 1.45 – 1.27 (m, 14H), 1.24 (dd, *J* = 7.0, 3.0 Hz, 16H), 1.18 (dd, *J* = 6.9, 2.2 Hz, 12H), 1.15 – 1.07 (m, 24H).

^{13}C{^{1}H} NMR (126 MHz, methylene chloride-d_2) δ / ppm = 177.1 (C_{NHC}), 160.8, 156.8, 152.1, 148.9, 148.7, 148.1, 146.2, 146.1, 145.7, 142.9, 141.4, 141.0, 135.8, 134.3, 132.8, 132.5, 132.0, 131.7, 130.7, 130.5, 130.0, 129.4, 128.7, 128.3, 128.0, 127.9, 126.1, 124.23, 124.15, 124.04, 123.98, 121.2, 120.6, 120.1, 118.7, 114.2, 100.25, 100.16, 73.1, 72.8, 68.2, 59.8, 31.2, 29.26, 29.21, 28.97, 28.93, 28.71, 28.66, 28.53, 28.23, 26.3, 25.8, 25.5, 24.5, 23.9, 23.8, 23.29, 23.27, 22.3, 17.1, 14.6, 13.8, 13.2, 12.2, 7.3.

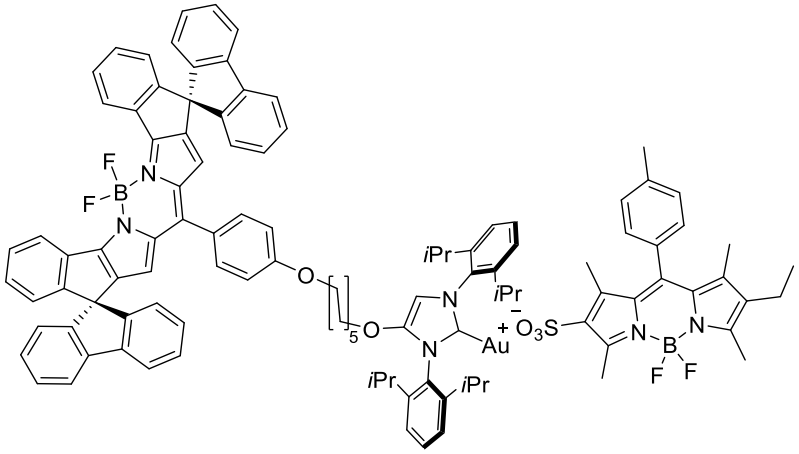

Synthesis of 126. In 25 mL round flask [AuCl(**119**_red)] (6.15 mg, 4.0 μmol) was dissolved in CH_2Cl_2 (10 mL) and a solution of $bdpSO_3Ag$ **114** (2.22 mg, 4.0 μmol) in acetonitrile (5 mL) was added. The AgCl precipitate formed immediately was separated by filtration through celite. The celite was washed with dichloromethane (10 mL) to extract the product completely. The combined filtrates were evaporated and dried overnight in high vacuum (7.8 mg, yield 99 %).

^{1}H NMR (500 MHz, methylene chloride-d_2) δ / ppm = 8.44 (d, *J* = 7.6 Hz, 2H), 7.83 (d, *J* = 7.6 Hz, 4H), 7.53 (t, *J* = 7.5 Hz, 2H), 7.49 – 7.45 (m, 2H), 7.38 (t, *J* = 7.5 Hz, 4H), 7.32 (d, *J* = 8.0 Hz, 4H), 7.29 – 7.22 (m, 6H), 7.17 (t, *J* = 7.5 Hz, 4H), 7.11 (d, *J* = 7.5 Hz, 2H), 6.94 (d, *J* = 7.6 Hz, 4H), 6.75 (d, *J* = 8.4 Hz, 2H), 6.63 (d, *J* = 7.7 Hz, 2H), 6.46 (s, 1H), 6.27 (s, 2H), 3.97 (t, *J* = 6.4 Hz, 2H), 3.83 (t, *J* = 6.4 Hz, 2H), 2.60 – 2.39 (m, 12H), 2.33 (q, *J* = 7.2 Hz, 2H), 1.68 – 1.61 (m, 4H), 1.34 – 1.13 (m, 42H), 0.99 (t, *J* = 7.5 Hz, 3H).

^{13}C{^{1}H} NMR (126 MHz, methylene chloride-d_2) δ / ppm = 161.69 (d, *J* = 4.4 Hz), 161.3, 159.2, 158.6, 157.4, 149.3, 148.7, 146.8, 146.4, 143.5, 143.0, 141.9, 141.6, 139.8, 139.7, 135.6, 135.1, 133.1, 132.6, 131.3, 131.2, 131.1, 131.0, 130.7, 130.4, 130.3, 129.5, 129.3, 128.62, 128.55, 128.47, 126.7, 124.80, 124.72, 124.66, 124.55, 121.2, 120.7, 114.7, 100.3,

73.4, 68.7, 60.3, 29.84, 29.79, 29.77, 29.73, 29.61, 29.55, 29.31, 29.25, 29.12, 26.4, 26.1, 24.9, 24.5, 24.3, 24.0, 21.8, 17.6, 14.7, 14.0, 13.3, 13.1, 12.4.
^{19}F NMR (471 MHz, methylene chloride-d_2) δ / ppm = -144, 26 (q, J(^{11}B-^{19}F) = 33 Hz) (green Bodipy), -146.43 (q, J(^{11}B-^{19}F) = 33 Hz) (red Bodipy).

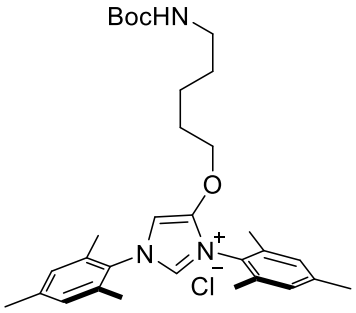

Synthesis of IMes·HCl. General Procedure G: BocNH$(CH_2)_5$OTs (90 mg, 0.25 mmol, 1.2 eq.), 4-hydroxy-1,3-dimesityl-1H-imidazol-3-ium chloride (75 mg, 0.21 mmol, 1.0 eq.), K_2CO_3 (29 mg, 0.21 mmol, 1.0 eq.), KI (105 mg, 0.63 mmol, 3 eq.) were placed in a dried 5 mL Schlenk flask and dissolved in dry acetone (3 mL). The crude product was purified by column chromatography (MeOH/CH_2Cl_2 = 1/15) and gave IMes·HCl as a white powder (55 mg, yield 48%).
^{1}H NMR (300 MHz, chloroform-d) δ / ppm = 9.28 (s, 1H), 7.30 (s, 1H), 7.02 (d, J = 10.4 Hz, 4H), 4.57 (s, 1H), 4.32 (t, J = 6.5 Hz, 2H), 3.03 (q, J = 6.7 Hz, 2H), 2.34 (d, J = 8.7 Hz, 6H), 2.22 (s, 6H), 2.14 (s, 6H), 1.84 – 1.60 (m, 3H), 1.50 – 1.14 (m, 12H).
^{13}C{^{1}H} NMR (75 MHz, chloroform-d) δ / ppm = 156.2, 147.7, 141.7, 141.5, 134.9, 134.2, 131.3, 130.9, 130.1, 126.8, 102.2, 74.9, 29.6, 28.5, 28.0, 22.7, 21.3, 18.0.
HRMS (ESI positive): m/z calcd. for $C_{31}H_{44}N_3O_3$: 506.33772 $[M\text{-}Cl]^+$; found 506.33840.

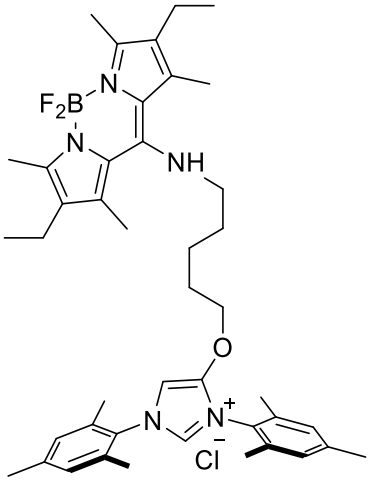

Synthesis of 127·HCl. The imidazolium salt IMes·HCl (40 mg, 0.074 mmol) was dissolved in freshly distilled CH_2Cl_2 (2 mL) in a dried 10 mL Schlenk flask, cooled to 0°C and treated with a solution of HCl in dioxane (4M, 28 µL, 0.11 mmol, 1.5 eq.) and stirred at rt for 15 h under nitrogen atmosphere. The volatiles was evaporated on the rotavap under reduced pressure, Et_3N (17.5 µL, 0.11 mmol, 1.7 eq) and *meso*-Cl Bodipy [273] (25 mg, 0.074 mmol) were added to the crude product, and the mixture dissolved in CH_2Cl_2:CH_3CN (1:1) (2 mL). The solution was stirred for 15 h at rt. Removal of the solvent on the rotavap under

reduced pressure and purification of the residue by silica gel column chromatography (CH_2Cl_2/MeOH = 1/1) as an eluent provides **127**·HCl as a yellow solid. Yield: 27 mg (49%).
^{1}H NMR (500 MHz, chloroform-*d*) δ / ppm = 9.26 (d, *J* = 1.7 Hz, 1H), 7.56 (d, *J* = 1.8 Hz, 1H), 7.00 (s, 4H), 5.39 (t, *J* = 5.3 Hz, 1H), 4.31 (t, *J* = 6.6 Hz, 2H), 3.47 (q, *J* = 6.3 Hz, 2H), 2.42 (s, 6H), 2.40 – 2.37 (m, 4H), 2.32 (d, *J* = 2.2 Hz, 6H), 2.26 (s, 6H), 2.20 (s, 6H), 2.09 (s, 6H), 1.71 – 1.64 (m, 6H), 1.37 – 1.31 (m, 2H), 1.03 (t, *J* = 7.5 Hz, 6H).
^{13}C{^{1}H} NMR (126 MHz, chloroform-*d*) δ / ppm = 151.4, 147.5, 145.0, 141.5, 141.3, 134.8, 134.1, 131.3, 131.0, 129.9, 129.8, 129.6, 128.6, 126.9, 122.7, 102.6, 74.3, 52.1, 31.7, 27.9, 22.5, 21.20, 21.16, 17.6, 17.2, 15.1, 13.2, 12.0.
^{19}F NMR (471 MHz, chloroform-*d*) δ / ppm = -144.43 (q, $J(^{11}B\text{-}^{19}F)$ = 33 Hz).
HRMS (ESI positive): m/z calcd. for $C_{43}H_{57}BF_2N_5O$: 708.46310 $[M\text{-}Cl]^+$; found 708.46187.

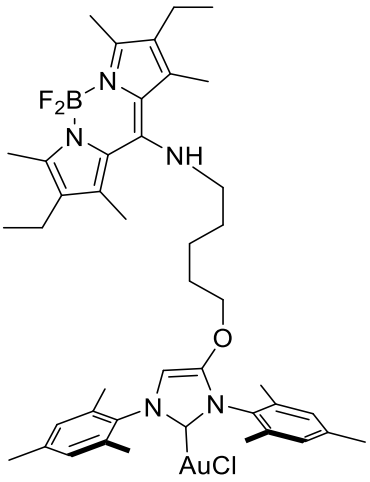

Synthesis of [AuCl(127_blue)]. To a 5 mL dried Schlenk flask equipped with a stirring bar containing **127·HCl** (15 mg, 0.02 mmol, 1.0 eq.) and Ag_2O (2.3 mg, 0.01 mmol, 0.5 eq.) under a flow of the nitrogen gas, dry 1,2-dichloroethane (2 mL) was added and the flask was sealed. After stirring in the dark for 90 min at 55 °C, [AuCl(SMe_2)] (5.9 mg, 0.02 mmol, 1.0 eq.) was added and the mixture was stirred for an additional 2 h at 60 °C. The resulting suspension was filtered through a short celite plug. The filtrate was collected and evaporated on the rotavap under reduced pressure. The product was purified by column chromatography (CH_2Cl_2) obtaining the product as a yellow solid (9.6 mg, yield 51%).
^{1}H NMR (500 MHz, chloroform-*d*) δ / ppm = 6.95 (d, *J* = 7.0 Hz, 4H), 6.30 (s, 1H), 5.18 (t, *J* = 5.7 Hz, 1H), 3.88 (t, *J* = 6.3 Hz, 2H), 3.42 (q, *J* = 6.6 Hz, 2H), 2.45 (s, 6H), 2.40 (q, *J* = 7.6 Hz, 4H), 2.32 (d, *J* = 7.0 Hz, 6H), 2.24 (s, 6H), 2.12 (s, 6H), 2.06 (s, 6H), 1.64 – 1.57 (m, 4H), 1.31 – 1.25 (m, 4H), 1.04 (t, *J* = 7.5 Hz, 6H).
^{13}C{^{1}H} NMR (126 MHz, chloroform-*d*) δ / ppm = 168.2 (C_{NHC}), 151.3, 147.7, 145.7, 139.79, 139.75, 135.42, 135.39, 134.9, 131.1, 129.9, 129.55, 129.47, 128.7, 98.8, 72.6, 52.3, 32.0, 28.2, 22.9, 21.34, 21.27, 18.0, 17.8, 17.3, 15.2, 13.2, 12.2.
^{19}F NMR (471 MHz, chloroform-*d*) δ / ppm = -145.17 (q, $J(^{11}B\text{-}^{19}F)$ = 28 Hz).
HRMS (ESI negative): m/z calcd. for $C_{43}H_{55}AuBClF_2N_5O$: 938.38274 $[M\text{-}H]^-$; found 938.38084.

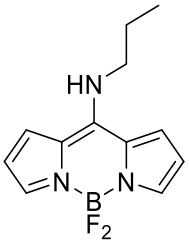

Synthesis of 128. General Procedure H.
^{1}H NMR (500 MHz, chloroform-*d*) δ / ppm = 7.68 (s, 1H), 7.44 (s, 1H), 7.09 (s, 1H), 6.80 (s, 1H), 6.58 (s, 1H), 6.51 (s, 1H), 6.29 (s, 1H), 3.50 (q, *J* = 6.5 Hz, 3H), 1.81 (h, *J* = 7.3 Hz, 3H), 1.08 (t, *J* = 7.4 Hz, 4H).
^{13}C{^{1}H} NMR (126 MHz, chloroform-*d*) δ / ppm = 148.3, 135.0, 132.2, 125.0, 123.9, 122.4, 114.9, 114.7, 113.8, 49.0, 22.3, 11.5.
HRMS (ESI positive): m/z calcd. for $C_{12}H_{15}BF_2N_3$: 250.13216 $[M+H]^+$; found 250.13233.
Yield: 108 mg (87%).

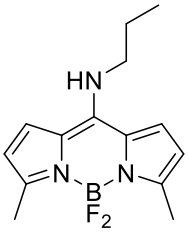

Synthesis of 129. General Procedure H.
^{1}H NMR (500 MHz, chloroform-*d*) δ / ppm = 6.83 (s, 2H), 6.13 (s, 2H), 6.02 (s, 1H), 3.41 (q, *J* = 6.5 Hz, 2H), 2.56 (s, 5H), 1.75 (h, *J* = 7.3 Hz, 2H), 1.04 (t, *J* = 7.4 Hz, 3H).
^{13}C{^{1}H} NMR (126 MHz, chloroform-*d*) δ / ppm = 147.5, 145.8, 123.3, 114.9, 48.8, 29.8, 22.6, 14.2, 11.5.
HRMS (ESI positive): m/z calcd. for $C_{14}H_{19}BF_2N_3$: 278.16346 $[M+H]^+$; found 278.16357.
Yield: 118 mg (85%).

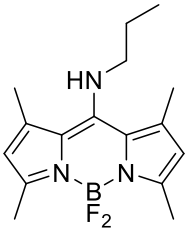

Synthesis of 130. General Procedure H.
^{1}H NMR (500 MHz, chloroform-*d*) δ / ppm = 6.01 (s, 2H), 5.46 (s, 1H), 3.50 (q, *J* = 6.4 Hz, 2H), 2.50 (s, 6H), 2.36 (s, 6H), 1.70 (h, *J* = 7.2 Hz, 2H), 0.98 (t, *J* = 7.4 Hz, 3H).
^{13}C{^{1}H} NMR (126 MHz, chloroform-*d*) δ / ppm = 152.3, 147.4, 131.8, 123.2, 118.2, 54.4, 25.7, 15.7, 14.3, 11.3.
HRMS (ESI positive): m/z calcd. for $C_{16}H_{23}BF_2N_3$: 306.19476 $[M+H]^+$; found 306.19482.
Yield: 113 mg (74%).

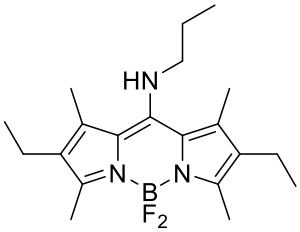

Synthesis of 131. General Procedure H.
^{1}H NMR (500 MHz, chloroform-*d*) δ / ppm = 5.38 (s, 1H), 3.47 (q, *J* = 6.3 Hz, 3H), 2.47 (s, 6H), 2.42 (q, *J* = 7.5 Hz, 4H), 2.29 (s, 6H), 1.69 (h, *J* = 7.2 Hz, 2H), 1.05 (t, *J* = 7.5 Hz, 6H), 0.97 (t, *J* = 7.3 Hz, 3H).
^{13}C{^{1}H} NMR (126 MHz, chloroform-*d*) δ / ppm = 151.5, 145.2, 129.7, 128.6, 122.9, 54.5, 25.7, 17.3, 15.2, 13.3, 12.2, 11.4.
HRMS (ESI positive): m/z calcd. for $C_{20}H_{31}BF_2N_3$: 362.25736 $[M+H]^+$; found 362.25743. Yield: 137 mg (76%).

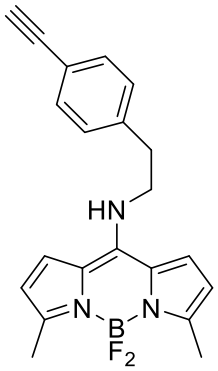

Synthesis of 133. *Tert*-butyl (4-ethynylphenethyl)carbamate (100 mg, 0.41 mmol) was dissolved in 3 mL of CH_2Cl_2, the reaction mixture was cooled to 0°C and treated with trifluoroacetic acid (200 μL) and stirred at rt for 1 h. The solution was evaporated and to the crude material was added 8-SMe Bodipy (110 mg, 0.41 mmol) and Et_3N (112 μL, 0.8 mmol) in the solvent mixture (1:1) of CH_2Cl_2 and CH_3CN (2 mL), and the solution was stirred for 24 h at rt. Solvent removal on the rotavap under reduced pressure and purification by column chromatography on silica gel using CH_2Cl_2 as an eluent gave Bodipy **133** as a yellow solid (68 mg, yield 46%).
^{1}H NMR (500 MHz, chloroform-*d*) δ / ppm = 7.51 (d, *J* = 7.9 Hz, 2H), 7.21 (d, *J* = 7.8 Hz, 2H), 6.79 (s, 2H), 6.16 (s, 2H), 5.99 (s, 1H), 3.83 (q, *J* = 6.5 Hz, 2H), 3.10 (s, 1H), 3.07 (t, *J* = 6.9 Hz, 2H), 2.56 (s, 6H).
^{13}C{^{1}H} NMR (126 MHz, chloroform-*d*) δ / ppm = 147.9, 145.5, 137.6, 133.1, 128.8, 123.3, 121.6, 115.3, 83.1, 78.0, 47.3, 34.9, 27.1, 14.3.
HRMS (ESI positive): m/z calcd. for $C_{21}H_{21}BF_2N_3$: 364.17911 $[M+H]^+$; found 364.17939.

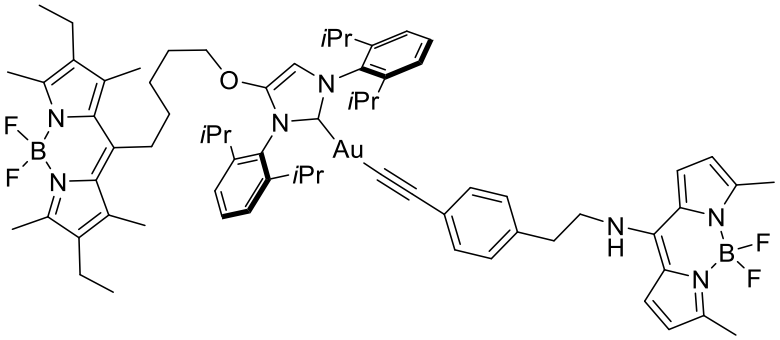

Synthesis of 134·dbu. A vial was charged with [AuCl(**122**_green)][244] (4.0 mg, 0.004 mmol, 1.0 eq.) and **133** (1.5 mg, 0.004 mmol, 1.0 eq.) and dissolved in a minimum amount of CH_2Cl_2 ~200 µL. To the reaction mixture, DBU (3.0 µL, 0.02 mmol, 5.0 eq.) was added and the solution stirred at rt for 15 h. The reaction mixture was diluted with CH_2Cl_2 (50 mL) and washed two times with brine (50 mL) and two times with water (50 mL). The organic layer was dried over $MgSO_4$, filtered and the volatiles evaporated on the rotavap under reduced pressure. The remaining orange solid **134·dbu** was used in further experiments without additional purification (5.9 mg, yield 99%).

^{1}H NMR (500 MHz, methylene chloride-d_2) δ / ppm = 7.55 (m, 2H, *p*-H_{Ar}), 7.35 (m, 4H, *m*-H_{Ar}), 7.23 (d, J = 8.0 Hz, 2H, *m*-$H_{Ar\text{-}bdp}$), 7.06 (d, J = 8.0 Hz, 2H, *o*-$H_{Ar\text{-}bdp\text{-}blue}$), 6.89 (br. s, 2H, γ-H bpd-blue), 6.45 (s, 1H, NC(OR)CHN), 6.17 (bs, 2H, β-H bdp-blue), 4.02 (t, J = 6.3 Hz, 2H, alkyl chain -CH_2O-), 3.86 (t, J = 7.0 Hz, 2H, alkyl chain -CH_2-Ar bdp-blue), 3.46 – 3.28 (m, 6H, DBU), 3.03 (t, J = 6.9 Hz, 2H, alkyl chain -CH_2-NH-bdp-blue), 2.91 (m, 4H, DBU + alkyl chain CH_2 bdp-green), 2.75 – 2.56 (m, 4H, CH *i*Pr), 2.48 (s, 6H, CH_3 bdp-blue), 2.45 (s, 6H, CH_3 bdp-green), 2.43 – 2.37 (m, 4H, $\underline{CH_2}CH_3$ bdp-green), 2.25 (s, 6H, CH_3 bdp-green), 2.12 – 1.89 (m, 2H, alkyl chain CH_2), 1.81 – 1.45 (m, 12H, DBU + alkyl chain), 1.41 – 1.31 (m, 12H, CH_3 *i*Pr), 1.26 (d, J = 6.7 Hz, 6H, CH_3 *i*Pr), 1.21 (d, J = 6.8 Hz, 6H, CH_3 *i*Pr), 1.05 (t, J = 7.5 Hz, 6H, $CH_2\underline{CH_3}$ bdp-green).

^{13}C{^{1}H} NMR (126 MHz, methylene chloride-d_2) δ / ppm = 185.1 (C_{NHC}), 166.2, 152.1, 148.7, 148.5, 146.4, 146.0, 145.9, 145.7, 144.3, 135.8, 135.0, 134.2, 132.8, 132.4, 130.7, 130.6, 130.5, 130.4, 130.4, 128.3, 125.4, 124.2, 124.2, 124.1, 124.0, 99.6, 72.4, 48.7, 47.4, 43.9, 41.1, 37.9, 34.5, 32.0, 31.9, 31.3, 29.6. 29.6, 29.4, 29.1, 29.0, 28.7, 28.2, 26.6, 26.3, 24.6, 24.4, 24.1, 24.0, 23.88, 23.84, 23.77, 23.37, 23.29, 22.7.

^{19}F NMR (471 MHz, methylene chloride-d_2) δ / ppm = -145.40 (q, J(^{11}B-^{19}F) = 33 Hz) (green Bodipy), -147.51 (q, J(^{11}B-^{19}F) = 28 Hz) (blue Bodipy).

HRMS (ESI positive): m/z calcd. for $C_{70}H_{87}AuB_2F_4N_7O$: 1336.67545 $[M+H]^+$; found 1336.67735.

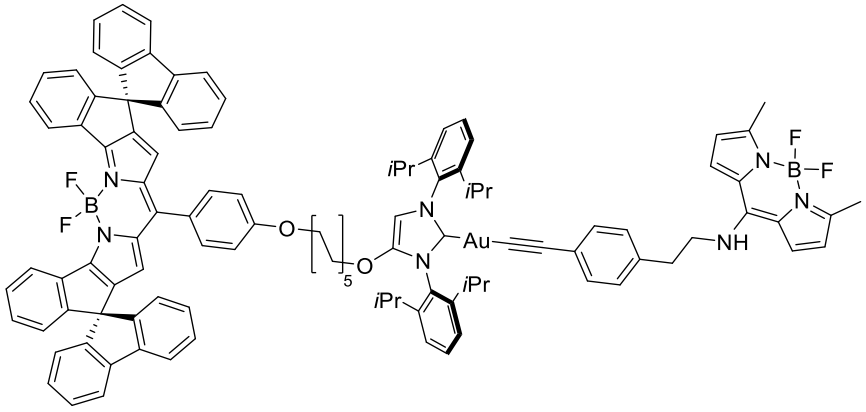

Synthesis of 136·dbu. A vial was charged with [AuCl(**119**_red)] (6.1 mg, 0.004 mmol, 1.0 eq.) and **133** (1.5 mg, 0.004 mmol, 1.0 eq.) and dissolved in a minimum amount of CH_2Cl_2 ~200 μL. To the reaction mixture, DBU (6.0 μL, 0.02 mmol, 10 eq.) was added and the solution was stirred at rt for 48 h. The reaction mixture was diluted with CH_2Cl_2 (50 mL), and washed two times with brine (50 mL) and two times with water (50 mL). The organic layer was dried over $MgSO_4$, filtered and the volatiles evaporated on the rotavap under reduced pressure. The remaining **136·dbu** as a red solid was used in further experiments without additional purification (8.0 mg, yield 99%).

^{1}H NMR (500 MHz, methylene chloride-d_2) δ / ppm = 8.44 (d, J = 7.6 Hz, 2H), 7.83 (d, J = 7.6 Hz, 4H), 7.57 – 7.50 (m, 4H), 7.40 – 7.32 (m, 10H), 7.27 – 7.22 (m, 4H), 7.17 (t, J = 7.5 Hz, 4H), 7.07 (d, J = 7.5 Hz, 2H), 6.94 (d, J = 7.6 Hz, 4H), 6.75 (d, J = 7.7 Hz, 2H), 6.63 (d, J = 7.7 Hz, 2H), 6.42 (s, 1H), 6.27 (s, 2H), 6.23 – 6.13 (m, 3H), 3.97 (t, J = 6.2 Hz, 2H), 3.91 – 3.80 (m, 4H), 3.46 – 3.32 (m, 6H, DBU) 3.02 (t, J = 6.7 Hz, 2H), 2.72 – 2.55 (m, 4H), 2.48 (s, 6H), 2.31 – 2.29 (m, 2H, DBU) 1.89 – 1.61 (m, 12H, DBU + alkyl chain), 1.38 – 1.19 (m, 40H, CH_3 *i*Pr + alkyl chain).

^{19}F NMR (471 MHz, methylene chloride-d_2) δ / ppm = -146.44 (q, J(^{11}B-^{19}F) = 31 Hz), -147.52 (q, J(^{11}B-^{19}F) = 31 Hz) (blue Bodipy).

HRMS (ESI positive): m/z calcd. for $C_{111}H_{104}AuB_2F_4N_7O_2$: 1862.8112 $[M+H]^+$; found 1862.8116.

6.1.2. Determination of fluorescence quantum yield.

Quantum yields were determined according to the literature procedure (U. Resch-Genger, K. Rurack, *Pure Appl. Chem*., **2013**, *85*, 2005–2026) using rhodamine 6G (from Sigma-Aldrich, BioReagent, suitable for fluorescence) as the standard. Absorption and emission spectra for all compounds and standards were obtained over a range of concentrations (200 nM to 0.5 μM, in acetonitrile) where a linear correlation between concentration and absorption was observed. The absorbance was within the range of 0.01 to 0.12. The quantum yield was calculated according to the equation:

$$\Phi_{\Delta} = \Phi_{st}\left(\frac{r_x}{r_{st}}\right)\left(\frac{\eta_x}{\eta_{st}}\right)^2 \qquad (6.1)$$

where the subscripts *st* and *x* denote standard and test respectively, Φ_{Δ} is the fluorescence quantum yield, *r* the gradient from the plot of integrated fluorescence intensity *vs*. absorbance, and η the refractive index of the solvent. Φ_{st} (rhodamine 6G) = 0.95 in EtOH; Φ_{st} (Coumarin 153) = 0.54 in EtOH.

6.1.3. Photooxidation of *p*-bromo-thioanisole.

Procedure: *p*-bromo-thioanisole (20.6 mg, 0.2 mmol), catalyst (0.002 mmol), 2-bromoanisole (internal standard, 25.67 μL, 0.2 mmol) or were added into a 2 mL transparent vial and dissolved in 0.5 mL of *t*-amyl alcohol and 0.5 mL of acetonitrile and the vial was irradiated under green LED. NMR was measured and the conversion to the product was calculated with respect to the internal standard.

6.1.4. Determination of singlet oxygen generation.

A mixture of 1,3-diphenylisobenzofuran (DPBF) (90 μM) and the respective photosensitizer (1.0 μM) was dissolved in the corresponding solvent (2 mL) and was irradiated under green LED light in a home-built photoreactor (Figure 104). The photooxidation of DPBF (Figure 103) was monitored over time at time intervals fdepending on the efficiency (rate) of the photocatalytic reaction.

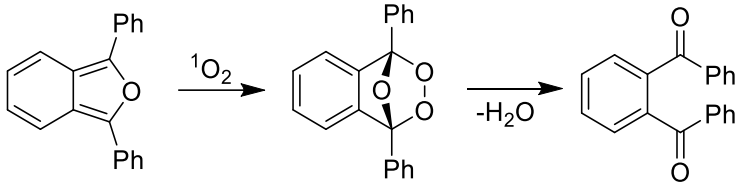

Figure 103 Reaction of DPBF photooxidation in the presence of a photocatalyst.

The time-dependent absorption graphs show the decrease in the DPBF absorbance at 410 nm and the corresponding linear regression from which the rate was calculated. $\Phi^{st}_{s.o.}$ data was obtained using 2,6-diiodobodipy ($\Phi^{st}_{s.o.}$ = 0.75 in acetonitrile; 0.94 in toluene) as the reference:[97,275]

$$\Phi_{\text{s.o.}} = \Phi^{st}_{\text{s.o.}}\frac{k}{k^{st}}\frac{I^{st}}{I} \qquad (6.2)$$

where (k) and (k^{st}) are the DPBF photooxidation rates in the presence of the corresponding photosensitizer (calculated from the decrease in absorbance at 410 nm), respectively; (I) and (I^{st}) are relative absorbance correction factors and were calculated according to the spectrum of the light source and the absorbance spectrum of the

photosensitizer. Relative absorbance (I) allows translation of the experimental data from photosensitizers with different absorbance spectrums using a non-monochromatic light source for the irradiation.

$$I = \int_{484}^{600} i(\lambda)\,(1 - 10^{-A(\lambda)})d(\lambda) \tag{6.3}$$

Where the integral of i, is the intensity of the light source at the specific wavelength (λ), with the corresponding absorbance value (A) at the given wavelength (λ).[276]

Figure 104 Home-built photoreactor for photocatalytic experiments.

6.1.5. General procedure for the synthesis of NHC-iridium based Bodipy-tagged ion paired complexes.

[IrCl(cod)(NHC)] ($2.05 \cdot 10^{-6}$ mol) was dissolved in CH_2Cl_2 (3 mL) and a solution of bdpSO_3Ag **114** ($2.00 \cdot 10^{-6}$ mol) in acetonitrile (2 mL) added. The AgCl precipitate formed immediately and was separated by filtration through celite pad. The celite was washed with dichloromethane (3 mL). The combined filtrates were evaporated and dried overnight in vacuum. The obtained solid was dissolved in 10.0 mL of toluene to obtain a $2.00 \cdot 10^{-4}$ M solution of the respective [Ir(bdpSO_3)(cod)(NHC)] complex.
This stock solution was kept under nitrogen atmosphere and used for measurements on the same day. Addition of this solution (10.0 µL, $2.00 \cdot 10^{-4}$ M, 2.00 nmol) to a cuvette charged with 1990 µL of solvent gave a $1.00 \cdot 10^{-6}$ M solution. The filled cuvette was then placed in the sample holder of the spectrometer, thermostatted to 25°C and the fluorescence determined.

6.1.6. General procedure for the titration fluorescence experiments.

All experiments were carried out in quartz cuvettes with path lengths of 10.0 mm. A cuvette was charged with 2000 µL of 1.0 µM solution of the respective [Ir(bdpSO_3)(cod)(NHC)] complex in toluene, 1,2-dichloroethane or acetonitrile. The temperature (T = 25 °C) was adjusted using a thermostat. Portions of purified solvent or a solution of salt in 1,2-dichloromethane were added to the cuvette in fixed amounts of 2

– 100 μL. For the fluorescence quenching experiment 0.2 *m*M NBu_4Br / NaBArF salt solutions in 1,2-dichloroethane were added to the cuvette (typical range 5 μL - 50 μL). After each aliquot, the fluorescence intensity was monitored. The next aliquot was added when the fluorescence level was found to remain constant, which is typically the case after 30 s of light exposure. The titration was terminated when addition of a new aliquot did not lead to a further increase in the fluorescence. The fluorescence data were finally corrected for dilution of the sample. In order to avoid mistakes in the preparation of solution of photocatalyst each fluorescence value of the 1.0 μM solution of the respective [Ir(bdpSO_3)(cod)(NHC)] complex in toluene were monitored prior to the photooxidation experiment. Following the photooxidation experiment of DPBF to obtain the respective fluorescence intensity for the fully separated ion pair, an 8 M solution of NBu_4Br in 1,2-dichloroethane was added (10 μL, $8.00 \cdot 10^{-5}$ mol, 40000 eq.).

6.1.7. FRET evaluation experiments.

Monitoring of gold acetylide/thiolate FRET experiments. To a quartz cuvette containing a solution of gold acetylide complex [AuCCPh(**124**_green)] (5.0 μM) in CH_2Cl_2, a stock solution of gold-NTf_2 complex [AuNTf_2(**119**_red)] (1.0 eq.) (stored at -20 °C until use), was added dropwise in one portion. The emission intensities at 535 and 648 nm were monitored every interval 5 seconds over the measurement time.

Monitoring of ion pairing using red-green FRET. All experiments were carried out in quartz cuvettes with path lengths of 10.0 mm. A cuvette was charged with the respective Bodipy ion-paired dyad **126** (2.0 mL, 1.00 μM) in toluene or 1,2-dichloroethane solution. Next, the measurement was started and the fluorescence intensity at the designated wavelength was observed (530 nm for the green emission and 648 nm for the red emission). After approximately 1 min (when the intensity of fluorescence signal remains constant), portions of freshly distilled DMAc or phenylacetylene in toluene solution (0.18M) were added to the cuvette (typical range 5 μL - 100 μL). After each aliquot, the fluorescence intensity at the specific wavelength was monitored. The next aliquot was added when the fluorescence level was found to remain constant after 30 s. The titration was terminated when addition of a new aliquot did not lead to further change in the fluorescence signal. The fluorescence data were finally corrected for dilution of the sample. In order to obtain the respective fluorescence intensity for the fully separated ion pair an (8M) solution of NBu_4Br in 1,2-dichloroethane was added (10 μL, 0.08 mmol).

Experimental evaluation of the blue-green-red triad. A quartz cuvette was filled with blue-green dyad **134·dbu** in 2 mL of 1,2-dichloroethane solution (5.0 μM). Next, the measurement was started and the fluorescence intensity at the emission maximum of the corresponding fluorophore was observed at the designated wavelength (at 535 nm for the green emission and at 652 nm for the red emission). After approximately 1 min (once the fluorescence signal intensity remained constant), a solution of [AuNTf_2(**119**_red)] (5 μM, 1.0 eq.) in 1,2-dichloroethane was added. The time of addition is indicated with arrows. After approx. 1-2 min more of the [AuNTf_2(**119**_red)] complex solution (5 μM, 1.0 eq.) in 1,2-dichloroethane was added and a formation of the Widenhoefer dimer was observed. The reported fluorescence are peak intensities. For selected examples, it was shown that changes in peak intensities are the same as changes in integrated intensities. This is possible since the Bodipy units are remote tags, which are not influenced to a significant extent by the nature of the organometallic complex.

7. List of Abbreviations

Ac	acetyl
Ar	aryl
BArF	tetrakis(3,5-bis(trifluoromethyl)phenyl)borate
Bodipy	4,4-difluoro-4-bora-3*a*,4*a*-diaza-*s*-indacene
Bu	butyl
cod	*cis*,*cis*-1,5-cyclooctadiene
Cp	cyclopentyl
Cy	cyclohexyl
CV	cyclic voltammetry
dbu	1,8-diazabicyclo[5.4.0]undec-7-ene
DCE	1,2-dichloroethane
DCM	dichloromethane
DDQ	2,3-dichloro-5,6-dicyano-1,4-benzoquinone
DFT	density functional theory
DIPEA	N, N-diisopropylethylamine
DMAc	dimethylacetamide
DMAP	4-dimethylaminopyridine
DMF	dimethylformamide
DMSO	dimethyl sulfoxide
DPBF	1,3-diphenylisobenzofurane
EC_{50}	half maximal effective concentration
EDG	electron-donating group
Et	ethyl
EWG	electron-withdrawing group
Fc	ferrocene
$FcMe_8$	octamethyl ferrocene
FRET	fluorescence or Förster resonance energy transfer
HAE	heavy atom effect
Hex	hexyl
hfa	hexafluoroacetylacetonat
HOMO	highest occupied molecular orbital
IC	internal conversion
*i*Pr	isopropyl
ISC	intersystem crossing

LUMO	lowest unoccupied molecular orbital
Me	methyl
Mes	mesityl
MS	mass spectrometry
Nf	nonafluorobutanesulfonyl
NHC	*N*-heterocyclic carbene
NIR	near-infrared region
NMR	nuclear magnetic resonance
PDT	photodynamic therapy
PET	photoinduced electron transfer
Ph	phenyl
phen	phenanthroline
PS	photosensitizer
py	pyridine
RET	resonance energy transfer
ROMP	ring-opening polymerization reaction
ROS	reactive oxygen species
rt	room temperature
S_NAr	nucleophilic aromatic substitution
S_EAr	electrophilic aromatic substitution
SMFM	single molecule fluorescence microscopy
TBET	through-bond energy transfer
Tf	triflate
TFA	trifluoroacetic acid
TIRF	total internal reflection fluorescence microscopy
Tos	tosylate
TTET	triplet-triplet energy transfer
UV/Vis	ultraviolet-visible

8. References

[1] J. R. Lakowicz, *Principles of Fluorescence Spectroscopy*, Springer, New York, **2006**.

[2] a) H. Yersin, A. F. Rausch, R. Czerwieniec, T. Hofbeck, T. Fischer, *Coord. Chem. Rev.* **2011**, *255*, 2622; b) K. Lazebnik, *Photochem. & Photobiol.* **2010**, *86*, 492.

[3] J. M. Lee, J. M. Park, H. K. Lee, H. M. Kim, J. H. Kim, J. P. Kim, *Dyes Pigm.* **2021**, *196*, 109662.

[4] B. Valeur, M. N. Berberan-Santos, *Molecular Fluorescence Principles and Applications*, WILEY - VCH, 2012.

[5] G. A. Jones, D. S. Bradshaw, *Front. Phys.* **2019**, *7*, 1.

[6] G. L. Closs, J. R. Miller, *Science* **1988**, *240*, 440.

[7] O. Eivgi, S. A. Blum, *Trends Chem.* **2022**, *4*, 5.

[8] B. Valeur, *Coord. Chem. Rev.* **2000**, *205*, 3.

[9] a) X. Tian, L. Murfin, L. Wu, S. Lewis, T. James, *Chem. Sci.* **2021**, *12*, 3406; b) Q. Shen, S. Wang, N.-D. Yang, C. Zhang, Q. Wu, C. Yu, *J. Lumin.* **2020**, *225*, 117338; c) M. Heilemann, S. van de Linde, A. Mukherjee, M. Sauer, *Angew. Chem. Int. Ed.* **2009**, *48*, 6903; d) J. V. Jun, D. M. Chenoweth, E. J. Petersson, *Org. Biomol. Chem.* **2020**, *18*, 5747; e) J. B. Grimm, L. D. Lavis, *Nat. Methods* **2022**, *19*, 149; f) J. Chan, S. C. Dodani, C. J. Chang, *Nat. Chem.* **2012**, *4*, 973.

[10] P. Kaur, K. Singh, *J. Mater. Chem. C* **2019**, *7*, 11361.

[11] T. Kowada, H. Maeda, K. Kikuchi, *Chem. Soc. Rev.* **2015**, *44*, 4953.

[12] N. Boens, V. Leen, W. Dehaen, *Chem. Soc. Rev.* **2012**, *41*, 1130.

[13] S. Kolemen, E. U. Akkaya, *Coord. Chem. Rev.* **2018**, *354*, 121.

[14] L. Huang, J. Zhao, S. Guo, C. Zhang, J. Ma, *J. Org. Chem.* **2013**, *78*, 5627.

[15] J. Zhao, K. Xu, W. Yang, Z. Wang, F. Zhong, *Chem. Soc. Rev.* **2015**, *44*, 8904.

[16] L. Bonardi, H. Kanaan, F. Camerel, P. Jolinat, P. Retailleau, R. Ziessel, *Adv. Funct. Mater.* **2008**, *18*, 401.

[17] P. de Bonfils, L. Péault, P. Nun, V. Coeffard, *Eur. J. Org. Chem.* **2021**, 1809.

[18] a) B. M. Squeo, L. Ganzer, T. Virgili, M. Pasini, *Molecules* **2020**, *26*, 155; b) D. Zhang, V. Martín, I. García-Moreno, A. Costela, M. E. Pérez-Ojeda, Y. Xiao, *Phys. Chem. Chem. Phys.* **2011**, *13*, 13026.

[19] E. Antina, N. Bumagina, Y. Marfin, G. Guseva, L. Nikitina, D. Sbytov, F. Telegin, *Molecules* **2022**, *27*, 1396.

[20] S. Saha, S. Mondal, *Photochemistry and Photophysics: Fundamentals to Applications*, IntechOpen, **2018**.

[21] A. Treibs, F.-H. Kreuzer, *Liebigs Ann. Chem.* **1968**, *718*, 208.

[22] J. A. van Koeveringe, J. Lugtenburg, *Recl. Trav. Chim. Pays-Bas* **1977**, *96*, 55.

[23] V. Lakshmi, M. Shaikh, M. Ravikanth, *J. Fluoresc.* **2013**, *23*, 519.

[24] R. W. Wagner, J. S. Lindsey, *Pure & Appl. Chem.* **1996**, *68*, 1373.

[25] T. V. Goud, A. Tutar, J.-F. Biellmann, *Tetrahedron* **2006**, *62*, 5084.

[26] V. Leen, P. Yuan, L. Wang, N. Boens, W. Dehaen, *Org. Lett.* **2012**, *14*, 6150.

[27] M. T. Rogers, *J. Chem. Soc.* **1943**, *0*, 590.

[28] a) W. Zhao, E. M. Carreira, *Angew. Chem. Int. Ed.* **2005**, *117*, 1705; b) W. Zhao, E. M. Carreira, *Chem. Eur. J.* **2006**, *12*, 7254.

[29] K. B. A. Loudet, *Chem. Rev.* **2007**, *107*, 4891.

[30] N. Boens, B. Verbelen, W. Dehaen, *Eur. J. Org. Chem.* **2015**, 6577.

[31] N. Boens, B. Verbelen, M. J. Ortiz, L. Jiao, W. Dehaen, *Coord. Chem. Rev.* **2019**, *399*, 213024.
[32] H. Lu, J. Mack, Y. Yanga, Z. Shen, *Chem. Soc. Rev.* **2014**, *70*, 691.
[33] I. Esnal, J. Bañuelos, I. López Arbeloa, A. Costela, I. Garcia-Moreno, M. Garzón, A. R. Agarrabeitia, M. José Ortiz, *RSC Adv.* **2013**, *3*, 1547.
[34] L. Jiao, W. Pang, J. Zhou, Y. Wei, X. Mu, G. Bai, E. Hao, *J. Org. Chem.* **2011**, *76*, 9988.
[35] B. Dhokale, T. Jadhav, S. M. Mobin, R. Misra, *Chem. Commun.* **2014**, *50*, 9119.
[36] T. Rohand, M. Baruah, W. Qin, N. Boens, W. Dehaen, *Chem. Commun.* **2006**, *3*, 266.
[37] a) E. Bodio, C. Goze, *Dyes Pigm.* **2019**, *160*, 700; b) A. L. Nguyen, P. Bobadova-Parvanova, M. Hopfinger, F. R. Fronczek, K. M. Smith, M. Vicente, H. Graça, *Inorg. Chem.* **2015**, *54*, 3228.
[38] T. Lundrigan, S. M. Crawford, T. S. Cameron, A. Thompson, *Chem. Commun.* **2012**, *48*, 1003.
[39] a) V. Leen, V. Z. Gonzalvo, W. M. Deborggraeve, N. Boens, W. Dehaen, *Chem. Commun.* **2010**, *46*, 4908; b) R. I. Roacho, A. Metta-Magaña, E. Peña-Cabrera, K. Pannell, *Org. Biomol. Chem.* **2015**, *13*, 995.
[40] V. Leen, M. van der Auweraer, N. Boens, W. Dehaen, *Org. Lett.* **2011**, *13*, 1470.
[41] B. Verbelen, S. Boodts, J. Hofkens, N. Boens, W. Dehaen, *Angew. Chem. Int. Ed.* **2015**, *127*, 4695.
[42] K. Rurack, M. Kollmannsberger, J. Daub, *Angew. Chem. Int. Ed.* **2001**, *40*, 385.
[43] a) L. Betancourt-Mendiola, I. Valois-Escamilla, T. Arbeloa, J. Banuelos, I. Lopez Arbeloa, J. Flores-Rizo, R. Hu, E. Lager, C. Gomez-Duran, J. Belmonte-Vazquez, M. Martínez-Gonzalez, I. Arroyo, C. Osorio-Martínez, E. Alvarado-Martínez, A. Urías-Benavides, B. Gutierrez-Ramos, B. Tang, E. Peña-Cabrera, *J. Org. Chem.* **2015**, *80*, 5771; b) J. Han, O. Gonzalez, A. Aguilar-Aguilar, E. Peña-Cabrera, K. Burgess, *Org. Biomol. Chem.* **2009**, *7*, 34; c) E. Peña-Cabrera, A. Aguilar-Aguilar, M. Gonzalez-Domínguez, E. Lager, R. Zamudio-Vazquez, J. Godoy-Vargas, F. Villanueva-García, *Org. Lett.* **2007**, *9*, 3985; d) G. Ulrich, A. Haefele, P. Retailleau, R. Ziessel, *J. Org. Chem.* **2012**, *77*, 5036; e) B. Verbelen, V. Leen, L. Wang, N. Boens, W. Dehaen, *Chem. Commun.* **2012**, *48*, 9129; f) T. Shimada, S. Mori, M. Ishida, H. Furuta, *Beilstein J. Org. Chem.* **2020**, *16*, 587; g) L. Luo, Di Wu, W. Li, S. Zhang, Y. Ma, S. Yan, J. You, *Org. Lett.* **2014**, *16*, 6080; h) W. Ren, H. Xiang, C. Peng, Z. Musha, J. Chen, X. Li, R. Huang, Y. Hu, *RSC Adv.* **2018**, *8*, 5542.
[44] V. Leen, E. Braeken, K. Luckermans, C. Jackers, M. van der Auweraer, N. Boens, W. Dehaen, *Chem. Commun.* **2009**, *30*, 4515.
[45] C. Gómez-Durán, I. García-Moreno, A. Costela, V. Martin, R. Sastre, J. Bañuelos, F. López Arbeloa, I. López Arbeloa, E. Peña-Cabrera, F. Azael, *Chem. Commun.* **2010**, *46*, 5103.
[46] a) Z. Wang, J. Zhao, *Org. Lett.* **2017**, *19*, 4492; b) E. Deniz, G. C. Isbasar, O. A. Bozdemir, L. T. Yildirim, A. Siemiarczuk, E. U. Akkaya, *Org. Lett.* **2008**, *10*, 3401; c) V. Leen, D. Miscoria, S. Yin, A. Filarowski, J. M. Ngongo, M. van der Auweraer, N. Boens, W. Dehaen, *J. Org. Chem.* **2011**, *76*, 8168; d) X. Zhou, Q. Wu, Y. Feng, Y. Yu, C. Yu, E. Hao, Y. Wei, X. Mu, L. Jiao, *Asian J. Chem.* **2015**, *10*, 1979.
[47] L. Li, J. Han, B. Nguyen, K. Burgess, *J. Org. Chem.* **2008**, *73*, 1963.
[48] a) J. Bañuelos, *Chem. Rec.* **2016**, *16*, 335; b) B. M. Squeo, M. Pasini, *Supramol. Chem.* **2020**, *32*, 56.

[49] a) M. Baruah, W. Qin, N. Basaric, W. De Borggraeve, N. Boens, *J. Org. Chem.* **2005**, *70*, 4152; b) M. Baruah, W. Qin, C. Flors, J. Hofkens, R. Vallee, D. Beljonne, M. Auweraer, W. Borggraeve and N. Boens, *J. Phys. Chem. A* **2006**, *110*, 5998; c) W. Qin, M. Baruah, M. van der Auweraer, F. C. de Schryver, N. Boens, *J. Phys. Chem. A* **2005**, *109*, 7371; d) W. Qin, T. Rohand, M. Baruah, A. Stefan, M. V. Auweraer, W. Dehaen, N. Boens, *Chem. Phys. Let.* **2006**, *420*, 562; e) T. Rohand, J. Lycoops, S. Smout, E. Braeken, M. Sliwa, M. van der Auweraer, W. Dehaen, W. M. de Borggraeve, N. Boens, *Photochem. Photobiol. Sci.* **2007**, *6*, 1061.

[50] M. Zhang, E. Hao, Y. Xu, S. Zhang, H. Zhu, Q. Wang, C. Yu, L. Jiao, *RSC Adv.* **2012**, *2*, 11215.

[51] H.-B. Cheng, X. Cao, S. Zhang, K. Zhang, Y. Cheng, J. Wang, J. Zhao, L. Zhou, X.-J. Liang, J. Yoon, *Adv. Mater.* **2022**, e2207546.

[52] W. Miao, C. Yu, E. Hao, L. Jiao, *Front. Chem.* **2019**, *7*, 825.

[53] R. Prieto-Montero, A. Prieto-Casta, R. Sola-Llano, A. R. Agarrabeitia, D. Garcia-Fresnadillo, I. Lopez-Arbeola, A. Villanueva, M. J. Ortiz, S. de la Moya, V. Martinez-Martinez, *Photochem. Photobiol.* **2020**, *96*, 458.

[54] E. Bassan, A. Gualandi, P. G. Cozzi, P. Ceroni, *Chem. Sci.* **2021**, *12*, 6607.

[55] a) H. Klfout, A. Stewart, M. Elkhalifa, H. He, *ACS Appl. Mater. Interfaces* **2017**, *9*, 39873; b) G. H. A. Bessetteab, *Chem. Soc. Rev.* **2014**, *43*, 3342.

[56] E. Fron, E. Coutiño-Gonzalez, L. Pandey, M. Sliwa, M. van der Auweraer, F. C. de Schryver, J. Thomas, Z. Dong, V. Leen, M. Smet, W. Dehaen, T. Vosch, *New J. Chem.* **2009**, *33*, 1490.

[57] R. Rao, M. Tiwari, J. Bellare, M. Ravikanth, *J. Org. Chem.* **2011**, *76*, 7263.

[58] O. Buyukcakir, O. A. Bozdemir, S. Kolemen, S. Erbas, E. U. Akkaya, *Org. Lett.* **2009**, *11*, 4644.

[59] S. Zhu, J. Zhang, G. Vegesna, A. Tiwari, F.-T. Luo, M. Zeller, R. Luck, H. Li, S. Green, H. Liu, *RSC Adv.* **2012**, *2*, 404.

[60] R. Hu, E. Lager, A. Aguilar-Aguilar, J. Liu, J. W. Y. Lam, H. H. Y. Sung, I. D. Williams, Y. Zhong, K. S. Wong, E. Peña-Cabrera, B. Z. Tang, *J. Phys. Chem. C* **2009**, *113*, 15845.

[61] J. Wang, N. Boens, L. Jiao, E. Hao, *Org. Biomol. Chem.* **2020**, *18*, 4135.

[62] a) M. Nakamura, H. Tahara, K. Takahashi, T. Nagata, H. Uoyama, D. Kuzuhara, S. Mori, T. Okujima, H. Yamada, H. Uno, *Org. Biomol. Chem.* **2012**, *10*, 6840; b) J. M. Cannon, R. Giovanelli, M. P. Haynes, S. Janowiecki, A. Parker, J. J. Salzer, E. A. K. Adams, E. Engstrom, S. Huang, K. B. W. McQuinn, J. Ott, A. Saintonge, E. D. Skillman, J. Allan, G. Erny, P. Fliss, A. Smith, *Tetrahedron* **2010**, *66*, 6895; c) Z. Zhou, J. Zhou, L. Gai, A. Yuan, Z. Shen, *Chem. Commun.* **2017**, *53*, 6621.

[63] a) H. Kim, A. Burghart, M. B. Welch, J. Reibenspies, K. Burgess, *Chem. Commun.* **1999**, *18*, 1889; b) J. Chen, A. Burghart, A. Derecskei-Kovacs, K. Burgess, *J. Org. Chem.* **2000**, *65*, 2900.

[64] a) R. Gresser, H. Hartmann, M. Wrackmeyer, K. Leo, M. Riede, *Tetrahedron* **2011**, *67*, 7148; b) A. Loudet, R. Bandichhor, L. Wu, K. Burgess, *Tetrahedron* **2008**, *64*, 3642; c) X. Zhang, H. Yu, Y. Xiao, *J. Org. Chem.* **2012**, *77*, 669.

[65] Z. Shi, X. Han, W. Hu, H. Bai, B. Peng, L. Ji, Q. Fan, L. Li, W. Huang, *Chem. Soc. Rev.* **2020**, *49*, 7533.

[66] a) A. Hayek, F. Bolze, J.-F. Nicoud, P. L. Baldeck, Y. Mély, *Photochem. Photobiol. Sci.* **2006**, *5*, 102; b) G. Zhang, S. Zheng, H. Liu, P. R. Chen, *Chem. Soc. Rev.* **2015**, *44*, 3405.
[67] a) S. Hohng, S. Lee, J. Lee, M. H. Jo, *Chem. Soc. Rev.* **2014**, *43*, 1007; b) Y. Zhang, A. Peng, X. Jie, Y. Lv, X. Wang, Z. Tian, *ACS Appl. Mater. Interfaces* **2017**, *9*, 13920; c) D. Ma, D. Kim, E. Seo, S.-J. Lee, K. H. Ahn, *Analyst* **2015**, *140*, 422.
[68] a) M. Zhu, C. Yang, *Chem. Soc. Rev.* **2013**, *42*, 4963; b) J.-H. Lee, C.-H. Chen, P.-H. Lee, H.-Y. Lin, M. Leung, T.-L. Chiu, C.-F. Lin, *J. Mater. Chem. C* **2019**, *7*, 5874; c) Z. Xu, B. Z. Tang, Y. Wang, D. Ma, *J. Mater. Chem. C* **2020**, *8*, 2614.
[69] I. Esnal, I. Valois-Escamilla, C. F. A. Gómez-Durán, A. Urías-Benavides, M. L. Betancourt-Mendiola, I. López-Arbeloa, J. Bañuelos, I. García-Moreno, A. Costela, E. Peña-Cabrera, *ChemPhysChem* **2013**, *14*, 4134.
[70] M. Farinone, J. Cybińska, M. Pawlicki, *Org. Chem. Front.* **2020**, *7*, 2391.
[71] A. Kaur, Z. Lim, K. Yang, E. J. New, *Fluorescent Sensors for Biological Metal Ions*, Elsevier, 2017.
[72] K. P. Carter, A. M. Young, A. E. Palmer, *Chem. Rev.* **2014**, *114*, 4564.
[73] a) A. W. Czarnik, *ACS Symp. Ser.* **1993**, *538*, 1; b) A. Prasanna de Silva, H. Nimal Gunaratne, T. Gunnlaugsson, A. Huxley, C. McCoy, J. Rademacher, T. Rice, *Chem. Rev.* **1997**, *97*, 1515.
[74] a) W. Qin, W. Dou, V. Leen, W. Dehaen, M. van der Auweraer, N. Boens, *RSC Adv.* **2016**, *6*, 7806; b) A. D. Johnson, R. M. Curtis, K. J. Wallace, *Chemosensors* **2019**, *7*, 22; c) N. Acha, C. Elosúa, J. Corres, F. Arregui, *Sensors* **2019**, *19*, 599; d) A. Kanegae, Y. Takata, I. Takashima, S. Uchinomiya, R. Kawagoe, K. Usui, A. Yamashita, J. Wongkongkatep, M. Sugimoto, A. Ojida, *Commun. Chem.* **2021**, *4*, 104.
[75] J. Huang, Y. Fang, W. Dehaen, *Chemosensors* **2020**, *8*, 51.
[76] X. Li, F. Li, G. Ji, *J. Fluoresc.* **2022**, *33*.
[77] a) L.-J. Fan, W. E. Jones, *J. Phys. Chem. B* **2006**, *110*, 7777; b) S. Zhang, W. Yuan, Y. Qin, J. Zhang, N. Lu, W. Liu, H. Li, Y. Wang, Y. Li, *Polyhedron* **2018**, *148*, 22; c) B. Daly, J. Ling, A. Prasanna de Silva, *Chem. Soc. Rev.* **2015**, *44*, 4203.
[78] L. Wu, C. Huang, B. P. Emery, A. C. Sedgwick, S. D. Bull, X.-P. He, H. Tian, J. Yoon, J. L. Sessler, T. D. James, *Chem. Soc. Rev.* **2020**, *49*, 5110.
[79] X. Zhang, Y. Xiao, X. Qian, *Angew. Chem.* **2008**, *120*, 8145.
[80] A. Barba-Bon, A. Costero, S. Gil, F. Sancenón, R. Martínez-Máñez, *Chem. Commun.* **2014**, *50*, 13289.
[81] A. Barba-Bon, L. Calabuig, A. Costero, S. Gil, R. Martínez-Máñez, F. Sancenón, *RSC Adv.* **2014**, *4*, 8962.
[82] a) K. Kim, O. G. Tsay, D. A. Atwood, D. G. Churchill, *Chem. Rev.* **2011**, *111*, 5345; b) G. H. Dennison, M. R. Sambrook, M. R. Johnston, *Chem. Commun.* **2014**, *50*, 195.
[83] M. N. Hopkinson, C. Richter, M. Schedler, F. Glorius, *Nature* **2014**, *510*, 485.
[84] R. Visbal, M. C. Gimeno, *Chem. Soc. Rev.* **2014**, *43*, 3551.
[85] N. Ségaud, C. Johnson, A. Farre, M. Albrecht, *Chem. Commun.* **2021**, *57*, 10600.
[86] (None), P. Kos, H. Plenio, *Chem. Eur. J.* **2015**, *21*, 1088.
[87] P. Kos, H. Plenio, *Angew. Chem. Int. Ed.* **2015**, *127*, 13491.
[88] J. Zhao, W. Wu, J. Sun, S. Guo, *Chem. Soc. Rev.* **2013**, *42*, 5323.
[89] X. Zhao, Y. Hou, L. Liu, J. Zhao, *Energy Fuels* **2021**, *35*, 18942.

[90] K. Chen, Y. Dong, X. Zhao, M. Imran, G. Tang, J. Zhao and Q. Liu, *Front. Chem.* **2019**, *7*, 821.
[91] Q.-Q. Zhou, Y.-Q. Zou, L.-Q. Lu, W.-J. Xiao, *Angew. Chem. Int. Ed.* **2019**, *58*, 1586.
[92] A. Baldacchino, M. Collins, M. Nielsen, T. Schmidt, D. McCamey, M. Tayebjee, *Chem. Phys. Rev.* **2022**, *3*, 21304.
[93] R. Pérez-Ruiz, *Top. Curr. Chem.* **2022**, *380*, 23.
[94] R. Baskaran, J. Lee, S.-G. Yang, *Biomater. Res.* **2018**, *22*, 25.
[95] a) Y. Liu, R. Qin, S. Zaat, E. Breukink, M. Heger, *J Clin Transl Res* **2015**, 140; b) L. Benov, *Med. Princ. Pract.* **2015**, *24*, 14.
[96] X. Zheng, L. Zhang, M. Ju, L. Liu, C. Ma, Y. Huang, B. Wang, W. Ding, X. Luan, B. Shen, *ACS Appl. Mater. Interfaces* **2022**, *14*, 46262.
[97] A. A. Buglak, A. Charisiadis, A. Sheehan, C. J. Kingsbury, M. O. Senge, M. A. Filatov, *Chem. Eur. J.* **2021**, *27*, 9934.
[98] W. Wang, L. Wang, Z. Li, Z. Xie, *Chem. Commun.* **2016**, *52*, 5402.
[99] a) T. Zhang, C. Ma, T. Sun, Z. Xie, *Coord. Chem. Rev.* **2019**, *390*, 76; b) D. Mai, C. Kim, J. Lee, T. Pegarro Vales, I. Badon, K. De, S. Cho, J. Yang, H.-J. Kim, *Sci. Rep.* **2022**, *12*, 2541.
[100] N. Aksakal, T. Eçik, H. Kazan, G. Çiftçi, F. Yuksel, *Photochem. Photobiol. Sci.* **2019**, *18*, 2012.
[101] H. Huang, S. Banerjee, P. J. Sadler, *ChemBioChem* **2018**, *19*, 1574.
[102] L. Qiao, J. Liu, Y. Han, F. Wei, X. Liao, C. Zhang, L. Xie, L. Ji, H. Chao, *Chem. Commun.* **2021**, *57*, 1790.
[103] T. C. Johnstone, K. Suntharalingam, S. J. Lippard, *Chem. Rev.* **2016**, *116*, 3436.
[104] A. Bera, S. Gautam, K. Raza, P. Kondaiah, A. Chakravarty, *J. Inorg. Biochem.* **2021**, *223*, 111526.
[105] E. Palao, R. Sola-Llano, A. Tabero, H. Manzano, A. Agarrabeitia, A. Villanueva, I. López-Arbeloa, V. Martinez, M. Ortiz, *Chem. Eur. J.* **2017**, *23*, 10139.
[106] M. Üçüncü, E. Karakuş, E. K. Demirci, M. Sayar, S. Dartar, M. Emrullahoğlu, *Org. Lett.* **2017**, *19*, 2522.
[107] a) R. C. McAtee, E. J. McClain, C. R. J. Stephenson, *Trends Chem.* **2019**, *1*, 111; b) G. E. M. Crisenza, P. Melchiorre, *Nat. Commun.* **2020**, *11*, 803; c) C.-S. Wang, P. H. Dixneuf, J.-F. Soulé, *Chem. Rev.* **2018**, *118*, 7532.
[108] a) J. Fischer, P. Nun, V. Coeffard, *Synthesis* **2020**, *52*, 1617; b) F. Strieth-Kalthoff, F. Glorius, *Chem* **2020**, *6*, 1888.
[109] C. B. Kelly, N. R. Patel, D. N. Primer, M. Jouffroy, J. C. Tellis, G. A. Molander, *Nat. Protoc.* **2017**, *12*, 472.
[110] J. Malone, S. Klaine, C. Alcantar, F. Bratcher, R. Zhang, *New J. Chem.* **2021**, *45*, 4977.
[111] a) M. D. Woodhouse, J. K. McCusker, *J. Am. Chem. Soc.* **2020**, *142*, 16229; b) S. Parisien-Collette, A. Hernandez-Perez, S. Collins, *Org. Lett.* **2016**, *18*, 4994.
[112] R. F. Higgins, S. M. Fatur, S. G. Shepard, S. M. Stevenson, D. J. Boston, E. M. Ferreira, N. H. Damrauer, A. K. Rappé, M. P. Shores, *J. Am. Chem. Soc.* **2016**, *138*, 5451.
[113] a) an Xie, Z.-H. Pan, M. Yu, G.-G. Luo, Di Sun, *Chin. Chem. Lett.* **2019**, *30*, 225; b) G.-G. Luo, K. Fang, J.-H. Wu, J.-C. Dai, Q.-H. Zhao, *Phys. Chem. Chem. Phys.* **2014**, *16*, 23884.
[114] P. de Bonfils, L. Péault, P. Nun, V. Coeffard, *Eur. J. Org. Chem.* **2021**, 1809.

[115] a) P. G. P. Saha, *Eur. J. Org. Chem.* **2022**, e202200733; b) K. L. Skubi, T. R. Blum, T. P. Yoon, *Chem. Rev.* **2016**, *116*, 10035.
[116] D. Wang, I. Pernik, S. T. Keaveney, B. A. Messerle, *ChemCatChem* **2020**, *12*, 5091.
[117] D. Wang, R. Malmberg, I. Pernik, S. K. K. Prasad, M. Roemer, K. Venkatesan, T. W. Schmidt, S. T. Keaveney, B. A. Messerle, *Chem. Sci.* **2020**, *11*, 6256.
[118] D. Wang, N. S. D. Solomon, I. Pernik, B. A. Messerle, S. T. Keaveney, *Aust. J. Chem.* **2020**, *73*, 979.
[119] K. C. Dissanayake, P. O. Ebukuyo, Y. J. Dhahir, K. Wheeler, H. He, *Chem. Commun.* **2019**, *55*, 4973.
[120] K.-K. Chen, S. Guo, H. Liu, X. Li, Z.-M. Zhang, T.-B. Lu, *Angew. Chem. Int. Ed.* **2020**, *59*, 12951.
[121] R.-Q. Xia, J. Zheng, R.-J. Wei, J. He, D.-Q. Ye, M.-D. Li, G.-H. Ning, D. Li, *Inorg. Chem. Front.* **2022**, *9*, 2928.
[122] R. H. Crabtree, *The Organometallic Chemistry of the Transition Metals*, WILEY - Interscience, **2014**.
[123] V. Sashuk, D. Schoeps, H. Plenio, *Chem. Commun.* **2009**, *7*, 770.
[124] T. Vorfalt, K. J. Wannowius, V. Thiel, H. Plenio, *Chem. Eur. J.* **2010**, *16*, 12312.
[125] M. Lelek, M. Gyparaki, G. Beliu, F. Schueder, J. Griffié, S. Manley, R. Jungmann, M. Lakadamyali and C. Zimmer, *Nat. Rev. Methods Primers 2* **2022**, *70*, 39.
[126] A. Kiel, J. Kovacs, A. Mokhir, R. Krämer, D.-P. Herten, *Angew. Chem. Int. Ed.* **2007**, *46*, 5049.
[127] N. M. Esfandiari, Y. Wang, J. Y. Bass, T. P. Cornell, D. A. L. Otte, M. H. Cheng, J. C. Hemminger, T. M. McIntire, V. A. Mandelshtam, S. A. Blum, *J. Am. Chem. Soc.* **2010**, *132*, 15167.
[128] N. M. Esfandiari, S. A. Blum, *J. Am. Chem. Soc.* **2011**, *133*, 18145.
[129] a) A. Garcia, S. J. Saluga, D. J. Dibble, P. A. López, N. Saito, S. A. Blum, *Angew. Chem. Int. Ed.* **2021**, *60*, 1550; b) S. Saluga, D. Dibble, S. Blum, *J. Am. Chem. Soc.* **2022**, *144*, 10591.
[130] C. Feng, D. W. Cunningham, Q. T. Easter, S. A. Blum, *J. Am. Chem. Soc.* **2016**, *138*, 11156.
[131] Q. T. Easter, S. A. Blum, *Acc. Chem. Res.* **2019**, *52*, 2244.
[132] D. Axelrod, *Traffic* **2001**, *2*, 764.
[133] a) J. C. Scaiano, A. E. Lanterna, *J. Org. Chem.* **2017**, *82*, 5011; b) M. Decan, S. Impellizzeri, M. Marin, J. Scaiano, *Nat. Commun.* **2014**, *5*, 4612.
[134] K. Kitagawa, S. A. Blum, *ACS Catal.* **2017**, *7*, 3786.
[135] J. Ng, S. Upadhyay, A. Marquard, K. Lupo, D. Hinton, N. Padilla, D. Bates, R. Goldsmith, *J. Am. Chem. Soc.* **2016**, *138*, 3876.
[136] J. Nasielski, N. Hadei, G. Achonduh, E. A. B. Kantchev, C. J. O'Brien, A. Lough, M. G. Organ, *Chem. Eur. J.* **2010**, *16*, 10844.
[137] S.-G. Lim, S. Blum, *Organometallics* **2009**, *28*, 4643.
[138] O. Halter, R. Vasiuta, I. Fernández, H. Plenio, *Chem. Eur. J.* **2016**, *22*, 18066.
[139] R. Vasiuta, H. Plenio, *Chem. Eur. J.* **2016**, *22*, 6353.
[140] a) Y. Urano, M. Kamiya, K. Kanda, T. Ueno, K. Hirose, T. Nagano, *J. Am. Chem. Soc.* **2005**, *127*, 4888; b) T. Ueno, Y. Urano, K.-I. Setsukinai, H. Takakusa, H. Kojima, K. Kikuchi, K. Ohkubo, S. Fukuzumi, T. Nagano, *J. Am. Chem. Soc.* **2004**, *126*, 14079.
[141] M. A. Filatov, *Org. Biomol. Chem.* **2019**, *18*, 10.

[142] T. Yogo, Y. Urano, Y. Ishitsuka, F. Maniwa, T. Nagano, *J. Am. Chem. Soc.* **2005**, *127*, 12162.
[143] K.-X. Teng, W.-K. Chen, L.-Y. Niu, W.-H. Fang, G. Cui and Q.-Z. Yang, *Angew. Chem. Int. Ed.* **2021**, *133*, 20065.
[144] a) F. Geist, A. Jackel, R. F. Winter, *Inorg. Chem.* **2015**, *54*, 10946; b) P. Irmler, R. Winter, *Dalton Trans.* **2016**, *45*, 10420.
[145] A. M. Costero, M. L. Betancourt-Mendiola, P. Gaviña, L. E. Ochando, S. Gil, K. Chulvi, E. Peña-Cabrera, *Eur. J. Org. Chem.* **2017**, *2017*, 6283.
[146] M. Whited, P. Djurovich, S. Roberts, A. Durrell, C. Schlenker, S. Bradforth, M. Thompson, *J. Am. Chem. Soc.* **2011**, *133*, 88.
[147] A. Potocny, J. Teesdale, A. Marangoz, G. Yap, J. Rosenthal, *Inorg. Chem.* **2019**, *58*, 5042.
[148] L. K. McKenzie, H. E. Bryant, J. A. Weinstein, *Coord. Chem. Rev.* **2019**, *379*, 2.
[149] X.-F. Zhang, X. Yang, B. Xu, *Phys. Chem. Chem. Phys.* **2017**, *19*, 24792.
[150] a) B. Bertrand, K. Passador, C. Goze, F. Denat, E. Bodio, M. Salmain, *Coord. Chem. Rev.* **2018**, *358*, 108; b) L. Gourdon, K. Cariou, G. Gasser, *Chem. Soc. Rev.* **2022**, *51*, 1167.
[151] H. V. Huynh, *Chem. Rev.* **2018**, *118*, 9457.
[152] D. Nelson, *Eur. J. Inorg. Chem.* **2015**, 2012.
[153] E. A. Martynova, N. V. Tzouras, G. Pisanò, C. S. J. Cazin, S. P. Nolan, *Chem. Commun.* **2021**, *57*, 3836.
[154] S. Leuthäußer, D. Schwarz, H. Plenio, *Chem. Eur. J.* **2007**, *13*, 7195.
[155] This is necessary, since the recorded ATR-IR frequencies are shifted significantly relative to the traditional transmission IR frequencies and furthermore also differ from one ATR-IR spectrometer to another one -depending on the nature of the detector and window material.
[156] G. Ciancaleoni, N. Scafuri, G. Bistoni, A. Macchioni, F. Tarantelli, D. Zuccaccia, L. Belpassi, *Inorg. Chem.* **2014**, *53*, 9907.
[157] S. Popov, H. Plenio, *Eur. J. Inorg. Chem.* **2021**, *2021*, 3708.
[158] G. M. Sheldrick, *Acta Cryst.* **2015**, *71*, 3.
[159] O. V. Dolomanov, L. J. Bourhis, R. J. Gildea, J. A. K. Howard, H. Puschmann, *J. Appl. Cryst.* **2009**, *42*, 339.
[160] R. A. Kelly, H. Clavier, S. Giudice, N. M. Scott, E. D. Stevens, J. Bordner, I. Samardjiev, C. D. Hoff, L. Cavallo, S. P. Nolan, *Organometallics* **2008**, *27*, 202.
[161] A packing effect is unlikely, since DFT calculations reproduce the tilting of the two planes.
[162] O. Halter, J. Spielmann, Y. Kanai, H. Plenio, *Organometallics* **2019**, *38*, 2138.
[163] O. Halter, I. Fernández, H. Plenio, *Chem. Eur. J.* **2017**, *23*, 711.
[164] O. Halter, H. Plenio, *Eur. J. Inorg. Chem.* **2018**, *2018*, 2935.
[165] Y. You, *Org. Biomol. Chem.* **2018**, *16*, 4044.
[166] W. Hu, M. Liu, X.-F. Zhang, M. Shi, M. Jia, X. Hu, L. Liu, T. Wang, *J. Phys. Chem. C* **2020**, *124*, 23558.
[167] F. Wilkinson, W. P. Helman, A. B. Ross, *JPCRD* **1995**, *24*, 663.
[168] a) S. Xu, Y. Yuan, X. Cai, C.-J. Zhang, F. Hu, J. Liang, G. Zhang, D. Zhang, B. Liu, *Chem. Sci.* **2015**, *6*, 5824; b) P.-T. Chou, Y. Chi, M.-W. Chung, C.-C. Lin, *Coord. Chem. Rev.*

2011, *255*, 2653; c) Y.-L. Chen, S.-W. Li, Y. Chi, Y.-M. Cheng, S.-C. Pu, Y.-S. Yeh, P.-T. Chou, *ChemPhysChem* **2005**, *6*, 2012.
[169] W. H. Lam, E. S.-H. Lam, V. W.-W. Yam, *J. Am. Chem. Soc.* **2013**, *135*, 15135.
[170] a) H. Plenio, M. Bergmann, *Eur. J. Inorg. Chem.* **2018**, *2018*, 2054; b) M. Bergmann, M. Egert, H. Plenio, *Chem. Eur. J.* **2017**, *23*, 13328.
[171] a) C. Bian, A. K. Singh, L. Niu, H. Yi, A. Lei, *Asian J. Org. Chem.* **2017**, *6*, 386; b) H. Guo, H. Xia, X. Ma, K. Chen, C. Dang, J. Zhao, B. Dick, *ACS Omega* **2020**, *5*, 10586; c) C. Ye, Y. Zhang, A. Ding, Y. Hu, H. Guo, *Sci. Rep.* **2018**, *8*, 2205.
[172] a) C. Schiwek, J. Meiners, M. Förster, C. Würtele, M. Diefenbach, M. C. Holthausen, S. Schneider, *Angew. Chem. Int. Ed.* **2015**, *127*, 15486; b) M. Selke, C. S. Foote, *J. Am. Chem. Soc.* **1993**, *115*, 1166.
[173] The Vaska complex posseses two donating phosphine ligands and only single electron-withdrawing CO.
[174] S. Carboni, C. Gennari, L. Pignataro, U. Piarulli, *Dalton Trans.* **2011**, *40*, 4355.
[175] A. Macchioni, *Chem. Rev.* **2005**, *105*, 2039.
[176] Y. Marcus, G. Hefter, *Chem. Rev.* **2006**, *106*, 4585.
[177] a) D. Zuccaccia, L. Belpassi, A. Macchioni, F. Tarantelli, *Eur. J. Inorg. Chem.* **2013**, 4121; b) B. Binotti, G. Bellachioma, G. Cardaci, C. Carfagna, C. Zuccaccia, A. Macchioni, *Chem. Eur. J.* **2007**, *13*, 1570.
[178] a) C. Merten, C. H. Pollok, S. Liao, B. List, *Angew. Chem. Int. Ed.* **2015**, *54*, 8841; b) H. Davis, M. Mihai, R. Phipps, *J. Am. Chem. Soc.* **2016**, *138*, 12759; c) C. Chiappe, B. Mennucci, C. Pomelli, A. Sanzonea and A. Marrab, *Phys. Chem. Chem. Phys.* **2010**, 1958.
[179] P. Rayner, P. Norcott, K. Appleby, W. Iali, R. John, S. Hart, A. Whitwood, S. Duckett, *Nat. Commun.* **2018**, *9*, 4251.
[180] R. Savka, H. Plenio, *J. Organomet. Chem.* **2012**, *710*, 68.
[181] R. Savka, H. Plenio, *Dalton Trans.* **2015**, *44*, 891.
[182] R. Alnoman, P. Stachelek, J. Knight, A. Harriman, P. Waddell, *Org. Biomol. Chem.* **2017**, *15*, 7643.
[183] G. Sipos, P. Gao, D. Foster, B. W. Skelton, A. N. Sobolev, R. Dorta, *Organometallics* **2017**, *36*, 801.
[184] H. W. Gibson, J. W. Jones, L. N. Zakharov, A. L. Rheingold, C. Slebodnick, *Chem. Eur. J.* **2011**, *17*, 3192.
[185] M. Trinchillo, P. Belanzoni, L. Belpassi, L. Biasiolo, V. Busico, A. D'Amora, L. D'Amore, A. Del Zotto, F. Tarantelli, A. Tuzi, D. Zuccaccia, *Organometallics* **2016**, *35*, 641.
[186] a) G. N. Lewis, M. Randall, *J. Am. Chem. Soc.* **1921**, *43*, 1112.; b) P. Debye, E. Hückel, *Z. Phys.* **1923**, *24*, 305.
[187] The relative fluorescence intensity is directly proportional to the "equilibrium constant".
[188] H. Clavier, S. Nolan, *Chem. Commun.* **2009**, *46*, 841.
[189] A. Poater, B. Cosenza, A. Correa, S. Giudice, F. Ragone, V. Scarano, L. Cavallo, *Eur. J. Inorg. Chem.* **2009**, 1759.
[190] Different default radii and different metal-C(NHC) values have also been employed, which leads to some arbitrarity in the buried volume values.
[191] D. Gusev, *Organometallics* **2009**, *28*, 6458.

[192] A. Gómez-Suárez, D. J. Nelson, S. P. Nolan, *Chem. Commun.* **2017**, *53*, 2650.
[193] L. Falivene, R. Credendino, A. Poater, A. Petta, L. Serra, R. Oliva, V. Scarano, L. Cavallo, *Organometallics* **2016**, *35*, 2286.
[194] L. Falivene, Z. Cao, A. Petta, L. Serra, A. Poater, R. Oliva, V. Scarano, L. Cavallo, *Nat. Chem.* **2019**, *11*, 872.
[195] A. V. Brethomé, S. P. Fletcher, R. S. Paton, *ACS Catal.* **2019**, *9*, 2313.
[196] D. J. Durand, N. Fey, *Acc. Chem. Res.* **2021**, *54*, 837.
[197] This is based on the reasonable assumption, that the true close ion paired complexes would display the same fluorescence intensity.
[198] The given value for corrected data corresponds to the deviation of fluorescence intensity from the linear fit, compensating for the electronic effect of the respective NHC.
[199] P. de Frémont, N. M. Scott, E. D. Stevens, S. P. Nolan, *Organometallics* **2005**, *24*, 2411.
[200] B. Truscott, D. Nelson, C. Lujan, A. Slawin, S. Nolan, *Chem. Eur. J.* **2013**, *19*, 7904.
[201] It should be mentioned, that in these DFT calculations a metal center was not included. The energies are only those of the plain carbene with different N-isopropyl group orientations.
[202] a) A. Macchioni, *ChemInform* **2005**, *36*; b) Z. Lu, T. Li, S. R. Mudshinge, B. Xu, G. B. Hammond, *Chem. Rev.* **2021**, *121*, 8452; c) A. R. Kennedy, W. J. Kerr, R. Moir, M. Reid, *Org. Biomol. Chem.* **2014**, *12*, 7927; d) D. Zuccaccia, L. Belpassi, A. Macchioni, F. Tarantelli, *Eur. J. Inorg. Chem.* **2013**, 4121.
[203] a) R. V. Honeychuck, W. H. Hersh, *Inorg. Chem.* **1989**, *20*, 2869; b) H. Mayfield, W. Bull, *J. Chem. Soc. A* **1971**, 2279.
[204] T. Dröge, F. Glorius, *Angew. Chem. Int. Ed.* **2010**, *49*, 6940.
[205] a) D. J. Durand, N. Fey, *Chem. Rev.* **2019**, *119*, 6561; b) D. Cremer, E. Kraka, *Dalton Trans.* **2017**, *46*, 8323.
[206] N. M. Scott, R. Dorta, E. D. Stevens, A. Correa, L. Cavallo, S. P. Nolan, *J. Am. Chem. Soc.* **2005**, *127*, 3516.
[207] A. Chianese, X. Li, M. Janzen, J. W. Faller, R. Crabtree, *Organometallics* **2003**, *22*, 1663.
[208] S. Wolf, H. Plenio, *J. Organomet. Chem.* **2009**, *694*, 1487.
[209] G. Ciancaleoni, N. Scafuri, G. Bistoni, A. Macchioni, F. Tarantelli, D. Zuccaccia, L. Belpassi, *Inorg. Chem.* **2014**, *53*, 9907.
[210] S. Leuthäußer, V. Schmidts, C.M. Thiele, H. Plenio, *Chem. Eur. J.* **2008**, *14*, 5465.
[211] H. V. Huynh, Y. Han, R. Jothibasu, J. A. Yang, *Organometallics* **2009**, *28*, 5395.
[212] K. Verlinden, H. Buhl, W. Frank, C. Ganter, *Eur. J. Inorg. Chem.* **2015**, 2416.
[213] D. Marchione, M. A. Izquierdo, G. Bistoni, R. W. A. Havenith, A. Macchioni, D. Zuccaccia, F. Tarantelli, L. Belpassi, *Chem. Eur. J.* **2017**, *23*, 2722.
[214] O. Back, M. Henry-Ellinger, C. D. Martin, D.Martin, G. Bertrand, *Angew. Chem. Int. Ed.* **2013**, *52*, 2939.
[215] A. Liske, K. Verlinden, H. Buhl, K. Schaper, C. Ganter, *Organometallics* **2013**, *32*, 5269.
[216] S. V. C. Vummaleti, D. J. Nelson, A. Poater, A. Gómez-Suárez, D. B. Cordes, A. M. Z. Slawin, S. P. Nolan, L. Cavallo, *Chem. Sci.* **2015**, *6*, 1895.

[217] D. Gatineau, D. Lesage, H. Clavier, H. Dossmann, C. H. Chan, A. Milet, A. Memboeuf, R. B. Cole, Y. Gimbert, *Dalton Trans.* **2018**, *47*, 15497.
[218] a) R. Credendino, L. Falivene, L. Cavallo, *J. Am. Chem. Soc.* **2012**, *134*, 8127; b) V. César, N. Lugan, G. Lavigne, *J. Am. Chem. Soc.* **2008**, *130*, 11286; c) M. Süssner, H. Plenio, *Chem. Commun.* **2005**, 5417.
[219] C. Hansch, A. Leo, R. Taft, *Chem. Rev.* **1991**, *91*, 165.
[220] T. Papp, L. Kollár, T. Kégl, *Chem. Phys. Let.* **2013**, *588*, 51.
[221] C. L. Perrin, *J. Chem. Educ.* **2017**, *94*, 669.
[222] Linear plots are historically important and better accessible to the eye. This is the reason, why a linear plot is also displayed, even though non-linear fits are convenient these days and often more precise - see ref. 221.
[223] The value is based on the average of the symmetric and the antisymmetric CO stretch, both absorbances tend to be broad and the resolution limit of the spectrometer being 0.5 wavenumbers.
[224] F. Wilkinson, W. P. Helman, A. B. Ross, *JPCRD* **1995**, *24*, 663.
[225] I. Krossing, I. Raabe, *Angew. Chem. Int. Ed.* **2004**, *43*, 2066.
[226] The small amount of solid NaBr formed does not lead to significant scattering of the excitation light in the fluorescence cuvette.
[227] Addition of NaBArF to a toluene solution of 2,6-diiodobodipy does not have any effect on the photosensitizing ability.
[228] a) S. Xu, Y. Yuan, X. Cai, C.-J. Zhang, F. Hu, J. Liang, G. Zhang, D. Zhang, B. Liu, *Chem. Sci.* **2015**, *6*, 5824; b) J. Zhang, W. Chen, R. Chen, X.-K. Liu, Y. Xiong, S. V. Kershaw, A. L. Rogach, C. Adachi, X. Zhang, C.-S. Lee, *Chem. Commun.* **2016**, *52*, 11744; c) J. Zhang, F. Fang, B. Liu, J.-H. Tan, W.-C. Chen, Z. Zhu, Y. Yuan, Y. Wan, X. Cui, S. Li, Q.-X. Tong, J. Zhao, X.-M. Meng, C.-S. Lee, *ACS Appl. Mater. Interfaces* **2019**, *11*, 41051; d) X. Zhao, S. Long, M. Li, J. Cao, Y. Li, L. Guo, W. Sun, J. Du, J. Fan, X. Peng, *J. Am. Chem. Soc.* **2020**, *142*, 1510; e) V.-N. Nguyen, Y. Yim, S. Kim, B. Ryu, K. M. K. Swamy, G. Kim, N. Kwon, C.-Y. Kim, S. Park, J. Yoon, *Angew. Chem. Int. Ed.* **2020**, *59*, 8957.
[229] TDDFT calculations to determine the respective S1 and T1 energies of the iridium complexes with an explicit solvation model were attempted, but did not provide a consistent data set.
[230] X. Li, A. H. G. David, L. Zhang, B. Song, Y. Jiao, D. Sluysmans, Y. Qiu, Y. Wu, X. Zhao, Y. Feng, L. Mosca, J. F. Stoddart, *J. Am. Chem. Soc.* **2022**, *144*, 3572.
[231] A. Nagarkar, S. Root, M. Fink, A. Ten, B. Cafferty, D. Richardson, M. Mrksich, G. Whitesides, *ACS Cent. Sci.* **2021**, *7*, 1728.
[232] Y. Wu, M. Frasconi, W.-G. Liu, R. M. Young, W. A. Goddard, M. R. Wasielewski, J. F. Stoddart, *J. Am. Chem. Soc.* **2020**, *142*, 11835.
[233] B. Bajar, E. Wang, S. Zhang, M. Lin, J. Chu, *Sensors* **2016**, *16*, 1488.
[234] M. Sustarsic, A. N. Kapanidis, *COSB* **2015**, *34*, 52.
[235] P. Rajdev, S. Ghosh, *J. Phys. Chem. B* **2019**, *123*, 327.
[236] a) R. Castellano, S. Craig, C. Nuckolls, J. Rebek, *J. Am. Chem. Soc.* **2000**, *122*, 7876; b) M. J. Mayoral, D. Serrano-Molina, J. Camacho-García, E. Magdalena-Estirado, M. Blanco-Lomas, E. Fadaei, D. González-Rodríguez, *Chem. Sci.* **2018**, *9*, 7809.
[237] L. Yuan, W. Lin, K. Zheng, S. Zhu, *Acc. Chem. Res.* **2013**, *46*, 1462.
[238] I. Johnson, M. Spence, *Molecular Probes Handbook - A Guide to Fluorescent Probes and Labeling Technologies*, **2010**.

[239] G. Ulrich, R. Ziessel, A. Harriman, *Angew. Chem. Int. Ed.* **2008**, *47*, 1184.
[240] A. Kiel, J. Kovacs, A. Mokhir, R. Krämer, D.-P. Herten, *Angew. Chem. Int. Ed.* **2007**, *46*, 5049.
[241] a) T. Cordes, S. Blum, *Nat. Chem.* **2013**, *5*, 993; b) Q. Easter, S. Blum, *Angew. Chem. Int. Ed.* **2018**, *130*, 1588; c) Q. T. Easter, V. Trauschke, S. A. Blum, *ACS Catal.* **2015**, *5*, 2290; d) A. Garcia, S. J. Saluga, D. J. Dibble, P. A. López, N. Saito, S. A. Blum, *Angew. Chem. Int. Ed.* **2021**, *60*, 1550.
[242] J. Fan, M. Hu, P. Zhan, X. Peng, *Chem. Soc. Rev.* **2013**, *42*, 29.
[243] I. Pochorovski, B. Breiten, W. B. Schweizer, F. Diederich, *Chem. Eur. J.* **2010**, *16*, 12590.
[244] O. Halter, H. Plenio, *Chem. Commun.* **2017**, *53*, 12461.
[245] Z. Wu, H. Fujita, N. C. M. Magdaong, J. R. Diers, D. Hood, S. Allu, D. M. Niedzwiedzki, C. Kirmaier, D. F. Bocian, D. Holten, J. S. Lindsey, *New J. Chem.* **2019**, *43*, 7233.
[246] Y. Tan, J. F. Hartwig, *J. Am. Chem. Soc.* **2011**, *133*, 3308.
[247] Y. Kanai, D. Müller-Borges, H. Plenio, *Adv. Synth. Catal.* **2022**, *364*, 679.
[248] N. K. Lee, A. N. Kapanidis, Y. Wang, X. Michalet, J. Mukhopadhyay, R. H. Ebright, S. Weiss, *Biophys. J.* **2005**, *88*, 2939.
[249] Y. Shinozaki, S. Popov, H. Plenio, *Chem. Sci.* **2023**, *14*, 350.
[250] T. J. Brown, R. A. Widenhoefer, *Organometallics* **2011**, *30*, 6003.
[251] The residual green fluorescence is not the result of incomplete conversion of the starting materials into the products, since re-dissolved samples from the preparative synthesis also display residual green fluorescence of comparable intensity. Very fast scrambling of the green/red labels is also unlikely since it should lead to much higher green fluorescence.
[252] Intermolecular gold shuffling with mixing of fluorescent labels does not take place during the observation time.
[253] Estimate is based on the extrapolation of the near linear central segment of the plot of distance *vs*. energy transfer efficiency.
[254] N. Salvi, L. Belpassi, D. Zuccaccia, F. Tarantelli, A. Macchioni, *J. Organomet. Chem.* **2010**, *695*, 2679.
[255] a) F. Zaccaria, L. Sian, C. Zuccaccia, A. Macchioni, *Adv. Organomet. Chem.* **2020**, *73*, 78; b) L. Sian, A. Macchioni, C. Zuccaccia, *ACS Catal.* **2010**, *10*, 1591; c) F. Zaccaria, L. Sian, C. Zuccaccia, A. Macchioni, *Adv. Organomet. Chem.* **2020**, *73*, 1.
[256] D. Zuccaccia, A. Del Zotto, W. Baratta, *Coord. Chem. Rev.* **2019**, *396*, 103.
[257] G. Duran-Sampedro, A. R. Agarrabeitia, I. Garcia-Moreno, L. Gartzia-Rivero, S. de La Moya, J. Bañuelos, Í. López-Arbeloa, M. J. Ortiz, *Chem. Commun.* **2015**, *51*, 11382.
[258] a) J. Bañuelos, V. Martín, A. Gómez-Durán, I. Arroyo Córdoba, E. Peña-Cabrera, I. García-Moreno, Á. Costela, E. Pérez-Ojeda, T. Arbeloa, Í. López Arbeloa, *Chem. Eur. J.* **2011**, *17*, 7261; b) C. A. Osorio-Martínez, A. Urías-Benavides, C. F. A. Gómez-Durán, J. Bañuelos, I. Esnal, I. López Arbeloa, E. Peña-Cabrera, *J. Org. Chem.* **2012**, *77*, 5434.
[259] The sudden change in the fluorescence indicates that the change in fluorescence is less likely caused by a chemical reaction (which should take some time), but is the result of the sudden increase in the concentration of the red Bodipy after addition of the solution of the red dye.

[260] This experiment was also used to correct the observed red fluorescence in the triad experiment for cross-talk intensity.
[261] B. T. Worrell, J. A. Malik, V. V. Fokin, *Science* **2013**, *340*, 457.
[262] S. H. Hong, A. G. Wenzel, T. T. Salguero, M. W. Day, R. H. Grubbs, *J. Am. Chem. Soc.* **2007**, *129*, 7961.
[263] a) V. Thiel, K. J. Wannowius, C. Wolf, C. M. Thiele, H. Plenio, *Chem. Eur. J.* **2013**, *19*, 16403; b) D. L. Nascimento, M. Foscato, G. Occhipinti, V. R. Jensen, D. E. Fogg, *J. Am. Chem. Soc.* **2021**, *143*, 11072.
[264] N. Jeddi, N. W. J. Scott, I. J. S. Fairlamb, *ACS Catal.* **2022**, *12*, 11615.
[265] S. Popov, H. Plenio, *Eur. J. Inorg. Chem.* **2022**, e202200335.
[266] S. Popov, H. Plenio, *Chem. Commun.* **2022**, *58*, 12669.
[267] K. Kadish, X. Mu, J. Anderson, *Pure & Appl. Chem.* **1989**, *61*, 1823.
[268] D. J. Nelson, A. Collado, S. Manzini, S. Meiries, A. M. Z. Slawin, D. B. Cordes, S. P. Nolan, *Organometallics* **2014**, *33*, 2048.
[269] R. Savka, S. Foro, H. Plenio, *Dalton Trans.* **2016**, *45*, 11015.
[270] W. J. Kerr, M. Reid, T. Tuttle, *Angew. Chem.* **2017**, *129*, 7916.
[271] T. Vorfalt, S. Leuthäußer, H. Plenio, *Angew. Chem. Int. Ed.* **2009**, *48*, 5191.
[272] T. Kowada, S. Yamaguchi, K. Ohe, *Org. Lett.* **2010**, *12*, 296.
[273] P. Irmler, F. S. Gogesch, A. Mang, M. Bodensteiner, C. B. Larsen, O. S. Wenger, R. F. Winter, *Dalton Trans.* **2019**, *48*, 11690.
[274] A. Kämpfe, E. Brendler, E. Kroke, J. Wagler, *Chem. Eur. J.* **2014**, *20*, 9409.
[275] a) A. M. Durantini, L. E. Greene, R. Lincoln, S. R. Martínez, G. Cosa, *J. Am. Chem. Soc.* **2016**, *138*, 1215; b) Z. Lou, Y. Hou, K. Chen, J. Zhao, S. Ji, F. Zhong, Y. Dede and B. Dick, *J. Phys. Chem. C* **2018**, *122*, 185.
[276] L. V. Lutkus, S. S. Rickenbach, T. M. McCormick, *J. Photochem. Photobiol.* **2019**, *378*, 131.

Erklärungen laut Promotionsordnung

§8 Abs. 1 lit. c der Promotionsordnung der TU Darmstadt

Ich versichere hiermit, dass die elektronische Version meiner Dissertation mit der schriftlichen Version übereinstimmt und für die Durchführung des Promotionsverfahrens vorliegt.

§8 Abs. 1 lit. d der Promotionsordnung der TU Darmstadt

Ich versichere hiermit, dass zu einem vorherigen Zeitpunkt noch keine Promotion versucht wurde und zu keinem früheren Zeitpunkt an einer in- oder ausländischen Hochschule eingereicht wurde. In diesem Fall sind nähere Angaben über Zeitpunkt, Hochschule, Dissertationsthema und Ergebnis dieses Versuchs mitzuteilen.

§9 Abs. 1 der Promotionsordnung der TU Darmstadt

Ich versichere hiermit, dass die vorliegende Dissertation selbstständig und nur unter Verwendung der angegebenen Quellen verfasst wurde.

§9 Abs. 2 der Promotionsordnung der TU Darmstadt

Die Arbeit hat bisher noch nicht zu Prüfungszwecken gedient.

Darmstadt, den ……..

(Name und Unterschrift)